LIPIDOMICS OF INFLUENZA VIRUS: IMPLICATIONS OF HOST CELL CHOLINE- AND SPHINGOLIPID METABOLISM

LUKAS BAHATI TANNER

M.Sc.

National University of Singapore & University of Basel

A THESIS SUBMITTED

FOR THE DEGREE OF DOCTOR OF PHILOSOPHY

NUS GRADUATE SCHOOL FOR INTEGRATIVE SCIENCES AND ENGINEERING (NGS)

NATIONAL UNIVERSITY OF SINGAPORE

2012

Declaration

I hereby declare that the thesis is my original work and it has been written by me in its entirety. I have duly acknowledged all the sources of information which have been used in the thesis.

This thesis has also not been submitted for any degree in any university previously.

Lukas Bahati Tanner

23rd December 2012

Acknowledgments

Surfing the Singaporean PhD wave was an exciting journey with many ups and downs. It would not have been possible without the help and support of so many people in so many ways…I am deeply grateful…

First and foremost, I would like to thank my supervisor Markus Wenk for his patience, guidance, support and the endless fruitful discussions we had. It sparked my passion and hunger for future endeavours in the exciting field of lipidomics.

I thank my two TAC members Paul MacAry and Vincent Chow who were always ready to answer my many questions and to provide me with useful suggestions throughout the project.

I am also very grateful to the many current and former members of the MRW lab. Especially, I would like to thank Charmaine Chng who was working with me, first as an honour's student, then as a master's student. Her help and contribution were invaluable for the success of this project and it was great to share my passion for biology with her. Many thanks goes to Amaury, Anne, Federico, Guanghou, Huimin, Husna, Jacklyn, Jingyan, Lissya, Lynette, Madhu, Martin, Pradeep, Sudar, Shareef, Weifun & Xueli for suggestions and help throughout the project, but also for their friendship and good times which was an invaluable enrichment besides the day-to-day lab routine.

I express gratitude to my collaborators Frederic Vigant & Benhur Lee (University of California, Los Angeles); Takayuki Nitta & Hung Fan (University of California, Irvine); Qian Zhang & Shee Mei Lok (Duke-NUS); Manuel Fernandez-Rojo & Rob Parton (University of Queensland); Fubito Nakatsu & Pietro De Camilli (Yale University); Stefania Luisoni, Pascal Roulin & Urs Greber (University of Zurich).

I am most grateful to my parents Suzanne and Marcel for their endless support and love in good times but also in difficult times. I express special thanks to my two sisters, Catherine and Sabine, for always being there for me. The support of our family is invaluable to reach my goals.

Last but not least, I show gratitude to my friends in Singapore but also back home in Switzerland. I've realized that without their good friendship I would not have the energy to fulfil my goals.

Table of Contents

Summary

Enveloped viruses consist of a host-derived lipid envelope which is a detailed representation of the lipid composition at budding sites. For example, influenza viruses hijack plasma membrane microdomains which are generally enriched in cholesterol, sphingolipids and in certain glycerophospholipid species. Enveloped viruses not only acquire such host lipids, but also have the capability to modify host cell metabolism for efficient replication.

In this study, we harnessed a comprehensive lipidomics approach using mass spectrometry to get a better understanding of the role of lipids during influenza A virus replication. We performed a detailed analysis of host cell lipid metabolism in a lung epithelial cell line. We identified a variety of sphingo- and glycerophospholipids to be differentially regulated in human lung epithelial cells during the course of an infection. Specifically, we observed an upregulation of sphingomyelin, ether linked and odd chain ester linked phosphatidylcholine species, but a concomitant decrease in even chain ester linked phosphatidylcholine species in infected cells. Consistent with a redirection of glycolytic flux into the biosynthesis of ether- and sphingolipids, we detected an early phosphorylation of pyruvate kinase M2 and a decrease in peroxisomal ß-oxidation. Significance of increased lipogenesis (ether and odd chain lipid biosynthesis) but decreased ß-oxidation in the peroxisome was further supported by the antiviral activity of a PPARα agonist.

The influenza virus induced changes in host cell lipid metabolism correlated with the lipid composition of purified virus particles. Further analysis revealed an influenza

specific remodelling of phosphatidylcholine species when compared to other enveloped viruses. We hypothesized that these changes reflected the requirement of polarized vesicular trafficking for influenza virus assembly and budding. Subsequently, we identified NS1 as a determinant modulating host cell lipid metabolism which was confirmed by distinct sphingolipid and phosphatidylcholine profiles of two closely related influenza virus strains differing in a non-conservative point mutation in NS1. We further showed that the influenza virus non-structural protein NS1 harbours a highly conserved putative peroxisome targeting sequence 2.

Based on these findings and published data, we proposed a model whereby influenza virus redirects glycolytic flux into the biosynthesis of ether linked- and sphingolipids, to facilitate proper virion morphogenesis in the exocytic pathway which correlates with virus pathogenicity. The importance of choline containing sphingo- and ether lipids was additionally highlighted by impaired virus production from cells either treated with a sphingomyelin synthase inhibitor or from ether lipid deficient cells.

Besides, we also detected a significant enrichment of ceramide in influenza virus envelopes despite not being differentially regulated in virus infected cells. Further scrutiny revealed a specific enrichment of ceramide in enveloped viruses fusing at late endosomal compartments, and we subsequently derived a model whereby ceramide/cholesterol ratios of cellular and viral membranes mediate intracellular trafficking.

List of Tables

List of Figures

List of Abbreviations

A549	Human alveolar adenocarcinoma cells
ACOX	Acyl-CoA oxidase
AGPS	Alkylglycerone phosphate synthase
ALV	Avian leukosis virus
AMPK	AMP activated protein kinase
ASAH	N-acylsphingosine amidohydrolase
BSA	Bovine serum albumin
CerS	Ceramide synthase
CHO-K1	Chinese hamster ovary cell line K1
CPE	Cytopathic effect
cRNA	Complementary RNA
CROT	Carnitine-O-octanoyltransferase
DAG	Diacylglycerol
DBI	Diazepam binding inhibitor
DHAP	Dihydroxyacetone phosphate
DHAPAT	Dihydroxyacetone phosphate acyl transferase
DM	Dense microsomes
DMEM	Dulbecco's modified eagle medium
DRM	Detergent resistant membrane
ENO	Enolase
Env	HIV envelope protein
ER	Endoplasmic reticulum
ESCRT	Endosomal sorting complex required for transport
ESI	Electro spray ionization
ETNK	Ethanolamine kinase
EV	Enrichment value
FADS	Fatty acid desaturase
FASN	Fatty acid synthase
FBS	Fetal bovine serum
FDPS	Farnesyl diphosphate synthase
Gag	HIV structural protein
GAPDH	Glyceraldehyde-3-phosphate dehydrogenase
GlcCer	Glucosyl/galactosyl ceramide
GM3	Ganglioside GM3
GP	Ebola virus glycoprotein
GSL	Glycosphingolipids
HA	Hemagglutinin
HCV	Hepatitis C virus
HIV	Human immunodeficiency virus
hpi	Hours post infection
HPLC	High performance liquid chromatography
HRP	Horse radish peroxidase

HSD17B4	Hydroxysteroid (17-beta) dehydrogenase 4
ICC	Immunocytochemistry
KDSR	3-ketodihydrosphingosine reductase
KO	Knockout
lo	Liquid-ordered
LPC	Lysophosphatidylcholine
M1	Matrix protein 1
M2	Matrix protein2
MAD	Median absolute deviation
MDCK	Madine Darby canine kidney cells
MEF	Mouse embryonic fibroblast
MLV	Murine leukemia virus
MLYCD	Malonyl-CoA decarboxylase
MOI	Multiplicity of infection
MRM	Multiple reaction monitoring
mRNA	Messenger RNA
MS	Mass spectrometry
MV	Microvesicles
MVB	Multivesicular bodies
NA	Neuraminidase
NAGA	N-acetylgalactosaminidase alpha
NEU	Sialidase
NLS	Nuclear localization signal
NP	Nucleocapsid protein
NPC	Nuclear pore complex
NS1	Non-structural protein 1
NS2	Non-structural protein 2
PA	Phosphatidic acid
PBS	Phosphate buffered saline
aPC	Phosphatidylcholine
ePC	Ether PC
PDMP	d,l-threo-1-phenyl-2-decanoylamino-3-morpholino-1-propanol
aPE	Phosphatidylethanolamine
ePE	Ether PE
PG	Phosphatidylglycerol
PGK	Phosphoglycerate kinase
PI	Phosphatidylinositol
PI4KIIIα	Phosphatidylinositol-4 kinase
PKM2	Pyruvate kinase M2
PPAR	Peroxisome proliferator-activated receptor
PS	Phosphatidylserine
PTDSS	PS synthase
PTS	Peroxisomal targeting sequence
QTOF	Quadrupole time of flight
RIPA	Radio immunoprecipitation assay

RLR	RIG-I-like receptor
RNA	Ribonucleic acid
RNP	Ribonucleoprotein
RT-qPCR	Reverse transcription quantitative polymerase chain reaction
S1P	Sphingosine-1-phosphate
SAMe	S-adenosylmethionine
SCD	Stearoyl-CoA desaturase
SDR	Short chain dehydrogenase/reductase domain
SEM	Scanning electron microscopy
Serinc	Serine incorporator
SFV	Semliki forest virus
SM	Sphingomyelin
SMS	Sphingomyelin synthase
SPL	S1P lyase
SREBP	Sterol-response element-binding protein
TAG	Triacylglycerol
TBST	Tris-buffered saline Tween
TLC	Thin layer chromatography
TPCK	L-(tosylamido-2-phenyl) ethyl chloromethyl ketone (TPCK)
VLDL	Very low density lipoprotein
VLP	Virus like particle
vRNA	Viral RNA
VSV	Vesicular stomatitis virus
VSV-G	VSV G protein
WT	Wild type

List of Publications

Original research articles

MSc Thesis:

Decision tree algorithms predict the diagnosis and outcome of dengue fever in the early phase of illness. **Tanner L**, Schreiber M, Low JG, Ong A, Tolfvenstam T, Lai YL, Ng LC, Leo YS, Thi Puong L, Vasudevan SG, Simmons CP, Hibberd ML, Ooi EE. *PLoS Negl Trop Dis. 2008 Mar 12;2(3):e196.*

Genomic epidemiology of a dengue virus epidemic in urban Singapore. Schreiber MJ, Holmes EC, Ong SH, Soh HS, Liu W, **Tanner L**, Aw PP, Tan HC, Ng LC, Leo YS, Low JG, Ong A, Ooi EE, Vasudevan SG, Hibberd ML. *J Virol. 2009 May;83(9):4163-73. Epub 2009 Feb 11*

PhD Thesis:

The stem region of premembrane protein plays an important role in the virus surface protein rearrangement during dengue maturation. Zhang Q, Hunke C, Yau YH, Seow V, Lee S, **Tanner LB**, Guan XL, Wenk MR, Fibriansah G, Chew PL, Kukkaro P, Biukovic G, Shi PY, Shochat SG, Grüber G, Lok SM. *J Biol Chem. 2012 Oct 3.*

PtdIns4P synthesis by PI4KIIIα at the plasma membrane and its impact on plasma membrane identity. Nakatsu F, Baskin JM, Chung J, **Tanner LB**, Shui G, Lee SY, Pirruccello M, Hao M, Ingolia NT, Wenk MR, De Camilli P. *J Cell Biol. 2012 Dec 10;199(6):1003-16.*

A Mechanistic Paradigm for Broad-Spectrum Antivirals that Target Virus-Cell Fusion. Frederic Vigant, Jihye Lee, Axel Hollmann, **Lukas B. Tanner**, Zeynep Akyol Ataman, Tatyana Yun, Guanghou Shui, Hector Aguilar-Carreno, Dong Zhang, David Meriwether, Gleyder Roman-Sosa, Lindsey R. Robinson, Terry L. Juelich, Hubert Buczkowski, Sunwen Chou, Miguel A.R.B. Castanho, Mike C. Wolf, Jennifer K. Smith, Ashley Banyard, Margaret Kielian, Srinivasa Reddy, Markus R. Wenk, Matthias Selke, Nuno C. Santos, Alexander N. Freiberg, Michael E. Jung, Benhur Lee. *Nat Chem Biol. Submitted.*

Lipidomics identifies a requirement of choline lipid metabolism for influenza virus replication. **Lukas B. Tanner**, Charmaine Chng and Markus R Wenk. *Manuscript in preparation.*

Review and opinion articles

PhD Thesis:

Implications for lipids during replication of enveloped viruses. Chan RB, **Tanner L**, Wenk MR. *Chem Phys Lipids. 2010 Jun;163(6):449-59. Epub 2010 Mar 15. Review.*

The position of sialic acid attachment in gangliosides dictates virus entry and trafficking. Madhu Sudhan Ravindran*, **Lukas B. Tanner*** and Markus R Wenk. *Traffic. In revision. (*Co-first authors).*

The ceramide and cholesterol composition as a determinant for vesicular trafficking. **Lukas B. Tanner** & Markus R Wenk. *Manuscript in preparation.*

Lipid metabolism during influenza virus infection. **Lukas B. Tanner** & Markus R Wenk. *Manuscript in preparation.*

1 Introduction

1.1 Overview

Influenza viruses are zoonotic pathogens circulating in many animal hosts including humans, birds, horses, dogs and pigs (Taubenberger and Morens, 2010). They are enveloped viruses with a segmented negative-strand RNA genome. They belong to the family of the *Orthomyxoviridae* consisting of the three virus types A, B and C, which differ in their host range and pathogenicity (Cox and Subbarao, 2000). Influenza A viruses, being the most common and virulent pathogens among the three influenza virus types, can be further divided into subtypes by the antigenic and genetic nature of their surface glycoproteins hemagglutinin (HA) and neuraminidase (NA). The high degree of antigenic variation in HA and NA is caused by two important mechanisms known as antigenic drift and antigenic shift. Antigenic drift is mediated by the high mutation rate of influenza A viruses through the accumulation of point mutations in HA and NA genes to escape neutralization by antibodies generated against previous strains (Cox and Subbarao, 2000). For example, it has recently been shown that positive Darwinian selection acts on antigenic sites in HA (Chen and Holmes, 2006; Fitch et al., 1997; Ina and Gojobori, 1994). Antigenic shift refers to the transmission of an animal or avian virus from an animal reservoir to humans or to the reassortment of the HA and NA gene segments between animal and human influenza A viruses caused by coinfection of the same host cell (Cox and Subbarao, 2000). Genetic reassortment has been commonly implicated in host switch events (Garten et al., 2009; Scholtissek et al., 1978; Taubenberger and Kash, 2010) and shown to participate in influenza A virus evolution (Dugan et al., 2008; Holmes et al., 2005). So far, viruses bearing all known 16 HA (H) and 9 NA (N) subtypes were

exclusively isolated from avian hosts, but only viruses of the H1N1, H2N3 and H3N2 subtypes have been associated with causing the febrile respiratory human disease, influenza, which is commonly referred to as the flu (Cox and Subbarao, 2000; Taubenberger and Morens, 2010).

Every year, seasonal influenza virus epidemics result in approximately three to five million cases of severe illness and in 250,000 to 500,000 deaths worldwide. While most of deaths occur among children below the age of two and adults above the age of 65 due to influenza and pneumonia (WHO Fact sheet N°211, April 2009), higher mortality rates can also be observed in patients predisposed to cardiopulmonary and other chronic diseases (Cox and Subbarao, 2000). However, pandemic influenza A virus strains with novel antigenic subtypes can occasionally emerge resulting in global outbreaks affecting up to 50% of the population with a 20-fold elevated risk for younger adults (Taubenberger and Kash, 2010). Hitherto, 14 influenza A virus pandemics have been reported over the last 500 years with the most recent outbreak in 2009 (Taubenberger and Kash, 2010; Taubenberger and Morens, 2010). The 2009 influenza virus pandemic was referred to as the “swine flu” since it was caused by a novel H1N1 virus derived from two unrelated swine H1N1 viruses (Garten et al., 2009). It spread over 214 countries resulting in >622,482 lab-confirmed cases and 18,449 lab-confirmed deaths (Cheng et al., 2012). The first H1N1 virus pandemic known as the “Spanish flu” occurred in 1918 and was the worst influenza virus pandemic ever recorded in history which killed over 50 million people worldwide (Johnson and Mueller, 2002). Isolation and reconstruction of the virus genome from victims’ tissues revealed an avian origin of the causative H1N1 influenza virus strain (Taubenberger et al., 2005) and its unique pathogenicity when compared to other

human influenza viruses (Tumpey et al., 2005). It is intriguing that direct descendants of the 1918 virus are still circulating in human populations and continuously contribute to the emergence of new viruses to cause epidemics and pandemics (Taubenberger and Kash, 2010). For instance, the 2009 H1N1 swine flu strain was a fourth generation descendant of the 1918 virus (Morens et al., 2009) illustrating the long-term epidemiologic success of influenza viruses.

Despite recent advances in the understanding of influenza virus outbreaks, prediction of future influenza virus pandemics is still a difficult challenge. Not only does it require global surveillance of genetic diversity of influenza viruses from their natural reservoirs, but also new advances in basic research are needed to obtain a combined picture of influenza virus host adaption and pathogenicity. Considering the recent surge in drug resistance (Le et al., 2005; Medina and Garcia-Sastre, 2011), advances in basic research are additionally instrumental with regard to the development of novel antiviral strategies to counteract future influenza virus pandemics. Currently, there are four drugs in use which directly target influenza viruses but they only constitute two families. Amantadine and Rimantadine belong to the first family of drugs inhibiting matrix protein 2 (M2), whereas Zanamivir and Oseltamivir are members of the second family of compounds targeting influenza virus NA. This limited number of antiviral drugs and targets against influenza virus demonstrates the need for broad-spectrum therapeutic approaches targeting viral and host factors in different life cycle stages to minimize the development of resistance. Especially, identification and understanding of host factors and their complex interaction with influenza virus are crucial in the search for host determinants in influenza virus pathogenesis.

1. Introduction

Contribution of host proteins to the influenza virus life cycle have been extensively addressed in recent years, yet, the role of host cell metabolites, such as lipids has been neglected so far. This is surprising since infectious influenza virions not only consist of a host derived lipid bilayer but also depend on host cell lipid metabolism for replication, budding and assembly (Hidari et al., 2006; Munger et al., 2008; Nayak et al., 2009; Nayak et al., 2004; Rossman et al., 2010; Rossman and Lamb, 2011; Takahashi et al., 2008). Despite recent advances in dissecting the lipid inventory of purified influenza virus particles (Blom et al., 2001; Gerl et al., 2012; Polozov et al., 2008; Scheiffele et al., 1999; van Meer and Simons, 1982), there is still a substantial lack in our understanding of how influenza virus regulates lipid metabolism to ensure biogenesis of functional viral envelopes with a particular lipid composition, and whether lipids are mediators of virus pathogenicity. Furthermore, host derived virus envelopes are inert biological membranes and represent attractive targets for antiviral therapy, minimizing the development of drug resistance (Vigant et al, *submitted*).

This chapter will first present a brief overview of recent literature about the structure and life cycle of influenza A viruses, followed by a second part which will specifically discuss the importance of host cell metabolites in the influenza virus life cycle. We will highlight emerging roles of cellular lipids within the context of host-virus interactions and will finally derive novel hypotheses that could have a potential share in advancing our current knowledge of lipid involvement during influenza virus infections.

1.2 The biology of influenza virus

1.2.1 The structure of influenza virus

Influenza viruses are negative-sense single stranded RNA viruses encoding 11 virus proteins, eight of which are expressed in infectious, enveloped virions (Rossman and Lamb, 2011). They are pleomorphic in structure and appear either as spherical with a diameter of 100nm or as filamentous particles, 100nm in diameter but more than 20µm in length. They are similar with regard to their genome and protein composition (Roberts et al., 1998; Rossman and Lamb, 2011), but the functional difference between filamentous and spherical influenza virus particles still remains uncertain. Nevertheless, it is thought that filamentous particles are mainly produced by *in vivo* infections (Chu et al., 1949; Kilbourne and Murphy, 1960) whereas spherical particles are the product of an adaptation to virus growth in eggs (Choppin et al., 1960).

The RNA genome of influenza viruses is divided into eight segments which are numbered in order of decreasing length (Figure 1-1A). The eight segments are separately packaged into ribonucleoprotein (RNP) particles composed of the RNA polymerase complex proteins PB1 (segment 2), PB2 (segment 1) and PA (segment 3), and the nucleocapsid protein NP (segment 5) which mediates packing and binding of the RNA genome. The matrix protein M1 (segment 7) bridges the RNP core to the host derived virus envelope and confers structure to influenza virus particles. Influenza virions express the two surface spike glycoproteins HA (segment 4) and NA (segment 6) as well as matrix protein M2 (segment 7) on their surface (Figure 1-1A).

While HA mediates receptor binding and fusion during the virus entry process into host cells, NA is mainly implicated at late stages of the virus life cycle, responsible for the release of virus progenies by the enzymatic cleavage of viral receptors on the host cell surface. The third integral membrane protein M2 is a multifunctional, proton selective ion channel which mediates virus assembly and budding, as well as virus entry into host cells (Rossman and Lamb, 2011). The proteins encoded on segment 8 are non-structural proteins NS1 and NEP/NS2 which are highly expressed in infected cells and mediate influenza virus replication, but they do not get incorporated into infectious influenza virions.

Besides viral proteins, additional evidence suggests a significant incorporation of (36 unique) host proteins into infectious influenza virions (Shaw et al., 2008). For instance, incorporation of annexin II into influenza virions is thought to mediate the proteolytic cleavage of HA through binding and activation of plasminogen into plasmin (LeBouder et al., 2008). Yet, the exact function of identified host proteins in influenza virus particles is not well understood.

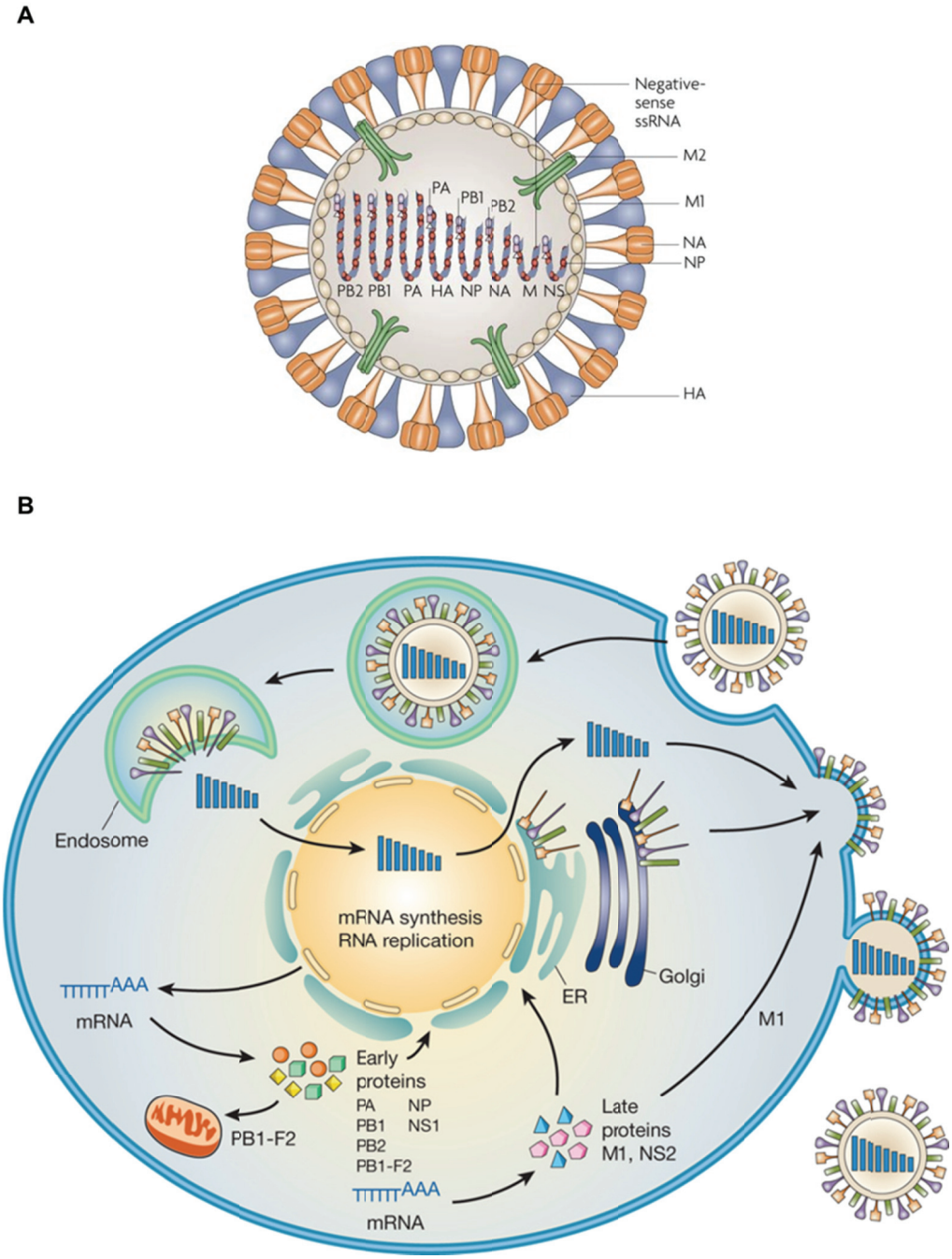

Figure 1-1: The structure and life cycle of influenza virus. (A) Influenza A virus particles express M2 and the two glycoproteins HA and NA on their surface. M1 is beneath the virus envelope and binds to the eight segments of vRNA packaged into RNPs. RNPs consist of PB1, PB2, PA and NP. Taken from (Nelson and Holmes, 2007). **(B)** The life cycle of influenza virus particles is initiated by the binding of HA to sialic acid containing receptors, leading to endocytosis of the virions. *pH* dependent fusion in late endosomal compartments releases the viral genome for replication and transcription in the nucleus. Finally, new virus progenies are assembled and bud at the plasma membrane. Taken from (Neumann et al., 2009).

1.2.2 The life cycle of influenza virus

1.2.2.1 Virus attachment and entry

The lifecycle of influenza virus is initiated by the binding of influenza virus particles to the host cell surface (Figure 1-1B). This is mediated by HA recognizing N-acetylneuraminic (sialic) acid residues of glycoproteins- and –lipids on the host cell surface (Chandrasekaran et al., 2008; Chu and Whittaker, 2004; de Vries et al., 2012; Kuiken et al., 2006; Maines et al., 2006; Russell et al., 2006; Shinya et al., 2006; Skehel and Wiley, 2000; van Riel et al., 2006). Sialic acids are acidic monosaccharides containing nine carbons and are usually attached to terminal galactose residues. The second carbon of sialic acid can either bind to carbon 3 or carbon 6 of galactose, resulting in α2-3 and α2-6 linkages, respectively. The various subtypes of HA have differential specificities towards the two different sialic acid linkages and human viruses preferentially bind to α2-6 linkages which are predominantly found in the upper respiratory tract (Bouvier and Palese, 2008). On the other hand, avian viruses have a greater specificity to α2-3 linkages which are widely expressed in the guts and respiratory tracts of bird species. The complex affinity of influenza A virus towards (α2-6)- and (α2-3)-linked sialic acids is believed to be a key mediator of airborne virus transmission (Bouvier and Palese, 2008; Olofsson et al., 2005). The ability of hemagglutinin to switch its preference from (α2-3)-linked sialic acids to (α2-6)-linked sialic acids is closely associated with the transmission from birds to sustained human to human transmissions and with its potential to cause widespread pandemic outbreaks (Bouvier and Palese, 2008; Herfst et al., 2012; Imai

et al., 2012; Olofsson et al., 2005). Recently, it has been shown that mutations in HA of avian H5N1 virus strains were able to confer airborne transmissibility between mammals due to adaption from avian α2-3 to the human α2-6 linkages (Herfst et al., 2012; Imai et al., 2012). In addition, a recent study showed that hemagglutinin specificity is not exclusively determined by sialic acid linkage but also by long sialylated glycans with characteristic structural topologies (Chandrasekaran et al., 2008).

Binding of influenza virus HA to host cell surface receptors initiates a signalling cascade, leading to endocytosis of the bound virus particle (Figure 1-1B). The exact mechanism is still obscure but a recent study showed that influenza virus binding results in clustering of plasma membrane lipids to establish "lipid-raft" based platforms for receptor tyrosine kinase signalling. This, in turn, mediates *de novo* formation of clathrin coated pits and enhances influenza virus uptake (Eierhoff et al., 2010; Rossman and Lamb, 2011; Rust et al., 2004). Moreover, influenza virus particles are also able to functionally enter host cells via a clathrin and caveolin independent entry pathway which has been identified as macropinocytosis (de Vries et al., 2011; Lakadamyali et al., 2004; Rust et al., 2004; Sieczkarski and Whittaker, 2002). The endocytosed influenza virus particle is transported to late endosomes where a low *pH* triggered conformational change of HA ($pH \approx 5$) induces membrane fusion (Figure 1-1B). In parallel, the low *pH* environment also activates the influenza virus ion channel M2 leading to the conduction of protons into the viral core. This influx of protons causes dissociation of RNPs from M1 proteins and subsequently releases the dissociated RNPs into the cytoplasm for transport to the nucleus where

virus replication takes place (Bouvier and Palese, 2008; Luo, 2012; Rossman and Lamb, 2011).

1.2.2.2 Virus replication

Transport of released RNPs into the nucleus via the nuclear pore complex (NPC) is mediated by NP carrying three nuclear localization signals (NLSs) which facilitate interaction and recruitment of various host factors (Cros and Palese, 2003). Once in the nucleus, viral RNA (vRNA) is transcribed into two positive sense RNA species by the vRNA dependent RNA polymerase: one serves as the capped, polyadenylated messenger RNA (mRNA) for host cell translation of viral proteins, and the other one is a complementary RNA (cRNA) which is used as a template to transcribe more copies of the negative-sense genomic vRNA (Figure 1-1B). Newly synthesized vRNAs are packaged into RNPs and their export from the nucleus into the cytoplasm is regulated by interactions of viral proteins NEP/NS2 und M1 with the nuclear pore complex (Bouvier and Palese, 2008; Nagata et al., 2008).

Virus replication within a host cell is a complex interplay of host and viral factors which involves hijacking of favourable cellular pathways but, at the same time, requires interference and inhibition of antiviral responses. Non-structural protein 1 (NS1), which is highly expressed in infected cells but not incorporated into infectious influenza virions, is considered to be the major viral factor regulating the balance between cellular pro- and antiviral activities. It is a multifunctional protein localized to the nucleus and cytoplasm consisting of a N-terminal RNA binding domain and a

C-terminal "effector" domain which mediates both, binding to host proteins and stabilizing the RNA binding domain. NS1 not only antagonizes interferon-α/ß mediated antiviral responses but also executes a plethora of other important functions to ensure proper virus replication including (1) regulation of vRNA synthesis, (2) mRNA splicing and translation, (3) virus particle morphogenesis, (4) suppression of apoptosis through activation of PI3K/Akt signalling and (5) contribution to virus pathogenesis (Hale et al., 2008).

1.2.2.3 Virus assembly and budding

After efficient viral protein synthesis and genome replication, viral constituents are individually transported to the assembly and budding sites at the apical plasma membrane. While it is well understood that HA, NA and M2 harness classical cellular exocytic transport pathways which are involved in polarized trafficking (Nayak et al., 2004), it is still unclear how M1 and vRNPs get transported to budding sites. M1 does not possess any determinants for polarized trafficking but has the capability to bind lipids, vRNPs as well as the tails of HA and NA. Thus, it is proposed that the apical transport of M1 involves its binding to the piggy-back of HA and NA (Nayak et al., 2009). Polarized trafficking of vRNPs to the budding site has been recently shown to be dependent on Rab11 positive recycling endosomes (Bruce et al., 2010; Eisfeld et al., 2011; Momose et al., 2011).

There is still no exact model of how the transported viral constituents get assembled into a virus particle and finally induce virus budding at the plasma membrane. One of

the major difficulties to derive a common model for influenza virus morphogenesis is found in the differences between virus like particle (VLP) budding and virus budding (Rossman and Lamb, 2011). While separate expression of influenza virus proteins HA, NA, M2 and membrane targeted M1 all have the capability to induce VLP budding, the driving force behind the spatial and temporal orchestration of these individual events into a combined functional framework for influenza virus budding is more complex. Unlike budding of retroviruses, such as human immunodeficiency virus (HIV), budding of influenza virus is not dependent on a functional endosomal sorting complex required for transport (ESCRT) (Bruce et al., 2009; Chen et al., 2007; Rossman et al., 2010), and involvement of other host proteins is not well understood. Rossman and Lamb (Rossman and Lamb, 2011) recently proposed a model whereby clustering of HA and NA initiates bud formation, followed by recruitment of M1 via binding to the cytoplasmic tails of HA and NA. M1 proteins subsequently serve as docking sites for vRNPs. Elongation of the budding virions is induced by polymerization of M1 proteins, leading to the polarized localization of vRNPs. M2 is later recruited to the periphery of budding sites through its interaction with M1. Insertion of the amphipathic helix of M2 at the lipid phase boundary leads to changes in membrane curvature and membrane scission of the budding virions. Finally, NA mediates the release of surface bound virions by cleaving off sialic acids from the host cell surface.

Yet controversial, “lipid rafts” are proposed to be the plasma membrane budding sites of influenza virus. The synergistic and lipid-driven packaging of cholesterol, sphingolipids and saturated glycerophospholipids into plasma membrane microdomains accounts for the unique biophysical characteristics of this liquid-

ordered (lo) state (Chan et al., 2010; Hanzal-Bayer and Hancock, 2007; Simons and Vaz, 2004). Evidence supporting involvement of "lipid rafts" in the influenza virus life cycle is mainly based on the intrinsic association of HA and NA with "lipid rafts" and/or on the effect of cholesterol depletion on virus production (Barman and Nayak, 2000; Chen et al., 2005; Leser and Lamb, 2005; Takeda et al., 2003). However, interpretation of such results might be exacerbated by two main problems: firstly, choosing an appropriate "lipid raft" marker is crucial and controversial (Briggs et al., 2003). Definition and extraction of "lipid rafts" is based on the conception that pre-existing lo-domains form insoluble detergent resistant membranes (DRM) when treated with low concentrations of a non-ionic detergent such as Triton X-100. Neither presence nor absence of proteins in DRM is sufficient to find "lipid raft" markers since it is clear that detergent treatment can alter lipid raft composition and can even induce phase separation (Hanzal-Bayer and Hancock, 2007). Secondly, cholesterol depletion from the plasma membrane by cyclodextrins is commonly used to disrupt "lipid rafts" and to proof "lipid raft" mediated processes. This is definitely insufficient because a recent study showed that cyclodextrin treatment has additional, cholesterol-independent effects on membrane protein mobility (Shvartsman et al., 2006). For example, HA contains three palmitoylated cysteine residues in the transmembrane domain which are responsible for its targeting to "lipid raft" domains (Chen et al., 2005; Scheiffele et al., 1997; Takeda et al., 2003). On the contrary, it is intriguing that HA dynamics at the plasma membrane do not follow "lipid raft" fluctuations (Hess et al., 2007; Nikolaus et al., 2010) and that HA does not co-localize with another "lipid raft" associated virus protein, HIV Gag (Khurana et al., 2007). Furthermore, influenza virus M2 proteins are excluded from such "raft" domains despite their requirement for influenza virus budding (Rossman and Lamb, 2011). M2

mediated changes in membrane curvature and membrane scission were closely associated with cholesterol levels whereby a high cholesterol concentration was inhibitory due to higher membrane rigidity (Rossman et al., 2010). In line with this, cholesterol depletion from the plasma membrane increased influenza virus but decreased budding of another "lipid raft" budding virus, HIV (Barman and Nayak, 2007; Ono and Freed, 2001; Pickl et al., 2001). Similarly, the Ebola virus glycoprotein (GP) , also a "lipid raft" associated protein, and HIV envelope protein (Env) did not co-localize with each other on the plasma membrane and HIV Gag pseudotyped VLPs exclusively carried either only GP or Env despite their expression in the same producer cell (Leung et al., 2008). These findings together suggest heterogeneous lipid and protein compositions of plasma membrane microdomains, and such heterogeneities were recently demonstrated in living cells (Itano et al., 2011; Neumann et al., 2010).

Induction of plasma membrane microdomains most probably is a general feature of enveloped virus budding and categorization of enveloped viruses into "lipid raft"-dependent or -independent is too simplified. Enveloped viruses, including vesicular stomatitis virus (VSV) and Semliki forest virus (SFV) which are "lipid raft" independent, generally show high levels of cholesterol (Blom et al., 2001; Brugger et al., 2006; Chan et al., 2008; Gerl et al., 2012; Kalvodova et al., 2009; Polozov et al., 2008; Scheiffele et al., 1999; van Meer and Simons, 1982). The high content of cholesterol possibly reflects its importance for structural integrity and organization of membranes as discussed below. Furthermore, several virus envelope proteins have been found to localize to or to induce "lipid raft" domains including the envelope protein of VSV (VSV-G) (Barman and Nayak, 2000; Chen et al., 2005; Harder et al.,

1998; Leser and Lamb, 2005; Luan and Glaser, 1994; Rousso et al., 2000; Takeda et al., 2003). Considering such compelling evidence, it is more likely to envision that arrival of virus surface proteins at the plasma membrane induces protein-lipid interactions generating unique plasma membrane domains required for virus budding (Nikolaus et al., 2010), rather than virus proteins are transported to pre-existing plasma membrane microdomains such as "lipid rafts". This would also explain observed differences in the lipid and protein composition of virus particles and would be in line with the recent discovery of specific lipid binding domains in transmembrane proteins (Contreras et al., 2012).

Comparing the proposed model for influenza virus budding (Rossman and Lamb, 2011) to a recent study showing that surface glycoproteins are actively recruited to virus assembly sites during pseudotyping of retrovirus particles (Jorgenson et al., 2009), there are two possible scenarios determining the unique protein and lipid compositions of enveloped viruses (Lorizate and Krausslich, 2011): The first mechanism is a matrix protein driven mechanism (pushing force) implicated in the budding of retroviruses. Surface glycoproteins transported to the plasma membrane induce aggregation of lo-like lipids and proteins in their proximity. Only concomitant expression of the matrix protein, Gag, leads to clustering of surface glycoproteins and induction of assembly sites for retrovirus particles. The second mechanism, observed during budding of influenza viruses, is a surface glycoprotein driven process (pulling force). The surface glycoproteins HA and NA are already expressed as clusters on the plasma membrane and are able to initiate bud formation on their own. As a result, the lipid composition of influenza virus particles is mainly mediated by HA and NA and slightly modified by the activity of M2 to induce membrane scission and bud closure.

Interestingly, influenza viruses carrying mutations in the cytoplasmic tails of HA and NA have been shown to exhibit distinct lipid compositions when compared to wild type viruses (Zhang et al., 2000).

1.2.3 The role of lipids in the influenza virus life cylce

The above described involvement of plasma membrane microdomains in influenza virus morphogenesis and their subsequent incorporation into virus envelopes highlights the importance of lipids in the influenza virus life cycle. In this respect, lipids are an important bridge of virus exit to virus entry, since induction of lipid and protein clusters at the plasma membrane are not solely important for virus budding but, in turn, the acquired lipid inventory is also essential for structural integrity, entry and fusion of infectious influenza virions. This suggests that enveloped viruses acquire their lipid inventory in an organized fashion to support subsequent steps in the virus life cycle. Hepatitis C virus (HCV) is a prominent virus example linking virus exit and entry for life cycle progression. HCV buds at lipid droplet associated ER membranes (Miyanari et al., 2007) and it has been shown that infectious HCV particles commonly associate with apolipoproteins and only Very Low Density Lipoprotein (VLDL)-HCV particles are successfully released from infected cells (Gastaminza et al., 2008; Gastaminza et al., 2006; Merz et al., 2011). In this way, HCV actually mimics the molecular identity of lipoproteins to hijack lipoprotein transport mechanism for entry into host cells (Agnello et al., 1999; Andre et al., 2002; Molina et al., 2007).

1.2.3.1 Structure of lipids

Lipids have been once neglected as structural and storage entities, and only recently, with the advance in technology, our understanding of functional roles of lipids is emerging (Guan et al., 2009; van Meer et al., 2008; Wenk, 2005). Lipids are structurally and chemically diverse molecules which either act as aggregates in subcellular membranes (e.g. plasma membrane microdomains and lipid droplets) but also as single entities (e.g. inflammatory mediators such as platelet activating factor and eicosanoids) (Figure 1-2A). The various combinations of fatty acids with functional head groups give rise to an estimated 10,000 to 100,000 different lipid species (Wenk, 2010). Mammalian lipids can be further classified into the five major classes known as fatty acyls, glycerolipids, glycerophospholipids, sterol lipids and sphingolipids (Figure 1-2A). Biological membranes predominantly consist of glycerophospholipids, sterol lipids (cholesterol) and sphingolipids and their distribution in cellular membranes is highly organized (Figure 1-2A) (van Meer et al., 2008). This compartmentalization is essential for proper functionality of biological systems and represents an attractive target for pathogens which is underlined by increasing evidence of lipid involvement in host-pathogen interactions (Wenk, 2006).

Glycerophospholipids usually consist of a glycerol backbone made of two fatty acyl moieties and a functional head group giving rise to phosphatidylcholine (PC), phosphatidylethanolamine (PE), phosphatidylserine (PS), phosphatidylinositol (PI), phosphatidic acid (PA) and phosphatidylglycerol (PG) (Figure 1-2A). In some cases, the fatty acid moieties in the glycerol backbone can also be attached by an ether

linkage rather than the usual ester linkage (Figure 1-2B). This gives rise to ether lipids which are mainly represented by two classes: The plasmanyl species and the plasmenyl (known as plasmalogens) species which have one of their fatty acids (usually at the sn-1 position) attached by an ether- or by a vinyl ether linkage respectively (Figure 1-2B). While the majority of ether lipids exist as PC and PE lipids, ether linkages in other glycerophospholipid classes have also been reported (Ivanova et al., 2010). With respect to this study, we will refer to ether PC (ePC) and PE (ePE) lipids as the combination of plasmanyl and plasmenyl structures.

Sphingolipids usually consist of a ceramide backbone attached to highly diverse sugar head groups. For example, gangliosides are characterised by sialylated sugar head groups (Figure 1-2A). The head group can also be represented by choline giving rise to sphingomyelin (SM). The ceramide backbone can either exist as dihydroceramide whereby a sphinganine (saturated sphingoid base) is attached to a fatty acid or as ceramide consisting of a sphingosine (unsaturated sphingoid base) attached to a fatty acid (Figure 1-2C). Recent evidence suggests a vast diversity of ceramide backbones based on the variations and modifications of sphingoid bases attached to distinct fatty acids (Merrill, 2011). With respect to this study, we will mainly focus on (dihydro)ceramide, glucosyl/galactosyl ceramide (GlcCer), ganglioside GM3 and SM species.

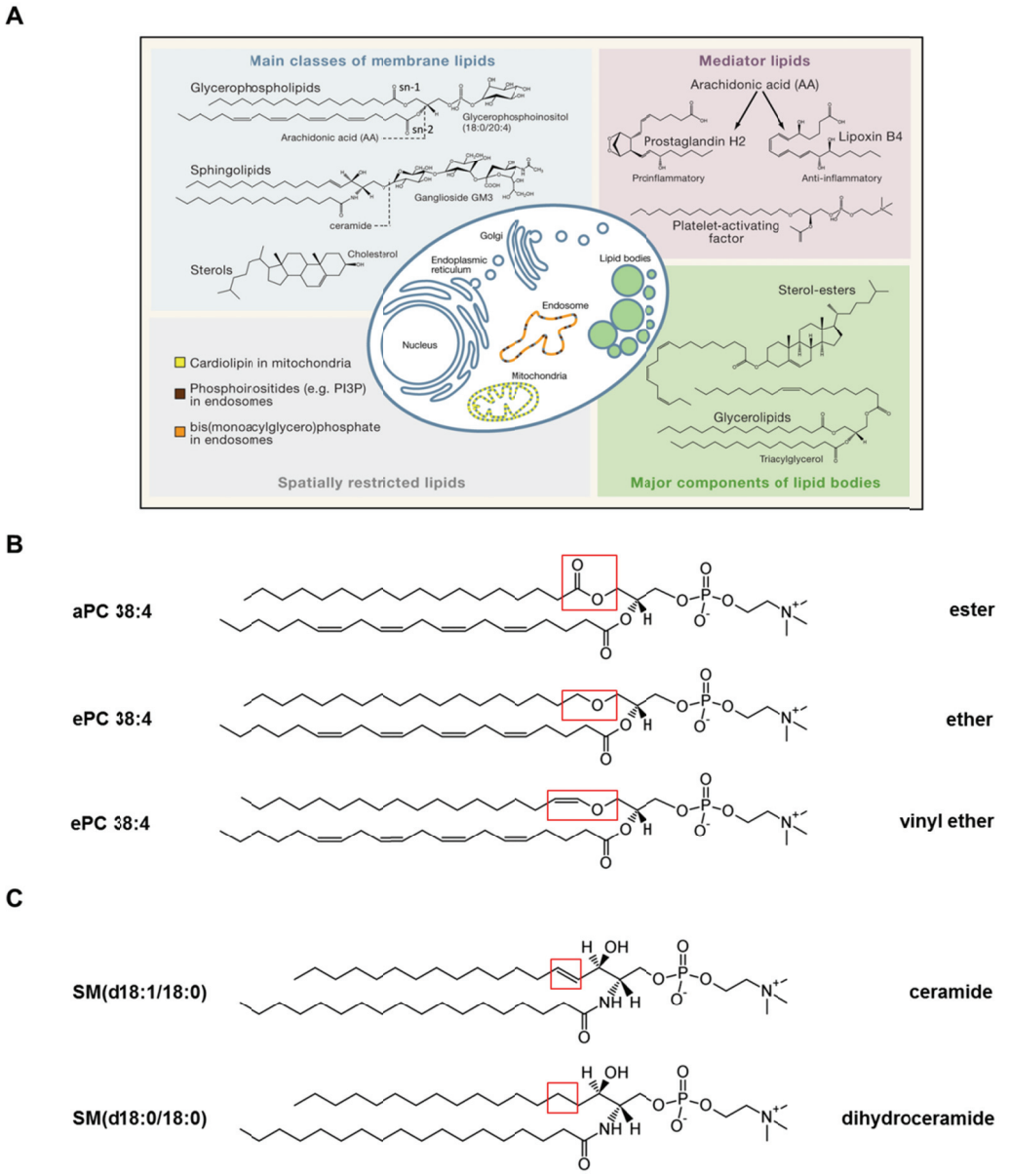

Figure 1-2: Lipid structure and function in mammalian cells. (A) Lipids are heterogeneously distributed in mammalian cells and their compartmentalization is essential for functionality. Lipids can be categorized into five major classes: fatty acyls (mediator lipids), glycerolipids (major components of lipid bodies or storage lipids), glycerophospholipids, sterol lipids and sphingolipids (main classes of membrane lipids). Taken from (Wenk, 2010). **(B)** The two fatty acids in glycerophospholipids are usually attached by an ester linkage. In some cases, fatty acids can be attached by an ether or vinyl ether linkage (mainly at the sn-1 position). Three representative structures of PC lipids are shown. Red box indicates the differences in fatty acid linkage. **(C)** The backbone of sphingolipids is highly diverse. For example, the sphingoid base in the ceramide backbone can be either saturated (sphinganine) or unsaturated (sphingosine) which gives rise to dihydroceramide and ceramide, respectively. Red box indicates the differences in the sphingoid base.

1.2.3.2 Role of lipids for influenza virus particle structure

Influenza virions are generally enriched in cholesterol, PS, PE, SM, GlcCer and ceramide species (Blom et al., 2001; Gerl et al., 2012; Polozov et al., 2008; Scheiffele et al., 1999; van Meer and Simons, 1982) (Figure 1-3). The high enrichment of cholesterol is a general feature of enveloped viruses required for membrane fluidity and structural integrity, and depletion of cholesterol from influenza virus envelopes decreased infectivity (Barman and Nayak, 2007; Chan et al., 2008; Takeda et al., 2003). Influenza virus envelope lipids are usually found in a disordered state at physiological temperatures but at very low temperatures, they are able to form solid-phase and gel-phase states which confer higher stability to virus particles (Polozov et al., 2008). This temperature dependent phase transition can be explained by the interaction and competition of cholesterol with ceramide in biological membranes (Goni and Alonso, 2009; Megha and London, 2004; Yu et al., 2005). Ceramide enriched gel domains are usually solubilized in biological membranes with high cholesterol content at physiological temperatures, but they reorganize into gel domains at lower temperatures (Castro et al., 2009). Hence, the relatively higher enrichment of ceramide species found in influenza virus particles as compared to other enveloped viruses (Chan et al., 2008; Gerl et al., 2012; Kalvodova et al., 2009) could mediate the increased stability and transmission of influenza viruses at lower temperature (Lowen et al., 2007; Polozov et al., 2008). This supports the notion that the acquired lipid inventory is specifically tailored for the virus life cycle.

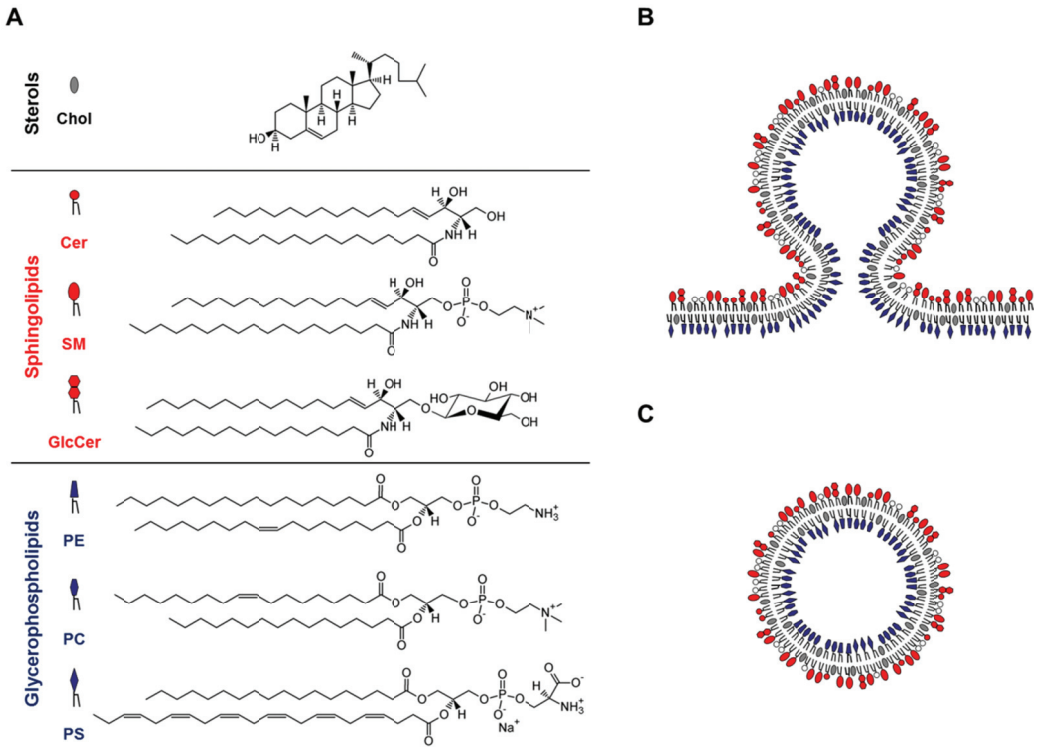

Figure 1-3: Major lipid classes of enveloped viruses. Adapted from (Chan et al., 2010). (A) Structure of major classes of lipids (cholesterol, ceramide, SM, GlcCer, PE, PC, PS) found in enveloped viruses and their asymmetric distribution in budding particles **(B)** and virions **(C)**.

Also, host lipids incorporated into virus envelopes are functionally important for virus entry and fusion. High levels of ether linked PE species which have also been observed in other enveloped viruses like HIV, SFV and VSV (Brugger et al., 2006; Chan et al., 2008; Kalvodova et al., 2009), have been associated with an important role during virus fusion due to their high fusogenicity (Glaser and Gross, 1994; Glaser et al., 2002). This is explained by the unique biophysical properties of PE lipids as they have the ability to intrinsically organize into a hexagonal phase which facilitates membrane curvature and membrane fusion (Chan et al., 2010; Glaser and Gross, 1994; Lohner, 1996).

Enrichment of PS species in influenza virus envelopes supports the reported involvement of annexin A5 as a secondary receptor during influenza virus entry (Chan et al., 2010; Huang et al., 1996) and reflects the incorporation of annexins into purified influenza virus particles (Shaw et al., 2008). Annexins are PS binding proteins which have been previously implicated in the entry of several enveloped viruses including influenza viruses by specifically mediating membrane fusion (Chan et al., 2010; Huang et al., 1996). Furthermore, the finding of macropinocytosis as an alternative entry pathway for influenza virus particles (de Vries et al., 2011) represents another possible role for PS during influenza virus entry. Vaccinia virus expresses PS on the outer layer of its envelope to mimic apoptotic material which commonly gets internalized by many cells using PS mediated macropinocytosis (Henson et al., 2001; Mercer and Helenius, 2008). Considering induction of apoptosis in influenza virus infected cells at later stages of infection (Gannage et al., 2009; Zhirnov and Klenk, 2007) and the associated externalization of PS from the cytoplasmic to the outer leaflet of the plasma membrane (Lee et al., 2012; Martin et al., 1995; Shiratsuchi et al., 2000), one could assume that PS species are possibly exposed on the surface of influenza virus particles. In line with this, it has been estimated that equal proportions of PS are found in the inner and outer surface of purified influenza virus membranes (Rothman et al., 1976).

The discussed lipid composition of influenza virus particles represents an extracellular stage but it is still an open question whether functionally relevant modifications occur during the virus entry process. Late endosomes harbour a variety of lipid degrading enzymes which have the potential to act on influenza virus envelopes. For example, acid sphingomyelinase has a *pH* optimum of around 5.5 (similarly to the *pH* required

for HA mediated fusion) and is highly active in late endosomes (Kolter and Sandhoff, 2010). It has been shown that phago-lysosomal fusion is dependent on ceramide generation by the activity of acid sphingomyelinase (Utermohlen et al., 2008; Utermohlen et al., 2003). In this respect, it would be interesting to see whether a similar mechanism is harnessed during influenza virus fusion in late endosomes. Ceramide, a conical lipid, induces negative curvature and facilitates formation of a fusion stalk which is discussed in further detail below (Chan et al., 2010; Chernomordik and Kozlov, 2003, 2008).

1.2.3.3 Role of lipids during influenza virus entry

Besides the importance of lipids incorporated into influenza virus envelopes, the functional role of host cell lipids is equally crucial during virus entry into host cells. Similar to sialylated glycoproteins, complex sialylated glycosphingolipids (GSL) expressed on the host cell plasma membrane can serve as functional receptors for influenza virus HA and mediate virus entry (Ablan et al., 2001; Chu and Whittaker, 2004; Gambaryan et al., 2004; Hidari et al., 2007; Kogure et al., 2006; Matrosovich et al., 2006b). The predominating occurrence of *O*-linked glycosylation in GSL but *N*-linked glycosylation in glycoproteins exposes some interesting differences with regard to their functionality. While macropinocytic entry of influenza virus was impaired into cells depleted of *N*-linked glycans, the classical endocytic pathway was not affected (de Vries et al., 2012). Conversely, influenza virus entry in the absence of *N*-linked glycans was more sensitive to NA inhibitors. These findings together suggest a specific involvement of NA in a GSL mediated endocytic route. One

possible explanation for a requirement of NA in a GSL mediated entry pathway comes from a recent literature mining study performed by us, revealing importance of internally sialylated GSL species in entry and trafficking of viruses fusing at late endosomes (Ravindran, Tanner & Wenk, *submitted*). Several *in vitro* studies showed that influenza virus preferentially binds to complex internally sialylated GSL species (Matrosovich et al., 2006b). However, specific binding of HA to internally sialylated GSL species in biological membranes is likely to be exacerbated, due to steric hindrance caused by the tight packaging of GSL in membranes (Hakomori, 2003). Therefore, cleavage of externally attached sialic acids from GSL by NA is required to facilitate binding of influenza virus HA to internally attached sialic acids of GSL and to mediate the successful entry of influenza viruses into host cells. Considering the high abundance of *O*-linked glycosylation in mucus and epithelial surfaces of airways (Fahy and Dickey, 2010), such an entry pathway might be relevant *in vivo* as reflected by the importance of NA to initiate influenza virus infection in human airway epithelium (Matrosovich et al., 2004). In contrary, a GSL mediated entry pathway is masked in laboratory conditions, due to the dominant role of *N*-linked glycosylated growth factor receptors promoting influenza virus entry *in vitro* (de Vries et al., 2011; Eierhoff et al., 2010). The rather supportive role of *O*-linked glycans during influenza virus entry *in vitro* is further backed by the insensitivity to NA inhibitors in the presence of *N*-linked glycans (de Vries et al., 2012) and by a three to four fold reduction of influenza virus infection into host cells lacking GSL (Matrosovich et al., 2006b).

Lipids are also mediators of subsequent influenza virus membrane fusion which has been extensively studied and reviewed (Chan et al., 2010; Chernomordik and Kozlov,

2003, 2008; Hamilton et al., 2012). Membrane lipid composition greatly influences fusion efficiency which is mainly due to spontaneous curvature of lipids, influenced by their individual geometries (Chan et al., 2010; Chernomordik and Kozlov, 2003, 2008). PA, cholesterol, ceramide, diacylglycerol (DAG) and PE are conical lipids having relatively small head groups in relation to their fatty acyl tails and promote negative spontaneous curvature. On the other hand, inverted-conical lipids having proportionally large head groups such as lysolipids induce positive spontaneous curvature (Chan et al., 2010; Chernomordik and Kozlov, 2003, 2008). Insertion of HA into the target membrane leads to positive curvature bringing the two membranes together (Fuhrmans and Marrink, 2012). Upon contact of the two membranes, formation of a fusion stalk is induced which is facilitated by conical lipids exhibiting negative spontaneous curvature. In line with that, influenza virus membrane fusion was inhibited by the inverted-conical lipid lysophasphatidylcholine (LPC) but promoted by conical lipids such as oleic acid and PE (Alford et al., 1994; Baljinnyam et al., 2002; Chernomordik et al., 1998; Chernomordik et al., 1997). In contrary, the subsequent opening of the fusion pore is mediated by inverted-conical shaped lipids due to their spontaneous positive curvature (Chernomordik and Kozlov, 2003). Finally, expansion of the fusion pore occurs and the viral genome is released into the host cell cytoplasm. It has been shown, that this final step is mediated by cholesterol but inhibited by sphingolipids (Biswas et al., 2008; Nussbaum et al., 1992; Razinkov and Cohen, 2000).

1.2.3.4 Role of lipids during intracellular stages of influenza virus replication

Loss of membrane mass by virus budding has to be compensated by biogenesis of new membranes. Therefore, enveloped viruses need to interfere with host cell metabolism redirecting metabolic intermediates into lipid biosynthesis (Chan et al., 2010). Several enveloped viruses have been shown to upregulate flux through the central carbon metabolism, including glycolysis, and its efflux to fatty acid and lipid biosynthesis (Liu et al., 2011; Munger et al., 2008; Perera et al., 2012; Roe et al., 2011). Only a few studies addressed the impact of influenza virus on host cell metabolism. A very early study reported increased glucose breakdown in influenza virus infected chick embryo cells (Klemperer, 1961) which is now backed with more recent evidence clearly associating influenza virus with host cell glycolysis: (1) purified influenza virus particles were highly enriched in glycolytic enzymes (Shaw et al., 2008), (2) expression of glycolytic enzymes was upregulated in influenza virus infected cells (Brown et al., 2010; Coombs et al., 2010; Dove et al., 2012; Kroeker et al., 2012) and their knockdown impaired influenza virus infection (Brass et al., 2009; Karlas et al., 2010; Shapira et al., 2009), and (3) influenza virus infected cells showed an increased glycolytic flux which was correlated with virus replication efficiency (Ritter et al., 2010). Especially, an upregulation of initial steps of glycolysis was observed, similar to the phenomenon of aerobic glycolysis called Warburg effect in cancer cells. Cancer cells primarily rely on the Warburg effect to convert nutrients into the biosynthesis of nucleotides, amino acids and lipids to support the biomass requirement for proliferative growth (Vander Heiden et al., 2009). For example, production of serine via redirection of glycolytic flux by phosphoglycerate

dehydrogenase has been shown to contribute to oncogenesis (Locasale et al., 2011). This could possibly reflect the high levels of glycosphingolipids and bioactive sphingolipids in cancer cells (Furukawa et al., 2012; Hakomori, 2000; Oskouian and Saba, 2010) since serine is a direct precursor for sphingolipid biosynthesis.

A recent metabolomics study identified differential regulation of fatty acid and cholesterol metabolites in influenza virus infected cells (Lin et al., 2010) which was supported by increased activities of enzymes catalysing intermediate steps of lipid biosynthesis (Janke et al., 2011). Increased expression of malonyl coenzyme A decarboxylase (MLYCD) but decreased expression of fatty acid desaturase 2 (FADS2) and FADS3 have been consistently observed in influenza virus infected cells (Coombs et al., 2010; Dove et al., 2012; Kroeker et al., 2012), together indicating an important role of *de novo* fatty acid biosynthesis. Furthermore, inhibition of fatty acid biosynthesis using pharmacological inhibitors or siRNA constructs greatly impaired influenza virus replication (Munger et al., 2008; Shapira et al., 2009; Sui et al., 2009). Interestingly, chronic influenza virus infections and more severe influenza virus pathologies such as encephalopathy have been linked to accumulation of very long chain fatty acids due to defects in ß-oxidation (Diaconita et al., 1985; Yao et al., 2007). Since ß-oxidation of very long chain fatty acids occurs in the peroxisome, the reported interaction of influenza virus NS1 with hydroxysteroid (17-beta) dehydrogenase 4 (HSD17B4) is of great interest (Lazarow, 2011; Wolff et al., 1996). HSD17B4 is an essential part of the peroxisomal ß-oxidation system and its overexpression reduced influenza virus protein expression and replication (Lazarow, 2011; Wolff et al., 1996). Such an inhibitory mechanism of influenza virus on peroxisomal ß-oxidation is also supported by the antiviral activity of acyl-CoA

oxidase 1 (ACOX1) (Shapira et al., 2009) and by the downregulation of carnitine-O-octanoyltransferase (CROT) in influenza virus infected cells (Kroeker et al., 2012). Both are crucial enzymes in the peroxisomal ß-oxidation cascade. Altogether this could explain the findings of reduced fatty acid ß oxidation in mice infected with influenza virus (Murphy et al., 1996; Trauner et al., 1988).

Interference with lipid metabolism has been proven to be a potent antiviral strategy, especially inhibition of cholesterol biosynthesis using statins which significantly reduced influenza related mortality (Vandermeer et al., 2012). Downregulation of cholesterol metabolism in immune cells upon virus infections has been identified to be part of the host antiviral response (Blanc et al., 2011). This is in line with the influenza virus induced expression of viperin inactivating farnesyl diphosphate synthase (FDPS) which is an essential enzyme for isoprenoid biosynthesis (Tan et al., 2012a; Wang et al., 2007). Its general downregulation upon influenza virus infections has been repeatedly observed (Billharz et al., 2009; Coombs et al., 2010; Dove et al., 2012; Kroeker et al., 2012). Cholesterol and fatty acid metabolism have been generally proposed to be essential for late stages in the virus life cycle, especially for the organization of virus assembly sites and generation of viral lipid envelopes (Janke et al., 2011; Munger et al., 2008; Tan et al., 2012a; Wang et al., 2007).

Involvement and regulation of glycerophospholipids and sphingolipids in influenza virus infection, on the other hand, have been addressed only to a lesser extent. Early studies suggested an increased incorporation of glucose breakdown products into neutral lipids with a concomitant inhibition of glycerophospholipid biosynthesis in influenza virus infected cells (Caric-Lazar et al., 1978; Frischholz and Scholtissek,

1984). Especially, the accumulation of the phospholipid precursor, phosphorylcholine, has been linked to a decrease in glycerophospholipid metabolism in influenza virus infected cells (Caric-Lazar et al., 1978). This is reflected by the virulence dependent downregulation of genes and proteins involved in glycerophospholipid metabolism during the course of an infection (Billharz et al., 2009; Dove et al., 2012; Josset et al., 2012; Kroeker et al., 2012; Ma et al., 2011b). One study especially revealed influenza virus NS1 as the major factor blocking expression of genes involved in host interferon and lipid metabolism pathways including expression of sterol-response element-binding protein 1 (SREBP1) (Billharz et al., 2009), a major regulator of phosphatidylcholine biosynthesis (Walker et al., 2011). SREBP1 has been shown to regulate the one-carbon cycle producing the methyl donor S-adenosylmethionine (SAMe) required for the *de novo* methylation pathway of PC biosynthesis (Walker et al., 2011). In contrast, there is clear proof of sphingolipids as positive mediators of influenza virus replication. It has been shown that pharmacological inhibition of ceramide synthase and glucosyl ceramide transferase impaired late stages of influenza virus replication (Hidari et al., 2006), while upregulation of sulfatide increased influenza virus replication through efficient translocation of NPs from the nucleus into the cytoplasm (Takahashi et al., 2008). In line with this, accumulation of sphingosine-1-phopshate (S1P), an important mediator of sphingolipid metabolism, stimulated influenza virus replication, whereas overexpression of S1P lyase (SPL), which irreversibly degrades S1P, led to the inhibition of influenza virus replication (Seo et al., 2010).

1.3 Aims of the thesis

The above described findings suggest an increase of glycolytic flux in influenza virus infected cells and a redirection of its intermediates into sphingolipid and fatty acid biosynthesis with a concomitant inhibition of glycerophospholipid metabolism. One explanation of this shift in metabolism is the requirement of new sphingolipid mass for membrane biogenesis during influenza virion morphogenesis since influenza virus envelopes are enriched in sphingolipids (Blom et al., 2001; Gerl et al., 2012). Importance of lipids and lipid metabolism is additionally illustrated by the increasing number of lipid metabolic enzymes that mediate influenza virus replication. For instance, the five recent siRNA screens together identified 110 lipid metabolic enzymes as mediators of influenza virus replication (Brass et al., 2009; Hao et al., 2008; Karlas et al., 2010; Konig et al., 2010; Shapira et al., 2009; Sui et al., 2009; Watanabe et al., 2010). This represented only 8% of the total hits and demonstrates the redundancy and post transcriptional regulation of metabolic pathways which exacerbate their identification on the basis of genes and proteins. For example, it has been shown, that lysine acetylation of metabolic enzymes plays a major role in metabolic regulation in response to nutrient availability and cellular metabolic state (Zhao et al., 2010). Therefore, more detailed studies are indispensable which directly address and measure the levels of lipid metabolites during influenza virus infection. For this purpose, we decided to harness a systems-scale lipidomics approach to investigate the role of lipids in the influenza virus lifecycle.

More specifically, we pursued the following aims:

1. Establishing a detailed temporal lipid profile of influenza virus infection in a human lung epithelial cell line (Chapter 2).

2. Linking lipid changes in virus infected host cells to influenza virus morphogenesis by analysing the lipid composition of purified influenza virus particles produced from human lung epithelial cells (Chapter 3).

3. Identifying severity related lipids by analysing the lipid composition of virus mutants exhibiting differences in pathogenicity and replication dynamics (Chapter 3).

4. Determining the functional importance of identified lipid species for influenza virus replication using a combination of genetic and pharmacological approaches to interfere with lipid metabolic pathways (Chapter 4).

2 Lipidomics of Virus Infected Cells

2.1 Introduction and rationale

Influenza viruses hijack host cell machineries and impact host cell metabolism to tailor cellular pathways and resources to their needs for efficient replication, assembly and budding. In recent years, systems-scale studies investigating the function of genes (Billharz et al., 2009; Brass et al., 2009; Geiss et al., 2002; Hao et al., 2008; Karlas et al., 2010; Konig et al., 2010; Shapira et al., 2009; Watanabe et al., 2010) and proteins (Coombs et al., 2010; Dove et al., 2012; Kroeker et al., 2012; Lietzen et al., 2011) during influenza virus infections have been extensively addressed, but there is still a significant lack in our understanding of how these complex networks interact with each other and function together as a system (Watanabe et al., 2010). Especially, understanding the regulation of host cell metabolism, not only in virus infected cells but also, for example, in cancer cells, is still in its fledgling stages. Only recently and as a consequence of the advance in technology, studies started to address the functional role of metabolites in various cellular contexts (Jain et al., 2012; Liu et al., 2011; Locasale et al., 2011; Munger et al., 2008; Vander Heiden et al., 2010; Vastag et al., 2011; Yuan et al., 2008).

Several studies investigated regulation of glycolysis and redirection of its intermediates into the biosynthesis of macromolecules such as nucleic acids and amino acids in virus infected cells (Liu et al., 2011; Munger et al., 2008; Ritter et al., 2010; Roe et al., 2011; Vastag et al., 2011). Yet, there exist only a limited number of more detailed studies addressing the regulation and role of lipids in virus infected cells. While there are systems-scale level analyses of lipid metabolism in dengue virus

(Perera et al., 2012), HCV (Roe et al., 2011) and human cytomegalovirus infected cells (Liu et al., 2011), there is still no detailed analysis of lipid metabolism during influenza virus infection despite its requirement for replication and morphogenesis of virus progenies (Munger et al., 2008). The envelope of influenza virus particles is a host-derived lipid bilayer from plasma membrane budding sites. Regardless of its well resolved lipid and protein composition (Blom et al., 2001; Gerl et al., 2012; Polozov et al., 2008; Scheiffele et al., 1999; Shaw et al., 2008; van Meer and Simons, 1982), yet, our knowledge of its biogenesis is not sufficient. Since biogenesis of cellular and viral membranes is directly linked to lipid metabolism, we were interested in harnessing a comprehensive lipidomics approach using mass spectrometry to identify differential regulated host lipids important for influenza virus replication.

In this chapter, we will discuss our findings of differentially regulated lipid species in influenza virus infected cells. We will first introduce several host sphingo- and glycerophospholipids which were altered in human lung epithelial cells during virus infection. Specifically, accumulation of saturated SM, odd chain aPC and ePC species with the concomitant decrease in even chain aPC species will be separately discussed within the context of existing literature. Subsequently, data supporting the role of decreased peroxisomal but increased glycolytic activity in virus infected cells will be introduced. The chapter will conclude with a general discussion combining our observations into a common model describing lipid metabolism in influenza virus infected cells.

2.2 Materials and methods

2.2.1 Cells, viruses and reagents

Human alveolar adenocarcinoma (A549) cells (CCL-185) and Madin Darby canine kidney (MDCK) cell lines (CCL-34) were originally obtained from ATCC; egg grown influenza virus A/PR/8/34 H1N1 was kindly provided by Mike Kemeney (Department of Microbiology, National University of Singapore); Ham's F12 GlutaMAX™, Dulbecco's Modified Eagle Medium (DMEM) GlutaMAX™, Fetal bovine serum (FBS), 100x streptomycin and penicillin (P/S) were obtained from Gibco®, Life Technologies Co. (San Diego, California, USA); Avicel Microcrystalline Cellulose was kindly provided by FMC Biopolymer (Philadelphia, USA); TPCK Trypsin, HPLC and analytical grade chloroform and methanol, ammonium hydroxide, 4% formaldehyde and crystal violet were all purchased from Sigma-Aldrich (St. Louis, USA); Lipid standards were purchased from Avanti Polar Lipids, Inc. (Alabama, USA) unless otherwise stated; Anti-influenza virus M2 (sc-32238) and anti-α-tubulin antibodies were purchased from Santa Cruz Biotechnology (Santa Cruz, CA, USA); Anti pyruvate kinase M2 (PKM2), anti-phospho PKM2 (Tyr-105) and anti-actin antibodies were obtained from Cell Signaling Technologies Inc. (Massachusetts, USA); Secondary antibodies goat anti-mouse and goat anti-rabbit IgG (H+L)-HRP conjugate were purchased from Biorad (California, USA).

2.2.2 H1N1 virus growth in A549 cells

A549 cells were grown in F12 GlutaMAX™ (10% FBS, 50u/ml penicillin & 50µg/ml streptomycin) in 12-well plates to confluency (80 to 100%) and infected with purified influenza virus at a multiplicity of infection of 5 (MOI 5). Influenza virus A/PR/8/34 H1N1 virus was purified over a sucrose gradient as discussed in chapter 3 (Shaw et al., 2008) and used to determine virus growth in a time dependent manner. 500µl of virus inoculum (serum free F12 GlutaMAX™ supplemented with 50u penicillin, 50µg streptomycin & 1µg/ml TPCK trypsin) was incubated for 1 hour (5% CO_2, 37^oC) before incubation in fresh serum free F12 GlutaMAX™ (50u penicillin & 50µg streptomycin) medium at 5% CO_2, 37^oC. Subsequently, virus supernatants and cell lysates were collected at 1, 3, 6, 12, 18, 24 and 30 hours post infection (hpi) to determine virus release and protein expression by plaque assay and western blot respectively. Duplicates were sampled for each time point and plaque assay was performed in duplicates for each replicate (n=4 per condition).

2.2.2.1 Plaque assay to determine influenza virus release

Plaque assay was done as previously described (Matrosovich et al., 2006a). Briefly, 2x10^5 MDCK cells were seeded into 24-well plates one day prior to infection and incubated in DMEM GlutaMAX™-I (10%FBS, 50u/ml penicillin & 50µg/ml streptomycin) at 5% CO_2, 37^oC. Cells were washed twice with serum free DMEM GlutaMAX™ (50u/ml penicillin & 50ug/ml streptomycin) and infected with 10-fold dilutions of virus supernatants in 200µl of serum free DMEM GlutaMAX™

supplemented with 1µg/ml TPCK trypsin. Virus inoculum was removed after 1 hour, exchanged with 2.4% Avicel in 2xDMEM (50u penicillin, 50µg streptomycin & 1ug/ml TPCK Trypsin) and incubated for another 60 to 70 hours at 5% CO_2, 37^{o}C. Subsequently, Avicel containing media was aspirated and cells were fixed with 4% formaldehyde for 20 minutes. Then, fixed cells were washed twice with 1x phosphate buffered saline (PBS) and stained for ten minutes with 1% crystal violet dissolved in 20% methanol and water.

2.2.2.2 Detection of virus and host protein expression by western blot

Cell lysates were washed twice with ice-cold 1xPBS prior to collection by a modified radio immunoprecipitation assay (RIPA) buffer with protease inhibitors (Roche Diagnostics, Rotkreuz, Switzerland). Cells were scraped, transferred to a fresh centrifuge tube (Axygen Inc, California, USA) and were mixed in a bench top ThermoStat (Eppendorf, Hamburg, Germany) for 20min at 4^{o}C. Then, samples were pelleted in a pre-chilled (4^{o}C) bench top centrifuge (Eppendorf, Hamburg, Germany) for 20min at maximum speed (25,000xg). The supernatant was transferred to a fresh centrifuge tube and protein concentration was determined in duplicates using a modified Lowry's assay (Biorad, California, USA) according to the manufacturer's protocol. Briefly, 25µl of a mixture (20µl of surfactant solution (Reagent S) in 1ml of alkaline copper tartrate (reagent A)) was added to 5µl of each sample in a 96-well plate, followed by addition of 200µl of a diluted folin solution (reagent B). 0 mg/ml, 0.2 mg/ml, 0.4 mg/ml, 0.6 mg/ml, 0.8 mg/ml, 1.0 mg/ml, 1.2 mg/ml, 1.4 mg/ml, 1.6 mg/ml, 1.8 mg/ml and 2.0 mg/ml bovine serum albumin (BSA) dilutions in RIPA

buffer were used to draw a standard curve. The plate was kept in the dark for 10 minutes before reading the intensity at an absorbance of 750nm using a SpectraMax190 micro titre plate reader (Molecular Devices LLC, California, USA).

For each sample, 10µg of protein was run on a 10% SDS-polyacrylamide gel, first at 80V (for stacking), then at 120V (for resolving). Separated proteins were transferred onto a nitrocellulose membrane using a semi-dry transfer blotter (Biorad, California, USA) (100mA for 1 hour). The membrane was then blocked in 10% non-fat milk in Tris-buffer saline Tween (TBST) for 1 hour and successively incubated with a primary antibody for 2 hours at room temperature or overnight at 4^{o}C. After 1 hour incubation with a secondary antibody conjugated to horse radish peroxidase (HRP), the blots were developed using Super signal West Dura chemiluminescent (Pierce, Rockford, USA). Mouse anti-influenza virus matrix protein 2 (M2) antibody (1:1000) was used to assess virus protein expression, mouse anti-α-tubulin antibody (1:1000) as a loading control and goat anti-mouse (1:10,000) as secondary antibody.

Determination of PKM2 phosphorylation and expression was performed using rabbit anti-PKM2 antibody (1:1000), rabbit anti-phospho-PKM2 (Tyr105) antibody (1:1000) and goat anti-rabbit secondary antibody (1:10,000). A549 cells were infected with MOI 2 and also collected on ice after 6, 12, 18 and 24hpi in modified RIPA buffer supplemented with protease (Roche Diagnostics, Rotkreuz, Switzerland) and phosphatase inhibitors cocktails 2 and 3 (Sigma-Aldrich, St. Louis, USA).

2.2.3 Collection of infected cells for lipid analysis

A549 cells were seeded into 10cm cell culture dishes 24 hours prior to infection and incubated in F12 GlutaMAX™ (10% FBS, 50u penicillin & 50µg streptomycin). 80 to 100% confluent A549 cells were infected with a 5ml inoculum of purified influenza virus A/PR/8/34 H1N1 at MOI 5 as described above. Virus-infected cells and mock infected cells were collected at 12, 18 and 24hpi. Three independent experiments were performed with three replicates each per condition (n=9 per condition). Prior to harvesting, cells were washed twice with ice cold 1xPBS and then scraped in 500µl ice cold methanol. Samples were collected in fresh centrifuge tubes (Axygen Inc, California, USA) and kept at -20^{o}C before lipid extraction. Lipid extraction for all conditions and replicates in any given experiment was performed at the same time.

2.2.4 Lipid extraction

Only pre-chilled HPLC grade reagents were used. Lipid extraction was conducted according to a modified Bligh and Dyer extraction method (Bligh and Dyer, 1959). Briefly, 250µl of ice cold chloroform was added to the scraped cells in 500µl of methanol (chloroform to methanol 1:2 volume to volume (v/v)). The cells were mixed at high speed for 1 hour at 4^{o}C. Subsequently, 250µl of ice cold chloroform and 275µl of ice cold distilled water were added to break phases. After additionally mixing the samples for 1 minute at high speed, samples were centrifuged in a 4^{o}C pre chilled bench top centrifuge (10,000rpm for 2 minutes). The organic phase, containing the

majority of lipids, was transferred to a fresh centrifuge tube and kept on ice. The aqueous phase was re-extracted with 500µl of chloroform, mixed again for 1 minute and spun down for 2 minutes (4^{o}C; 10,000rpm). The organic phase was collected again and combined with the organic phase of the first extraction. Samples were dried under vacuum using a miVac Duo Concentrator (Genevac Ltd, Suffolk, UK). Samples were stored at -80^{o}C until further analysis by mass spectrometry.

2.2.5 Quantitative analysis of cellular phospho- and sphingolipids by high performance liquid chromatography multiple reaction monitoring mass spectrometry (HPLC MS/MS; operated in MRM mode)

The three independent experiments (Supplementary Table 7-1) were run separately and mass spectrometry analysis of phospho- and sphingolipid species was performed as previously described (Shui et al., 2011b). Briefly, dried cellular lipid extracts were dissolved in 60 to 80µl of chloroform:methanol (1:1 v/v). 20µl of sample were spiked with 20µl of 2x internal standard mixture containing representative standards for PS (dimyristoyl-glycero-phosphoserine or DMPS; final concentration 2µg/ml), PE (1,2-dimyristoyl-glycero-3-phosphoethanolamine or DMPE; final concentration 10µg/ml), PI (2-dioctanoyl-glycero-3-phosphoinositol or C8PI; final concentration 1µg/ml), PC (1,2-dimyristoyl-glycero-3-phosphocholine or DMPC; final concentration 10µg/ml), SM (lauroyl sphingomyelin or LSM; final concentration 2µg/ml), Ceramide (N-heptadecanoyl-D-erythro-sphingosine or C17Cer; final concentration 1µg/ml) and GlcCer (D-glucosyl-ß1-1'-N-octanoyl-D-erythro-sphingosine or C8GlcCer; final concentration 1µg/ml) species.

Sample injection volume was 15µl and prior to introduction into a triple quadrupole instrument ABI 3200 QT (Applied Biosystems, California, USA), lipid classes were separated by high performance liquid chromatography (HPLC) using a Luna 3-µm silica column (Phenomenex Inc, California, USA) coupled to an Agilent 1200 HPLC system (Agilent, California, USA). A linear two-gradient setup was used consisting of mobile phase A (chloroform:methanol:ammonium hydroxide, 89.5:10:0.5) and mobile phase B (chloroform:methanol:ammonium hydroxide:water, 55:39:0.5:5.5). The flow rate was kept at 300 µl/min; 5% mobile phase B for 3 minutes, then linearly switched to 30% mobile phase B in 24 minutes and maintained for 5 minutes, and then linearly changed to 70% mobile phase B in 5 minutes and maintained for 7 minutes. Then, the composition of the mobile phase was returned to the original ratio over 5 minutes and maintained for 6 minutes before the next sample was analysed (Shui et al., 2011b). Lipids were ionized by electro spray ionization (ESI) and analysed by a targeted multiple reaction monitoring (MRM) approach measuring 159 unique transitions (Supplementary Table 7-6). The samples were first run in the negative ion mode measuring transitions corresponding to PS, PE, PI and GM3 species and afterwards PC, SM, Cer and GlcCer specific transitions were analysed in the positive ion mode. Odd chain PC species were distinguished from ePC species by their different elution time.

2.2.5.1 Analysis of MS raw data

Signal intensities for each lipid species were extracted according to their retention time using an in-house developed MATLAB algorithm (Bowen Li, National

University of Singapore) (MathWorks, Massachusetts, USA) and imported into Excel (Microsoft, Washington, USA). Concentrations of measured lipid species were calculated by normalization to the representative spiked internal standards. GM3 levels were normalized to the PI internal standard (C8PI). Lipid species were represented as a molar fraction of the total amount of measured lipid species (Chan et al., 2008). The data of the three independent experiments were combined and significant differences between influenza virus infected and mock infected cells were identified by two criteria to account for experimental variations and differences between independent analytical mass spectrometry runs: 1) A given lipid species had to be statistically significant (unpaired Student's t-test; two-tailed; $p<0.05$) at 18hpi and/or 24hpi in at least one experiment between mock and virus infected cells, and (2) the identified lipid specie followed the same trend in all three independent experiments. A lipid species was considered to follow the same trend as long as the interval [Average(log(H1N1/mock)) - StdDev(log(H1N1/mock)); Average(log(H1N1/mock)) + StdDev(log(H1N1/mock))] calculated by the log(H1N1/mock) values of all three independent experiments did not include zero. The fold-ratio was used to present the data and to make the three independent experiments comparable with regard to lipid changes between infected and mock infected cells. The variations of absolute values between independent experiments were high and hence, identification of small changes would not have been possible to detect by combining the absolute values of the three independent experiments. The differences of significantly regulated lipid species were plotted as log(H1N1/mock) ratios in a heat plot generated by an in-house developed MATLAB algorithm (Bowen Li, National University of Singapore) (MathWorks, Massachusetts, USA) or by basic bar plots with standard deviations drawn in Excel (Microsoft, Washington, USA).

Finally and similar to gene expression data, we harnessed a one-tailed Fisher's exact test (right/greater tail; $p<0.05$) to identify significant enrichment of a certain lipid class in the identified differentially regulated lipid species using an online tool (http://www.langsrud.com/fisher.htm) (Supplementary Table 7-2). This analysis was used to account for overrepresentation of a certain lipid class in our MRM list covering 175 lipid species.

2.2.6 Quantitative analysis of neutral lipids

Neutral lipids were measured for only two of the three independent experiments. 20µl of the same lipid extracts used for HPLC/MS/MS (operated in MRM mode) were mixed with a standard mixture containing standards for TAG (d_5-TAG 48:0 (5µg/ml)), cholesterol ester (d_6-C18 cholesterol ester (10µg/ml)), DAG (4-methyl 16:0 diether DAG (3µg/ml)) and cholesterol (d_6-cholesterol (5µg/ml)). Internal standards for TAG, cholesterol ester and cholesterol were obtained from C/D/N Isotopes Inc. (Quebec, Canada). 30µl of sample plus standard mixture were injected and neutral lipids (DAG and TAG species, cholesterol ester and cholesterol) were analysed by reverse phase HPLC/ESI/MS on an ABI 3200QT (Applied Biosystems, Foster City CA) instrument coupled to an Agilent 1200 HPLC system (Agilent, California, USA) as previously described (Shui et al., 2010; Shui et al., 2011b; Tan et al., 2012b). Neutral lipids were separated from polar lipids using an Agilent Zorbax Eclipse XDB-C18 column (inner diameter 4.6x150mm) (Agilent, California, USA) with an isocratic gradient (chloroform, methanol, 0.1M ammonium acetate 100:100:4 (v/v/v)) at a flow rate of 250 µl/min. 84 ions (Supplementary Table 7-7) were

monitored in the positive mode and corresponding intensities were extracted based on their elution profile by an automated in-house developed MATLAB algorithm (Bowen Li, National University of Singapore) (MathWorks, Massachusetts, USA) and imported into Excel (Microsoft, Washington, USA). Intensities were normalized to internal standards and represented as a ratio to the total amount of measured phospholipids. Significant differences were identified by an unpaired Student's t-test (two-tailed; $p<0.05$).

2.2.7 Catalase assay in virus infected cells

A549 cells were seeded into 12-well plates and grown in F12 GlutaMAX™ (10% FBS, 50u penicillin & 50µg streptomycin) at 5% CO_2, 37°C. Confluent monolayers (80% to 100%) were infected with influenza virus A/PR/8/34 H1N1 (MOI 2) as described above and infected cells were incubated for another 18 hours. Afterwards, cells were washed twice with 1xPBS and collected in 60µl of RIPA buffer. Catalase was measured according to the manufacturer's protocol using a commercial kit purchased from Sigma-Aldrich (St. Louis, USA). Two independent experiments with triplicates per condition were performed at room temperature. Briefly, 10µl of samples were added to 65µl of 1x Assay Buffer (50mM potassium phosphate buffer, *pH* 7.0) and transferred to a fresh centrifuge tube. Subsequently, 25µl of the Colorimetric Assay Substrate Solution (adjusted to 200mM H_2O_2 in 1x Assay Buffer) were added and the reaction was kept for 1 to 5 minutes. The reaction was stopped by adding 900µl of Stop Solution (15mM sodium azide in water) and 10µl aliquots of the catalase enzymatic reactions were transferred to a fresh centrifuge tube. 1ml of Color

Reagent (30µl of Peroxidase Solution in 30ml of Chromogen Solution) was added and absorbance at 520nm was measured after 15 minutes incubation using a SpectraMax190 micro titre plate reader (Molecular Devices LLC, California, USA). Values of both experiments represented relative to mock infected cells were combined and significant differences were calculated by an unpaired Student's t-test (two-tailed*;* $p<0.05$).

2.3 Results and discussion

2.3.1 Influenza virus infection had a stringent but significant effect on host cell phospho- and sphingolipid metabolism

To systematically characterize phospho- and sphingolipid metabolism during influenza virus infection, we used HPLC-MS/MS (operated in MRM mode) to identify differentially regulated lipid species during the course of an infection in A549 cells (Figure 2-1A). First we established the growth of purified MDCK cell culture derived influenza virus A/PR/8/34 H1N1 in A549 cells to select time points that fall into late stages of virus growth, to allow for *de novo* lipid biosynthesis and complete virion morphogenesis. On this note, a recent study investigating major metabolic pathways (such as glycolysis and amino acid biosynthesis) during influenza virus infection, detected virus related changes only after 10 to 12hpi (Ritter et al., 2010). A549 cells were infected with MOI 5 and a synchronized one round of infection was assumed. MOI 5 was chosen based on another study investigating the impact of influenza virus infection on host cell metabolism (Ritter et al., 2010). Virus supernatant and cell protein extracts were collected at 3, 6, 12, 18, 24 and 30hpi and virus titre, as well as virus protein expression, were assessed by plaque assay and western blot, respectively. The peak of virus growth was determined to be at 18hpi. As a result, we decided to sample the 12, 18 and 24hpi time points for the analysis of influenza virus specific changes in lipid metabolism (Figure 2-1A).

Three independent experiments with three replicates per condition (three mock and three infected at 12hpi, 18hpi and 24hpi) were conducted. Since virus infection was done in serum free conditions, it was necessary to additionally probe for mock infection during the time course to exclude any metabolic changes that were not virus related but rather due to serum free conditions (Ritter et al., 2010). Samples were collected and subjected to lipid extraction prior to the targeted analysis of 175 different lipid species by HPLC-MS/MS (operated in MRM mode). The collected data were combined and differentially regulated lipid species were identified using two criteria to account for variations between independent analytical mass spectrometry runs: (1) a given lipid species had to be statistically significant (unpaired Student's t-test; two-tailed; $p<0.05$) at 18hpi and/or 24hpi in at least one experiment, and (2) the lipid followed the same trend in all three independent experiments. A lipid species was considered to follow the same trend as long as the interval [Average(log(H1N1/mock)) - StdDev(log(H1N1/mock)); Average(log(H1N1/mock)) + StdDev(log(H1N1/mock))] calculated by the log(H1N1/mock) values of all three independent experiments did not include zero.

Applying these two criteria allowed us to identify 78 differentially regulated lipid species in virus infected cells as compared to mock infected cells grown in serum free conditions (Figure 2-1C). The 78 differentially regulated species were mainly enriched in choline containing lipids ($p<0.001$) and sphingolipid species ($p<0.01$) as calculated by a one-tailed (right/greater tail) Fisher's exact test ($p<0.05$) (Figure 2-1B & Supplementary Table 7-2). More specifically, there was a general increase in ePC and odd chain aPC, SM and GlcCer species with a concomitant decrease in even chain aPC and ganglioside GM3 species (Figure 2-1B&D). PS, PI and PE species

were only affected to a lesser extent (Figure 2-1B) whereas total amounts of aPE species continuously decreased during the course of an influenza virus infection (Figure 2-1D). There was a general increase of saturated lipid species within most of the investigated lipid classes in influenza virus infected A549 cells (Figure 2-1E). For example, PS 32:0 was the only differentially regulated PS and was increased across all three time points. Furthermore, the saturated ester linked PC species (aPC 34:0a, aPC 36:0a and aPC 38:0a) showed a similar upregulation in infected cells as opposed to the general downregulation of unsaturated aPC species (Figure 2-1C).

A

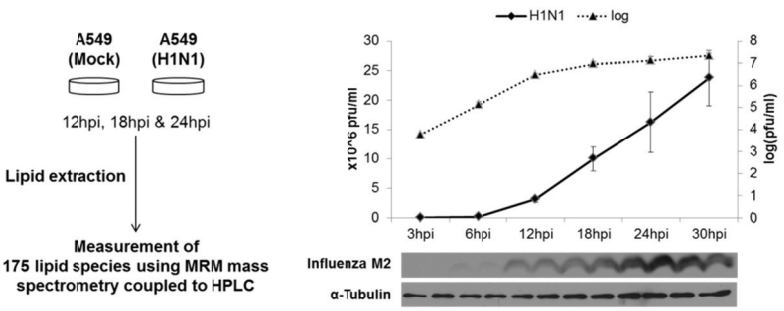

B

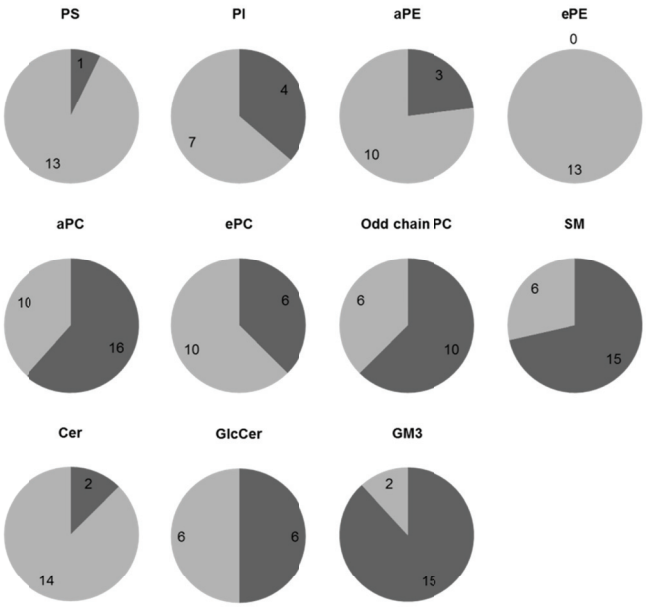

Lipid Class	*p-value*
GM3	0.000129
Choline	0.000267
Sphingo	0.005588
SM	0.007969
PC	0.034117

Lipid Class	*p-value*
GlcCer	0.460104
PI	0.809013
Phospho	0.997832
Cer	0.999295
PS	0.999835
PE	0.999985

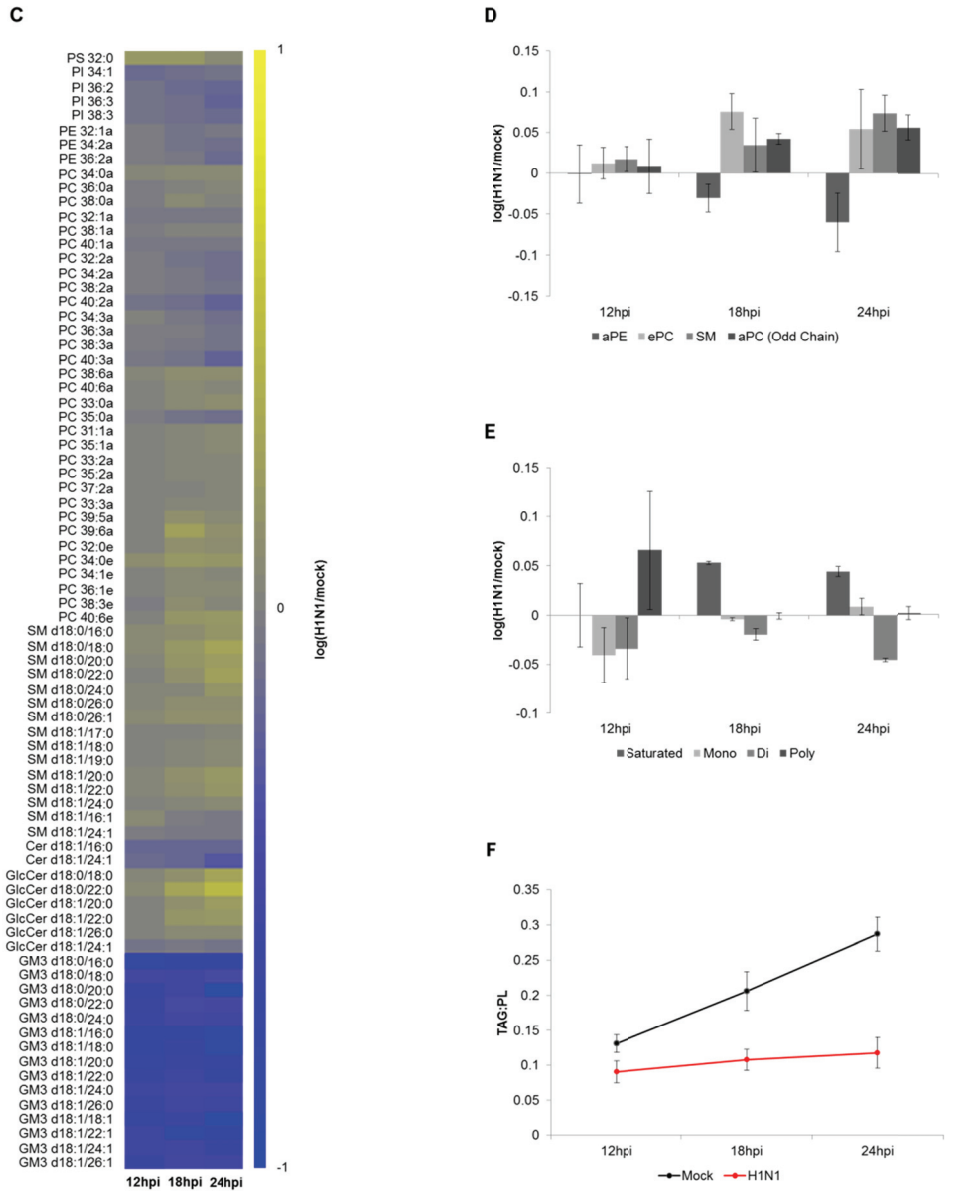

Figure 2-1: Lipidomics of influenza virus infected cells. (A) Mock and influenza virus H1N1/PR8 infected A549 cells (MOI 5) were collected at late stages of virus growth (12hpi, 18hpi and 24hpi). Samples were subjected to lipid extraction and analysis by HPLC MS/MS (operated in MRM mode) measuring 175 lipid species. **(B)** The majority of differentially regulated species were observed in choline- and sphingolipids classes. Percentages of unchanged (light grey) and differentially regulated (dark grey) lipid species over three independent experiments are shown as pie charts; *p-values* were calculated by a Fisher's exact test and lipid classes significantly enriched (*$p<0.05$)* were coloured in yellow. **(C)** 78 lipid species were found to be differentially regulated over three independent experiments using the two criteria described in the text. **(D)** Total amounts of aPE, ePC, SM and odd chain aPC were found to be differentially regulated in influenza virus infected cells. **(E)** Saturated phospholipid species were generally upregulated whereas unsaturated species were downregulated in infected cells. Data is represented as the averages of the log(H1N1/mock) calculated from the three independent experiments normalized to the total phospholipid content. Error bars represent standard deviations. **(F)** TAG levels were decreased in infected cells as compared to mock infected cells. Data shows TAG levels in relation to the total amount of measured phospho- and sphingolipids from two independent experiments (n=6). Error bars depict standard deviations.

2.3.1.1 aPC species were decreased while ePC, odd chain aPC and SM species were increased in influenza virus infected cells

A specific remodelling within the PC lipid class was observed, resulting in an increase of ether-linked and odd chain aPC species but a decrease in even chain aPC species (Figure 2-1C&D). The increase in ether linked PC species peaked at 18hpi whereas the increase in odd chain and the decrease in even chain aPC species peaked at 24hpi (Figure 2-1C&D). The reduced levels of aPC species in influenza virus infected cells have been previously proposed to be related to an impairment in aPC biosynthesis by measuring metabolite rates of phospholipid precursors and by global gene and protein expression experiments (Billharz et al., 2009; Caric-Lazar et al., 1978; Kroeker et al., 2012). Especially SREBP1, which is a major regulator of the one-carbon cycle producing the methyl donor SAMe required for the de novo methylation pathway for aPC biosynthesis, was significantly downregulated in influenza virus infected cells (Billharz et al., 2009; Walker et al., 2011). These changes at 24hpi coincided with the upregulation of another choline containing lipid, SM, which suggested an important correlation of influenza virus replication with choline lipid metabolism (Figure 2-1D). For example increase in SM and decrease in PC species could be explained by the fact that sphingomyelin synthases SMS1 and SMS2 use PC as a substrate to transfer the choline head group onto a ceramide backbone. Another valuable observation made in the gene expression study by Billharz et al (2009) was the significant downregulation of ethanolamine kinase 1 (ETNK1) which is a rate-controlling step in PE biosynthesis. Indeed, in our temporal lipid profile we also observed a continuous downregulation of PE biosynthesis (Figure 2-1D). It could be argued that the

downregulation of ETNK1 generally decreased PE species but within the choline containing species, exclusively aPC species were downregulated, due to the decrease in SREBP1 expression. On the other hand ePC and SM species were upregulated because their rate-controlling steps in the form of choline kinases were not affected by virus infection.

2.3.1.2 Sphingolipids with a dihydroceramide backbone were upregulated while sphingolipids with a ceramide backbone were downregulated in influenza virus infected cells

The differential regulation of sphingolipids was striking, especially the general increase in SM and GlcCer species accompanied by the decrease in GM3 species (Figure 2-1C). The decrease of GM3 species was most probably related to influenza virus NA activity, cleaving the externally attached sialic acid on the sugar head group (Sato et al., 1998). Most likely, this did not reflect the general increase in sphingolipid biosynthesis since influenza virus replication has been shown to be dependent on sphingolipids (Gerl et al., 2012; Hidari et al., 2006; Takahashi et al., 2008). GM3 species were thus excluded from further data analysis under the assumption that their downregulation did not reflect the general upregulation of sphingolipid biosynthesis.

For a more detailed analysis, levels of sphingolipid species (Cer, GlcCer and SM) were represented relative to the total amount of measured sphingolipids. Specific changes with regard to the (un-)saturation of the sphingoid base backbone as well as to the chain length and (un-)saturation of the fatty acyl moiety were revealed. For

example, there was an overall increase of dihydroceramide containing sphingolipids during the course of an infection, whereas ceramide containing sphingolipids were slightly downregulated (Figure 2-2A). However, it was evident that sphingolipids consisting of a ceramide backbone with a saturated fatty acyl chain showed a slightly increasing trend whereas ceramide containing sphingolipids with an unsaturated fatty acyl moiety in their ceramide backbone were substantially downregulated during the course of the infection (Figure 2-2C). This is in line with our general observation of increased incorporation of saturated fatty acyl moieties into phospholipid species in virus infected cells (Figure 2-1C) which might cause increased lipid order required for virus assembly and budding.

Infected cells also showed an increased incorporation of C20, C22 and C26 fatty acyl moieties into sphingolipid species (Figure 2-2B). Especially, saturated C18:0, C20:0, C22:0 and C26:0 fatty acyls, whereas saturated C16:0 and unsaturated C16:1 and C24:1 fatty acyls were decreased (Figure 2-2D). On the other hand, C20:1 and C26:1 were the only unsaturated fatty acyl moieties in sphingolipid species which were upregulated in virus infected cells (Figure 2-2D). Incorporation of fatty acid moieties into sphingolipids is catalysed by six ceramide synthases (CerS1-6) specific for fatty acid chain lengths (Levy and Futerman, 2010; Mullen et al., 2012). Based on this, the observed increased incorporation of C20, C22 and C26 fatty acids into sphingolipid species possibly reflected a CerS2 mediated upregulation of sphingolipid biosynthesis (Levy and Futerman, 2010; Mullen et al., 2012). Differences in ceramide fatty acid composition can greatly influence cellular function (Grosch et al., 2012) and for instance, depletion of CerS2 results in impaired vesicular trafficking (Markham et al., 2011; Silva et al., 2012). Therefore, increased incorporation of very long chain fatty

acids into sphingolipids might be essential to maintain the need for vesicular trafficking required for influenza virus morphogenesis.

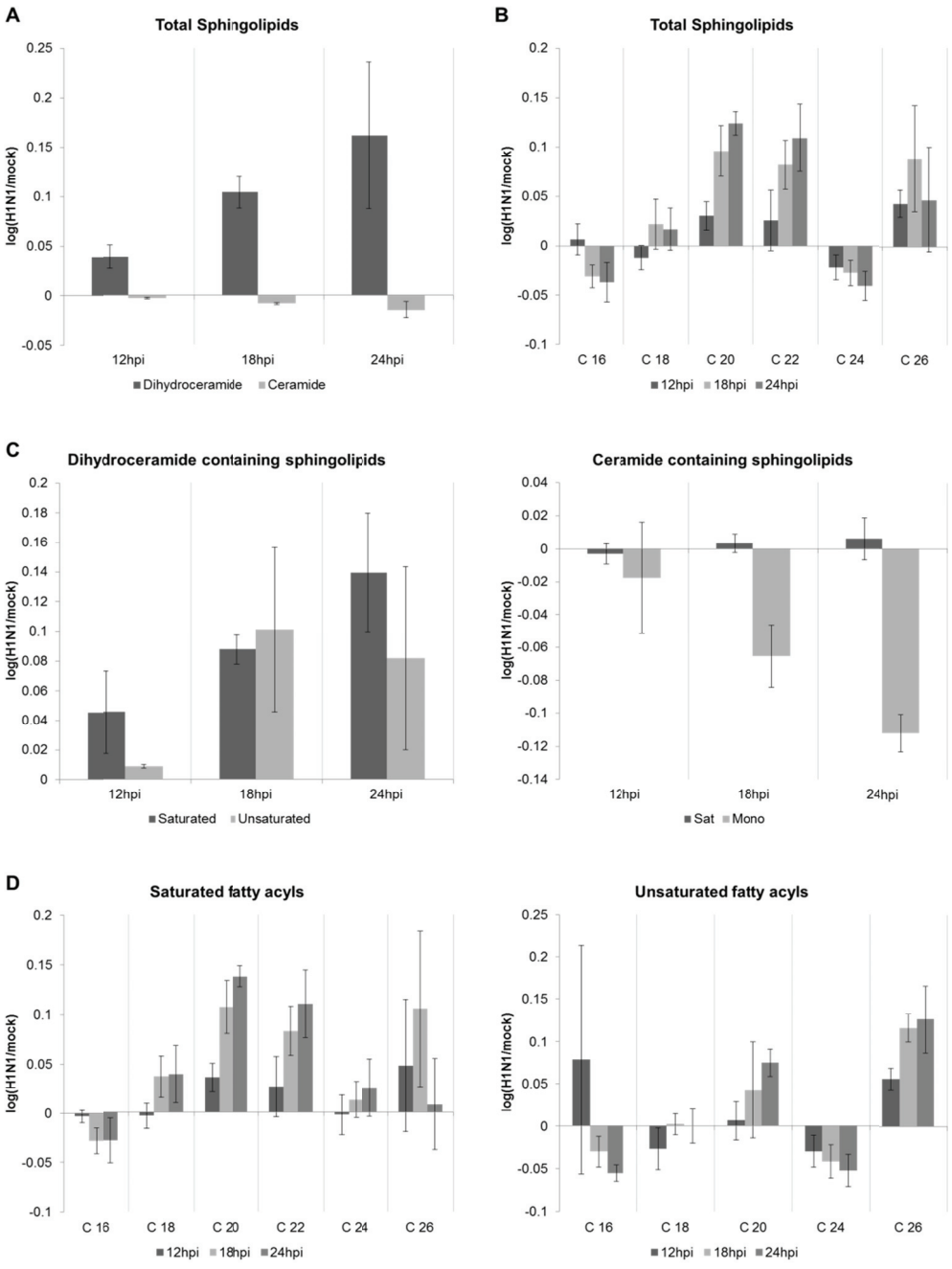

Figure 2-2: Differential regulation of sphingolipids in influenza virus infected cells. Sphingolipid species (SM, GlcCer & Cer) were normalized to the total sphingolipid content and classified according to their **(A)** ceramide backbone (dihydroceramide versus ceramide) and **(B)** according to their fatty acyl chain length. **(C)** Dihydroceramide and ceramide containing species were further categorized into

consisting of either saturated or unsaturated fatty acyl chains. **(D)** Chain length and saturation of fatty acyl moieties of sphingolipid species were also investigated. Data is shown as the average of the log(H1N1/mock) calculated from the three independent experiments. Error bars represent standard deviations.

2.3.1.3 Peroxisomal catalase activity was decreased in influenza virus infected cells

The increase of ePC and odd chain aPC species led us to investigate peroxisomal activity since biosynthesis of ether lipids and production of odd chain fatty acyl moieties by one cycle α-oxidation of very long chain fatty acids solely occurs in the peroxisome (Guo et al., 2010; Wallner and Schmitz, 2011; Wanders et al., 2000). For this purpose, we measured peroxisomal catalase activity which correlates with peroxisomal ß-oxidation. ß-oxidation in the peroxisome is not coupled to ATP synthesis but instead produces hydrogen peroxide which consequently gets converted into oxygen and water by catalase (Perichon and Bourre, 1995). We infected cells with MOI 2 to ensure synchronized infection of host cells. We found a 20% decrease in catalase activity in infected cells indicative of decreased ß-oxidation in the peroxisome. This is in line with our temporal lipid data showing an enrichment of C26:0 and C26:1 but a decrease of C24:1 fatty acyl moieties in sphingolipid species (Figure 2-2D). Accumulation of C26:0 and C26:1 fatty acid moieties in sphingolipids have been proposed to be diagnostic markers for diseases caused by defects in peroxisomal ß-oxidation (Pettus et al., 2004). It has been shown that accumulation of C26:0 fatty acids was inhibitory to the biosynthesis of C24:1 fatty acids (Sargent et al., 1994). C24:1 fatty acids were upregulated by increased peroxisomal ß-oxidation mediated by increased ACOX1 activity (Vluggens et al., 2010). ACOX1 has also been identified to be antiviral among other host factors implicated in influenza virus

replication (Shapira et al., 2009). This is further backed by a different report showing that overexpression of another essential enzyme involved in the peroxisomal ß-oxidation cascade, HSD17B4, inhibits influenza virus protein expression (Wolff et al., 1996). On the contrary, proteins involved in peroxisomal α-oxidation such as PHYHIP have been identified to be proviral (Brass et al., 2009).

In summary, accumulation of odd-chain aPC species might be a result of increased α-oxidation of very long chain fatty acids in the peroxisome which are unable to get further metabolized due to decreased peroxisomal ß-oxidation. As a consequence, they might get incorporated as odd chain fatty acyls into phospho- and sphingolipids. Such a mechanism has been observed in differentiating adipocytes where increased α-oxidation was also coupled prior to fatty acid Δ9-desaturation (Su et al., 2004). Interestingly, knockdown of the enzyme stearoyl-CoA desaturase (Δ9-desaturase; SCD) essential for the synthesis of unsaturated lipids has also been found to decrease influenza virus replication (Hao et al., 2008).

Due to the tight balance between anabolism and catabolism, accumulation of ePC species in virus infected cells could be explained by a relative increase in lipogenesis in the peroxisome since the catabolic arm of peroxisomal ß-oxidation was decreased. The possibility that the identified lipid changes in virus infected cells represented a specific impairment of peroxisomal ß-oxidation could be further supported by the decreased levels of TAG in virus infected cells (Figure 2-1F). We observed a continuous accumulation of TAG levels in mock infected cells most likely due to the serum free growth condition leading to an increase in glycolytic flux and neutral lipid biosynthesis. Alternatively, levels of TAG in virus infected cells seemed to increase

only slightly or remained unchanged (Figure 2-1F). Our results in combination with other studies showing essentiality of fatty acid biosynthesis (Coombs et al., 2010; Munger et al., 2008; Shapira et al., 2009; Shaw et al., 2008) in influenza virus infection/replication, led us to conclude that upregulation of fatty acid biosynthesis occurred concomitantly with increased lipid catabolism in the mitochondrion. Earlier findings of long chain fatty acid accumulation in acute and more severe pathologies, such as encephalopathy in influenza virus infected mice, further support a specific inhibition of peroxisomal catabolism since peroxisomal ß-oxidation is required for the shortening and degradation of long chain fatty acids (Diaconita et al., 1985; Yao et al., 2007).

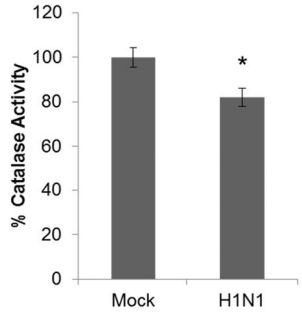

Figure 2-3: Catalase activity in influenza virus infected A549 cells. Cells were infected with influenza virus and catalase activity was measured at 18hpi using a Catalase Assay Kit (Sigma-Aldrich, St. Louis, USA). Virus infection reduced catalase activity by 20%. *indicates a significant *p-value* (unpaired Student's t-test; two-tailed; $p<0.05$).

2.3.1.4 Influenza virus infection induced early phosphorylation of PKM2

Ether lipid biosynthesis is directly linked to glycolysis by its metabolic intermediate dihydroxyacetone phosphate (DHAP) which gets converted into acyl-DHAP by dihydroxyacetone phosphate acyl transferase (DHAPAT) and subsequently to alkyl-DHAP by alkyldihydroxyacetone phosphate synthase (AGPS) in the peroxisome. It has been shown that influenza virus infection upregulates upstream glycolytic intermediates similarly to the Warburg effect in cancer cells (Ritter et al., 2010). The phosphorylated and less active dimeric form of PKM2 has been postulated to be a major driver for the Warburg effect redirecting upstream glycolytic intermediates into the biosynthesis of nucleotides, amino acids and lipids (Eigenbrodt et al., 1992; Hitosugi et al., 2009), explaining the relatively high levels of ether lipids found in cancerous cells (Magnusson and Haraldsson, 2011; Wallner and Schmitz, 2011). Based on this, we decided to measure expression and phosphorylation levels of PKM2 in virus infected A549 cells. We infected cells with MOI 2 to ensure synchronized infection of host cells. We observed a slightly increased (in two independent experiments between 6hpi and 12hpi) PKM2 phosphorylation in infected cells as compared to mock infected cells. The differences in phosphorylation of PKM2 between infected and non-infected cells were small, which was most probably due to the already high levels of PKM2 and its phosphorylated form in A549 cells since they are of cancerous origin (Hitosugi et al., 2009). Nevertheless, the importance of PKM2 in influenza virus replication was additionally supported by its 100-fold upregulation in a primary human tracheobronchial airway epithelial cell line infected with influenza virus and by its association with purified influenza virus particles (Kroeker

et al., 2012; Shaw et al., 2008). The recent observation of PKM2 controlling *de novo* serine biosynthesis from glycolysis (Ye et al., 2012) could also reflect increased sphingolipid biosynthesis in influenza virus infected cells (Figure 2-1), since serine is a direct precursor for the biosynthesis of sphingoid bases.

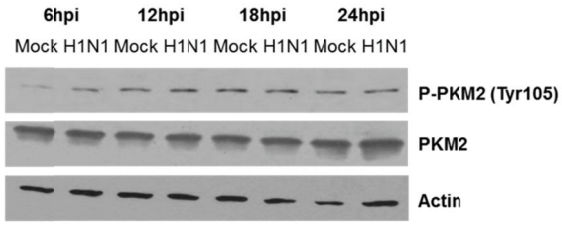

Figure 2-4: PKM2 phosphorylation during influenza virus infection. Cells were infected with influenza virus and cellular protein lysates were collected at 18hpi. Expression and phosphorylation of PKM2 was probed by western blot. Actin was used as the loading control. Results from one experiment are shown which are representative of two independent experiments.

2.4 Conclusion

In this chapter, we established for the first time a detailed temporal lipid profile of an influenza virus infection in A549 cells. Our findings were in agreement with previous studies based on gene and protein expression data, generally pointing towards an increase in sphingolipid but a decrease in glycerophospholipid biosynthesis in influenza virus infected cells (Figure 2-1) (Billharz et al., 2009; Caric-Lazar et al., 1978; Coombs et al., 2010; Dove et al., 2012; Kroeker et al., 2012). Especially, the increase in SM and GlcCer in combination with decreased levels of aPE and aPC species (Figure 2-1) reflected the previously described lipid composition of purified influenza virus particles from MDCK cell lines (Gerl et al., 2012). This suggested that influenza virus tailors host cell lipid metabolism to its needs for virion morphogenesis and tempted us to further investigate the lipid composition of A549 produced influenza virus (addressed in Chapter 3). The increase in SM could be linked to a decrease in aPC species, since biosynthesis of SM is catalysed by SMS1 and SMS2 which transfer the choline of PC onto the ceramide backbone. Ceramide levels remained constant or only decreased slightly due to a general stimulation of sphingolipid biosynthesis in virus infected cells (Figure 2-1) (Hidari et al., 2006; Takahashi et al., 2008). Furthermore, the identified specific remodelling within the PC lipid class, consisting of an increase in ePC and odd chain aPC species but of a concomitant decrease in aPC species, implied an important role of the peroxisome for influenza virus replication (Figure 2-1). In line with increased lipogenesis and decreased ß-oxidation in the peroxisome, we found a significant reduction in catalase activity which reflected decreased peroxisomal ß-oxidation (Figure 2-3). We

speculated that decreased peroxisomal ß-oxidation was accompanied by a concomitant increase in mitochondrial peroxisomal ß-oxidation since TAG levels were significantly reduced in influenza virus infected cells (Figure 2-1), despite the importance of fatty acid biosynthesis for influenza virus replication (Munger et al., 2008).

In combination with previous findings from our laboratory (Lukas Tanner & Xueli Guan, *unpublished*), upregulation of sphingolipids (via increased endogenous production of serine and incorporation into ceramide) and ePC species (via increased levels of DHAP) led us to hypothesize that lipid biosynthesis in infected cells could be linked to the previously reported increase in glycolysis during influenza virus infection (Ritter et al., 2010) in a similar manner as observed in cancer cells exhibiting high levels of sphingolipids and ether lipids (Magnusson and Haraldsson, 2011; Wallner and Schmitz, 2011). In line with this, PKM2 levels were highly upregulated in influenza virus infected cells (Kroeker et al., 2012) and we observed an early induction of PKM2 phosphorylation (Figure 2-4).

Finally, we were able to integrate our findings with data from siRNA screens (Brass et al., 2009; Karlas et al., 2010; Konig et al., 2010; Shapira et al., 2009; Sui et al., 2009; Watanabe et al., 2010), protein expression (Coombs et al., 2010; Dove et al., 2012; Kroeker et al., 2012) and gene expression data (Billharz et al., 2009) to manually derive and propose a cellular lipid flux model during influenza virus infection (Figure 2-5). We hypothesized that lipid flux in influenza virus infected cells is regulated by high glucose consumption under the control of PI3K/Akt signalling which is induced upon influenza virus infection (Charmaine Chng & Lukas Tanner,

unpublished) (Ehrhardt and Ludwig, 2009; Zhirnov and Klenk, 2007). Activation of Akt has been shown to induce PKM2 upregulation and phosphorylation via the mTOR complex which could possibly explain observations of PKM2 upregulation (Kroeker et al., 2012) and phosphorylation (Figure 2-5) in influenza virus infected cells. Consequently, this leads to an increase in glycolytic flux (Ritter et al., 2010) similar to the Warburg effect in cancer cells which inhibits AMP activated protein kinase (AMPK) activity. In contrast, AMPK activity has been shown to suppress tumour growth (Shackelford and Shaw, 2009) and AMPK agonists have successfully been used to treat influenza virus infected mice (Moseley et al., 2010). Therefore, the antagonistical regulation of downstream effectors by PI3K/Akt signalling and AMPK activity might determine the balance between anabolic and catabolic functions in influenza virus infected cells. The rather descriptive and hypothetical nature of our proposed model needs further experimental validation, but it can serve as the basis for future studies addressing role and regulation of lipid metabolism in influenza virus infected cells. It would be of great interest to repeat a similar study in primary lung cells due to the cancerous nature of the used A549 cells. It is well known that metabolism of cancer cells is extensively different to non-cancerous cells. Hence, differences observed in lipid metabolism during influenza virus infection could be even more striking in primary cells. This is supported by the finding of a 100-fold upregulation of PKM2 in a primary human tracheobronchial airway epithelial cell line infected with influenza virus (Kroeker et al., 2012).

2. Lipidomics of Virus Infected Cells

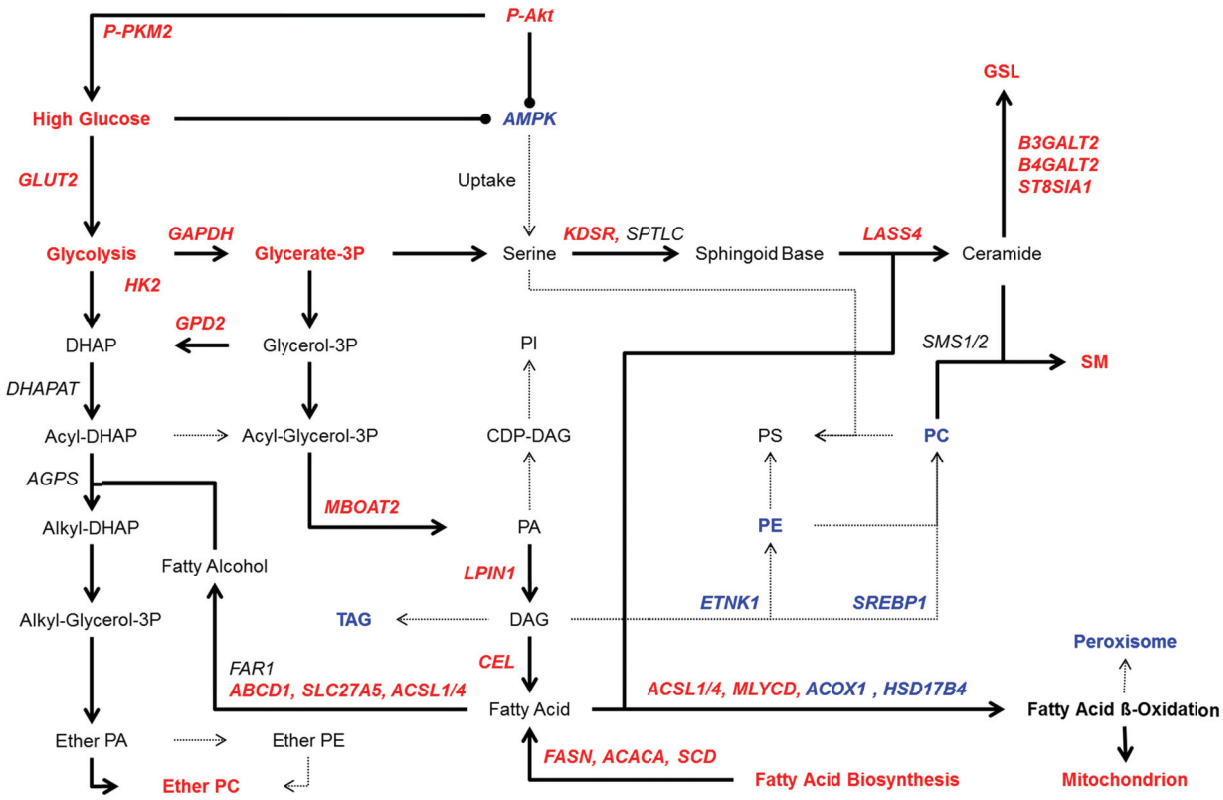

Figure 2-5: Proposed lipid flux in influenza virus infected cells (Page 64): The model was derived by combining our lipid data with published data from siRNA screens (Brass et al., 2009; Karlas et al., 2010; Konig et al., 2010; Shapira et al., 2009; Sui et al., 2009; Watanabe et al., 2010), protein expression studies (Coombs et al., 2010; Dove et al., 2012; Kroeker et al., 2012) and gene expression studies (Billharz et al., 2009). Genes, proteins and metabolites reported to affect influenza virus replication are depicted in black (no change or not identified), bold red (proviral or upregulated) and bold blue (antiviral or downregulated); Bold arrows and dashed arrows represent proposed increased and decreased fluxes, respectively; Bold black lines with round ends indicate an inhibition of expression or activity; ATP-binding cassette, sub-family D 1 (ABCD1), acetyl-CoA carboxylase alpha (ACACA), acyl-CoA oxidase 1 (ACOX1), acyl-CoA synthetase long-chain family member 1/4 (ACSL1/4), alkylglycerone phosphate synthase (AGPS), AMP activated protein kinase (AMPK), N-acylsphingosine amidohydrolase (acid ceramidase) 1 (ASAH1) , UDP-Gal:betaGlcNAc beta 1,3-galactosyltransferase, polypeptide 4 (B3GALT2), UDP-Gal:betaGlcNAc beta 1,4-galactosyltransferase polypeptide 4 (B4GALT2), carboxyl ester lipase (CEL), diacylglycerol (DAG), dihydroxyacetone phosphate (DHAP), DHAP acyl transferase (DHAPAT), ethanolamine kinase 1 (ETNK1), fatty acid reductase 1 (FAR1), fatty acid synthase (FASN), glyceraldehyde-3-phopshate dehydrogenase (GAPDH), facilitated glucose transporter 2 (GLUT2), glycerol-3-phosphate dehydrogenase 2 (GPD2), glycosphingolipids (GSL), hexokinase 2 (HK2), hydroxysteroid (17-beta) dehydrogenase 4 (HSD17B4), 3-ketodihydrosphingosine reductase (KDSR), ceramide synthase 4 (LASS4), lipin 1 (LPIN1), membrane bound O-acyltransferase domain containing 2 (MBOAT2), malonyl-CoA decarboxylase (MLYCD), phosphatidic acid (PA), phosphatidylcholine (PC), phosphatidylethanolamine (PE), phopsphatidylinositol (PI), pyruvate kinase 2 (PKM2), phosphatidylserine (PS), stearoyl-CoA desaturase (SCD), fatty acid transporter 5 (SLC27A5), sphingomyelin (SM), sphingomyelin synthase 1/2 (SMS1/2), sterol regulatory element binding transcription factor 1 (SREBP1) & triacylglycerol (TAG).

3 Lipidomics of Influenza Virus

3.1 Introduction and rationale

After establishing a detailed temporal lipid profile in influenza virus infected cells, we were wondering whether the lipid composition of influenza virus particles correlates with the enrichment of certain lipid species in virus infected host cells. Influenza A viruses are enveloped viruses which derive their lipid-bilayer from the host plasma membrane during budding. Their envelope is a detailed representation of the lipid composition at the budding site and can provide additional insights into the importance of lipids in the virus life cycle. Several studies scrutinized the lipid composition of purified influenza virus particles (Blom et al., 2001; Gerl et al., 2012; Polozov et al., 2008; Scheiffele et al., 1999; van Meer and Simons, 1982) without addressing its regulation and link to host cell lipid metabolism. Consequently, we applied our targeted lipidomics approach to first establish the lipid composition of purified A549 grown influenza virus A/PR/8/34 H1N1 in comparison to its producer cell. Then, we looked at the lipid composition of two closely related influenza virus A/Aichi/2/68 H3N2 strains, which exhibit differences in pathogenicity and replication dynamics, to identify potential viral determinants interfering with host cell lipid metabolism.

In this chapter we will first introduce the lipid composition of purified A549 grown influenza virus A/PR/8/34 H1N1 in relation to other published enveloped viruses. We will specifically emphasize on the increase of SM and ePC species and on the decrease of aPC species which were consistent with our findings of a differentially regulated host cell lipid metabolism during influenza virus infection.

Secondly, we will discuss the enrichment of ceramide species in influenza virus particles which were not differentially regulated in virus infected cells and in combination with extensive literature mining, we will propose a novel concept of how ceramide species regulate influenza virus particle trafficking.

In the third part, we will present the lipid composition of two closely related influenza virus A/Aichi/2/68 H3N2 strains differing in a point mutation in NS1 and propose NS1 to be a potential regulator of viral lipid composition and host cell lipid metabolism. We will then bring together the different datasets on host cell lipid metabolism, influenza virus lipid composition and virulence related lipids by hierarchical clustering revealing severity dependent clusters of co-regulated lipid species.

Finally, we will highlight the importance of lipids in the virus life cycle by confirming the broad-spectrum antiviral activity of two new compounds which oxidize phospholipids in virus envelopes. The chapter will conclude with a general discussion on the described results in relation to each other and within the context of recent literature.

3.2 Materials and methods

3.2.1 Cells, viruses and reagents

Egg grown human influenza virus strain A/Aichi/2/68 H3N2 P0 and egg grown mouse adapted human influenza virus strain A/Aichi/2/68 H3N2 P10 were kindly provided by Vincent Chow (Department of Microbiology, NUS); Sucrose and Glutaraldehyde were purchased from Sigma-Aldrich (St. Louis, USA); All other reagents were from identical sources as described in chapter 2 unless stated otherwise.

3.2.2 Virus purification

Virus stocks were prepared by passaging egg grown virus strains once in MDCK cells. Purified viruses used for lipid analysis represented the second passage in any given producer cell to minimize virus adaption through passaging. Viruses were not grown for more than three passages in any given cell line.

Purification of influenza viruses was carried out as previously described (Shaw et al., 2008) (Supplementary Figure 7-1). Two independent preparations were conducted for virus production in A549 cells (Supplementary Table 7-3). A549 cells were grown in 20x15cm tissue culture dishes and, when confluent (80 to 100%), infected with influenza virus A/PR/8/34 H1N1 (MOI <0.05) which has been passaged only once in MDCK cells. Infection was done as described above and 12.5ml serum free F12 GlutaMAX™ supplemented with penicillin (50u/ml), streptomycin (50µg/ml) and

TPCK trypsin (1µg/ml) per culture dish were used as inoculum. Medium was exchanged after 1 hour and 12.5ml of fresh serum free F12 GlutaMAX™ (50u penicillin & 50µg streptomycin) were added. Virus supernatant (250ml) was collected after incubation for 72 to 96 hours (37^{o}C, 5%CO_2) and clarified twice by centrifugation for ten minutes in a pre-chilled bench top centrifuge at 4000rpm (4^{o}C) (Eppendorf, Hamburg, Germany). 10x25ml of clarified supernatant was subsequently layered over 7ml of 20% sucrose cushions (dissolved in 1xPBS) and concentrated by centrifugation at 112,600xg (33PA tubes; swing bucket rotor P28S) for 2 hours at 4^{o}C in a HIMAC CP100WX ultracentrifuge (Hitachi, Japan). Virus pellets were dissolved in 100µl 1xPBS (a total of 1ml of concentrated virus) and carefully dislodged overnight at 4^{o}C before layering 2x500µl of concentrated virus over 30% to 60% sucrose gradients (seven 1.4ml steps freshly prepared from the bottom in a 10PA tube: 60%, 55%, 50%, 45%, 40%, 35% and 30% in 1xPBS). The gradient was centrifuged at 112,600xg (swing bucket rotor P40ST) for 3 hours at 4^{o}C in a HIMAC CP100WX ultracentrifuge (Hitachi, Japan) and the banded virus (1.18g/cm^3 to 1.19 g/cm^3; interface between 40% and 45% sucrose) was carefully collected, combined and diluted with 1xPBS. Finally, purified influenza viruses were pelleted by centrifugation for 2 hours at 4^{o}C (swing bucket rotor P28S; 33PA tubes) in a HIMAC CP100WX ultracentrifuge (Hitachi, Japan) and pellet was carefully dislodged in 200µl 1xPBS over night at 4^{o}C after carefully aspirating the supernatant. Purified viruses were aliquoted and stored at -80^{o}C until further analysis by SDS gel electrophoresis (virus purity), plaque assay (virus titre) and analysis by mass spectrometry (lipid composition).

Other virus strains discussed in this chapter were purified using the same protocol. For MDCK grown influenza viruses (influenza virus A/PR/8/34 H1N1, influenza virus A/Aichi/2/68 H3N2 P0 & influenza virus A/Aichi/2/68 H3N2 P10), only 10x 15cm culture dishes of confluent MDCK cells were used. Cells were incubated with viruses in 12.5ml serum free DMEM GlutaMAX™ (50u/ml penicillin, 50µg/ml streptomycin & 2µg/ml TPCK trypsin) and exchanged after 1 hour with fresh serum free medium still supplemented with 2µg/ml TPCK trypsin. Virus supernatant was collected when at least 75% of the infected MDCK cell monolayer exhibited virus induced cytopathic effect (CPE) characterized by cell shedding. Purification of influenza virus A/PR/8/34 H1N1 was routinely done and 3 independent preparations for influenza virus A/Aichi/2/68 H3N2 P0 and influenza virus A/Aichi/2/68 H3N2 P10 were performed.

3.2.3 Assessment of virus purity by SDS gel electrophoresis and scanning electron microscopy (SEM)

Virus purity was assessed by running 15µl of purified virus samples on precast Tris-HCl 4 to 15% gradient gels (Biorad, California, USA). Samples were run at 120V and proteins were visualized using Coomassie Brilliant Blue R-250 Dye (Life Technologies Co, San Diego, USA) dissolved in 45% methanol, 45% water and 10% acetic acid) and identified based on their molecular size in comparison to recent published literature on influenza virus purification (Gerl et al., 2012; LeBouder et al., 2008; Shaw et al., 2008). Initial SEM pictures were taken from negative stained purified MDCK grown influenza virus A/Aichi/2/68 H3N2 P10 virus particles (fixed

in 1% glutaraldehyde in 1xPBS) with the help from Weifun Cheong (National University of Singapore) (Supplementary Figure 7-2).

3.2.4 Lipid extraction of purified influenza virus particles

Lipids of purified influenza virus particles were extracted using a modified Bligh and Dyer protocol (Bligh and Dyer, 1959; Chan et al., 2008) as described in chapter 2. 150µl of influenza virus preparations were split into 50µl replicates in fresh centrifuge tubes (Axygen Inc, California, USA) and 600ul of choloroform:methanol (1:1 v/v) were added. Samples were mixed for 1 hour at high speed and at 4^{o}C using a ThermoStat mixer (Eppendorf, Hamburg, Germany). Subsequently, 300µl of chloroform and 200µl of KCl were added, followed by 2 min centrifugation (9000rpm) at 4^{o}C in a bench top centrifuge (Eppendorf, Hamburg, Germany). Samples were dried under vacuum using a miVac Duo Concentrator (Genevac Ltd, Suffolk, UK) and stored at -80^{o}C until further analysis by mass spectrometry.

Samples consisted of the following biological replicates (Supplementary Table 7-3): for A549 grown H1N1 virus: two independent experiments split into three replicates (n=6); for MDCK grown influenza virus A/PR/8/34 H1N1: one preparation split into three replicates (n=3); for influenza virus A/Aichi/2/68 H3N2 P0 and P10 strains: three independent experiments split into three replicates (n=9 for each virus strain: 1 replicate of each virus and independent experiment (n=3) was used for high resolution quadrupole time of flight (QTOF) analysis; 2 replicates of each virus and independent experiment (n=6) were used for targeted HPLC-MS/MS (operated in MRM mode)).

3.2.5 Quantitative analysis by HPLC-MS/MS (operated in MRM mode)

Dried virus lipid extracts were dissolved in 60µl of chloroform:methanol (1:1 v/v). Targeted analysis of 159 species of phospho- and sphingolipids from purified influenza virus particles and data analysis were conducted as described in chapter 2. Two independent experiments with three replicates each were used for the lipid analysis of purified A549 grown influenza virus A/PR/8/34 H1N1 (n=6), whereas three independent experiments with two replicates each were analysed to determine the lipid composition of the two different influenza virus A/Aichi/2/68 H3N2 P0 and P10 strains (n=6 for each virus strain).

3.2.6 Untargeted analysis of PC lipid species using a high resolution QTOF mass spectrometer

After testing the technical reproducibility, each of the three biological replicates of influenza virus A/Aichi/2/68 H3N2 P0 and P10 viruses were analysed (n=3 per virus strain). Dried virus lipid extracts were dissolved in 60µl of solvent B (95% acetonitrile in water containing 25mM ammonium formate pH 4.6) and 20µl of sample were mixed with 20µl of DMPC standard resulting in a final standard concentration of 10µg/ml. Untargeted high resolution mass spectrometry coupled to liquid chromatography was performed using an Agilent 1200 series HPLC-Chip LC system connected to an Agilent 6540 QTOF mass spectrometer (Agilent Technologies, California, USA). A custom synthesized HILIC chip with a 160nl trapping column and a 75µmx150mm analytical column consisting of Amide-80

stationary phase with 5µm particle size and 80Å pore size (Tosoh Bioscience LLC, Pennsylvania, USA) was used for lipid separation. The chip cube was operated in back flush mode and the run time per sample was 19 minutes. 0.4µl of samples were injected onto the trapping column by a capillary pump. Lipid separation was performed by a gradient elution of two mobile phases (solvent A: 50% acetonitrile in water containing 25mM ammonium formate *pH* 4.6; solvent B: 95% acetonitrile in water containing 25mM ammonium formate *pH* 4.6) controlled by a nano pump. Samples were injected with 100% solvent B for 1.5 minutes in the enrichment column at a flow rate of 4µl/minute. Then the valve was switched to place the trapping column in line with the analytical column and samples were eluted at a flow rate of 400nl/minute, first with 85% solvent B for 1.5 minutes, then with 80% solvent B for 8.5 minutes. Subsequently, the mobile phase was changed to 100% solvent A for 2 minutes and the column was re-equilibrated by 100% solvent B for 5.5 minutes. Separated lipids were introduced into the Agilent 6540 QTOF mass spectrometer operated in positive ion mode by ESI and voltage was set at 1800V; temperature at 300°C; drying gas at 4l/min and fragmentor voltage set at 175V. The instrument was operated in auto MS/MS mode at fixed collision energy. MS and MS/MS spectra were acquired in the range of m/z 110-1300 and at an acquisition rate of 4spectra/second and 2spectra/second respectively. Reference masses (121.05087300 and 922.00979800) were simultaneously injected for automatic mass correction during the analysis.

For data analysis, only PC species were considered. Recorded mass spectra of PC species were extracted based on their elution time (7 to 7.5 minutes) with an intensity threshold of 10. The data was imported into Excel (Microsoft, Washington, USA) and

two different data analysis methods were performed. In the first method, mass spectra from 700 to 850 m/z were plotted and represented in relation to the highest intensity peak (aPC34:1). PC species were identified based on their exact mass and on a previously established list of 36 PC species in mammalian cells (Kuerschner et al., 2012). In the second approach, the 36 identified PC intensities were first normalized to the spiked internal DMPC standard and finally, to the total measured PC amount. Significantly different levels of PC species between the two influenza virus strains were identified by a paired Student's t-test (two-tailed; $p<0.05$) only including species that had the same trend in all three independent experiments. Similarly to the time course experiment (Chapter 2), species having the same trend in all three independent experiments were determined by calculating a log(P10/P0) value for each pair (n=3) and the interval [Average(log(P10/P0))-Stdev(log(P10/P0)); Average(log(P10/P0))+StdDev(log(P10/P0))] must not include zero. Significant PC species were represented in a heat plot calculated by the log(P10/P0) ratios and plotted by an in-house developed MATLAB algorithm (Bowen Li, National University of Singapore) (MathWorks, Massachusetts, USA).

3.2.7 Hierarchical clustering of lipid species

The MRM data from eight independent experiments describing virulence (differences between influenza virus A/Aichi/2/68 H3N2 P0 and P10 strains; 3 independent experiments), viral lipids (the lipid profile of influenza virus A/PR/8/34 H1N1 compared to its A549 producer cell; 2 independent experiments) and host response (virus induced changes in A549 cells at 18hpi and 24hpi; three independent

experiments) were considered for clustering. Lipid species with missing values were excluded which resulted in a list of 146 lipid species. An average of log(fold-ratios) for each lipid class in a given experiment was calculated. Three log(H3N2 P10/H3N2 P0) were calculated from duplicates in the three independent experiments (Supplementary Table 7-4). Six log(H1N1/A549) were calculated from two independent preparations of purified virus particles (three replicates in each experiment) and three independent experiments of mock infected A549 cells at 12hpi (three replicates in each experiment). The two H1N1 preparations were separately compared to the three independent experiments of mock infected A549 cells at 12hpi and represented viral lipids (Supplementary Table 7-4). Six log(H1N1/mock) were calculated from triplicates in the three independent experiments describing influenza virus induced changes (host response) at 18 and 24hpi (Supplementary Table 7-4). Subsequently, the data was clustered by hierarchical clustering using Pearson correlation distances (uncentered) with average-linkage implemented in the open ware clustering software *Cluster3.0* (de Hoon et al., 2004). Since there are 2^{N-1} (2^{145}) ordering consistent with any tree of N (146) items (lipid species), a GORDER value consistent with the order of the input data was assigned. The input data was sorted according to lipid classes (PS, PI, GM3, aPE, ePE, aPC, ePC, SM, Cer, GlcCer) followed by saturation and chain length and the assigned GORDER values increased for each lipid species based on its position in the list order (1 to 146). This ensured that the lipid order produced by clustering was as close as possible (without violating the structure of the dendrogram) to the original lipid order.

The calculated dendrogram was visualized using the open ware software *Java TreeView* (Saldanha, 2004) with the colours red (upregulation), blue (downregulation)

and white (no change). Patterns in identified clusters were further analysed by Excel (Microsoft, Washington, USA).

3.2.8 Determination of IC_{50} of LJ001 and JL103 by plaque assay

Antiviral compounds LJ025 (negative control), LJ001 and JL103 were kindly provided by our collaborators Frderic Vigant and Benhur Lee (University of California, Los Angeles, USA). 10mM stock solutions of LJ025, LJ001 and JL103 were prepared by dissolving the compounds in DMSO. The same batch of purified MDCK grown influenza virus A/PR/8/34 H1N1 virus was used for all three independent experiments. 3 fold serial dilutions of compounds were prepared in 440µl of serum free DMEM GlutaMAX™ to obtain 2x concentrations of compounds to be tested. The concentrations of LJ025 and LJ001 were in the micro molar range (10µM, 3.33µM, 1.11µM, 0.37µM, 0.12µM and DMSO control) whereas the concentrations for JL103 were in the nano molar range (0.1µM, 0.033µM, 0.011µM, 0.0037µM, 0.0012µM, DMSO control). Viruses were also prepared in 440µl of serum free DMEM GlutaMAX™ ($5x10^5$pfu/ml) and afterwards added to the previously prepared serial dilutions of LJ025, LJ001 and JL103. Viruses and compounds were incubated in transparent centrifuge tubes under light exposure for 10 minutes. Subsequently, 10 fold serial dilutions (10^{-1} to 10^{-4}) of treated viruses were prepared in 261µl of serum free DMEM GlutaMAX™ supplemented with 50u/ml penicillin, 50µg/ml streptomycin and 2µg/ml TPCK trypsin. Plaque assay was done in triplicates per each compound and treatment condition and confluent monolayers of MDCK cells which were seeded 1 day prior into 24-well plates were infected with 200µl of virus

dilutions. The inoculum was removed after 1 hour, exchanged with 2.4% Avicel in 2xDMEM (50u/ml penicillin, 50µg/ml streptomycin & 1µg/ml TPCK Trypsin) and incubated for another 60 to 70 hours at 5% CO_2, 37^{o}C. Avicel containing media was aspirated and cells were fixed with 4% formaldehyde for 20 minutes. Then, fixed cells were washed twice with 1x PBS and stained for ten minutes with 1% crystal violet dissolved in 20% methanol and water. The final virus concentration in each treatment condition and replicate was calculated to be $2.41x10^5$ pfu/ml and the observed average virus titre in all control samples across three independent experiments was $1.27x10^5$ pfu/ml. Data was plotted relative to the control samples and IC_{50} of LJ001 and JL103 were determined by our collaborator Frederic Vigant (University of California, Los Angeles, USA) using GraphPad PRISM^{TM} (GraphPad Software Inc, California, USA).

3.2.9 Mass spectrometry analysis of oxidized lipids in influenza virus envelopes

Two independent experiments were performed using two independent purified MDCK grown influenza virus A/PR/8/34 H1N1 preparations. 120µl of purified viruses (in 1xPBS) were divided into 6x20µl aliquots (2 for LJ025; 2 for LJ001; 2 for JL103) and 20µl of 2x concentrations (10µM) of compounds in 1xPBS were added to obtain a final treatment concentration of 5µM. Viruses were incubated with 5µM compounds for 1 hour under light exposure, followed by the addition of 600µl of chloroform:methanol 1:2 (v/v). Subsequent steps were performed at 4^{o}C and samples were mixed under vacuum on a ThermoStat mixer (Eppendorf, Hamburg, Germany). Afterwards, 300µl of chloroform and 200µl of distilled water were added, mixed for another 15 minutes and afterwards spun down for 2 minutes at 9000rpm. Samples

were dried under vacuum using a miVac Duo Concentrator (Genevac Ltd, Suffolk, UK) and stored at -80^{o}C until further analysis by mass spectrometry. Mass spectrometry was performed with the help of Guanghou Shui (National University of Singapore) and samples were analysed using a high resolution Thermo LTQ-Orbitrap mass spectrometer (Thermo Fisher Scientific Inc, Massachusetts, USA) and an ABI 3200 QTRAP mass spectrometer (Applied Biosystems, California, USA) after liquid chromatography separation (Davis et al., 2008; Shui et al., 2011b). Data was represented either as a molar fraction of the total amount of measured lipids or as a single stage positive ion mass spectrum (over a m/z range of 1 Dalton).

3.3 Results & discussion

3.3.1 The composition of A549 produced influenza A virus H1N1

A549 grown influenza virus A/PR/8/34 H1N1 virus was purified over a sucrose gradient as described previously (Shaw et al., 2008) (Figure 3-1A & Supplementary Figure 7-1). Virus purity was assessed by SDS gel electrophoresis and coomassie blue staining. We detected six major bands which corresponded to the molecular weight of the six most abundant influenza virus particle proteins such as hemagglutinin (HA0, HA1 & HA2), NP, NA and M1 (Figure 3-1B). There were also two fainter bands visible which did not correspond to any virus proteins but were identified as actin and annexins based on their size and recent literature on purified influenza virus particles (LeBouder et al., 2008; Shaw et al., 2008) (Figure 3-1B). We considered our influenza virus preparations pure due to the high reproducibility (similar results were obtained in independent replicate experiments and using H1N1 as well as H3N2 influenza virus strains produced in MDCK cells; see below) and the high consistency with previous studies using pure influenza virus particles (LeBouder et al., 2008; Shaw et al., 2008). Furthermore, SEM pictures taken from MDCK grown purified influenza virus A/Aichi/2/68 H3N2 P10 (see below) showed clear virus particles devoid of cellular debris (Supplementary Figure 7-2). For lipid analysis, two independent experiments with three replicates each were performed (n=6) (Supplementary Table 7-3). Mass spectrometry analysis (measuring 159 MRM transitions; excluding odd chain aPC species) of all samples was conducted in the same run and collected data were compared to the average of serum starved mock infected cells at 12hpi (n=9)

(Supplementary Table 7-1) from the previously described time course experiment (Chapter 2). The phospholipid composition of influenza virus particles was characterized by decreased levels of total PC, PE and PI content and slightly increased levels of PS in comparison to the uninfected A549 producer cell (Figure 3-1C&D). There was a general enrichment of ether linked lipid species with only a relatively small decrease of ePE and a marginal increase in ePC species. SM, GlcCer and Cer were generally enriched in influenza virus with SM being the most abundant lipid class. On the other hand, there was an overall decrease in ganglioside GM3 species as compared to uninfected producer cells (Figure 3-1C&D). The observed trends were not only consistent with recent literature on the lipid composition of influenza virus particles (Blom et al., 2001; Gerl et al., 2012; Polozov et al., 2008; Scheiffele et al., 1999; van Meer and Simons, 1982) but also supported our observations from influenza virus infected A549 cells. The nearly absence of ganglioside GM3 species and the enrichment of dihydrosphingolipid, SM and GlcCer species in influenza virus envelopes were in line with a very recent study (Gerl et al., 2012) and also reflected the host response during influenza virus infection (Figure 3-1C&D).

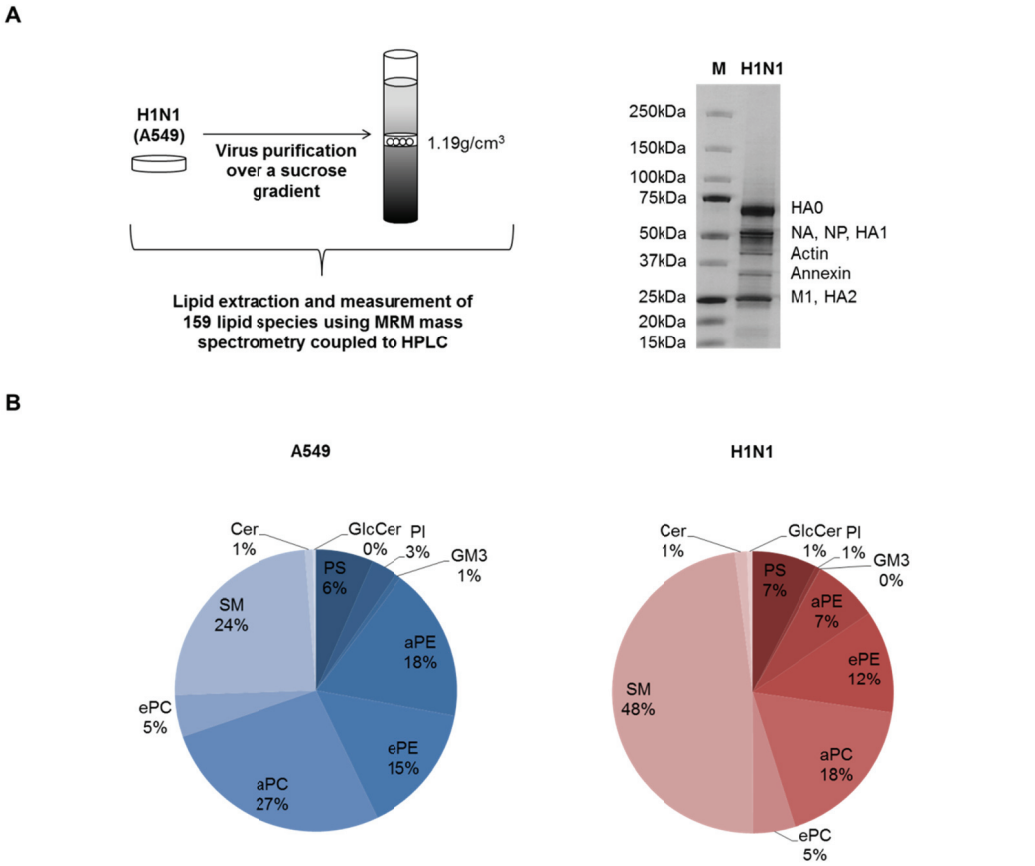
A
H1N1
(A549)
Virus purification
over a sucrose
gradient
1.19g/cm3
Lipid extraction and measurement of
159 lipid species using MRM mass
spectrometry coupled to HPLC
M
H1N1
250kDa
150kDa
100kDa
75kDa
50kDa
37kDa
25kDa
20kDa
15kDa
HA0
NA, NP, HA1
Actin
Annexin
M1, HA2
B
A549
H1N1
Cer 1%
GlcCer 0%
PI 3%
GM3 1%
PS 6%
SM 24%
aPE 18%
ePC 5%
ePE 15%
aPC 27%
Cer 1%
GlcCer 1%
PI 1%
GM3 0%
PS 7%
aPE 7%
ePE 12%
SM 48%
aPC 18%
ePC 5%
C
Molar concentration [%]
0.6
0.5
0.4
0.3
0.2
0.1
0
PS
aPE
ePE
aPC
ePC
SM
PI
GM3
Cer
GlcCer
0.05
0.04
0.03
0.02
0.01
0

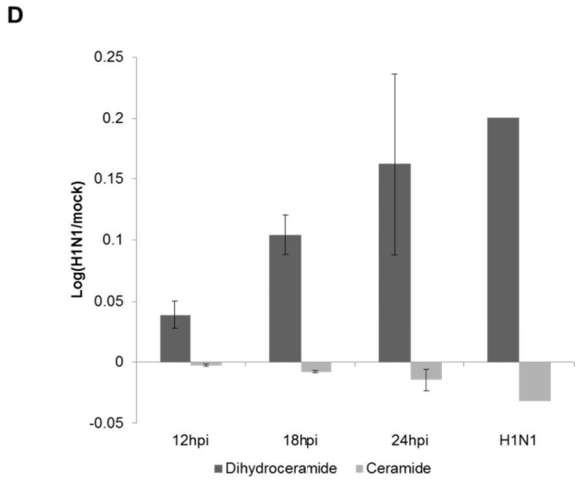

Figure 3-1: Lipidomics of influenza virus A/PR/8/34 H1N1 produced from lung epithelial cells. **(A)** Influenza virus A/PR/8/34 H1N1 was grown in A549 cells, purified over a sucrose gradient (Shaw et al., 2008) and subsequently, lipids were analysed by HPLC-MS/MS (operated in MRM mode). **(B)** Virus purity was assessed by SDS gel electrophoresis and the six major influenza virus proteins (HA0, NA, NP, HA1, M1, HA2) were detected. **(C)** The lipid profile of influenza virus A/PR/8/34 H1N1 (red) was compared to the lipid composition of uninfected A549 cells at 12hpi (blue). Error bars represent standard deviation of three biological replicates (A549; n=9) and two biological replicates (H1N1; n=6) respectively. Unpaired Student's t-test was used to calculate statistically significance (two-tailed); **p<0.05*; ***p<0.005*; ****p<0.0005*. **(D)** Sphingolipid species (Cer, GlcCer & SM) were normalized to the total amount of measured sphingolipids and analysed according to their backbone structure. Influenza viruses were significantly enriched in dihydroceramide containing sphingolipids (two-tailed; *p<0.001*) but decreased in ceramide containing sphingolipids (two-tailed; *p<0.001*) as calculated by an unpaired Student's t-test. The virus was compared to the data of the time course experiment log(H1N1/mock) and the differences were represented as a log(H1N1/$A549_{12hpi}$). Error bars represent standard deviations.

3.3.1.1 The increased ePC/aPC ratio was specific for influenza virus particles

The distinct remodelling of PC species in influenza virus infected A549 cells was also evident in purified influenza virus particles (Figure 2-1D, Figure 3-1C&D & Figure 3-2). The decrease in aPC species was not surprising due to the relatively low levels of this lipid class at the plasma membrane and it also confirmed the previous findings by Gerl et al (2012). It was intriguing that we also observed a slight but significant increase of ether linked PC species in the virus envelope which was in line with the upregulation of ether linked PC species during the course of an influenza virus

infection (Figure 2-1D & Figure 3-1C&D). This was in contrast to Gerl et al's study (2012) which did not report any significant changes regarding ePC species. Nevertheless, when looking at the ratio of ether linked to ester linked PC species in influenza virus particles, it became evident that both results were in agreement and consistent with the idea of an influenza virus dependent remodelling of PC species (Figure 3-2).

We then asked ourselves whether this remodelling of PC species was influenza virus specific or whether it was just a common feature of enveloped viruses. For this purpose, we collected published and unpublished data on the lipid composition of several enveloped viruses in comparison to their producer cells including HIV and murine leukemia virus (MLV) (Chan et al., 2008)[1], VSV and SFV (Kalvodova et al., 2009) as well as HCV (Merz et al., 2011) and dengue virus[2]. We calculated their respective ePC/aPC ratios to make the different lipidomics data sets comparable since comparison of absolute values would not have been possible due to differences in analysis platforms. This clearly demonstrated that influenza virus particles were the only viruses with a higher ePC/aPC ratio as compared to their producer cells (unpaired Student's t-test; two-tailed; $p<0.005$) suggesting a functional and specific link between influenza virus replication and PC class remodelling (Figure 3-2D). We observed similar trends when we analysed purified MDCK grown influenza viruses including the influenza virus A/PR/8/34 H1N1 strain as well as influenza virus A/Aichi/2/68 H3N2 P0 and P10 strains (Figure 3-2) which are discussed in further

[1] The lipid profiles of two MLV strains (43D and 17-5) produced from NIH cells were part of a collaborative effort with Hung Fan at the University of California, Irvine.
[2] The lipid profile of dengue virus was part of a collaborative effort with Zhang Qian and Shee Mei Lock at Duke-NUS, Singapore and has recently been submitted to *JCB* (Qian et al, 2012).

details below. On the contrary, there was no such specific remodelling regarding the high levels of ePE and low levels of aPE found in influenza virus particles, which rather supported the notion that enrichment of ePE species is a general feature of enveloped viruses (Brugger et al., 2006; Chan et al., 2008; Kalvodova et al., 2009). One explanation for this finding might be the biophysical properties of PE lipids, as they can intrinsically organize into a hexagonal phase which facilitates membrane curvature and membrane fusion (Chan et al., 2010).

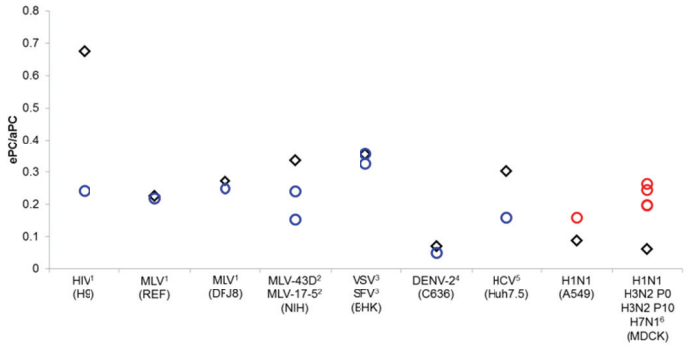

	HIV[1] (H9)	MLV[1] (REF)	MLV[1] (DFJ8)	MLV 43D[2] (NIH)	MLV 17-5[2] (NIH)	VSV[3] (BHK)	SFV[3] (BHK)	DENV[4] (C636)	HCV[5] (Huh7.5)	H1N1 (A549)	H1N1 (MDCK)	H3N2 P0 (MDCK)	H3N2 P10 (MDCK)	H7N1[6] (MDCK)
ePC/aPC (Virus)	0.24	0.22	0.25	0.24	0.15	0.33	0.36	0.05	0.16	0.16	0.26	0.20	0.25	0.20
ePC/aPC (Cell)	0.68	0.23	0.27	0.34	0.34	0.36	0.36	0.07	0.30	0.09	0.06	0.06	0.06	0.06
$\Delta_{Virus-Cell}$	**-0.44**	**-0.01**	**-0.02**	**-0.1**	**-0.19**	**-0.03**	**0**	**-0.02**	**-0.14**	**0.07**	**0.2**	**0.14**	**0.19**	**0.14**

Non-flu: average ($\Delta_{Virus-Cell}$)=-0.11±0.14; Flu: average ($\Delta_{Virus-Cell}$)=3.15±0.05; unpaired Stucent's t-test (two-tailed; *p<0.001*)

Figure 3-2: ePC/aPC ratio of several enveloped viruses. ePC/aPC ratios of influenza viruses (red circles) were compared to other enveloped viruses (blue circles) and represented in relation to uninfected producer cells (black diamonds); [1](Chan et al., 2008), [2](Viruses provided by Hung Fan and lipid analysis performed by us), [3](Kalvodova et al., 2009), [4](Viruses provided by Shee Mei Lock and lipid analysis performed by us; Qian et al, 2012), [5](Merz et al., 2011), [6](Gerl et al., 2012). The difference $\Delta_{Virus-Cell}$ was significant between flu viruses and non-flu viruses (unpaired Student's t-test; two-tailed; $p<0.001$).

3.3.1.2 The ceramide levels were high in purified influenza virions when compared to other enveloped viruses

We noted relatively high levels of ceramide species in purified influenza virus particles from A549 cells but no specific upregulation of ceramide species in infected A549 cells (Figure 2-1B&D). In our study, there were around 1.7 times higher ceramide levels in H1N1 influenza particles whereas the H7N1 virus analysed by Gerl et al (2012) had similar levels in comparison to the lipid composition of their host cells (Figure 3-3A). The two other analysed H3N2 strains (discussed in further details below) exhibited a similar enrichment of ceramide as compared to the analysed MDCK producer cell by Gerl et al, 2012 (Figure 3-3A). Again, this was in contrast to other enveloped viruses such as HIV, MLV, VSV, SFV which had around three times lower ceramide levels (unpaired Student's t-test; two tailed; $p<0.02$) than their producer cells (Chan et al., 2008; Kalvodova et al., 2009). This suggested that ceramide species were locally enriched at the plasma membrane budding site and that they represented an influenza virus specific requirement during the virus life cycle (Figure 3-3A).

The reported close interaction between ceramide and cholesterol in membranes and subcellular organelles (Castro et al., 2009; Goni and Alonso, 2009; Guan et al., 2009; Kolter and Sandhoff, 2010; Megha and London, 2004; Silva et al., 2009; Yu et al., 2005) prompted us to further investigate their relationship in enveloped viruses. Since we did not analyse cholesterol levels in the A549 grown influenza virus, we solely focused on the published literature. We first calculated an absolute

ceramide/cholesterol ratio for VSV and SFV (Kalvodova et al., 2009), influenza virus H7N1 (Gerl et al., 2012) and their producer cells and found a much higher ratio in influenza virus particles (0.007) as compared to the ratios of VSV, SFV and producer cells (0.0015-0.0025) (Figure 3-3B). At first, this did not seem to be surprising since VSV and SFV are viruses which do not bud from classical "lipid raft" domains (Kalvodova et al., 2009) whereas influenza virus has been thought to be "raft-dependent" (Gerl et al., 2012). For that reason, we decided to additionally include other plasma membrane budding viruses which are "raft-dependent" such as HIV and MLV (Chan et al., 2008). Since the method to normalize cholesterol was different in the study describing the lipid composition of HIV and MLV (Chan et al., 2008), we came up with a new concept to investigate the ceramide/cholesterol ratio in relation to the plasma membrane. We calculated an enrichment value (*EV*)[3] for HIV and MLV (Chan et al., 2008), VSV and SFV (Kalvodova et al., 2009), avian leukosis virus (ALV) (Robin Chan, *unpublished* data) and H7N1 (Gerl et al., 2012) which confirmed the high enrichment of ceramide species in influenza viruses (Figure 3-3C). Surprisingly, HIV and MLV had an *EV* in the range of VSV and SFV, whereas ALV had also a high ceramide/cholesterol ratio comparable to the ratio found in the H7N1 influenza virus. Considering that ALV and influenza virus are dependent on a low *pH* (late endosomal compartments; $pH<5.6$), but VSV and SFV on an intermediate *pH* (early endosomal compartments; $pH<6.4$) and MLV and HIV on a neutral *pH* (plasma membrane or early endosomal compartments; $pH<7.4$) for fusion (Mercer et al., 2010), we hypothesized that the ceramide/cholesterol ratio could be representative of the virus entry pathway. This was also reflected by the low ceramide/cholesterol ratio

[3] $EV = \frac{\frac{ceramide\,(virus)}{ceramide\,(plasma\,membrane)}}{\frac{cholesterol\,(virus)}{cholesterol\,(plasma\,membrane)}}$

with the nearly absence of ceramide in purified HCV virus particles which fuse in early endosomal compartments (Merz et al., 2011).

Functional differences with regard to cholesterol and ceramide dependency were observed during influenza virus and HIV entry into host cells. For instance, accumulation of ceramide species in host cells facilitated influenza virus infection but, in turn, abolished HIV replication due to an increased activity of host cell endocytosis (Finnegan and Blumenthal, 2006). This was in line with the finding that ceramide production by sphingomyelinase activity inhibited HIV fusion (Finnegan et al., 2007). On the other hand, depletion of cholesterol from host cells inhibited HIV virus entry due to impaired clustering of co-receptors into "lipid rafts" (Nguyen and Taub, 2002; Popik et al., 2002). Different requirements with regard to cholesterol and ceramide during virus entry could be explained by the cellular gradient of ceramide and cholesterol within eukaryotic cells. It has been proposed, that the highest enrichment of cholesterol is found at the plasma membrane with a gradual decrease towards the cell body, whereas ceramide is low at the plasma membrane but increases along the endocytic pathway with highest levels in highly acidic compartments due to the activity of sphingolipid degrading enzymes (Figure 3-2D) (Kolter and Sandhoff, 2010). This is illustrated by a recent lipidomics study where the fraction of intracellular vesicles (dense microsomes; DM) had a much higher absolute ceramide/cholesterol ratio than the plasma membrane (Dennis et al., 2010) (Figure 3-3B).

We propose that the virus lipid composition mimics the ceramide and cholesterol content of intra-/extracellular vesicles and fusion occurs more efficiently if the

ceramide/cholesterol ratios between the virus and the target membrane are similar. Such a model could be extrapolated to the general trafficking and membrane mixing of intracellular vesicles (Figure 3-2D). For example, microvesicles (MV) which are derived by shedding or budding from the plasma membrane by a similar mechanism harnessed by retroviruses (Wurdinger et al., 2012), transfer their intraluminal content to neighbouring cells by direct fusion at the plasma membrane (Nabhan et al., 2012). Interestingly, their ceramide/cholesterol ratio is low and similar to viruses (e.g. HIV and MLV) which directly fuse at the plasma membrane (Chan et al., 2008) (Figure 3-3C). In contrast, exosomes which are derived by inward budding from the limiting membrane into the intraluminal space of multivesicular bodies (MVB) are enriched in ceramide due to the action of sphingomyelinases which are essential for this process (Trajkovic et al., 2008; Yuyama et al., 2012). Exosomes are then further released into the extracellular space via the secretory pathway and one could imagine that the high ceramide content of the intraluminal exosomes diminishes the chance of fusion with the secretory endosomal membrane which has decreased ceramide but high cholesterol content (Figure 3-2D) (Klemm et al., 2009). Alternatively, fusion events at late endosomal compartments are dependent on high ceramide levels as shown by the importance of acid sphingomyelinase activity for phago-lysosomal fusion (Schramm et al., 2008; Utermohlen et al., 2008; Utermohlen et al., 2003). Synaptic vesicles have also a high ceramide/cholesterol ratio but their fusion occurs at the presynaptic membrane (Takamori et al., 2006) (Figure 3-3B) which would not support the proposed concept (Figure 3-2D). However, it has been shown that ceramidase is required for efficient completion of vesicle priming and fusion (Rohrbough et al., 2004) which would suggest that ceramidase activity decreases the ceramide content (Figure 3-2D) and as a result, the ceramide/cholesterol ratio in the synaptic vesicle, to

mediate fusion at the plasma membrane which is made of a low ceramide/cholesterol ratio (Figure 3-3B).

It is well understood, that the ceramide/cholesterol ratio is not the sole driver of vesicular membrane mixing and fusion but, for example, it could possibly influence the fluidity and rigidity of the direct lipid environment of virus fusion proteins (Ge and Freed, 2011; Luan and Glaser, 1994). It has been shown, that transmembrane domains of virus fusion proteins are critical determinants for virus entry (Armstrong et al., 2000; Bissonnette et al., 2009; Gravel et al., 2011; Popa et al., 2012). Recently, transmembrane domains have also been implicated to have specific requirements and affinities for certain lipid species which mediate protein functionality and trafficking (Contreras et al., 2012; Ronchi et al., 2008). In this respect, our proposed concept argues in favour of a link between virus exit and virus entry. The induced ceramide/cholesterol ratio required for budding is a determinant for virus fusion since it determines the lipid environment of HA which could be favourable for its function. Furthermore, the high ceramide content might be also responsible for the stability and transmission of influenza viruses at low temperatures due to induction of gel like phases (Castro et al., 2009; Lowen et al., 2007; Polozov et al., 2008). It would be interesting to see whether activities of endosomal enzymes such as sphingomyelinases further increase the ceramide enrichment in influenza virus envelopes, to trigger efficient virus fusion in late endosomal compartments.

3. Lipidomics of Influenza Virus

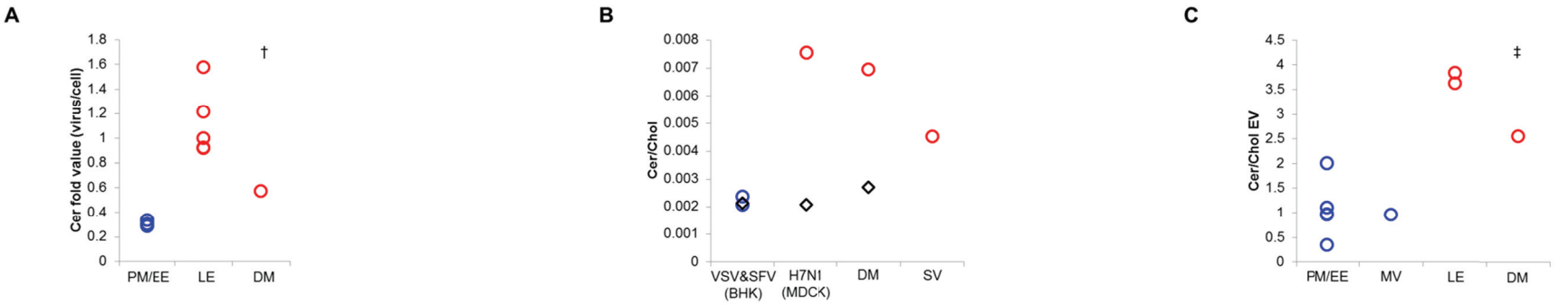

		Fusion at the plasma memrbane (PM) or early endosomes (EE)					Fusion at late endosomes (LE)					Cellular vesicles		
		HIV[1] (H9)	HIV[1] (MDM)	MLV[1] (REF)	VSV[2] (BHK)	SFV[2] (BHK)	ALV[3] (DFJ8)	H1N1 (A549)	H3N2 P0 (MDCK)	H3N2 P10 (MDCK)	H7N1[4] (MDCK)	MV[1] (MDM)	Microsomes[5] (RAW264.7)	Synaptic Vesicle[6]
	Cer (Virus)	1.5		1.4	0.09	0.1	2.3	1.4	1.2	1.1	1.1*		0.09	
	Cer (Cell)	5.3		4.2	0.3	0.3	1.9	0.9	1.2	1.2	1.2*		0.16	
A	**Fold value**	**0.3**		**0.3**	**0.3**	**0.3**	**1.2**	**1.6**	**1.0**	**0.9**	**0.9**		**0.57**	
	Cer (Virus)				0.09	0.1					0.4		0.09	0.1
	Chol (Virus)				43.6	42.4					51.8		13.5	29.0
B	**Cer/Chol**				**0.002**	**0.002**					**0.008**		**0.007**	**0.005**
	Cer (Virus)	1.5	1.6	1.4	0.09	0.1	2.3				0.39	2.3	0.09	
	Cer (PM)	1.6	0.6	0.8	0.09	0.09	0.3				0.09	0.6	0.09	
	Chol (Virus)	0.14	0.12	0.11	43.6	42.4	0.06				51.8	0.36	13.5	
	Chol (PM)	0.05	0.09	0.06	42.1	42.1	0.03				45.2	0.09	33.3	
C	**Cer/Chol EV**	**0.34**	**2.0**	**0.96**	**0.97**	**1.1**	**3.8**				**3.6**	**0.96**	**2.6**	

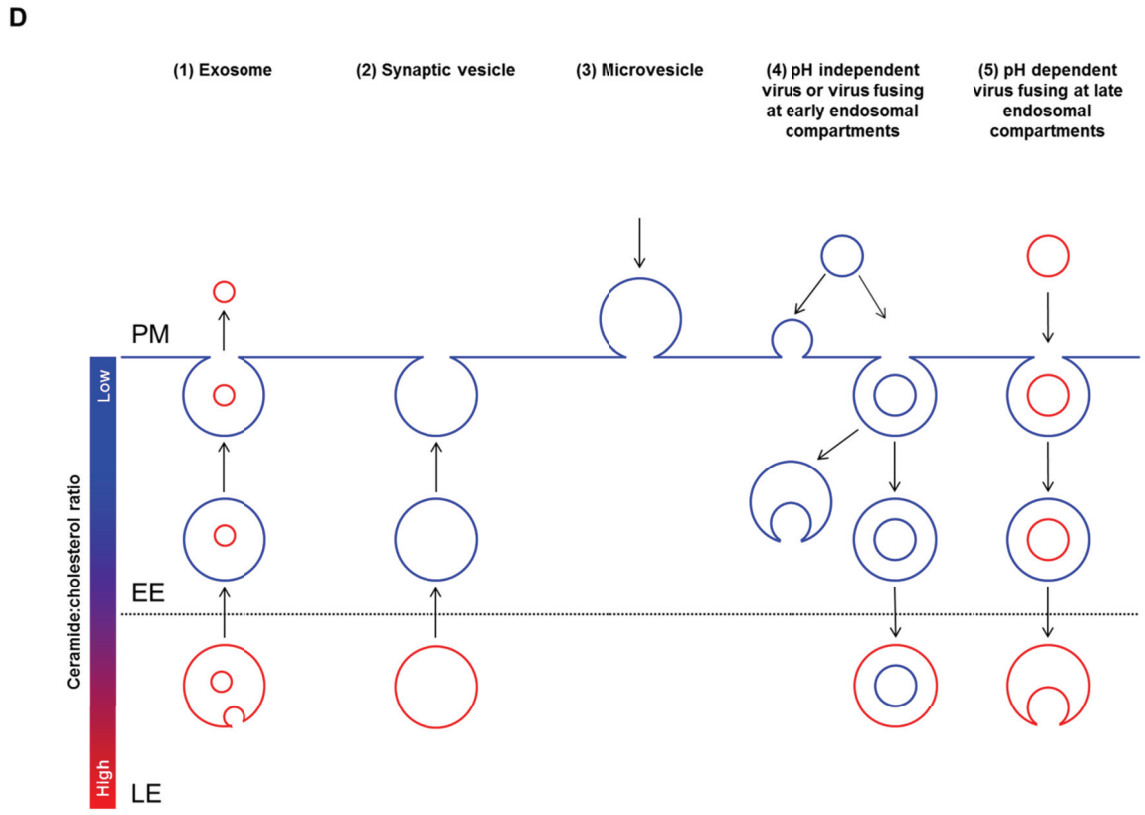
D
(1) Exosome
(2) Synaptic vesicle
(3) Microvesicle
(4) pH independent virus or virus fusing at early endosomal compartments
(5) pH dependent virus fusing at late endosomal compartments
PM
EE
LE
Low
High
Ceramide:cholesterol ratio

Figure 3-3: Enrichment of ceramide in enveloped viruses and cellular vesicles (Page 91&92). (A) An enrichment value of total ceramide content in enveloped viruses and cellular vesicles in comparison to producer cells was calculated. [*]Values from this study were normalized to our list of measured lipid classes to make the results comparable. The normalized values for MDCK cell lines were also used to compare MDCK grown viruses analysed in this study to producer cells (H1N1, H3N2 P0, H3N2 P10). [†]Depicts a significant difference calculated by an unpaired Student's t-test between plasma membrane (PM)/early endosome (EE) entering viruses (blue) and late endosome (LE) entering viruses and dense microsomes (DM) vesicles (red) (two-tailed; $p<0.005$). **(B)** An absolute ceramide/cholesterol (Cer/Chol) ratio was calculated for studies that represented cholesterol and ceramide data in a similar way. Black diamond represents the Cer/Chol ratio of the PM of respective producer cells. **(C)** Data is represented in comparison to the plasma membrane and an enrichment value (EV) as described in the main text has been calculated. [‡]Depicts a significant difference calculated by an unpaired Student's t-test between PM/EE entering viruses plus microvesicles (MV) and LE entering viruses plus DM vesicles (two-tailed; $p<0.05$). [1](Chan et al., 2008); [2](Kalvodova et al., 2009); [3]Robin Chan (*unpublished*); [4](Gerl et al., 2012); [5](Andreyev et al., 2010); [6](Takamori et al., 2006). **(D)** A proposed model of how the ceramide/cholesterol ratio modulates vesicular trafficking as described in the main text. Ceramide (red) and cholesterol (blue) enriched vesicles are presented as part of trafficking pathways in mammalian cells. (1) Exosomes are produced by inward budding due to ceramide generation by sphingomyelinase activity at multivesicular bodies (MVB) (Trajkovic et al., 2008; Yuyama et al., 2012). Exosomes are enriched in ceramide preventing fusion with the limiting secretory vesicle membrane which is high in cholesterol content, but allows their release into the extracellular space. (2) Synaptic vesicles are also high in ceramide content (Takamori et al., 2006) but fusion occurs with the plasma membrane after decreasing the ceramide/cholesterol ratio by ceramidase activity (Rohrbough et al., 2004). (3) Microvesicles are shed from the plasma membrane similarly to retrovirus budding (Nabhan et al., 2012; Wurdinger et al., 2012) and exhibit a high cholesterol content. They transfer their content to target cells by direct fusion at the plasma membrane (Nabhan et al., 2012). (4) Retroviruses exhibit a low ceramide/cholesterol content and enter host cells either by direct fusion at the plasma membrane or by fusion at early endosomal compartment (Miyauchi et al., 2009). Interestingly, retrovirus particles which are targeted to late endosomal compartments do not successfully infect target cells (Finnegan and Blumenthal, 2006). (5) Influenza viruses exhibiting a high ceramide/cholesterol ratio are targeted to late endosomal compartments which also exhibit high ceramide content.

3.3.2 The lipid composition of two different MDCK cell culture derived influenza A virus H3N2 strains: implications for virus severity

The consistent enrichment of certain lipid species in purified influenza virus particles as well as in virus infected cells tempted us to have a closer look at a potential regulatory mechanism. Despite the limited knowledge of how influenza virus impacts host cell lipid metabolism, there are a few reports mainly showing the downregulation of phospholipid biosynthesis (Billharz et al., 2009; Caric-Lazar et al., 1978; Kroeker et al., 2012). In particular, one study investigating changes in host gene expression

induced by different influenza viruses having the same genomic background but carrying distinct NS1 proteins reported that NS1 of the 1918 pandemic virus blocked host lipid metabolism to a greater extent than the NS1 of a less pathogenic influenza virus (Billharz et al., 2009). There is additional evidence that NS1 might be implicated in lipid metabolism due to its interaction with HSD17B4 which is an essential part of the peroxisomal ß-oxidation cascade (Wolff et al., 1996). As a result, we decided to look at the lipid profile of purified influenza viruses carrying the same genetic background but mutations in NS1. We focused on two influenza virus H3N2 strains which differ solely in two point mutations and which exhibit differences in pathogenicity (Narasaraju et al., 2009). In this study, an influenza A strain A/Aichi/2/68 H3N2 was adapted by ten passages in mice which ultimately showed higher virulence with enhanced replication ability caused by non-conservative mutations in HA (Gly218Glu) and NS1 (Asp125Gly) (Narasaraju et al., 2009). Furthermore, the mutation in NS1 (Asp125Gly) has been independently found to be selected upon mouse adaption producing high virus titres with enhanced interferon-ß antagonism (Forbes et al., 2012). We assumed a negligible effect of the mutation in HA (Gly218Glu) on host lipid metabolism since the mutation lies in a region involved in sialic acid linkage recognition, important for entry rather than influenza virus replication within the host cell (Narasaraju et al., 2009).

Virus strains were grown in MDCK cell lines to obtain high virus titres. The mouse adapted and more virulent influenza H3N2 A/Aichi/2/68 virus strain was referred to as P10, and the original H3N2 influenza A/Aichi/2/68 virus strain was referred to as P0. We performed three independent experiments with three replicates for each virus strain. One replicate of each experiment was used for measuring choline containing

lipids by an untargeted approach using a high-resolution QTOF instrument and two replicates of each experiment were analysed by a targeted MRM approach.

3.3.2.1 The ePC/aPC ratio was higher in the more virulent P10 influenza virus strain

In a first approach, we analysed three biological replicates (one replicate of each independent experiment) of both virus strains by high-resolution mass spectrometry to investigate whether remodelling of PC species was also apparent in purified influenza virus particles differing in their NS1 proteins. The data were represented in two ways. Firstly, a mass spectrum normalized to the most abundant peak (aPC 34:1) was plotted for the elution period of PC species (7.0 min to 7.5 min) (Figure 3-4A) and secondly, 36 PC species were identified based on their exact mass, normalized to an internal standard and finally, to the total amount of PC species (Figure 3-4B). Significant differences in lipid levels between the two influenza virus strains were identified by a paired Student's t-test (two-tailed; $p<0.05$) only including species that had the same trend in all three independent biological replicates. Similarly to the time course experiment, species having the same trend in all three independent experiments were determined by calculating a log(P10/P0) value for each pair (n=3) and the interval [Average(log(P10/P0))-StdDev(log(P10/P0)); Average(log(P10/P0))+StdDev(log(P10/P0))] must not include zero. Indeed, we observed a similar remodelling in PC species with an increase in ePC species (e.g. ePC 34:1 and ePC 40:6) but decreased levels of aPC species (e.g. aPC 36:1 and aPC 36:2) (Figure 3-4B). We then also described the data by the ePC/aPC ratio and despite some variations between the three independent experiments (the ePC/aPC ratios in the

first experiment differed slightly from the ratios in the other two experiments) (Figure 3-4C), the differences Δ_{P10-P0} between the P10 and P0 strains were consistent as calculated by a paired Student's t-test (two tailed; $p<0.02$) (Figure 3-4C). This suggested that influenza viruses with different NS1 proteins do not only impact host lipid metabolism but also affect the lipid composition of virus particles.

3.3.2.2 PS, GlcCer and SM species were additionally enriched in the P10 virus strain

To get a better idea of whether NS1 has a more global effect on the lipid composition of purified influenza virus particles, we analysed 159 lipid species using a targeted MRM approach. The data were normalized to the respective internal standards measured for each lipid class and subsequently, to the total amount of measured lipid species. Significant differences were identified using an unpaired Student's t-test (two tailed; $p<0.05$). The P10 virus had a significant increase in most of the PS and GlcCer species but only in some SM and ePC species (Figure 3-5). Instead, there was a general downregulation of aPC species in the more virulent P10 strain as compared to the parent P0 strain and the increased ePC/aPC ratios were consistent in both, the untargeted QTOF and targeted MRM approaches (Figure 3-4C&D). We concluded that the differences in the ePC/aPC ratios between the two virus strains were mainly due to depletion of aPC species rather than an enrichment of ePC species.

3. Lipidomics of Influenza Virus

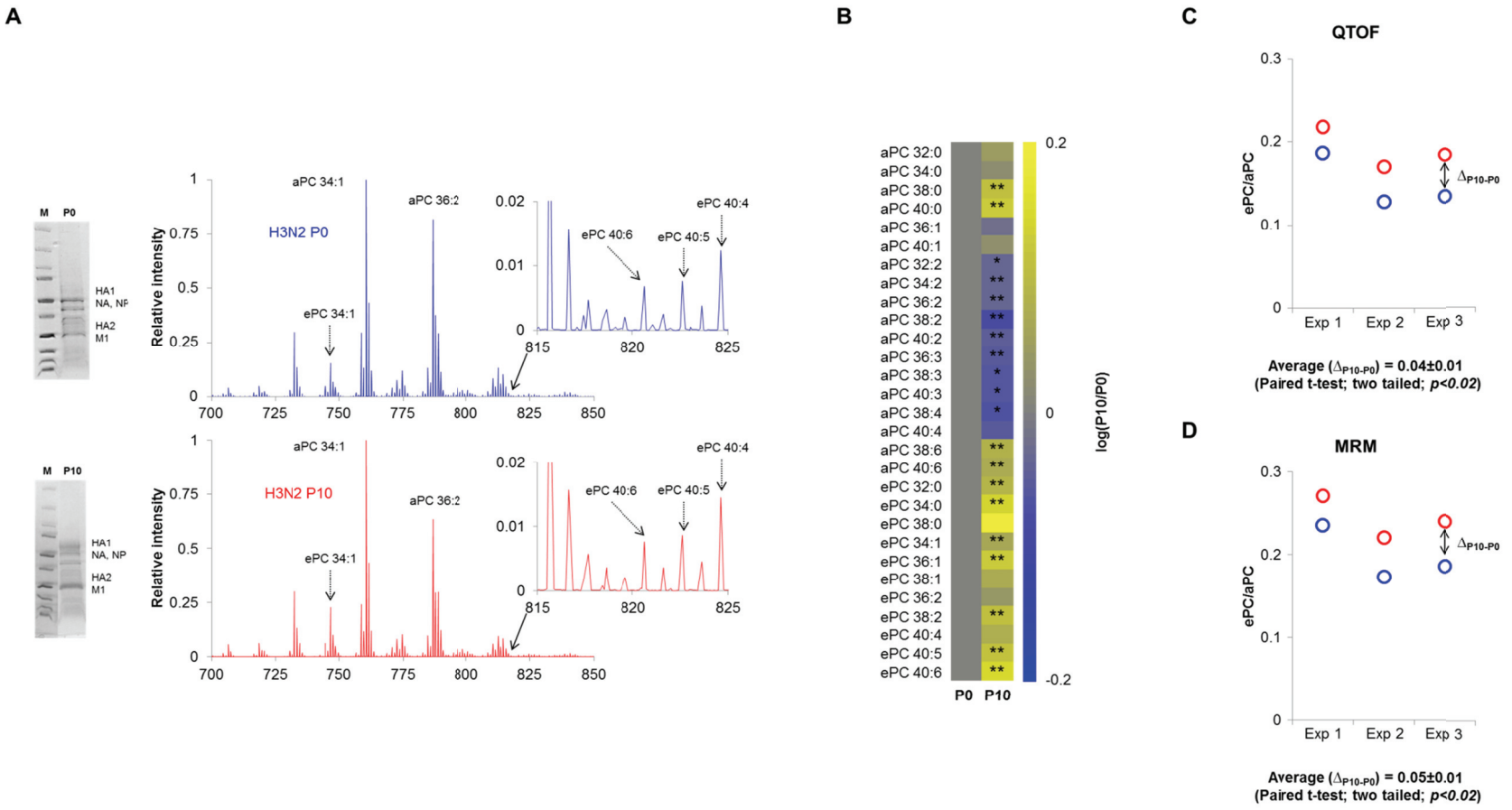

Figure 3-4: Untargeted QTOF approach to identify PC class specific changes between H3N2 P10 and H3N2 P0 strains (Page 97): (A) Untargeted mass spectrum of PC species normalized to the maximum intensity (aPC 34:1). **(B)** Identified PC species were normalized to the total PC intensity and represented as a heat plot showing the log-fold differences between H3N2 P0 and H3N2 P10 strains. Significance levels were calculated by a paired Student's t-test; *(two-tailed; $p<0.1$); **(two-tailed; $p<0.05$). **(C&D)** The ePC/aPC ratios for each pair from three independent experiments were calculated and plotted from QTOF (one biological replicate per condition) and MRM data (average of two biological replicates per condition). The significance levels of the differences between P10 (red) and P0 (blue) $\Delta_{P10\text{-}P0}$ were calculated by a paired Student's t-test.

The increase in GlcCer and some SM and ePC species and the decrease in aPC species clearly followed the same trends as the time course and purified virus lipid data from A549 cells (Figure 2-1, Figure 3-1 & Figure 3-5). On the other hand, the high levels of PS species in the P10 mutant virus were not as striking in the time course and purified virus data from A549 cells even though they also showed an increasing trend. We did not anticipate such strong differences between two viruses only differing in two non-conservative point mutations since one would assume that they would follow similar replication and assembly/budding mechanisms. However, similar trends have been previously observed between different influenza virus strains, but they remained undiscovered (Polozov et al., 2008). In this study, the overall lipid compositions of two different influenza virus strains (Influenza virus A X-31, A/Aichi/68 and influenza virus A/2/Japan/305/57) were analysed by thin layer chromatography (TLC). The X-31 strain showed increased PS and SM levels, but decreased PC levels when compared to the Japan strain, whereas levels of PE species remained unchanged (Polozov et al., 2008).

Our results and their study support the importance of increased sphingolipid but decreased phospholipid metabolism (mainly aPC species) and strengthen the idea of NS1 being a major regulator of host cell lipid metabolism during virus infection. This

is not surprising considering reports showing different kinetics of cell signalling, cellular metabolism and apoptosis induced by different influenza virus strains carrying mutations in NS1 (Ehrhardt and Ludwig, 2009; Gannage et al., 2009; Heynisch et al., 2010; Ritter et al., 2010; Seitz et al., 2010; Zhirnov and Klenk, 2007). For example, it is well understood that induction of apoptosis leads to an upregulation of PS biosynthesis combined with the exposure of PS on the cell surface (Lee et al., 2012; Martin et al., 1995; Shiratsuchi et al., 2000; Yu et al., 2004). More specifically, opposite trends of decreasing aPC but increasing PS species which, in contrary, were not upregulated in virus infected cells, point towards a localized increase of PS biosynthesis at the plasma membrane since PC can be used as a substrate for PS synthase 1 (PTDSS1) which exchanges the choline head group of PC with serine. Serine exchange reactions using PC as a substrate have been reported to additionally occur at the plasma membrane despite their predominant localization to mitochondrial-associated membranes (Mozzi et al., 1997; Siddiqui and Exton, 1992; Vance, 2008). The increase of PS species in the more virulent P10 strain could thus reflect its increased apoptotic potential in virus infected cells.

In addition, metabolites from glycolysis can be redirected into lipid metabolism, especially, PS and sphingolipid biosynthesis through the production of serine from 3-phosphoglycerate and ether lipid biosynthesis by acylation of dihydroxyacetone phosphate. Since induction of glycolysis was retarded in a slower replicating influenza virus strain as compared to a fast replicating strain which expressed different NS1 variants (Ritter et al., 2010), we could argue that more virulent viruses do not only have a greater impact on glycolytic flux but additionally on lipid metabolism. This is supported by gene expression studies showing a greater impact of

more virulent viruses expressing distinct NS1 proteins on lipid metabolism (Billharz et al., 2009).

Serine incorporator (Serinc 1-5) has been proposed to be at the forefront linking glycolysis, PS and sphingolipid biosynthesis together, by providing a membrane embedded scaffold for glycolytic and serine biosynthetic enzymes at various cellular membranes, including the plasma membrane (Inuzuka et al., 2005). Interestingly, Serinc5, also known as TPO1, expression in influenza virus infected cells was dependent on the presence of NS1 (Geiss et al., 2002) and it has been shown to localize to sphingolipid rich domains in cellular membranes including the plasma membrane (Fukazawa et al., 2006; Krueger et al., 1997). Overexpression of Serinc proteins led to the increased incorporation of serine into phosphatidylserine and sphingolipids (Inuzuka et al., 2005). Since the observed differences in the two purified influenza virus H3N2 strains possibly reflected localized changes of PS, PC and GlcCer species at plasma membrane budding sites, we could speculate that such effects were due to differences in lipid metabolism redirected from glycolytic intermediates at the plasma membrane which would be in line with upregulation (Kroeker et al., 2012) and early phosphorylation (Figure 2-4) of PKM2 in influenza virus infected cells. This could also explain the enrichment of glycolytic enzymes PKM2, enolase 1 (ENO1), glyceraldehyde-3-phosphate dehydrogenase (GAPDH) & phosphoglycerate kinase 1 (PGK1)) and lipid metabolic proteins (fatty acid synthase (FASN) & diazepam binding inhibitor (DBI)) in influenza virus envelopes (Shaw et al., 2008).

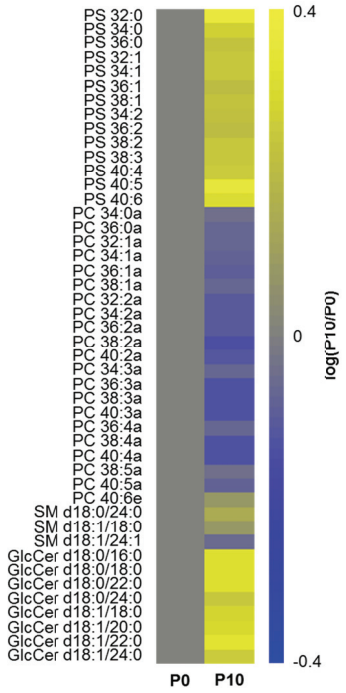

Figure 3-5: Significant phospholipid differences between two different H3N2 strains. 159 lipid species were measured from three biological replicates with duplicates each (n=6 for each virus strain). Only lipid species that showed the same trend in all three independent experiments and were significantly different as calculated by a Student's t-test (two-tailed; $p<0.05$) were plotted. Heat plot represents the log-fold ratio (P10/P0).

3.3.3 Hierarchical clustering of lipids identified lipid clusters associated with virus severity

After collecting data from several conditions (time course data in A549 cells (host response), lipid profile of virus particles produced from A549 cells (viral lipids) & lipid profile of viruses exhibiting different virulence (virulence)), we were interested in obtaining a more general picture of lipid involvement in virus infection. For this purpose we solely included the collected MRM data and harnessed hierarchical clustering using Pearson correlation distances (uncentered) with average-linkage. Similarly, this has previously been used to identify cancer associated metabolic

changes (Jain et al., 2012). Being interested in qualitative rather than quantitative differences and to make the datasets from various independent experiments comparable, we transformed the data points (146 lipid species; species with missing values were excluded) of each experiment into a log(fold-ratio) (Supplementary Table 7-4): for the time course data we obtained six log(H1N1/mock) from the three independent experiments at two time points (18hpi and 24hpi); for the lipid profile of H1N1 virus produced from A549 cells, we obtained six log(H1N1/A549) by dividing the averages of each of the two independent experiments for H1N1 by the three averages of mock infected A549 cells at 12hpi obtained from the three independent time course experiments; and for the differences between H3N2 P0 and H3N2 P10, we obtained three log(P10/P0) representing three independent experiments (Supplementary Table 7-4). The obtained dataset was clustered using the open source clustering software *Cluster3.0* (de Hoon et al., 2004) and the clustered data was visualized using *Java TreeView* (Saldanha, 2004) with red indicating an upregulation, blue a downregulation and white no change (Figure 3-6A). 22 clusters were identified with unique patterns of lipid regulation within the three groups (virulence associated lipids: log(P10/P0); viral lipids: log(H1N1/A549); host response: log(H1N1/mock)) which clearly illustrated the increase in sphingolipid and the decrease in phospholipid species in influenza virus particles and virus infected cells (Figure 3-6A&B). The majority of lipid species belonging to the same class clustered together suggesting a lipid class rather than a species dependent regulation of lipid metabolism during influenza virus infection (Figure 3-6A). For example, cluster 8 consisted of 38 or 40 carbon containing saturated aPC species (aPC 38:0 & aPC 40:0) and unsaturated ePC species (ePC 38:3; ePC40:4 & ePC40:6) which were decreased in purified influenza virus particles but slightly increased in virus infected cells and in more virulent virus

particles (Figure 3-6A&C). This possibly reflected changes important for intracellular stages of influenza virus replication rather than requirements for virion morphogenesis. Cluster 9 solely contained unsaturated aPC and aPE species which were downregulated in all three groups (Figure 3-6A&C) and clearly represented the inhibitory effect of influenza virus on lipid metabolism. Cluster 14 was considered the severity related cluster since it solely included PS species which were enriched in more severe P10 virus particles as compared to the P0 strain but showed only slightly increasing trends in virus infected cells and purified virus particles (Figure 3-6A&C). Cluster 17 was comprised of ceramide contain sphingolipids (SM, Cer and GlcCer species) with short chain saturated fatty acids (C16-C18) and of ether linked PE and PC species which were enriched in purified influenza virus particles but did not exhibited any specific severity and host response related signature (Figure 3-6A&C). Clustering of sphingolipids containing ceramides with short chain saturated fatty acids together with ePE and ePC in virus envelopes could reflect a special requirement for plasma membrane organization and influenza virion morphogenesis. It has been reported that shorter chain sphingolipids were enriched in the plasma membrane in relation to longer chain sphingolipids which were found to be predominantly localized to intracellular vesicles (Koivusalo et al., 2007). This would explain the involvement of CerS2 in intracellular trafficking events since it is responsible for the production of long chain fatty acid containing sphingolipids. Hence, as previously proposed (Chapter 2), upregulation of long chain fatty acid containing sphingolipids in virus infected cells likely reflects the need for vesicular trafficking. On the other hand, cluster 19 described sphingomyelin species with fatty acid chain moieties >C18 which were upregulated in virus infected cells and purified virus particles (Figure 3-6A&C) which probably reflected a general requirement of sphingomyelin biosynthesis for

influenza virus replication. Finally, cluster 20 combined SM and GlcCer species with saturated fatty acid moieties which were upregulated in virus infected cells and their enrichment in purified particles was also severity dependent (Figure 3-6A&C). These findings could indicate the severity related upregulation of sphingolipid biosynthesis in influenza virus infected cells due to increased glycolytic activity.

Hierarchical clustering clearly summarized the separately introduced findings in the previous paragraphs and illustrated once more the general importance of PC lipid class remodelling and sphingolipid biosynthesis (GlcCer and SM species) for influenza virus replication. We additionally identified a severity specific regulation of GlcCer and PS species.

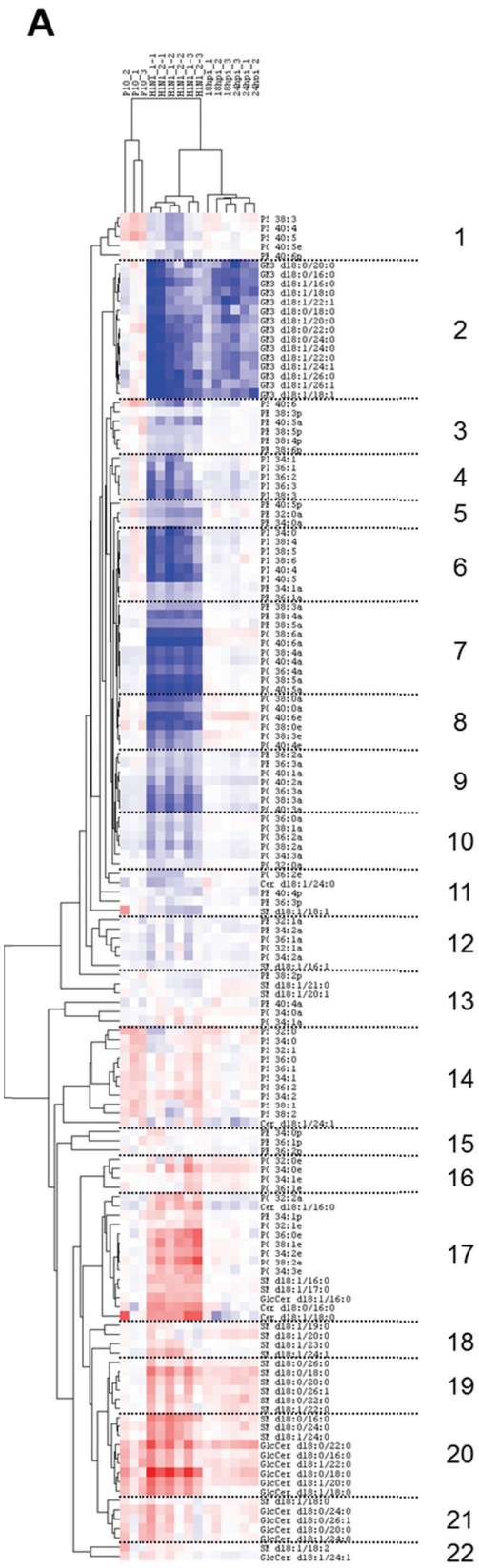
A
1
2
3
4
5
6
7
8
9
10
11
12
13
14
15
16
17
18
19
20
21
22

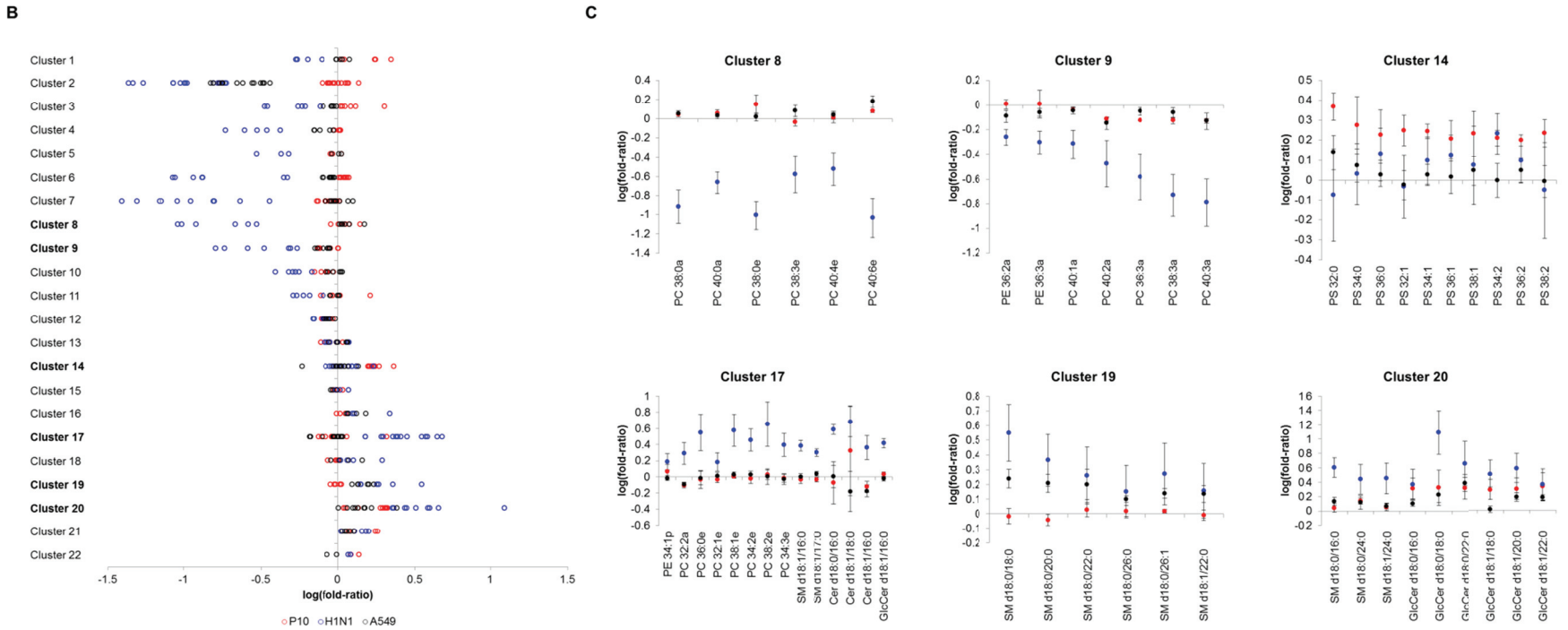

Figure 3-6: Hierarchical clustering of lipid species measured by MRM mass spectrometry. (A) Dendrogram showing the hierarchical clustering of the log(fold-ratios) of 146 lipid from eight independent experiments; blue, red and white indicating downregulation, upregulation and no change respectively. **(B)** Overview of 21 identified clusters representing the averages of log(P10/P0) (red), log(H1N1/A549) (blue) and log(H1N1/mock) (black) for measured lipid species. For simplicity reasons, the 18hpi and 24hpi time points were combined and considered as one condition. **(C)** Lipid distribution in six chosen clusters with error bars representing standard deviations.

3.3.4 Lipid composition of purified H1N1 influenza viruses treated with a broad spectrum antiviral[4]

Our results on purified influenza viruses revealed specific and common features in relation to other enveloped viruses. The common features of host-derived lipid bilayers of enveloped viruses are important to maintain biophysical characteristics such as membrane fluidity and membrane curvature which are not only essential for structural integrity but also for functionality during the virus life cycle, including membrane fusion during infection of host cells. For example, the general enrichment of cholesterol in enveloped viruses ensures proper packing and fluidity whereas enrichment of PE species maintains a hexagonal phase in virus envelopes which are essential for membrane curvature and fusion. In addition, virus membranes are inert and do not have any reparative capabilities like biogenic cellular membranes. Such characteristics, which are common between enveloped viruses but distinct in comparison to mammalian cells, present an attractive target for antiviral therapy. This has been recently addressed by several groups (Boriskin et al., 2008; Kesel, 2011; St Vincent et al., 2010; Wolf et al., 2010; Zasloff et al., 2011) and LJ001 has been identified as a membrane-binding broad spectrum antiviral which inhibits all tested enveloped viruses in a very late stage of the fusion cascade (just prior to membrane merger and fusion) without exhibiting any cytotoxic effects on host cells (Wolf et al., 2010) (Vigant et al, *submitted*). Interestingly, the inhibitory potential of LJ001 was not observed in non-enveloped viruses (Wolf et al., 2010) and it was not dependent on

[4] This work was part of a collaborative effort with Federic Vigant and Benhur Lee at the University of California, Los Angeles (UCLA) and is under review for publication in *Nat Chem Biol* (Vigant et al, *submitted*).

the presence of cholesterol since SFV produced from cholesterol depleted cells did not show any differential sensitivity (Vigant et al, *submitted*).

This sparked our interest to investigate the effect of LJ001 on the phospholipid composition of influenza virus particles. First, we established the IC_{50} for LJ001 and for a second generation compound with higher antiviral potency, JL103, on purified MDCK grown H1N1 influenza virus. Three independent experiments were performed and virus was exposed for ten minutes to light with three-fold dilutions of compound concentrations followed by plaque assay (Figure 3-7A). Light exposure was necessary due to the photosensitizing characteristics of the compounds (Vigant et al, *submitted*). We determined the IC_{50} to be 25.7nM and 1.7nM for LJ001 and JL103 respectively which was in the similar IC_{50} range of the other tested enveloped viruses (Vigant et al, *submitted*) (Figure 3-7B).

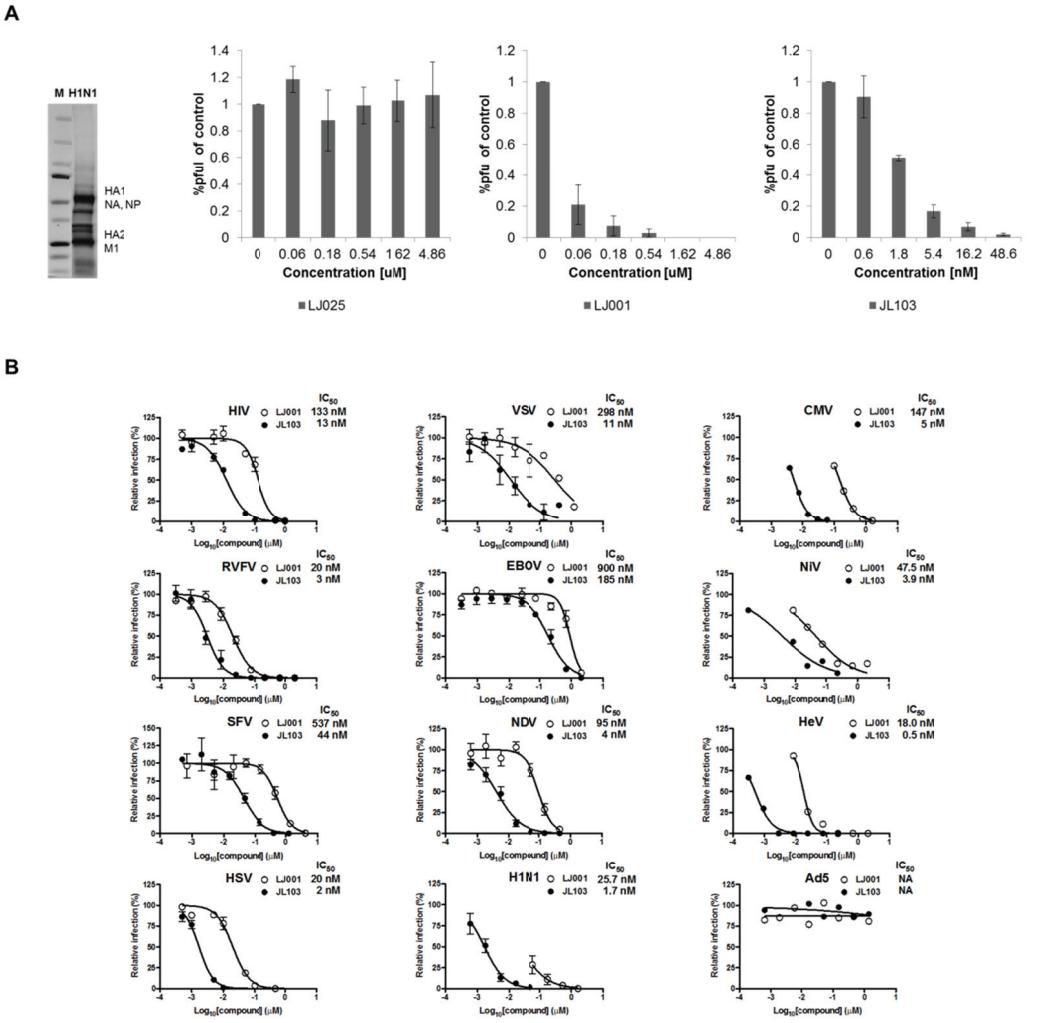

Figure 3-7: Inhibitory potential of LJ025 (control), LJ001 and JL103. (A) Purified MDCK grown H1N1 influenza viruses were treated with compounds for 10 min under light exposure and infectivity was assessed by plaque assay. Data are from three independent experiments and represented relative to DMSO control. Error bars are standard errors. **(B)** IC_{50}'s of LJ001 and JL103 on different enveloped viruses (taken from Vigant et al, *submitted*). IC_{50} on influenza virus infectivity was determined to be 25.7nM and 1.7nM for LJ001 and JL103 respectively.

3.3.4.1 LJ001 and JL103 oxidized phospholipids without affecting the total amount of lipids

Subsequently, we proceeded to analyse the lipid composition of purified influenza virus particles treated with 5μM of LJ001, JL103 or LJ025 (control compound). In an initial experiment viruses were treated and exposed to light for 10min. Samples were analysed using a high resolution Thermo LTQ-Orbitrap mass spectrometer and an ABI 3200 QTRAP mass spectrometer after liquid chromatography separation (Davis et al., 2008; Shui et al., 2011b). Despite the observed antiviral potency, we did not detect any lipid related changes (Lukas Tanner & Guanghou Shui, *unpublished*). Hence, we decided to increase the incubation period to an hour, to saturate and maximize the anticipated lipid modifications. We performed two independent experiments with two replicates for each condition. The total phospholipid composition and class distribution did not change in LJ001 and JL103 treated influenza virus particles but promptly, there was an up to 300-fold increase in unsaturated oxidized phospholipid species as compared to the control LJ025 treated viruses (Figure 3-8A). Furthermore, we also noted a consistent higher-fold increase of oxidized phospholipids in JL103 treated samples as compared to LJ001 which likely illustrated its higher antiviral potency (Figure 3-7A & Figure 3-8A). The precision of our measurements (Δ < 1ppm) allowed us to distinguish the spectrum of oxidized (OO)PC 36:2 (m/z=818.5910) from (unoxidized) ePC 40:6 (m/z=818.6063). The former was present in the LJ001 and JL103 treated samples, but almost completely absent in the LJ025 sample (Figure 3-8B). Based on these findings, our collaborators confirmed the oxidizing capability of the compounds on liposomes with a defined

phospholipid composition and scrutinized the detailed mechanism of action (Vigant et al, *submitted*). They finally proposed that after insertion into the virus membrane, LJ001 and JL103 are activated by light, generating singlet oxygen ($^1O_2$) which oxidizes the unsaturated fatty acyl moieties of several phospholipid species. Oxidation of unsaturated phospholipids in membranes leads to formation of microdomains through the clustering of oxidized lipids due to the presence of a polar group (hydroperoxy- or hydroxyl-) and to tighter positive curvature due to *cis-to-trans* isomerization of double bonds caused by the "singlet oxygen ene" reaction (Vigant et al, *submitted*). These modifications lead to decreased membrane fluidity (or increased membrane rigidity) in virus envelopes which consequently impairs membrane fusion.

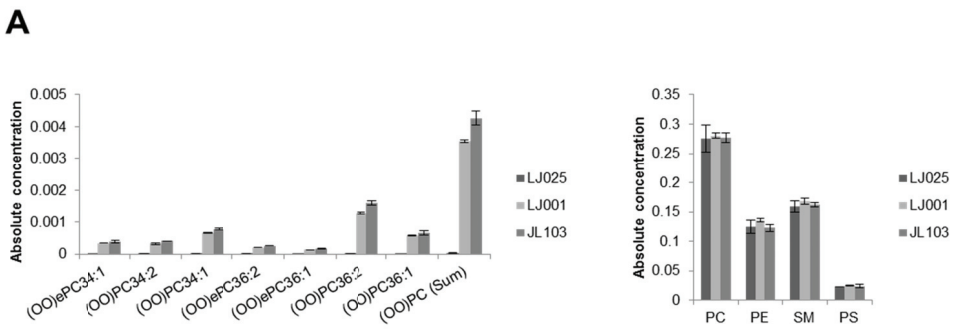

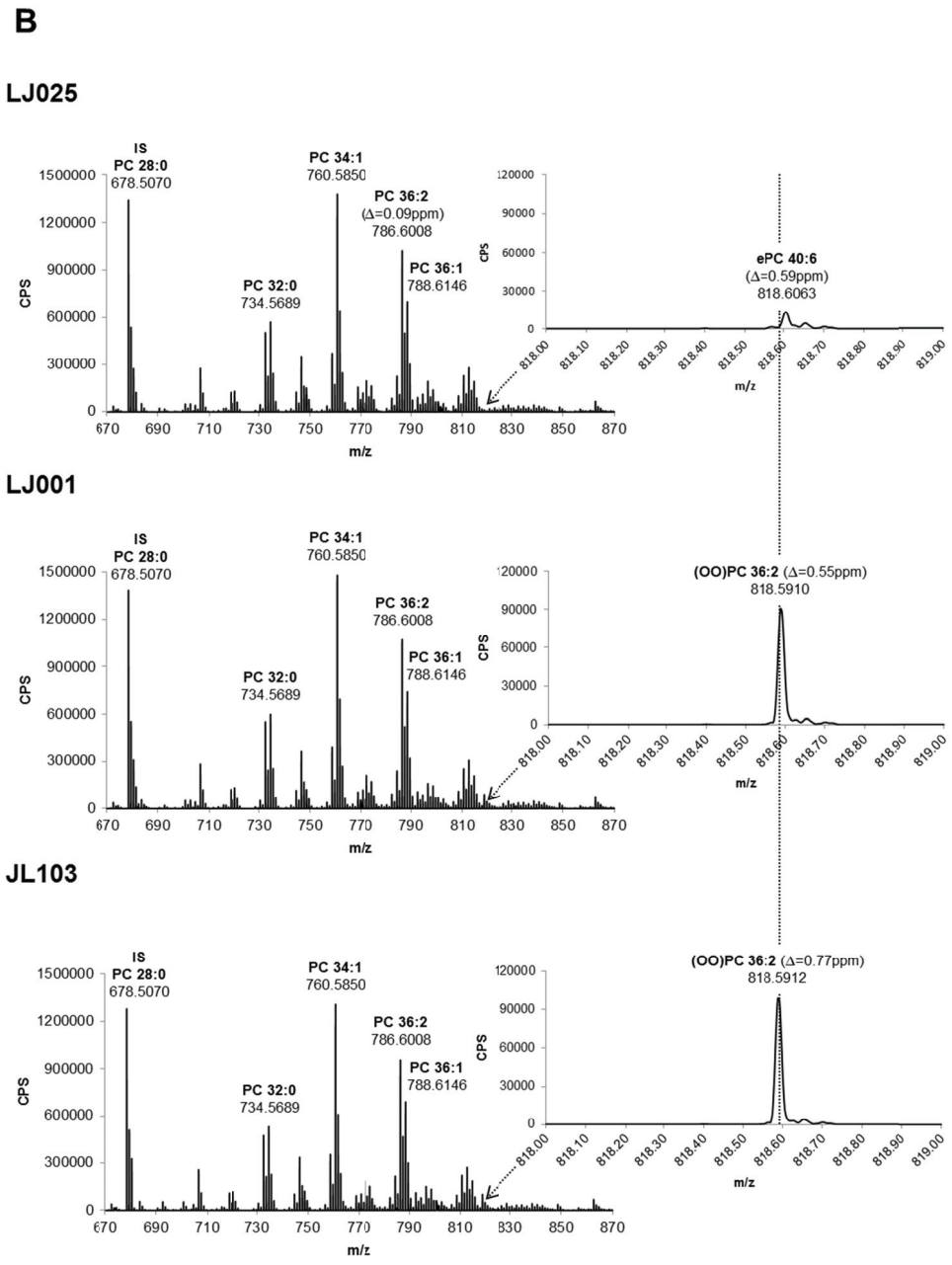

Figure 3-8: Lipid profile of LJ025, LJ001 and JL103 treated influenza virus particles. Influenza virus was treated with 5uM of LJ025 (control), LJ001 and JL103, exposed to light for 1h, and subsequently subjected to lipid extraction. Analyses of lipids, including oxidized species, were carried out using a high-resolution Thermo LTQ-Orbitrap mass spectrometer and an ABI 3200 QTRAP mass spectrometer after liquid chromatography separation. Similar results were obtained in two independent experiments. **(A)** The composition of major lipid classes (PC, PE, SM, PS) did not change whereas an up-to 300-fold increase in oxidized lipid species was observed. **(B)** Data is represented as a single stage positive ion mass spectrum (over a m/z range of 1Da). The hydroperoxide (OO)PC 36:2 is shown as an example of the prominent changes in (A). The precision of our measurements (Δ < 1ppm) allow us to distinguish the spectrum of oxidized (OO)PC 36:2 (m/z=818.5910) from (unoxidized) ePC 40:6 (m/z=818.6063). The former is present in the LJ001 and JL103 treated samples, but almost completely absent in the LJ025 control sample.

3.4 Conclusion

In this chapter we investigated the lipid compositions of different influenza virus strains and showed their functional importance. For the first time, we reported the lipid composition of purified influenza virus particles produced from A549 lung epithelial cells which highlighted the capability of influenza virus to tailor host cell metabolism to its needs (Chapter 2 & Figure 3-1). Furthermore, the lipid composition of A549 produced virus particles also showed high similarity to the previously reported MDCK grown influenza virus particles (Gerl et al., 2012). For example, in both influenza viruses, an increased remodelling of PC lipid species was evident due to an increased ePC/aPC ratio in comparison to their producer cells (Figure 3-2). The increased ePC/aPC ratio was specific for influenza virus particles when compared to the lipid composition of other enveloped viruses which suggested a functional importance of ePC species for influenza virus replication (Figure 3-2 & addressed in Chapter 4). We strikingly identified remodelling of PC class lipids to be severity dependent as shown by distinct lipid compositions of two influenza strains differing in a non-conservative point mutation in NS1 (Asp125Gly) conferring a higher degree of pathogenicity (Forbes et al., 2012; Narasaraju et al., 2009) (Figure 3-4). More detailed analyses revealed additional differences with regard to PS and GlcCer lipid species (Figure 3-5) which further supported the assumption that lipid biosynthesis was linked to increased glycolytic flux in a severity dependent manner. In summary, we established NS1 to be a regulator of influenza virus particle lipid composition which reflected its ability to interfere with host lipid metabolism on a gene expression level (Billharz et al., 2009).

We also identified a high enrichment of ceramide species in influenza virus particles when compared to their producer cells despite no differential regulation in infected A549 cells (Figure 2-1 & Figure 3-3). We speculated that an enrichment of ceramide levels possibly reflected a localized change at the plasma membrane important for virus budding and structure. Integration of our findings with existing literature led us to the conclusion that the ceramide/cholesterol ratio in viruses and cellular vesicles represents an important determinant for intracellular trafficking and mirrors influenza virus entry at late endosomes (Figure 3-3).

The described data illustrated the importance of host lipid species for the lifecycle progression of influenza virus and other enveloped viruses. This was conclusively confirmed by new antiviral compounds (LJ025 & JL103) which significantly reduced virus infection by oxidation of phospholipids in the virus envelope (Figure 3-7 & Figure 3-8).

4 Functional Role of Lipids in Virus Infection and Cell Organization

4.1 Introduction and rationale

In chapters 2 & 3, we identified distinct lipid patterns which are not only associated with influenza virus infections but also with purified influenza virus particles and virus pathogenicity. For example, the influenza virus specific remodelling of PC class lipids with an increase in ePC but a decrease in aPC species, combined with the general upregulation of SM species, pointed towards a specific requirement of choline containing lipids for influenza virus replication, which was additionally supported by previous reports (Billharz et al., 2009; Caric-Lazar et al., 1978). This prompted us to harness a siRNA and a pharmacological approach to interfere with choline containing ether- and sphingolipids to elucidate their functional role during an influenza virus infection.

In this chapter we will elaborate on the functional roles of lipids during influenza virus infection with a special focus on ether- and sphingolipids. First, we will show that influenza virus replication is impaired in ether lipid deficient cells by using a cell line impaired in DHAPAT activity and a siRNA approach targeting AGPS which both are essential enzymes in ether lipid biosynthesis. We will subsequently propose the involvement of ether lipids in polarized vesicular trafficking by harnessing an extensive literature mining approach and an interaction of influenza viruses with host cell peroxisomes. This will be underlined by our findings of a putative peroxisomal targeting sequence in NS1 and by the inhibitory activity of a PPARα agonist on influenza virus replication.

In the second part, we will address the function of sphingolipids, especially sphingomyelin species, during influenza virus replication by using D609, a pharmacological inhibitor of sphingomyelin synthase. The results will be put into context with recent literature and based on additional lipid data of D609 treated cells, we will propose an involvement of a sphingomyelin salvage pathway which requires *de novo* sphingolipid biosynthesis.

Finally, we will underline the general importance of lipids in cellular organization and trafficking by presenting the vast impact of phosphatidylinositol-4 kinase type 3 alpha (PI4KIIIα) on cellular lipid metabolism. The chapter will conclude with a general discussion of the introduced findings in the context of existing literature and in relation to each other.

4.2 Materials and methods

4.2.1 Cells, viruses and reagents

Wild type Chinese hamster ovary cell line (CHO-K1) cells and its ether lipid deficient variant NRel-4 were kindly provided by Raphael A. Zoeller (Boston University, USA). Validated silencer select siRNA constructs targeting AGPS (s16248 and s16249) and Rab11a (s16703 and s16704) and a control scrambled silencer select siRNA were purchased from Ambion (Texas, USA); Anti-AGPS antibody (HPA030209) was purchased from Sigma Aldrich (St. Louis, USA), anti-GAPDH antibody (sc-47724) from Santa Cruz (California, USA) and anti-Rab11a antibody (ab78337) from Abcam (Cambridge, UK); The PPARα agonist GW7647 and the sphingomyelin synthase inhibitor D609 were obtained from Tocris Bioscience (Bristol, UK); All other reagents were from identical sources as described in chapters 2 and 3 unless stated otherwise.

4.2.2 Lipid profiling of influenza virus infected CHO-K1 and NRel-4 cells

Wild type CHO-K1 and ether lipid deficient NRel-4 cells were routinely grown in F12 GlutaMAX™ (10% FBS, 50u/ml penicillin & 50µg/ml streptomycin) and infection with influenza virus was performed as described above. Briefly, 24 hours prior to infection, CHO-K1 and NRel-4 cells were seeded into 10cm tissue culture dishes und subsequently grown to confluency at 37^{o}C, 5%CO_2. One experiment with three replicates per condition was performed (CHO-K1 mock (n=3); CHO-K1

infected (n=3); NRel-4 mock (n=3); NRel-4 infected (n=3)) and cells were infected with influenza virus A/PR/8/34 H1N1 (MOI 5). Cells were collected after 18hpi and lipid extraction followed by mass spectrometry analysis (excluding odd chain aPC species) was performed as described in chapter 2. Analysed data was compared to the 18hpi time point of the A549 time course experiment (n=9; Chapter 2) solely including the 68 differentially regulated lipid species identified in A549 cells (excluding odd chain aPC species). Data was represented in a heat plot calculated by the log(H1N1/mock) ratios for the three cell types (A549, CHO-K1 & NRel-4).

4.2.3 Impact of DHAPAT deficiency on influenza virus replication

To investigate the impact of ether lipid deficiency on influenza virus replication, CHO-K1 and NRel-4 cells grown in 12-well plates were infected with influenza virus A/PR/8/34 H1N1 (MOI <1) and virus replication was assessed by western blot and plaque assay after 18 hours of infection. A small MOI was used to ensure capturing of effects on virus growth. Three independent experiments were performed and infection, western blot and plaque assays were executed as in chapter 2. Anti-influenza virus M2 (1:1000) and anti-GAPDH antibodies (1:1000) were used to determine influenza virus protein expression and as a loading control respectively.

4.2.4 Impact of AGPS knockdown on influenza virus infection

4.2.4.1 Knockdown of AGPS and Rab11a by siRNA interference

Two siRNA constructs for AGPS (s16248 and s16249) and Rab11a (s16703 and s16704) were used. At least three independent experiments with duplicates per condition were performed. Reverse transfection of siRNA constructs into A549 cells was performed in 12-well plates according to the manufacturer's protocol. Three different concentrations (3nM, 6nM and 12nM) were used and for each experiment, two replicates of water and scrambled siRNA controls were performed. Briefly, 200µl of OptiMEM (Gibco®, Life Technologies Co. (San Diego, California, USA)) containing 6µl of appropriate stock siRNA concentration and 2µl of lipofectamine RNAiMAX reagent (Invitrogen®, Life Technologies Co. (San Diego, California, USA)) were added to 24-well plates and incubated for 20min at room temperature. Afterwards, A549 cells were seeded into the wells in antibiotics free F12 GlutaMAX™ supplemented with 10% FBS. Seeded cell density was around 30% of confluency and cells were collected after 48 hours incubation at 37^{o}C, 5%CO_2. Knockdown efficiency was assessed by reverse transcription quantitative polymerase chain reaction (RT-qPCR) and immunoblotting. Cell viability was assessed using a MTT cell viability assay (Invitrogen®, Life Technologies Co. (San Diego, California, USA)) and degree of ether lipid depletion was measured by mass spectrometry.

4.2.4.2 Real time PCR

RNA of transfected A549 cells was extracted using QIAshredder and RNeasy mini kit (QIAGEN, Hilden, Germany) according to the manufacturer's protocol. Concentration of extracted RNA was determined using a NanoDrop system (Thermo Fisher Scientific Inc, Massachusetts, USA) and cDNA for RT-qPCR was synthesized using reverse transcription by the Superscript III First-strand synthesis supermix purchased from Invitrogen, Life Technologies Co. (San Diego, California, USA). Annealing buffer, Oligo-dT nucleotides, 2x first-strand reaction mix and reverse transcriptase enzyme mix were added as described in the manufacturer's protocol. Subsequently, synthesized cDNA was mixed together with pre-designed primers targeting the gene of interest and with the TaqMan Universal PCR Master Mix (Applied Biosystems, California, USA). qPCR was run using the Realtime 3200 system (Roche Diagnostics, Rotkreuz, Switzerland) and for each run, an endogenous control (18s) was included.

4.2.4.3 MTT cell viability assay

Cell viability after knockdown of genes of interest was assessed by the Vybrant MTT cell proliferation assay kit (V13154) (Invitrogen®, Life Technologies Co. (San Diego, California, USA)). Measurement of cell viability was conducted in at least three independent experiments. The assay was performed in a 96-well plate and siRNA transfection was performed as described above. After 48 hours, cells were subjected to serum starvation (to mimic infection conditions) in antibiotics free F12

GlutaMAX™ and after 18 hours, cell culture media was replaced with 100µl of fresh serum and antibiotics free F12 media without phenol red (Caisson Labs, Utah, USA). Subsequently, 10µl of MTT stock solution was added to each well and cells were incubated for two hours at 5%CO_2, 37^{o}C. Then, 85µl of media was removed from the wells and replaced with 50µl of DMSO. After an additional incubation at 5%CO_2, 37^{o}C for 10 minutes, cell viability was determined by measuring absorbance at 540nm using a SpectraMax190 micro titre plate reader (Molecular Devices LLC, California, USA).

4.2.4.4 Determination of protein expression by western blot

Knockdown efficiency was additionally determined on the level of protein expression. siRNA transfected A549 cells grown in 12-well plates were collected after 48 hours and subjected to immunoblotting as described in chapter 2. Antibodies against Rab11a (1:1000) and AGPS (1:2000) were used in combination with anti-GAPDH (1:1000) and anti-α-tubulin (1:1000) antibodies as loading controls. At least three independent experiments with duplicates per condition were performed.

4.2.4.5 Lipid measurements in AGPS depleted cells

Finally, knockdown efficiency was validated on the metabolite level using our established HPLC-MS/MS (operated in MRM mode) approach (Chapter 2). Two independent experiments with three replicates per condition were conducted. Lipids were harvested from cells grown in 10cm dishes for 48 hours and either transfected

with AGPS (s16248 and s16249) or scrambled siRNA constructs. Subsequent mass spectrometry analysis was performed as described in chapter 2.

4.2.4.6 Effect of AGPS knockdown on influenza virus replication

After establishing knockdown efficiency of transfected siRNA constructs on gene and protein expression as well as on metabolite levels, at least three independent experiments were conducted to determine the effect of AGPS knockdown on influenza virus replication. siRNA transfection and subsequent virus infection were done as described above. Briefly, siRNA transfected cells grown for 48 hours in 12-well plates were infected with influenza virus (MOI <1). A small MOI was used to ensure capturing of effects on virus growth. Cell lysates and virus supernatants were collected after an additional incubation for 18 hours, subjected to immunoblotting for virus protein expression (anti-influenza virus M2 (1:1000) and α-tubulin (1:1000) as loading control) and plaque assay according to the above described protocols (Chapter 2).

4.2.5 Bioinformatics analysis of ether lipid enrichment in trafficking pathways

Hits from a recent systems-scale siRNA screen on endocytosis (Collinet et al., 2010) were reanalysed. The list of 4609 gene hits was filtered based on *lipid* in any of the annotation categories using Excel (Microsoft, Washington, USA). This resulted in a list of 372 genes which had an association with lipid metabolism. Subsequently, this list was used to identify enriched lipid pathways as defined by the KEGG

PATHWAY database (http://www.genome.jp/kegg/pathway.html#lipid). A manual annotation was performed and out of the 372 genes, 240 genes were associated with any of the 15 defined lipid pathways. Significant enrichment was assessed using a one-tailed Fisher's exact t-test (right/greater tail) calculated using an online tool (http://www.langsrud.com/fisher.htm). Two criteria were used to describe pathway enrichment. The first criteria represented the general gene enrichment in a given lipid pathway whereas the second criteria described coverage of nodes in a pathway. Nodes in KEGG PATHWAY usually contain more than one homologue and the node was considered covered as long as one homologue was identified in the gene list. Each lipid pathway was scored according to its ranks based on gene enrichment (1 (lowest enrichment) to 15 (highest enrichment)), node coverage (1 (lowest enrichment) to 15 (highest enrichment)) and based on its Fisher's exact test *p-value* (1 (highest *p-value*) to 15 (lowest *p-value*)). The three individual scores for each lipid pathway were combined (combined rank score) and the distribution was described by the *median* and *median absolute deviation* (*MAD*). A significant enrichment of a lipid pathway was considered when the individual combined rank score of a lipid pathway was greater than (*median*+*MAD*).

4.2.6 Impact of PPARα agonist (GW7647) on influenza virus replication

A549 cells were infected with influenza virus (MOI <1) as described above and after 1 hour of infection, virus inoculum was exchanged with serum and antibiotics free F12 GlutaMAX™ supplemented with 1µM, 2µM and 5µM GW7647. Three independent experiments were performed in duplicates per condition. Virus

supernatants were collected after incubation for another 18 hours and subjected to determination of virus titres by plaque assay according to the protocol in chapter 2. Additionally, cell viability of GW7647 treated cells was assessed by the above described MTT assay in one experiment with three replicates.

4.2.7 Impact of the SMS1/2 inhibitor D609 on influenza virus replication

A549 cells were infected with influenza virus (MOI <1) in 12-well plates as described above and incubated for 12 hours in serum and antibiotics free F12 GlutaMAX™ at 5%CO_2, 37^{o}C. Then, medium was exchanged with fresh serum and antibiotics free F12 GlutaMAX™ supplemented with 10µM and 100µM D609. Cells were incubated for another 6 hours at 5%CO_2, 37^{o}C prior to collection of cell lysates and supernatants for the determination of virus protein expression by western blot and virus titres by plaque assay (Chapter 2). Three independent experiments were conducted and for one experiment, cell viability of D609 treated cells was also assessed by the previously described MTT assay.

For lipid analysis by mass spectrometry, A549 cells were treated with 10µM D609 in serum and antibiotics free F12 GlutaMAX™ for 18hpi. Collected cells were subjected to lipid extraction followed by mass spectrometry as outlined in chapter 2. One experiment with duplicates per condition was performed.

4.2.8 Lipid profile of PI4KIIIα KO fibroblasts

Dried lipid extracts prepared from WT and PI4KIIIα KO mouse embryonic fibroblasts (MEF) according to the modified Bligh & Dyer protocol as described in chapter 2 were obtained from our collaborators (Fubito Nakatsu & Pietro De Camilli, Yale University, USA) (Nakatsu et al, 2012). Dried lipid extracts were dissolved in 100 to 200µl chloroform:methanol 1:1. 20µl and 5µl aliquots were used for quantitative measurements of phospholipids and cholesterol respectively.

4.2.8.1 Quantitative analysis of cellular phospho- and sphingolipids by HPLC-MS/MS (operated in MRM mode)

Quantitative analysis of phospholipids was performed as described in chapter 2 except for using a slightly modified list of MRM transitions also including transitions for PA and lysolipid species (Supplementary Table 7-6). 20µl of samples were combined with 20µl of 2x standard mixture also containing a representative standard for PA (1,2-ditetradecanoyl-sn-glycero-3-phosphate or DMPA; 0.25ug/ml final concentration) besides the previously introduced standards.

4.2.8.2 Cholesterol analysis by HPLC APCI mass spectrometry

Free cholesterol was analysed as described previously (Shui et al., 2011a). Only HPLC grade solvents were used and the deuterated cholesterol standard (cholesterol-26,26,26,27,27,27-*d6*) was obtained from CDN Isotopes Inc. (Quebec, Canada).

Briefly, 5µl of dissolved cell lipid extracts were diluted in 25µl chlororform:methanol 1:1 and combined with 20µl of a 2x standard mix containing the cholesterol-*d6* (final concentration 2.5µg/ml) standard. Samples were analysed using an Agilent HPLC1100 system (Agilent, California, USA) coupled to an Applied Biosystems 3200 QTrap mass spectrometer (Applied Biosystems, California, USA). MRM transitions for endogenous cholesterol (369.4/161.0) and cholesterol-*d6* (375.4/161.0) were monitored in the positive atmospheric pressure chemical ionization (APCI) mode. Measured cholesterol levels were first normalized to the cholesterol-*d6* standard and finally presented relative to the measured phospholipid concentration to account for sample-to-sample variation. Statistically significant differences ($p<0.05$) were calculated using an unpaired two tailed Student's t-test.

4.3 Results and discussion

4.3.1 Influenza virus replication is impaired in ether lipid deficient cells[5]

4.3.1.1 Influenza virus replication was reduced in ether lipid deficient CHO cells

Based on our results showing an influenza virus specific remodelling of PC lipids, especially an upregulation of ePC but a downregulation of aPC species, in virus infected cells and also in purified virus particles, we decided to use an ether lipid deficient cell line to investigate the importance of ether lipids during influenza virus infection. We infected a wild type CHO-K1 and its ether lipid deficient variant, NRel-4 (Nagan et al., 1998), with influenza virus A/PR/8/34 H1N1 to check for differential regulation of lipid metabolism as well as impairment in virus replication. The ether lipid deficient NRel-4 cells exhibit significant lower levels of ether lipids due to DHAPAT activity (Nagan et al., 1998). DHAPAT is localized in the peroxisome and attaches a fatty acid moiety onto the glycolytic intermediate DHAP which is essential for ether lipid biosynthesis.

Control and mutant CHO cells were infected with influenza virus at an MOI 5 and virus titres and lipid changes were assessed after 18hpi. For lipid analysis, we performed one experiment with three replicates each measuring the 159 lipid species

[5] This work was part of a MSc project completed by Charmaine Chng under my supervision: Designed the experiments (Lukas Tanner & Charmaine Chng), performed the experiments (Charmaine Chng) and analyzed the data (Lukas Tanner & Charmaine Chng).

(excluding odd chain aPC species) which were also analysed in the previous time course experiment in A549 cells (Chapter 2). Subsequently, we compared the identified 68 lipid species which were differentially regulated in influenza virus infected A549 cells (excluding odd chain aPC species; Figure 2-1) to the lipid changes in infected wild type and mutant CHO cells (Figure 4-1A). The general changes induced by influenza virus infection in CHO cells were consistent with the changes in A549 cells, with an upregulation of sphingolipids (mainly GlcCer and some SM species) and a clear downregulation of gangliosides GM3, aPE and some aPC species (Figure 4-1A). The relatively small changes in SM species in CHO cells at 18hpi were most probably due to delayed influenza virus replication kinetics in CHO cells since these cells are less supportive for influenza virus replication as observed by decreased virus titres when compared to A549 cells (Narasaraju et al., 2009). However, there was an obvious upregulation of the total amount of ePC species in wild type CHO cells (unpaired Student's t-test; two-tailed; $p<0.05$) but not in its ether lipid deficient variant NRel-4 cells, which reflected their reported impairment in ether lipid biosynthesis (Figure 4-1A). Furthermore, the saturated aPC species (aPC 36:0 and aPC 38:0), which were usually upregulated in infected A549 and CHO-K1 cells, were downregulated in the mutant NRel-4 cell line, suggesting again a crucial involvement of PC species in influenza virus replication. In contrary, total amount of aPE species showed an increasing trend in virus infected NRel-4 cells, as opposed to decreased levels in A549 and unchanged levels in CHO WT cells (Figure 4-1A).

After establishing the differential regulation of PC species in influenza virus infected ether lipid deficient NRel-4 cells as compared to infected wild type CHO and A549

cells, we analysed the effect of ether lipid deficiency on influenza virus infection. Ether lipid deficient NRel-4 cells consistently exhibited slightly lower expression levels of influenza virus proteins NS1 and M2 and a three- to four-fold decrease in infectious virus particle formation when compared to wild type CHO-K1 cells (Figure 4-2B). These results conclusively emphasized a possible requirement for ether lipids in influenza virus replication.

4.3.1.2 Influenza virus replication was also reduced in AGPS depleted A549 cells

Since DHAP can also be redirected into TAG biosynthesis under high glucose consumption (Hajra et al., 2000) and since the two CHO cell variants were not isogenic, we decided to use a siRNA approach targeting AGPS in A549 cells to obtain a clearer picture of ether lipid involvement in influenza virus replication. AGPS exchanges the fatty acid of acyl-DHAP with a fatty alcohol introducing the characteristic ether bond at the sn-1 position or less frequently at the sn-2 position. This irreversible step lies just downstream of DHAPAT and is also localized in the peroxisome. Two siRNA constructs (s16248 and s16249) targeting AGPS were transfected into A549 cells and three different concentrations were used to validate the knockdown efficiency of AGPS mRNA, protein and ether lipid metabolite levels by RT-qPCR, western blot and mass spectrometry, respectively. Validation of off-target effects was beyond this study since purchased siRNA constructs have been tested for off-target effects as stated by the manufacturer. Cell viability after knockdown was assessed by MTT assay. We observed a significant reduction (>90%) of AGPS mRNA expression for both constructs (s16248 and s16249) across all three

different concentrations without affecting cell viability after 48 hours in three independent experiments (Supplementary Figure 7-3). Subsequently, we decided to use the 12nM concentration for further experiments and immunoblotting additionally confirmed the knockdown efficiency showing decreased AGPS protein expression in cells transefected with AGPS targeting siRNA constructs as compared to water and non-targeting siRNA control expressing cells (Figure 4-1C).

We then proceeded in testing whether ether lipid levels were also affected by the siRNA treatment. Two independent experiments with three replicates each were performed and lipids were extracted after 48 hours of transfection. We observed a small (around 1.5-fold) but significant decrease in ether linked lipid species (ePC and ePE) with a concomitant increase in ester linked lipid levels (aPC and aPE) whereas other phospho- and sphingolipid classes remained unchanged (Figure 4-1D). These results underlined the tight balance between ester linked- and ether linked lipid species and posed a good system to further investigate the functional role of ether lipids in influenza virus infection.

AGPS deficiency resulted in two- to three-fold reduced levels of infectious virus particles as observed by plaque assay (Figure 4-1C). Taking into account the relatively small decrease in ether linked lipids (<1.5-fold) upon AGPS knockdown (Figure 4-1D), we considered the two- to three-fold reduction in infectious virus titres biologically significant. Furthermore, the effects on influenza virus infection were similar to our positive control targeting Rab11a which has been previously shown to be essential for late stages of influenza virus replication, in particular assembly and budding (Amorim et al., 2011; Bruce et al., 2010; Eisfeld et al., 2011). Rab11a was

chosen as a positive control since we assumed that changes in lipid metabolism might be directly or indirectly linked to virus morphogenesis or assembly/budding due to their relatively late occurrence (between 18hpi and 24hpi) in virus infected cells and due to their enrichment in purified virus particles.

Levels of virus proteins in AGPS depleted A549 cells were similar to control cells, which was in contrast to the observed reduction in virus protein expression in ether lipid deficient NRel-4 cells (Figure 4-1). One explanation might be that the differences in ether lipid levels between the two CHO cell types were much more substantial than between AGPS depleted and control A549 cells. Furthermore, we cannot exclude the fact that the two CHO cells are not of isogenic nature and the possibility that they might exhibit additional phenotypic differences.

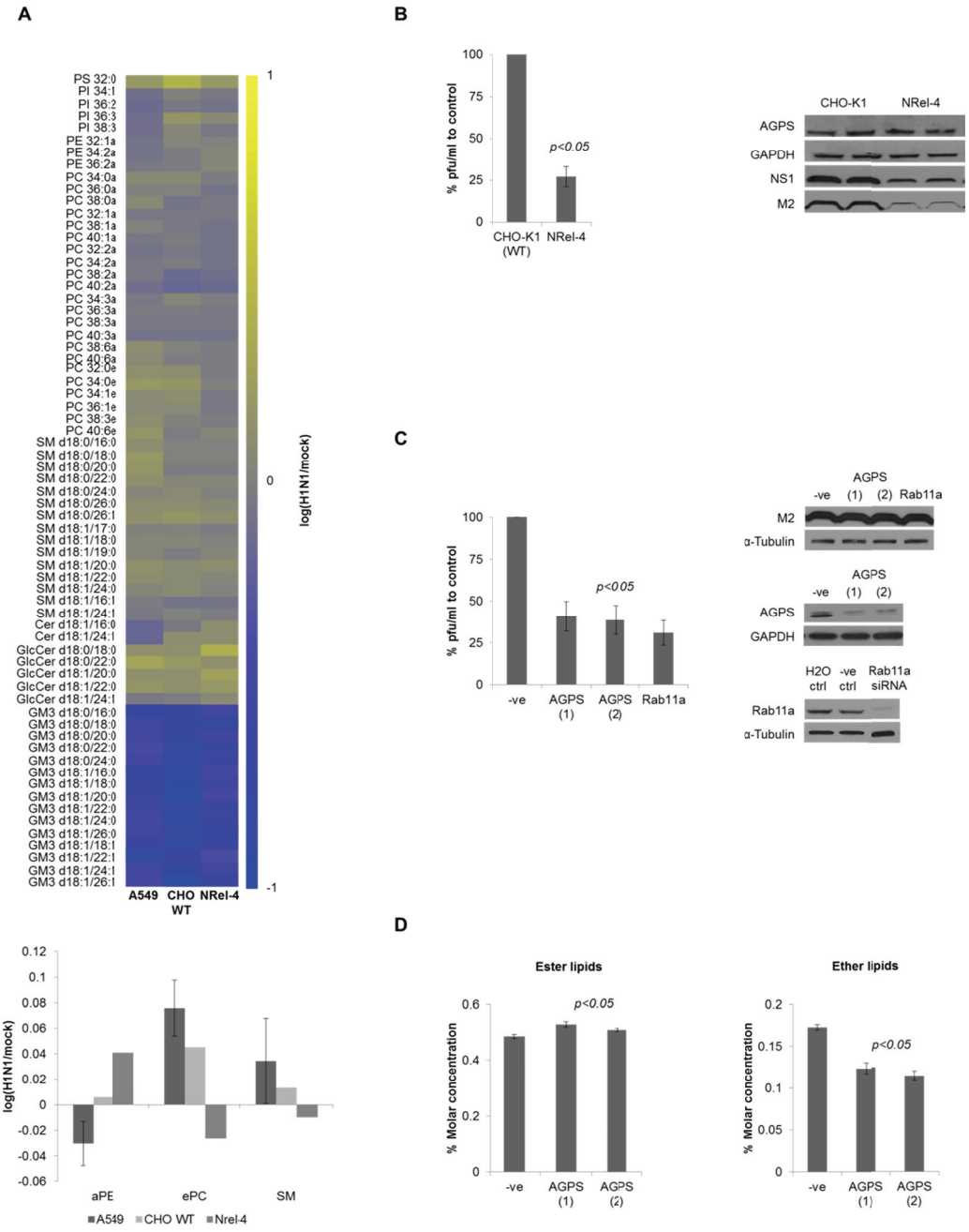

Figure 4-1: Ether lipid deficiency impacts influenza virus replication (adapted from Charmaine Chng). (A) Lipid changes induced in CHO WT and ether lipid deficient cells in comparison to the changes observed in A549 cells 18hpi. CHO WT cells and ether lipid deficient CHO cells (NRel-4) were infected with influenza virus and lipids were extracted and analysed 18hpi. Results were compared to the differentially regulated lipids in A549 cells. One experiment was performed with three replicates per condition. Data was presented as the log(H1N1/mock) ratio. Changes in total ePC levels were significantly increased in CHO WT infected cells as calculated by an unpaired Student's t-test (two-tailed; $p<0.05$). **(B)** Wild type CHO-K1 and ether lipid deficient CHO NRel-4 cells were infected with influenza virus and virus titre was assessed after 18hpi. There was a decrease in virus protein expression with a concomitant three to four fold reduction in virus titre over three independent experiments. Western blot from one experiment is shown which is representative of three independent experiments. **(C)** A549 cells were transfected with s16248 (1) and s16249 (2) siRNA constructs which

also resulted in a two to three-fold reduction in virus titres while virus protein expression was not affected. Negative controls (-ve) are scrambled siRNAs. Data is from at least three independent experiments and error bars depict standard errors. Western blot from one experiment is shown which is representative of three independent experiments. **(D)** AGPS knockdown slightly but significantly reduced ether lipid levels while ester linked lipid levels were increased as measured by mass spectrometry. Data are from two independent experiments and error bars represent standard deviations.

4.3.2 Ether lipids are possibly involved in polarized trafficking

The necessity of ether lipids during influenza virus infection was highlighted by (1) the upregulation of ePC species during the course of an influenza virus infection, (2) by the influenza virus specific enrichment of ether lipid species in the virus envelope and (3) by the impairment of virus replication in ether lipid deficient cells. Hitherto, there is still limited knowledge about the functional role of ether lipids, especially ether PC species, in cell as well as virus biology. The majority of studies on ether lipids investigated ethanolamine species due to their higher abundance. Nevertheless, recent evidence pointed towards a role in vesicular trafficking, since ether lipids have been shown to be enriched in vesicles originating from the endo-/exosomal system such as synaptic vesicles, exosomes and enveloped viruses (Chan et al., 2008; Gerl et al., 2012; Honsho et al., 2008; Takamori et al., 2006). The functional importance of such an enrichment in cellular vesicles could possibly reflect their role in membrane fusion due to their high fusogenicity (Glaser et al., 2002; Han et al., 1998) and in membrane integrity due to their enrichment, along with cholesterol, in plasma membrane microdomains (Pike et al., 2002). Cells lacking ether lipids also exhibited a partial reduction in protein secretion (Munn et al., 2003) and a potential co-regulation and –segregation of ether lipids with cholesterol was further supported by studies

showing defective cholesterol homeostasis in ether lipid deficient cells (Mankidy et al., 2010; Munn et al., 2003; Thai et al., 2001).

To get a better view on the involvement of ether lipids in membrane trafficking, we decided to harness a bioinformatics approach and to reanalyse data from a systems-wide siRNA screen on endocytosis (Collinet et al., 2010). This study identified 4609 genes grouped into 14 clusters which played an essential part in the organization and control of the endocytic system (Collinet et al., 2010). We filtered 372 (~8%) genes being associated with lipid metabolism with high enrichment in phospholipid and fatty acid metabolism (Figure 4-2A). We used two criteria to determine the degree of pathway enrichment and coverage. The first measure represented how many gene homologues in the KEGG pathway were covered accompanied by a significance level calculated by the Fisher's exact test. The second criteria accounted for the general coverage of the pathway or how many nodes were covered since a node in KEGG pathways can consist of several homologues (Figure 4-2A). Lipid pathways were scored according to their rank based on each criterion (1 for lowest coverage and highest *p-value* to 15 for highest coverage and lowest *p-value*). Subsequently, a combined rank score including the score for *p-value* was calculated (Figure 4-2B). The pathways that scored highest (glycerophospholipid (39), glycerolipid (35) and ether lipid metabolism (33.5)) were considered functionally important in vesicular trafficking, since their rank score was greater than the *median* (27.5) plus the median absolute deviation (*MAD;* 5.5) which was 33. Genes involved in ether lipid metabolism showed a relatively high gene coverage rate (29%; Fisher's exact test; two tailed; $p<10^{-38}$) and the highest pathway coverage of 80% (Figure 4-2A&B).

The unique feature of a high ePC/aPC ratio in influenza virus particles, which was not observed in other enveloped viruses (Chapter 3), pointed us towards a specificity of virus budding at the apical membrane which is a characteristic feature for influenza virus. As a result, we reanalysed the data of a recent study investigating lipid regulation during epithelial cell polarization (Sampaio et al., 2011) and similarly, we found an increased ePC/aPC ratio which was characterized by increasing ePC but decreasing aPC species peaking at day five with the initiation of epithelial cell polarity (Figure 4-2C) (Sampaio et al., 2011). Establishment of cell polarity is tightly linked to the secretory system by polarized trafficking of newly synthesized components to the plasma membrane (Golachowska et al., 2010; Rodriguez-Boulan et al., 2005). Hence, lipid changes at an early stage of cell polarization would hypothetically represent a massive induction of secretory vesicle formation. Influenza virus assembly and budding also requires the controlled and polarized transport of virus components to the site of particle morphogenesis at the plasma membrane. Based on this, remodelling of PC species leading to a high ePC/aPC ratio in influenza virus infected cells as well as in influenza virus particles might represent an unique requirement for polarized trafficking. Influenza virus particles showed a higher enrichment of short chain ePC species, whereas long chain ePC species were predominantly upregulated in infected cells (Figure 3-6). Similarly, this could reflect a chain length dependent requirement for trafficking, as identified by hierarchical clustering in sphingomyelin species (Figure 3-6). Experimental evidence of an importance of PC metabolism in the secretory pathway is compelling. For example in yeast, it is well understood that PC metabolism and the major PC/PI transfer protein Sec14p are required for vesicular transport from the Golgi (Bankaitis et al., 1989; Cleves et al., 1991). Sec14p regulates the phospholipid composition at the Golgi and

the recruitment of downstream effectors such as Ypt31p, a RabGTPase involved in vesicular trafficking. Ypt31p is the yeast Rab11 homologue which has been shown to be required for influenza virus replication (Amorim et al., 2011; Bruce et al., 2010; Eisfeld et al., 2011) (Figure 4-1C). In addition, Golgi organization and vesicular trafficking in mammalian cells were also shown to be dependent on functional PC metabolism (Litvak et al., 2005; Sarri et al., 2011; Testerink et al., 2009).

A

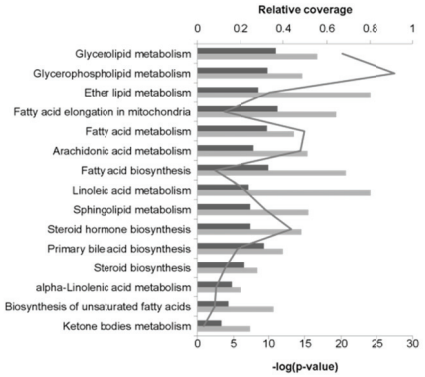

B

KEGG lipid pathway	P-value	Gene enrichment	Node enrichment	Combined Rank Score
Glycerolipid metabolism	14	14	11	39
Glycerophospholipid metabolism	15	12	8	35
Ether lipidmetabolism	10	9	14.5	33.5
Fatty acid elongation in mitochondria	5	15	12	32
Fatty acid metabolism	13	11	6	30
Fatty acid biosynthesis	3	13	13	29
Arachidonic acid metabolism	12	8	9	29
Linoleic acid metabolism	8	5	14.5	27.5
Sphingolipid metabolism	9	7	10	26
Steroid hormone biosynthesis	11	6	7	24
Primary bile acid biosynthesis	7	10	5	22
Steroid biosynthesis	6	4	3	13
alpha-Linolenic acid metabolism	4	3	1	8
Biosynthesis of unsaturated fatty acids	2	2	4	8
Ketone bodies metabolism	1	1	2	4

C

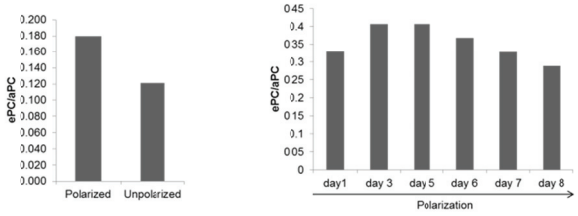

Figure 4-2: Ether lipids and their association with vesicular trafficking. (A) 4609 genes identified in a recent siRNA screen (Collinet et al., 2010) were reanalysed. 372 (8%) of the genes were associated with lipid metabolism and their coverage of KEGG pathways revealed significant enrichment in ether lipid metabolism. The pathways were sorted according to their combined rank score as described in the main text. Dark grey bars indicate coverage of KEGG genes, light grey bars indicate coverage of KEGG nodes and grey line represents -log(*p-value*) calculated by a Fisher's exact test. **(B)** Table showing the distribution of calculated rank scores for each of the three categories. Yellow box highlights the pathways that were enriched based on a greater combined rank score than *median* (27.5) + *MAD* (5.5) = 33. **(C)** Lipid data from polarizing epithelial cells (Sampaio et al., 2011) were reanalysed and the ePC/aPC ratio was plotted indicating an early enrichment of ePC species during epithelial cell polarization.

4.3.3 Activation of PPARα impaired influenza virus replication

The decrease in peroxisomal fatty acid ß-oxidation but the increase in peroxisomal phospholipid (ether lipid) synthesis during the course of an influenza virus infection was strikingly reflected by (1) accumulation of ether and odd chain phospholipids (Figure 2-1C&D) with a concomitant increased incorporation of long chain C26 fatty acids into sphingolipid species (Figure 2-2B), by (2) the decreased catalase activity in influenza virus infected cells (Figure 2-3) and by (3) the identification of HSD17B4, ACOX1, CROT as antiviral mediators (Figure 2-5) (Kroeker et al., 2012; Shapira et al., 2009; Wolff et al., 1996). Peroxisomal function and metabolism are mainly regulated by the three peroxisome proliferator-activated receptors which exist as three isoforms (PPARα, PPARß/δ and PPARγ) (Peters et al., 2012; Schupp and Lazar, 2010). PPARα and PPARγ play major roles in the regulation of genes involved in lipid anabolism and catabolism. PPARγ has been implicated in fatty acid uptake, transport, and storage whereas PPARα mainly regulates fatty acid oxidation and has been shown to be involved in the metabolic switch between glucose usage and lipid oxidation (Peters et al., 2012; Ribet et al., 2010). Recent studies showed that activation of PPARα increased peroxisomal fatty acid ß-oxidation but decreased glycolysis and diminished lipogenesis (Lee et al., 1995; Ribet et al., 2010). In contrary, activation of PPARγ had no effect on fatty acid oxidation and glycolysis (Ribet et al., 2010). Since influenza virus infection had exactly the opposite effect on lipogenesis and –lysis as described in chapter 2, we decided to use a highly specific PPARα agonist (GW7647) to investigate its impact on influenza virus infection. A549 cells were infected with influenza virus and GW7647 agonist was added 1 hour after

infection. Virus supernatant was collected 18hpi and virus titre was assessed by plaque assay. We observed a significant reduction in infectious virus particle formation in three independent experiments (Figure 4-3A). These results supported the observed changes in cellular metabolism and together established activation of PPARα and expression of its downstream effectors to be antiviral. PPARα agonists have been previously proposed as alternative treatments for influenza virus infections and a recent study showed their antiviral activity *in vivo* since gemfibrozil increased survival in a severe influenza infection mouse model (Budd et al., 2007; Fedson, 2008).

The recent finding that peroxisomes are initial sites of antiviral signalling inducing interferon independent expression of host defence factors via the RIG-I-like receptor (RLR) adaptor protein MAVS (Dixit et al., 2010) confirms a possible interaction between influenza virus and peroxisomal function. In this study, the effects were observed using a NS1 depleted influenza virus strain, since NS1 antagonizes interferon signalling and the antiviral host immune response in general (Dixit et al., 2010; Hale et al., 2008). NS1 proteins exhibiting a higher inhibitory impact on the host antiviral response also impacted expression of lipid metabolic genes to a greater extent (Billharz et al., 2009). This highlights NS1 to be the potential virus factor interfering with peroxisomal function and its interaction with the peroxisomal HSD17B4 protein (Wolff et al., 1996) would suggest a functional important targeting of NS1 to the peroxisome. Targeting of proteins to the peroxisome is mediated by two distinct peroxisome targeting sequences (PTS1 and PTS2) (Ma et al., 2011a) and hence, we were interested in whether NS1 harbours a putative PTS sequence.

We identified a putative PTS2 sequence 30 amino acids downstream of the N-terminus, similar to the PTS2 sequence of AGPS, by screening NS1 of influenza virus A/PR/8/34 H1N1 using the PTS2 Block algorithm (*www.peroxisomedb.org*) (Figure 4-3B). We further investigated the identified sequence with a recently described PTS2 predictor (Kunze et al., 2011)[6] which revealed the predicted sequence to be a weak targeting sequence (Supplementary Figure 7-5). Consistent with a function as a putative PTS2 targeting signal, the predicted sequence forms an amphipathic helix but, significantly deviates from other PTS2 sequences by having the expected positive charge histidine (H) at S3 replaced with a negatively charged serine (S) (Figure 4-3 & Supplementary Figure 7-5). The predicted sequence also lies in the RNA binding region of NS1 defined by the two highly conserved arginines (R). Therefore, it would rather exhibit a secondary function as a peroxisomal targeting sequence with limited evolutionary perfection to not interfere with RNA binding. Dual functionality of the predicted PTS2 sequence would not be of great surprise due to the multifunctional nature of NS1 (Hale et al., 2008), the fact that peroxisomes have been identified to be secondary localization sites for several proteins (Freitag et al., 2012) and since many proteins carry hidden peroxisomal targeting sequences (Neuberger et al., 2004). Additional experiments using immunocytochemistry and site-.directed mutagenesis are currently under way to further scrutinize the functionality of this predicted sequence.

[6] Predictions using the recently described PTS2 predictor (Kunze et al, 2011) were kindly performed by Sebstian Maurer-Stroh and Frank Eisenhaber at the Bioinformatics Institute (BII), Singapore.

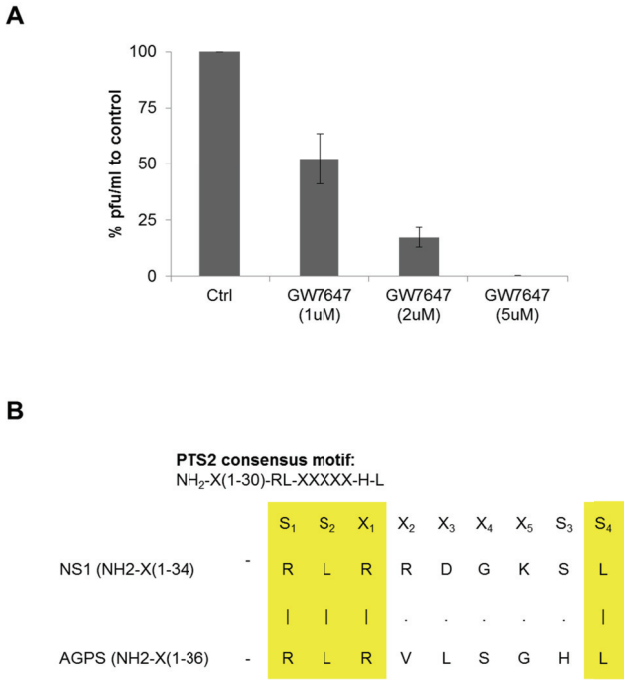

Figure 4-3: PPARα agonist impairs influenza virus replication. (A) A549 cells were infected with influenza virus and the PPARα agonist (GW7647) was added 1 hour after infection. Supernatant was collected 18hpi and reduced levels of virus titres were observed by plaque assay. Error bars depict standard errors and the decrease was statistically significant for all concentrations as calculated by an unpaired Student's t-test (two-tailed; at least $p<0.002$). **(B)** A putative N-terminal PTS2 sequence in influenza virus NS1 was identified using the PTS2 Block algorithm *(www.peroxisomedb.org)*. The sequence was further characterized using a recently described PTS2 predictor (Kunze et al., 2011) (Supplementary Figure 7-5).

4.3.4 Inhibition of sphingomyelin synthesis at a late stage of infection impaired influenza virus replication

Besides the influenza virus specific remodelling of PC species, a significant upregulation of sphingolipids, mainly GlcCer and SM species, was also measured. This was not only supported by the temporal lipid profile but also by their enrichment in purified influenza virus particles (Figure 2-1C&D & Figure 3-1B&C). The general upregulation of SM species in influenza virus infected cells peaked at 24hpi and supported previous findings that sphingolipid biosynthesis was required for late stages

in the virus life cycle (Hidari et al., 2006; Takahashi et al., 2008). SM is synthesized from PC by SMS1 and SMS2 which are either solely located at the Golgi (SMS1) or additionally located to the plasma membrane (SMS2) (Huitema et al., 2004). Both isoforms transfer a phosphocholine moiety from PC onto ceramide producing SM and DAG. Such an activity would be in line with our observations of decreased levels in aPC species but increased levels in SM species during an influenza virus infection (Figure 2-1C&D). SMS activity is essential for controlling cellular ceramide and DAG levels, and SM levels have generally been implicated in the functional and structural organization of cellular membranes (Subathra et al., 2011). For example, SMS activity at the Golgi generating DAG has been shown to be an important requirement for vesicular trafficking (Subathra et al., 2011). On the other hand, sphingomyelin biosynthesis at the plasma membrane mediates integrity of plasma membrane microdomains (Li et al., 2007).

We proceeded to investigate the role of sphingomyelin species at later stages of influenza virus infection in further details using a pharmacological inhibitor (D609) of both SMS isoforms (Adibhatla et al., 2012). D609 was originally discovered to inhibit PC-PLC specific activity (Amtmann, 1996). While the bacterial PC-PLC has been cloned and purified, the mammalian protein still remains unknown. Most of the studies measured PC-PLC activity based on accumulation of DAG and decreasing levels of PC (Adibhatla et al., 2012). Later studies evidently proved that D609 also actively inhibits SMS activity due to the similarity of the two enzymes, both cleaving the phosphocholine head group from the DAG backbone (Luberto and Hannun, 1998; Luberto et al., 2000).

A549 cells were infected with influenza virus and D609 was added after 12 hours of infection. Virus supernatant was collected after an additional incubation of 6 hours and virus titre was assessed by plaque assay. Three independent experiments were performed and, despite no impact on cell viability (Supplementary Figure 7-3), influenza virus production was inhibited in a dose dependent manner, with nearly no plaques observed at the highest concentration used (100μM). Influenza virus M2 protein expression was only decreased slightly at 100μM without any significant changes at 10μM. This suggested that PC-PLC and/or SMS activity might be essential for influenza virus assembly/budding. Subsequently, we performed one more experiment to check for changes in lipid metabolism after treatment with D609. For this purpose, we used the 10μM concentration and incubated the cells for 18 hours before lipid extraction and mass spectrometry. Two (control) and three (D609 treated samples) independent measurements were performed and we did not observe any substantial changes in the total levels of phospholipid classes except an increase in ePC species which was paralleled by the accumulation of Cer, GlcCer and ganglioside GM3 species (Figure 4-4B). The increase in ePC species most probably reflected decreased PC-PLC and/or SMS activity since ePC species appeared to be a better substrate than aPC species (Albi and Viola Magni, 2004). Surprisingly, we did not detect any obvious changes in the levels of SM but our results were in line with evidence indicating an induction of *de novo* sphingolipid biosynthesis (Perry and Ridgway, 2004) which was reflected by increased Cer, GlcCer and ganglioside GM3 levels in D609 treated cells (Figure 4-4B). This was explained by the inhibitory activity of D609 on a SM salvage (resynthesis) pathway (Luberto and Hannun, 1998; Luberto et al., 2000) rather than *de novo* SM biosynthesis since incorporation of serine into Cer and subsequently into SM was also stimulated (Perry and Ridgway,

2004). In the light of that, we could argue that late stages of influenza virus replication, including budding and/or assembly, are dependent on a SM salvage pathway, which could be initiated by NA activity leading to the observed decrease of ganglioside GM3 levels in influenza virus infected cells (Gerl et al., 2012; Sato et al., 1998). It has been shown that GM3 degradation by sialidase activity at the plasma membrane resulted in the production of Cer and subsequently of sphingosine, which was recycled for sphingolipid synthesis including the formation of SM and GlcCer species (Valaperta et al., 2006). The possibility that ganglioside degradation might be directly implicated in a SM salvage pathway during influenza virus infection is underlined by the antiviral effects of two inhibitors targeting different arms of sphingolipid biosynthesis on influenza virus replication (Hidari et al., 2006). Fumonisin B1 acting on ceramide synthases inhibits *de novo* biosynthesis and resynthesis of sphingolipids whereas *d,l-threo*-1-phenyl-2-decanoylamino-3-morpholino-1-propanol (PDMP) is a specific inhibitor of glycosphingolipid biosynthesis by acting on glucosylceramide synthase. While both inhibitors impaired influenza virus replication, only fumonisin B1 also significantly decreased SM levels (Hidari et al., 2006) suggesting, together with the D609 data, a specific requirement of glycosphingolipid synthesis in the formation of SM through a salvage pathway.

Additional indirect evidence pointing towards a possible role of a sphingolipid salvage pathway during influenza virus replication comes from a recent study showing increased virus titres produced from SPL, the enzyme responsible for the irreversible degradation of S1P, deficient cells (Seo et al., 2010). SPL deficiency leads to accumulation of S1P and induction of sphingolipid formation via recycling at the expense of *de novo* sphingolipid biosynthesis (Hagen-Euteneuer et al., 2012); indeed

dephosphorylation of S1P leads to the production of sphingosine which can be recycled for sphingolipid synthesis (Fyrst and Saba, 2010; Kitatani et al., 2008). Contrariwise, overexpression of SPL led to the inhibition of influenza virus replication (Seo et al., 2010), possibly due to the inhibition of sphingolipid recycling.

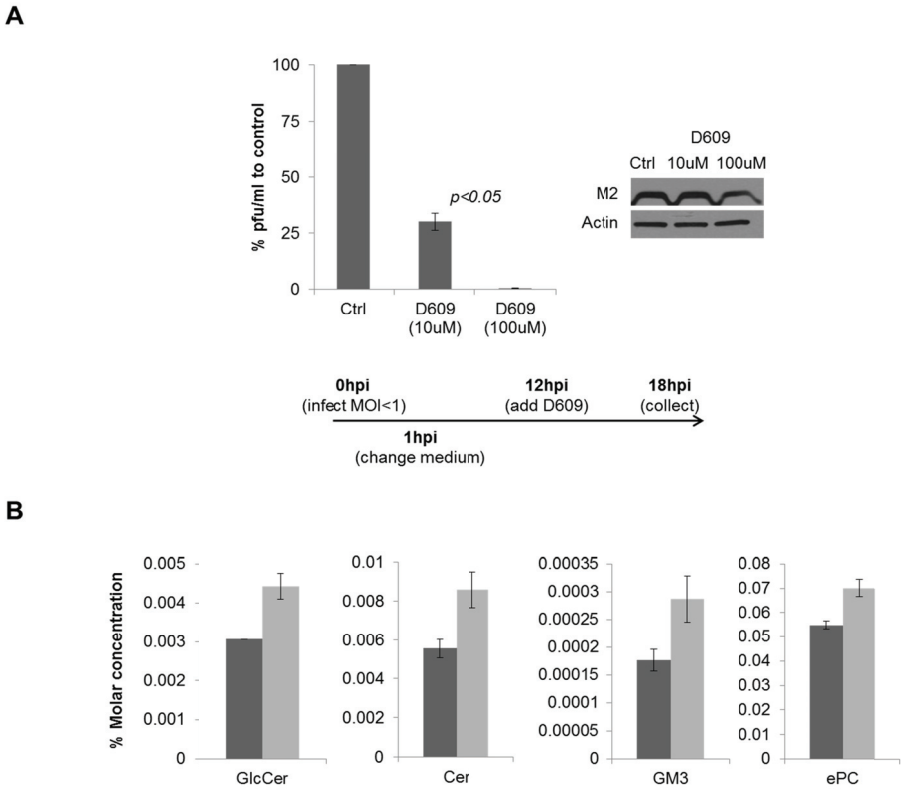

Figure 4-4: Inhibition of sphingomyelin biosynthesis impairs influenza virus replication. (A) A549 cells were infected with influenza virus and the sphingomyelin synthase inhibitor (D609) was added at 12hpi. Supernatant was collected at 18hpi and significantly reduced levels of virus titres were assessed by plaque assay (unpaired Student's t-test; two tailed $p<0.05$). Data is from three independent experiments and error bars depict standard errors. **(B)** A549 cells were treated with 10µM of D609 for 18 hours and mainly sphingolipid and ePC species were differentially regulated. Two (control) and three (D609 treated samples) independent measurements were performed. Error bars represent standard deviations.

4.3.5 PI4KIIIα as a major regulator of lipid metabolism[7]

Our findings of differentially regulated lipid species and their potential roles during influenza virus replication, combined with extensive literature, underline an important function of lipids, not only in mediating membrane structure and energy storage but also in regulating cellular organization and signalling. For example, one of the best understood lipid class implicated in cell physiology are phosphoinositides, which are generated by the phosphorylation of PI at the 3, 4 and 5 positions of the inositol ring and are minor components of cellular membranes (Di Paolo and De Camilli, 2006). Different degrees of phosphorylation of their head groups confer structural and functional diversity to the seven phosphoinositide species which are heterogeneously distributed in cellular membranes. Their head groups are exposed on the cytosolic leaflet of membranes and facilitate binding of a plethora of proteins generating a code for membrane identity (Lemmon, 2008).

PI4P is the most abundant phosphoinositide and plays fundamental roles in the structure and function of the Golgi, endosomal system as well as the plasma membrane (D'Angelo et al., 2008). It is synthesized at the Golgi and plasma membrane by phosphorylation of PI through the activity of four encoded PI4-kinases (PI4KIIα, PI4KIIß, PI4KIIIα and PI4KIIIß). Despite the evidence that PI4KIIIα activity is responsible for the generation of PI4P at the plasma membrane, its cellular localization, regulation and downstream implications are still obscure (Balla and

[7] This work was part of a collaborative effort with Fubito Nakatsu and Pietro De Camilli at Yale University and is in revision for publication in *JCB* (Nakatsu et al, 2012).

Balla, 2006). Recent findings suggest a critical dependency of HCV replication on PI4KIIIα (Alvisi et al., 2011; Berger et al., 2009; Borawski et al., 2009; Tai et al., 2009; Trotard et al., 2009) which further highlights the need to start elucidating its subcellular localization and the role of its generated PI4P pool in cell physiology.

For this purpose, our collaborators (Fubito Nakatsu & Pietro DeCamilli, Yale University) generated and characterized PI4KIIIα KO MEFs (Nakatsu et al, 2012). They revealed by immunocytochemistry (ICC) that, in comparison to WT MEFs, PI4KIIIα KO MEFs exhibited decreased levels of cholesterol at the plasma membrane but its accumulation in intracellular vesicles (Figure 4-5C). We further analysed cholesterol levels by mass spectrometry as described previously (Shui et al., 2011a) and found a small but significant increase in free cholesterol in PI4KIIIα KO MEFs (n=12 for WT and n=12 for KO MEFs; generated over four independent experiments) which together suggested a regulatory role of PI4KIIIα in cholesterol homeostasis.

We also analysed the lipidome of PI4KIIIα KO MEFs in relation to control MEFs. The 12 WT and 12 KO samples were analysed by HPLC MS/MS (operated in MRM mode) as described above (Chapter 2), but using a slightly modified MRM list to also include lysolipids and PA species (Supplementary Table 7-6). KO MEFs exhibited higher levels of total PI and PA species while PC levels were only increased to a lesser extent (Figure 4-5A&B). The accumulation in PI levels most probably reflected decreased PI4KIIIα activity since PI is the substrate for PI4KIIIα. In line with this, PI4KIIIα KO MEFs also exhibited decreased levels of PI4P (Nakatsu et al, 2012). Since PA is a strong allosteric activator of PIPKIs (Jenkins et al., 1994), accumulation of PA supported the findings of a modest reduction in $PI(4,5)P_2$ levels in PI4KIIIα KO

MEFs, due to a massive compensatory upregulation of PIPKIs converting PI4P to $PI(4,5)P_2$. This was in contrast to decreased levels of PS in PI4KIIIα KO cells which probably reflected inhibition of the PI4P 4-phosphatase Sac1 since PS has recently been shown to be its allosteric activator (Zhong et al., 2012). Thus, loss of PI4KIIIα leads to initiation of homeostatic mechanisms by activation of PIP kinases and inhibition of PI4P phosphatases to restore $PI(4,5)P_2$ levels (Nakatsu et al, 2012).

Despite no overall or only small changes in the PE and PC classes respectively, there was a remodelling with regard to their ether and ester linkages (Figure 4-5A). While the increase in ePE species was accompanied by decreased aPE species, the PC class lipid species showed the reverse trend with decreasing levels of ePC but increasing levels of aPC species in PI4KIIIα KO MEFs (Figure 4-5A). The opposite regulation of ester and ether lipids was consistent with our time course data of influenza virus infected cells (Chapter 2). This suggested an important cellular balance between ether and ester linked lipids and was further supported by other studies showing the reverse regulation of ester and ether linked lipid species (Nagan et al., 1998; Raa et al., 2009). For example, there were significantly higher levels of ester linked lipid species in AGPS depleted cells (Figure 4-1D) and DHAPAT deficient cells (Nagan et al., 1998).

Upregulation of ePE species was of great interest with regard to the defect in cholesterol homeostasis observed in PI4KIIIα KO MEFs (Figure 4-5C). While it is evident that ether lipid deficiency impairs cholesterol homeostasis, there is still no consensus with regard to a plausible mechanism (Mandel et al., 1998; Mankidy et al., 2010; Munn et al., 2003; Thai et al., 2001). Nonetheless, our findings support the reported defect in cholesterol transport (Munn et al., 2003; Thai et al., 2001) on the

basis of vesicular trafficking since PI4KIIIα knockdown increased endocytosis (Collinet et al., 2010). This would support our findings of cholesterol depletion from the plasma membrane but its accumulation in intracellular vesicles (Figure 4-5C). In line with increased trafficking from, but decreased trafficking to the plasma membrane in PI4KIIIα KO MEFs, we observed a decrease in ePC species, which would be in line with our proposed hypothesis about their involvement in the secretory pathway (Figure 4-2). Such opposite actions of ePC and ePE species could explain contradictory findings between different studies on ether lipids with regard to their involvement in cholesterol homeostasis since distribution of ePC and ePE levels might be different between cell lines and dependent on cellular function.

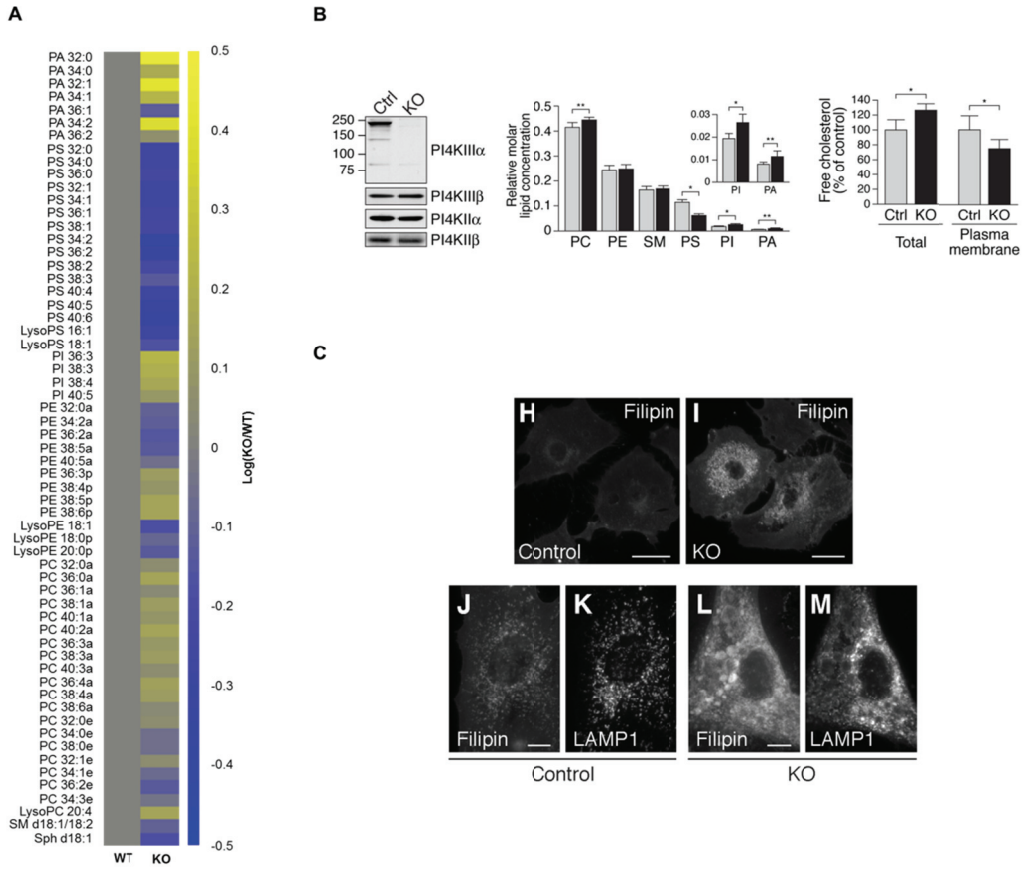

Figure 4-5: PI4KIIIα as a major regulator of cellular lipid metabolism. (A) Heat plot representing the log(KO/WT) of differentially regulated lipid species (WT: n=12; KO: n=12; unpaired Student's t-test; two-tailed; $p<0.05$). **(B)** Overview of phospholipid classes and cholesterol levels in KO fibroblasts. (*$p<0.0001$; **$p<0.001$). **(C)** Fluorescence imaging of WT and KO fibroblasts showing the accumulation of cholesterol in late endosomal and/or lysosomal compartments. Figures in B & C were taken from Nakatsu et al, 2012.

4.4 Conclusion

In this chapter, we confirmed the functional importance of choline containing lipid species for influenza virus infection. We showed the importance of PC lipid class remodelling for influenza virus replication (Figure 4-1) and based on a data mining approach, we hypothesized a specific involvement of ePC species in polarized vesicular trafficking facilitating influenza virus budding at the apical plasma membrane (Figure 4-2). We also demonstrated a requirement of SM biosynthesis for late stages of influenza virus infection and hypothesized a possible involvement of a salvage pathway rather than *de novo* biosynthesis (Figure 4-4). Our findings warrant future studies to further dissect the function of choline containing lipid species for influenza virus replication. On this note, we are in the process of performing EM experiments to check for an influenza virus budding phenotype at the plasma membrane of ether lipid deficient A549 cells and of cells treated with a sphingomyelin synthase inhibitor.

We additionally confirmed the functional importance of the hypothesized differentially regulated peroxisomal balance between anabolic (increased biosynthesis of ether lipids) and catabolic activities (decreased catalase activity and accumulation of C26 fatty acid containing sphingolipids) by observing an inhibitory effect of a PPARα agonist on influenza virus replication (Figure 4-3). This supported the therapeutic potential of PPARα agonists (Budd et al., 2007; Fedson, 2008). Based on the distinct lipid compositions of two influenza virus strains differing by a point mutation in NS1 (Figure 3-4 & Figure 3-5) and on recent literature (Billharz et al.,

2009; Wolff et al., 1996), we further proposed NS1 as a regulator of lipid metabolism and found a putative peroxisomal targeting sequence in NS1 (Figure 4-3). Although supported by the reported interaction of NS1 with the peroxisomal protein HSD17B4 (Wolff et al., 1996), these findings need further experimental validation to prove localization of NS1 with peroxisomes.

Finally, we illustrated the complex regulation and the multifunctional diversity of lipids by presenting the vast impact of PI4KIIIα deficiency on lipid metabolism and cellular function (Nakatsu et al, 2012). We were able to combine the observed cholesterol homeostasis phenotype in PI4KIIIα KO MEFs to our postulated concept of ether lipid involvement in vesicular trafficking, whereby ePE and ePC species exert opposite activities in endocytic and exocytic pathways respectively. Based on these findings, PI4KIIIα KO MEFs represent an attractive model to further investigate the regulatory mechanism behind dependency of cholesterol and vesicular trafficking on ether lipid metabolism.

5 Final Discussion & Conclusion

5.1 Final discussion

With this work, we presented for the first time a detailed temporal lipid profile of influenza virus infection in a lung epithelial cell line (A549) which correlated with the lipid composition of purified influenza virus particles (Chapters 2 & 3). We confirmed the functional importance of PC class remodelling and SM biosynthesis for influenza virus replication (Chapter 4) and additionally showed that influenza virus NS1 is a determinant for the lipid composition of influenza virions, bridging virus pathogenicity to host cell lipid metabolism (Chapter 3).

5.1.1 Lipid metabolism in influenza virus infected cells (Figure 5-1)

We were able to derive a model of lipid flux in influenza virus infected cells (Figure 2-5) by combining our lipid data from the initial time course experiment (Chapter 2) to existing genomics (Billharz et al., 2009; Karlas et al., 2010; Konig et al., 2010; Shapira et al., 2009; Sui et al., 2009; Watanabe et al., 2010) and proteomics data (Coombs et al., 2010; Dove et al., 2012; Kroeker et al., 2012). Subsequently, we modified the proposed model (Figure 5-1) by integrating additional data describing the lipid composition of different influenza virus strains (Chapter 3) and showing the functional importance of sphingolipids and ether lipids for influenza virus replication (Chapter 4).

5.1.1.1 Incorporation of serine into sphingolipid and phosphatidylserine biosynthesis is localized to the plasma membrane (Figure 5-1)

We hypothesized that the observed lipid changes were directly linked to a redirection of glycolytic flux due to an upregulation of early glycolytic steps, similar to aerobic glycolysis (Warburg effect) in cancer cells (Ritter et al., 2010) (Paragraph 2.4). This was supported by the upregulation (Kroeker et al., 2012) and early phosphorylation of PKM2 in virus infected cells (Figure 2-4) which has been shown to be the major driver for aerobic glycolysis and tumour growth (Vander Heiden et al., 2009). In the light of that, the observed increase in sphingolipid biosynthesis, especially GlcCer and SM species, can be explained by the increased endogenous synthesis of serine from glycolytic intermediates via phosphoglycerate dehydrogenase (Locasale et al., 2011). In line with this, enhanced serine biosynthesis upon influenza virus infection has been previously reported (Ritter et al., 2010).

Similar trends were also reflected by distinct lipid compositions of two influenza virus strains exhibiting different degrees of pathogenicity due to a point mutation in NS1 (D125G) (Figure 3-5). In addition to higher levels of GlcCer and some SM species, there was also an enrichment of PS species in the more virulent strain (Figure 3-5) despite no changes in PS levels during the course of an infection (Figure 2-1). This suggested a severity dependent regulation of host cell lipid metabolism, which was supported by a recent study showing a NS1 dependent expression of lipid metabolic genes (Billharz et al., 2009). Furthermore, our results pointed towards localized changes of host cell metabolism at the plasma membrane and highlighted a possible

involvement of serine incorporator 5 (Serinc5 or TPO1). Serinc5 is localized to sphingolipid rich domains in cellular membranes (Fukazawa et al., 2006; Krueger et al., 1997) and provides a membrane embedded scaffold for enzymes involved in glycolysis, sphingolipid- and serine metabolism (Inuzuka et al., 2005). Overexpression of Serinc5 stimulates PS and sphingolipid biosynthesis by facilitating serine exchange with other lipid head groups and ceramide biosynthesis, respectively (Inuzuka et al., 2005). Therefore, enrichment of PS in more virulent influenza virions can be directly linked to the decrease in aPC species (Figure 3-5) via activity of PTDSS1, exchanging the choline head group of PC with serine to generate PS. Similar reverse trends between PS and PC species have been recently observed in different influenza virus strains (Polozov et al., 2008) and together strengthen the NS1 dependent upregulation of Serinc5 expression in influenza virus infected cells (Geiss et al., 2002).

5.1.1.2 A salvage pathway is responsible for the increase of SM biosynthesis in influenza virus infected cells (Figure 5-1)

A more general picture was observed for sphingolipids (GlcCer and SM) since they were upregulated in virus infected cells (Figure 2-1), enriched in purified influenza virus particles (Figure 3-1) and even showed some dependency on severity (Figure 3-5). For example, increased levels of SM species were usually accompanied by decreased levels of aPC species which likely reflected SMS1 and SMS2 activities. Importance of SM biosynthesis for late stages of influenza virus replication was confirmed by impairment of infectious virus particle production after treatment with

the SMS1/2 inhibitor D609 (Figure 4-4A). Incorporation of additional experiments showing antiviral activity of different sphingolipid inhibitors, such as fumonisin B1 and PDMP (Hidari et al., 2006), generated an interesting hypothesis with regard to an involvement of a SM salvage pathway. We hypothesized that such a SM salvage pathway is mediated by influenza virus NA activity and dependent on *de novo* sphingolipid biosynthesis (Paragraph 4.2.7). The possible involvement of a SM salvage pathway is further highlighted by the identification of both, sphingolipid biosynthetic- and sphingolipid degrading enzymes which support influenza virus replication. For example, recent siRNA screens identified ceramide synthase 4 (LASS4) and 3-ketodihydrosphingosine reductase (KDSR), which are involved in sphingolipid biosynthesis, and N-acetylgalactosaminidase alpha (NAGA), sialidase 1 (lysosomal) (NEU1) and N-acylsphingosine amidohydrolase (acid ceramidase) 1 (ASAH1) which mediate sphingolipid degradation (Figure 5-1).

5.1.1.3 The increased lipogenesis but decreased ß-oxidation in the peroxisome is a mediator of lipid flux (Figure 5-1)

In contrast to a decrease in aPC species, we detected a severity independent increase in ePC species during influenza virus infection (Figure 2-1, Figure 3-4 & Figure 3-5). Upregulation of ePC biosynthesis can similarly be explained by increased glycolytic activity since DHAP is a direct precursor for ether lipid biosynthesis. We confirmed the functional importance of ether lipid biosynthesis by observing reduced virus titres produced from DHAPAT deficient cells and from AGPS depleted cells (Figure 4-1B&C). Consistent with enhanced peroxisomal lipogenesis, we also detected an

accumulation of odd chain aPC species (Figure 2-1). Alternatively, we observed a reduction in peroxisomal ß-oxidation which was supported by declined catalase activity (Figure 2-3), enrichment of C26 fatty acids, but depletion of C24:1 fatty acids in sphingolipids (Figure 2-2B&D), and by the inhibitory activity of a PPARα agonist (GW7647) on influenza virus replication (Figure 4-3A). We hypothesized that reduction in fatty acid ß-oxidation was specific to the peroxisome as we continuously observed low levels of TAG in influenza virus infected cells (Figure 2-1 & Paragraph 2.3.1.3). Identification of enzymes involved in the peroxisomal ß-oxidation cascade being antiviral, further strengthened our findings (Figure 5-1).

Especially, the identification of a putative PTS2 sequence in NS1 (Figure 4-3B & Supplementary Figure 7-5) and its inhibitory interaction with the peroxisomal protein HSD17B4 (Wolff et al., 1996) sparked our interest. It has been reported that increased glycolysis in differentiating adipocytes induced TAG synthesis but, in contrary, ether lipid levels remained constant despite high DHAPAT activity (Hajra et al., 2000). This was explained by the concomitant activity of acyl-DHAP reductase generating acyl-glycerol-3-phopshate (Hajra et al., 2000). While the yeast acyl-DHAP reductase is known as Ayr1p (Athenstaedt and Daum, 2000), so far, the mammalian homologue has not been identified. We decided to perform a blast search[8] on the human genome using Ayr1p (33kDa) as a query sequence, identifying HSD17B1 (DHB1) with the highest degree of similarity (*Score:* 74.7; *E value:* 2e-17). HSD17B1 is a 35kDa protein and belongs to the same protein family as HSD17B4. Subsequent alignment of HSD17B1, HSD17B4 (80kDa) and Ayr1p (35kDa) revealed a high conservation of

[8] The blast search was performed by BLASTP 2.2.27+ (Altschul et al., 1997; Altschul et al., 2005) run on http://blast.ncbi.nlm.nih.gov using standard settings.

active sites in the N-terminus which corresponded to the region responsible for its (3R)-hydroxyacyl-CoA dehydrogenase activity (Supplementary Figure 7-6). This sequence is characterized by its short chain dehydrogenase/reductase (SDR) motif which is found in 73 human proteins (Bray et al., 2009). Since the mammalian acyl-DHAP reductase has been proposed to be localized to the peroxisomal membrane (Ghosh and Hajra, 1986; Hajra et al., 2000), we decided to screen all reported peroxisomal proteins (Wiese et al., 2007) for a SDR motif. We identified 29 peroxisomal proteins carrying a SDR motif, and in combination with the predicted size of 75kDa for the mammalian acyl-DHAP reductase (Datta et al., 1990), we ended up with five candidates having a size between 70 and 80kDa (Supplementary Figure 7-7). However, HSD17B4 was the only candidate with a classical SDR sequence similar to Ayr1p. In combination with increased catalase activity upon induction of acyl-DHAP reductase (Hajra et al., 2000), these results collectively suggested HSD17B4 being a potential candidate responsible for the mammalian acyl-DHAP reductase activity.

Putting these findings into the context of an influenza virus infected cell with high glycolytic activity, we propose that NS1 is not solely modulating lipid metabolism by differentially regulating gene expression (Billharz et al., 2009), but also, due to its inhibitory interaction with HSD17B4, impairing peroxisomal fatty acid ß-oxidation and TAG accumulation, facilitating lipogenesis (ether lipid and odd chain lipid biosynthesis) in the peroxisome. Future studies should address whether HSD17B4 accounts for the mammalian acyl-DHAP reductase activity and whether its inhibition leads to impaired lipid flux under high glycolytic activity. Subsequently, it would be interesting to determine whether the interaction of NS1 with HSD17B4 is severity

dependent. This would be of great significance since the peroxisome has recently been identified as a major site for initial steps of antiviral signalling (Dixit et al., 2010).

NS1 most probably is just one part of a complex network incorporating cellular and viral factors to regulate host cell lipid metabolism. For example, the balance between metabolite levels is crucial to maintain lipid flux. This could explain our inability to rescue influenza virus production from ether lipid deficient cells (Supplementary Figure 7-4). 1-*O*-hexadecyl-sn-glycerol (HG) enters ether lipid metabolism downstream of AGPS and its addition rescues ether lipid deficiency (Nagan et al., 1998). However, we were not able to rescue virus production suggesting importance of metabolic flux through ether lipid metabolism rather than sole dependency on ether lipid metabolites. Impairment of DHAPAT and AGPS under high glucose conditions/influenza virus infection probably leads to the accumulation of glycolytic intermediates and to a redirection in glycolytic flux which might disturb the metabolic balance needed for influenza virus production. Therefore, addition of HG might have additional, non-ether lipid related effects which could be inhibitory for virus production. It would be interesting to scrutinize the effects of higher glycolytic flux in DHAPAT deficient and AGPS depleted cells.

5. Final Discussion & Conclusion

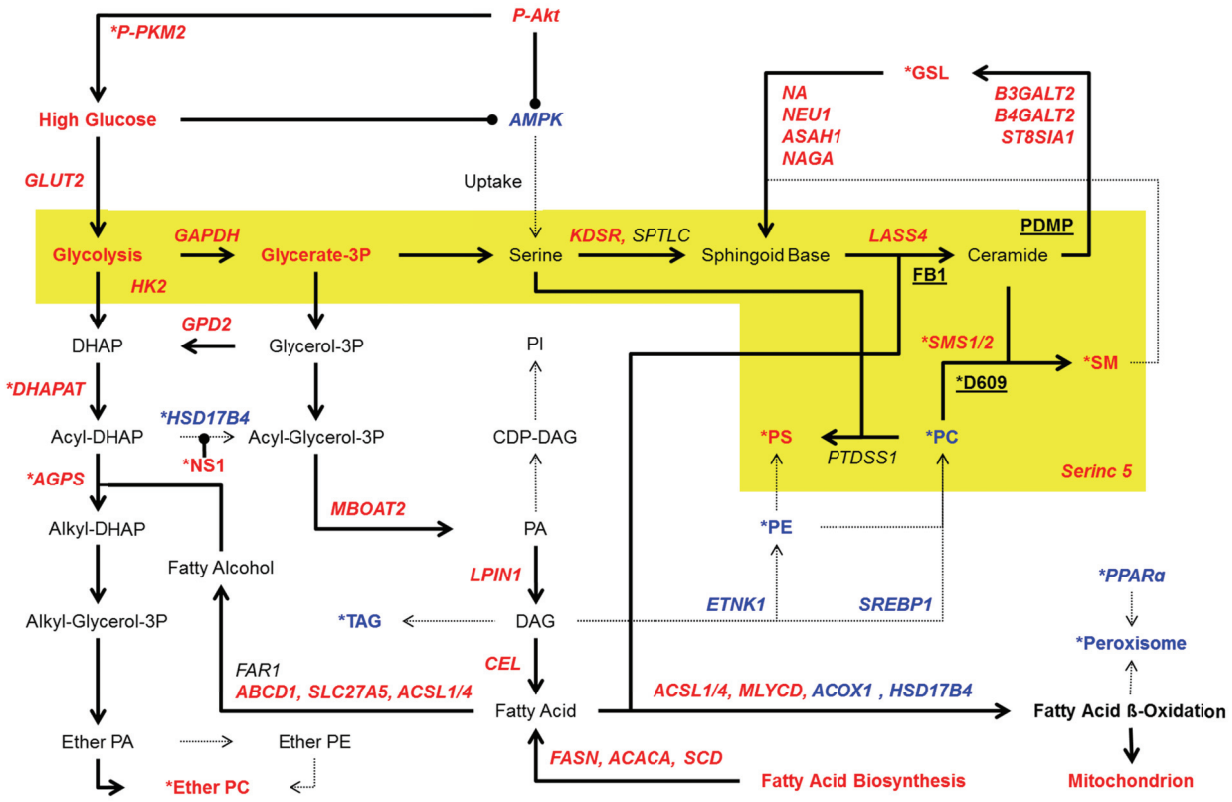

Figure 5-1: Final model of proposed lipid flux in influenza virus infected cells (Page 159). The model was derived by modifying the proposed lipid flux model (Chapter 2; Figure 2 5) with additional data from chapters 3and 4. Our data was combined with published data from siRNA screens (Brass et al., 2009; Karlas et al., 2010; Konig et al., 2010; Shapira et al., 2009; Sui et al., 2009; Watanabe et al., 2010), protein expression studies (Coombs et al., 2010; Dove et al., 2012; Kroeker et al., 2012) and gene expression studies (Billharz et al., 2009). Genes, proteins and metabolites reported to affect influenza virus replication are depicted in black (no change or not identified), bold red (proviral or upregulated) and bold blue (antiviral or downregulated); Bold arrows and dashed arrows represent proposed increased and decreased fluxes, respectively; Bold black lines with round ends indicate an inhibition of expression or activity; ATP-binding cassette, sub-family D 1 (ABCD1), acetyl-CoA carboxylase alpha (ACACA), acyl-CoA oxidase 1 (ACOX1), acyl-CoA synthetase long-chain family member 1/4 (ACSL1/4), alkylglycerone phosphate synthase (AGPS), AMP activated protein kinase (AMPK), N-acylsphingosine amidohydrolase (acid ceramidase) 1 (ASAH1) , UDP-Gal:betaGlcNAc beta 1,3-galactosyltransferase, polypeptide 4 (B3GALT2), UDP-Gal:betaGlcNAc beta 1,4-galactosyltransferase polypeptide 4 (B4GALT2), carboxyl ester lipase (CEL), diacylglycerol (DAG), dihydroxyacetone phosphate (DHAP), DHAP acyl transferase (DHAPAT), ethanolamine kinase 1 (ETNK1), fatty acid reductase 1 (FAR1), fatty acid synthase (FASN), glyceraldehyde-3-phopshate dehydrogenase (GAPDH), facilitated glucose transporter 2 (GLUT2), glycerol-3-phosphate dehydrogenase 2 (GPD2), glycosphingolipids (GSL), hexokinase 2 (HK2), hydroxysteroid (17-beta) dehydrogenase 4 (HSD17B4), 3-ketodihydrosphingosine reductase (KDSR), ceramide synthase 4 (LASS4), lipin 1 (LPIN1), membrane bound O-acyltransferase domain containing 2 (MBOAT2), malonyl-CoA decarboxylase (MLYCD), influenza virus neuraminidase (NA), N-acetylgalactosaminidase alpha (NAGA), sialidase 1 (lysosomal) (NEU1), influenza virus NS1 (NS1), phosphatidic acid (PA), phosphatidylcholine (PC), phosphatidylethanolamine (PE), phopsphatidylinositol (PI), pyruvate kinase 2 (PKM2), peroxisome proliferator-activated receptor alpha (PPARα), phosphatidylserine (PS), stearoyl-CoA desaturase (SCD), serine incorporator 5 (SERINC5), fatty acid transporter 5 (SLC27A5), sphingomyelin (SM), sphingomyelin synthase 1/2 (SMS1/2), sterol regulatory element binding transcription factor 1 (SREBP1), sialyltransferase 8 (ST8SIA1) & triacylglycerol (TAG); yellow box indicates the scaffold provided by serine incorporator 5 (SERINC5); Pharmacological inhibitors inhibiting influenza virus infection are depicted in underlined bold black; *identified in this study; Sphingomyelin synthase inhibitor (D609), ceramide synthase inhibitor (fumonisin B1; FB1) & glucosyltransferase inhibitor (d,l-threo-1-phenyl-2-decanoylamino-3-morpholino-1-propanol; PDMP).

5.1.2 Lipid composition of influenza virus particles

We concluded that influenza viruses tailor host lipid metabolism according to their needs for virion morphogenesis, due to similarities observed between influenza virus lipid composition (Figure 3-1) and influenza virus induced changes in host cell lipid metabolism (Figure 2-1). Especially, enrichment of SM, GlcCer, and ePC but decrease in aPC species in virus particles correlated with the temporal lipid profile. In contrast, ceramide species exhibited a relatively high enrichment in influenza virus particles without being differentially regulated in influenza virus infected cells. This

suggested a localized change at the plasma membrane budding site (Figure 2-1 & Figure 3-1). Subsequently, we were able to combine differences in ceramide enrichment of enveloped viruses and cellular vesicles to a lipid mediated model of intracellular trafficking (Figure 3-3). Collectively, our data underlined the importance of lipids in the virus life cycle and highlighted the general antiviral potential of disturbing the lipid composition of virus envelopes (Figure 3-7 & Figure 3-8).

5.1.2.1 The ePC/aPC ratio is unique for influenza virus and implies a need for polarized vesicular trafficking

Besides the described enrichment of SM and GlcCer species in influenza virus particles, we observed distinct remodelling within the PC lipid class. This was clearly in line with the lipid changes in influenza virus infected cells whereby enrichment of ePC species was accompanied by depletion of aPC species (Figure 2-1 & Figure 3-1). The increased ePC/aPC ratio was not only conserved across four different influenza virus strains, but also unique to influenza when compared with other enveloped viruses (Figure 3-2). Additionally, more virulent influenza virions exhibited an increased ePC/aPC ratio which was due to lower levels of aPC species rather than increased ePC species (Figure 3-4 & Figure 3-5), highlighting a general requirement of ePC species for influenza virus replication. Importance of ether lipid metabolism was further supported by decreased production of infectious virus particles from DHAPAT deficient and AGPS depleted cells (Figure 4-1). As discussed previously, the virulence dependent downregulation of aPC species most likely reflected increased SM and PS biosynthesis at the plasma membrane (Figure 5-1), and

supported the severity dependent regulation of SREBP1 (Billharz et al., 2009), a major regulator of aPC biosynthesis (Walker et al., 2011). In line with budding of influenza virus at the apical plasma membrane, using an *in silico* approach, we hypothesized a possible involvement of ePC species in polarized vesicular trafficking (Figure 4-2). Analysis of PI4KIIIα KO MEFs exhibiting greatly impaired lipid metabolism with increasing levels of ePE, but decreasing levels of ePC species, showed an accumulation of cholesterol in intracellular vesicles but its near absence from the plasma membrane (Figure 4-5). This was supported by evidence showing the involvement of ether lipids in cholesterol homeostasis, especially in regulating cholesterol transport (Mandel et al., 1998; Munn et al., 2003; Thai et al., 2001). Therefore, we explained accumulation of cholesterol in intracellular vesicles by increased endocytic activities due to PI4KIIIα depletion (Collinet et al., 2010). Considering higher enrichment of ePC species in intracellular membranes but increased levels of ePE species at the plasma membrane (Andreyev et al., 2010), we could envision reverse functionalities between ePC (exocytic) and ePE (endocytic) species.

Differential regulation of ePE and ePC species is of high interest. For example, upregulation of ePC species in influenza virus infected cells was intriguing since ePE species, despite being present in much higher abundance in mammalian cells, did not exhibit any differential regulation upon influenza virus infection. This clearly points towards specific fine tuning of ether lipid metabolism, which might be of relevance for cell physiology. Clearly, our experiments on ether lipid deficient cells were not conclusive with respect to functional differences between ePC and ePE species, but the hypothetical opposite functionality in trafficking between ePC and ePE highlights

the necessity of addressing ePE and ePC functions separately, rather than treating ether lipids as a whole.

5.1.2.2 The ceramide/cholesterol ratio is a determinant of vesicular trafficking

No substantial changes were observed in ceramide species during the course of an influenza virus infection (Figure 2-1). Nevertheless, influenza virus particles were generally enriched in ceramide species (Figure 3-1 & Figure 3-3A), consistent with an earlier study (Gerl et al., 2012). Further analysis revealed specific ceramide enrichment in viruses fusing at late endosomal compartments (Figure 3-3A) and subsequently we derived a model linking the ceramide/cholesterol ratio of cellular and viral membranes to vesicular trafficking (Figure 3-3B,C&D). On the basis of an increasing ceramide/cholesterol gradient from the plasma membrane towards the cell body of mammalian cells, we hypothesized that vesicular fusion occurs most efficiently when the ceramide/cholesterol ratio of the fusing membranes are similar (Figure 3-3). For example, influenza virus having a high ceramide/cholesterol ratio fuses at late endosomal membranes (Figure 3-3) whereas retroviruses such as HIV fusing at the plasma membrane, or at early endosomal compartments, exhibit a low ceramide/cholesterol ratio. We were also able to describe several cellular trafficking events using ceramide/cholesterol ratios. We concluded that intracellular fusion events occur at target membranes with a high ceramide/cholesterol ratio, whereas vesicles with a low ceramide/cholesterol ratio more likely fuse at the plasma membrane (Figure 3-3).

The high activity of sphingolipid degrading enzymes in late endosomal compartments (Kolter and Sandhoff, 2010) and the general sphingolipid enrichment of influenza virus particles (Figure 3-1) (Gerl et al., 2012), made us wonder whether further modifications to the virus lipid content occur to mediate fusion. For example, high activity of acid sphingomyelinase in the late endosome might also degrade SM in the virus envelope, generating ceramide and increasing the ceramide/cholesterol ratio to mediate virus fusion. Modifications to the sphingolipid content have been shown to mediate fusion whereby sphingomyelinase activity (ceramide generating) is needed for phago-lysosomal fusion (Utermohlen et al., 2008; Utermohlen et al., 2003), and ceramidase activity (ceramide degrading) primes synaptic vesicles for fusion at the plasma membrane (Rohrbough et al., 2004). This clearly demonstrates the functional importance of lipid composition in cellular membranes. On this note, it has been observed that influenza virosomes[9], having a distinct lipid composition than natural influenza viruses, get trafficked to different intracellular compartments than wild type influenza viruses, despite similar uptake mediated by HA (Bernd Wollscheid, *personal communication*). One possible explanation could be impairment in virus fusion due to the different lipid compositions, in spite of normal function of HA. This collectively underlines the significance of lipid-protein relationships as mediators of cell physiology.

[9] An influenza virosome is a liposome made of synthetic and natural phospholipids carrying wild type HA and NA.

5.2 Conclusion

In summary, this is the first in-depth study specifically addressing host lipid metabolism and function during influenza virus infection. It further highlighted lipidomics as a powerful tool to derive novel hypotheses for virus and cell biology.

Firstly, we revealed and proposed a detailed lipid flux model for influenza virus infection which warrants further studies, especially addressing its regulation for virion morphogenesis with respect to virus severity. It also raises the question whether different lipid compositions of influenza virus particles are mediators of virulence by conferring higher stability and infectivity to influenza virions. For instance, it would be exciting to extend our lipidomics approach to a wide range of other influenza virus strains exhibiting differences in pathogenicity.

Secondly, our findings put lipids at the forefront of cell organization and regulation. We introduced a concept of lipid composition mediated intracellular trafficking hijacked by enveloped viruses. Identification and understanding the mechanism of how viruses and vesicles tailor their lipid compositions to functionality is crucial. For example, it would be interesting to screen the lipid compositions of diverse virus like particles pseudotyped with different virus surface glycoproteins (e.g. *pH* dependent or *pH* independent) to understand whether protein functionality is directly linked to lipid environment.

6 Bibliography

Ablan, S., Rawat, S.S., Blumenthal, R., and Puri, A. (2001). Entry of influenza virus into a glycosphingolipid-deficient mouse skin fibroblast cell line. Archives of virology *146*, 2227-2238.

Adibhatla, R.M., Hatcher, J.F., and Gusain, A. (2012). Tricyclodecan-9-yl-xanthogenate (D609) mechanism of actions: a mini-review of literature. Neurochemical research *37*, 671-679.

Agnello, V., Abel, G., Elfahal, M., Knight, G.B., and Zhang, Q.X. (1999). Hepatitis C virus and other flaviviridae viruses enter cells via low density lipoprotein receptor. Proceedings of the National Academy of Sciences of the United States of America *96*, 12766-12771.

Albi, E., and Viola Magni, M.P. (2004). The role of intranuclear lipids. Biology of the cell / under the auspices of the European Cell Biology Organization *96*, 657-667.

Alford, D., Ellens, H., and Bentz, J. (1994). Fusion of influenza virus with sialic acid-bearing target membranes. Biochemistry *33*, 1977-1987.

Altschul, S.F., Madden, T.L., Schaffer, A.A., Zhang, J., Zhang, Z., Miller, W., and Lipman, D.J. (1997). Gapped BLAST and PSI-BLAST: a new generation of protein database search programs. Nucleic acids research *25*, 3389-3402.

Altschul, S.F., Wootton, J.C., Gertz, E.M., Agarwala, R., Morgulis, A., Schaffer, A.A., and Yu, Y.K. (2005). Protein database searches using compositionally adjusted substitution matrices. The FEBS journal *272*, 5101-5109.

Alvisi, G., Madan, V., and Bartenschlager, R. (2011). Hepatitis C virus and host cell lipids: an intimate connection. RNA biology *8*, 258-269.

Amorim, M.J., Bruce, E.A., Read, E.K., Foeglein, A., Mahen, R., Stuart, A.D., and Digard, P. (2011). A Rab11- and microtubule-dependent mechanism for cytoplasmic transport of influenza A virus viral RNA. Journal of virology *85*, 4143-4156.

Amtmann, E. (1996). The antiviral, antitumoural xanthate D609 is a competitive inhibitor of phosphatidylcholine-specific phospholipase C. Drugs under experimental and clinical research *22*, 287-294.

Andre, P., Komurian-Pradel, F., Deforges, S., Perret, M., Berland, J.L., Sodoyer, M., Pol, S., Brechot, C., Paranhos-Baccala, G., and Lotteau, V. (2002). Characterization of low- and very-low-density hepatitis C virus RNA-containing particles. Journal of virology *76*, 6919-6928.

Andreyev, A.Y., Fahy, E., Guan, Z., Kelly, S., Li, X., McDonald, J.G., Milne, S., Myers, D., Park, H., Ryan, A.*, et al.* (2010). Subcellular organelle lipidomics in TLR-4-activated macrophages. Journal of lipid research *51*, 2785-2797.

Armstrong, R.T., Kushnir, A.S., and White, J.M. (2000). The transmembrane domain of influenza hemagglutinin exhibits a stringent length requirement to support the hemifusion to fusion transition. The Journal of cell biology *151*, 425-437.

Athenstaedt, K., and Daum, G. (2000). 1-Acyldihydroxyacetone-phosphate reductase (Ayr1p) of the yeast Saccharomyces cerevisiae encoded by the open reading frame YIL124w is a major component of lipid particles. The Journal of biological chemistry *275*, 235-240.

Baljinnyam, B., Schroth-Diez, B., Korte, T., and Herrmann, A. (2002). Lysolipids do not inhibit influenza virus fusion by interaction with hemagglutinin. The Journal of biological chemistry *277*, 20461-20467.

Balla, A., and Balla, T. (2006). Phosphatidylinositol 4-kinases: old enzymes with emerging functions. Trends in cell biology *16*, 351-361.

Bankaitis, V.A., Malehorn, D.E., Emr, S.D., and Greene, R. (1989). The Saccharomyces cerevisiae SEC14 gene encodes a cytosolic factor that is required for transport of secretory proteins from the yeast Golgi complex. The Journal of cell biology *108*, 1271-1281.

Barman, S., and Nayak, D.P. (2000). Analysis of the transmembrane domain of influenza virus neuraminidase, a type II transmembrane glycoprotein, for apical sorting and raft association. Journal of virology *74*, 6538-6545.

Barman, S., and Nayak, D.P. (2007). Lipid raft disruption by cholesterol depletion enhances influenza A virus budding from MDCK cells. Journal of virology *81*, 12169-12178.

Berger, K.L., Cooper, J.D., Heaton, N.S., Yoon, R., Oakland, T.E., Jordan, T.X., Mateu, G., Grakoui, A., and Randall, G. (2009). Roles for endocytic trafficking and phosphatidylinositol 4-kinase III alpha in hepatitis C virus replication. Proceedings of the National Academy of Sciences of the United States of America *106*, 7577-7582.

Billharz, R., Zeng, H., Proll, S.C., Korth, M.J., Lederer, S., Albrecht, R., Goodman, A.G., Rosenzweig, E., Tumpey, T.M., Garcia-Sastre, A.*, et al.* (2009). The NS1 protein of the 1918 pandemic influenza virus blocks host interferon and lipid metabolism pathways. Journal of virology *83*, 10557-10570.

Bissonnette, M.L., Donald, J.E., DeGrado, W.F., Jardetzky, T.S., and Lamb, R.A. (2009). Functional analysis of the transmembrane domain in paramyxovirus F protein-mediated membrane fusion. Journal of molecular biology *386*, 14-36.

Biswas, S., Yin, S.R., Blank, P.S., and Zimmerberg, J. (2008). Cholesterol promotes hemifusion and pore widening in membrane fusion induced by influenza hemagglutinin. The Journal of general physiology *131*, 503-513.

Blanc, M., Hsieh, W.Y., Robertson, K.A., Watterson, S., Shui, G., Lacaze, P., Khondoker, M., Dickinson, P., Sing, G., Rodriguez-Martin, S.*, et al.* (2011). Host defense against viral infection involves interferon mediated down-regulation of sterol biosynthesis. PLoS biology *9*, e1000598.

Bligh, E.G., and Dyer, W.J. (1959). A rapid method of total lipid extraction and purification. Canadian journal of biochemistry and physiology *37*, 911-917.

Blom, T.S., Koivusalo, M., Kuismanen, E., Kostiainen, R., Somerharju, P., and Ikonen, E. (2001). Mass spectrometric analysis reveals an increase in plasma membrane polyunsaturated phospholipid species upon cellular cholesterol loading. Biochemistry *40*, 14635-14644.

Borawski, J., Troke, P., Puyang, X., Gibaja, V., Zhao, S., Mickanin, C., Leighton-Davies, J., Wilson, C.J., Myer, V., Cornellataracido, I.*, et al.* (2009). Class III phosphatidylinositol 4-kinase alpha and beta are novel host factor regulators of hepatitis C virus replication. Journal of virology *83*, 10058-10074.

Boriskin, Y.S., Leneva, I.A., Pecheur, E.I., and Polyak, S.J. (2008). Arbidol: a broad-spectrum antiviral compound that blocks viral fusion. Current medicinal chemistry *15*, 997-1005.

Bouvier, N.M., and Palese, P. (2008). The biology of influenza viruses. Vaccine *26 Suppl 4*, D49-53.

Brass, A.L., Huang, I.C., Benita, Y., John, S.P., Krishnan, M.N., Feeley, E.M., Ryan, B.J., Weyer, J.L., van der Weyden, L., Fikrig, E.*, et al.* (2009). The IFITM proteins mediate cellular resistance to influenza A H1N1 virus, West Nile virus, and dengue virus. Cell *139*, 1243-1254.

Bray, J.E., Marsden, B.D., and Oppermann, U. (2009). The human short-chain dehydrogenase/reductase (SDR) superfamily: a bioinformatics summary. Chemico-biological interactions *178*, 99-109.

Briggs, J.A., Wilk, T., and Fuller, S.D. (2003). Do lipid rafts mediate virus assembly and pseudotyping? The Journal of general virology *84*, 757-768.

Brown, J.N., Palermo, R.E., Baskin, C.R., Gritsenko, M., Sabourin, P.J., Long, J.P., Sabourin, C.L., Bielefeldt-Ohmann, H., Garcia-Sastre, A., Albrecht, R.*, et al.* (2010). Macaque proteome response to highly pathogenic avian influenza and 1918 reassortant influenza virus infections. Journal of virology *84*, 12058-12068.

Bruce, E.A., Digard, P., and Stuart, A.D. (2010). The Rab11 pathway is required for influenza A virus budding and filament formation. Journal of virology *84*, 5848-5859.

Bruce, E.A., Medcalf, L., Crump, C.M., Noton, S.L., Stuart, A.D., Wise, H.M., Elton, D., Bowers, K., and Digard, P. (2009). Budding of filamentous and non-filamentous influenza A virus occurs via a VPS4 and VPS28-independent pathway. Virology *390*, 268-278.

Brugger, B., Glass, B., Haberkant, P., Leibrecht, I., Wieland, F.T., and Krausslich, H.G. (2006). The HIV lipidome: a raft with an unusual composition. Proceedings of the National Academy of Sciences of the United States of America *103*, 2641-2646.

Budd, A., Alleva, L., Alsharifi, M., Koskinen, A., Smythe, V., Mullbacher, A., Wood, J., and Clark, I. (2007). Increased survival after gemfibrozil treatment of severe mouse influenza. Antimicrobial agents and chemotherapy *51*, 2965-2968.

Caric-Lazar, M., Schwarz, R.T., and Scholtissek, C. (1978). Influence of the infection with lipid-containing viruses on the metabolism and pools of phospholipid precursors in animal cells. European journal of biochemistry / FEBS *91*, 351-361.

Castro, B.M., Silva, L.C., Fedorov, A., de Almeida, R.F., and Prieto, M. (2009). Cholesterol-rich fluid membranes solubilize ceramide domains: implications for the structure and dynamics of mammalian intracellular and plasma membranes. The Journal of biological chemistry *284*, 22978-22987.

Chan, R., Uchil, P.D., Jin, J., Shui, G., Ott, D.E., Mothes, W., and Wenk, M.R. (2008). Retroviruses human immunodeficiency virus and murine leukemia virus are enriched in phosphoinositides. Journal of virology *82*, 11228-11238.

Chan, R.B., Tanner, L., and Wenk, M.R. (2010). Implications for lipids during replication of enveloped viruses. Chemistry and physics of lipids *163*, 449-459.

Chandrasekaran, A., Srinivasan, A., Raman, R., Viswanathan, K., Raguram, S., Tumpey, T.M., Sasisekharan, V., and Sasisekharan, R. (2008). Glycan topology determines human adaptation of avian H5N1 virus hemagglutinin. Nature biotechnology *26*, 107-113.

Chen, B.J., Leser, G.P., Morita, E., and Lamb, R.A. (2007). Influenza virus hemagglutinin and neuraminidase, but not the matrix protein, are required for assembly and budding of plasmid-derived virus-like particles. Journal of virology *81*, 7111-7123.

Chen, B.J., Takeda, M., and Lamb, R.A. (2005). Influenza virus hemagglutinin (H3 subtype) requires palmitoylation of its cytoplasmic tail for assembly: M1 proteins of two subtypes differ in their ability to support assembly. Journal of virology *79*, 13673-13684.

Chen, R., and Holmes, E.C. (2006). Avian influenza virus exhibits rapid evolutionary dynamics. Molecular biology and evolution *23*, 2336-2341.

Cheng, V.C., To, K.K., Tse, H., Hung, I.F., and Yuen, K.Y. (2012). Two years after pandemic influenza A/2009/H1N1: what have we learned? Clinical microbiology reviews *25*, 223-263.

Chernomordik, L.V., Frolov, V.A., Leikina, E., Bronk, P., and Zimmerberg, J. (1998). The pathway of membrane fusion catalyzed by influenza hemagglutinin: restriction of lipids, hemifusion, and lipidic fusion pore formation. The Journal of cell biology *140*, 1369-1382.

Chernomordik, L.V., and Kozlov, M.M. (2003). Protein-lipid interplay in fusion and fission of biological membranes. Annual review of biochemistry *72*, 175-207.

Chernomordik, L.V., and Kozlov, M.M. (2008). Mechanics of membrane fusion. Nature structural & molecular biology *15*, 675-683.

Chernomordik, L.V., Leikina, E., Frolov, V., Bronk, P., and Zimmerberg, J. (1997). An early stage of membrane fusion mediated by the low pH conformation of influenza hemagglutinin depends upon membrane lipids. The Journal of cell biology *136*, 81-93.

Choppin, P.W., Murphy, J.S., and Tamm, I. (1960). Studies of two kinds of virus particles which comprise influenza A2 virus strains. III. Morphological characteristics: independence to morphological and functional traits. The Journal of experimental medicine *112*, 945-952.

Chu, C.M., Dawson, I.M., and Elford, W.J. (1949). Filamentous forms associated with newly isolated influenza virus. Lancet *1*, 602.

Chu, V.C., and Whittaker, G.R. (2004). Influenza virus entry and infection require host cell N-linked glycoprotein. Proceedings of the National Academy of Sciences of the United States of America *101*, 18153-18158.

Cleves, A.E., McGee, T.P., Whitters, E.A., Champion, K.M., Aitken, J.R., Dowhan, W., Goebl, M., and Bankaitis, V.A. (1991). Mutations in the CDP-choline pathway for phospholipid biosynthesis bypass the requirement for an essential phospholipid transfer protein. Cell *64*, 789-800.

Collinet, C., Stoter, M., Bradshaw, C.R., Samusik, N., Rink, J.C., Kenski, D., Habermann, B., Buchholz, F., Henschel, R., Mueller, M.S.*, et al.* (2010). Systems survey of endocytosis by multiparametric image analysis. Nature *464*, 243-249.

Contreras, F.X., Ernst, A.M., Haberkant, P., Bjorkholm, P., Lindahl, E., Gonen, B., Tischer, C., Elofsson, A., von Heijne, G., Thiele, C.*, et al.* (2012). Molecular recognition of a single sphingolipid species by a protein's transmembrane domain. Nature *481*, 525-529.

Coombs, K.M., Berard, A., Xu, W., Krokhin, O., Meng, X., Cortens, J.P., Kobasa, D., Wilkins, J., and Brown, E.G. (2010). Quantitative proteomic analyses of influenza virus-infected cultured human lung cells. Journal of virology *84*, 10888-10906.

Cox, N.J., and Subbarao, K. (2000). Global epidemiology of influenza: past and present. Annual review of medicine *51*, 407-421.

Cros, J.F., and Palese, P. (2003). Trafficking of viral genomic RNA into and out of the nucleus: influenza, Thogoto and Borna disease viruses. Virus research *95*, 3-12.

D'Angelo, G., Vicinanza, M., Di Campli, A., and De Matteis, M.A. (2008). The multiple roles of PtdIns(4)P -- not just the precursor of PtdIns(4,5)P2. Journal of cell science *121*, 1955-1963.

Datta, S.C., Ghosh, M.K., and Hajra, A.K. (1990). Purification and properties of acyl/alkyl dihydroxyacetone-phosphate reductase from guinea pig liver peroxisomes. The Journal of biological chemistry *265*, 8268-8274.

Davis, B., Koster, G., Douet, L.J., Scigelova, M., Woffendin, G., Ward, J.M., Smith, A., Humphries, J., Burnand, K.G., Macphee, C.H.*, et al.* (2008). Electrospray ionization mass spectrometry identifies substrates and products of lipoprotein-associated phospholipase A2 in oxidized human low density lipoprotein. The Journal of biological chemistry *283*, 6428-6437.

de Hoon, M.J., Makita, Y., Imoto, S., Kobayashi, K., Ogasawara, N., Nakai, K., and Miyano, S. (2004). Predicting gene regulation by sigma factors in Bacillus subtilis from genome-wide data. Bioinformatics *20 Suppl 1*, i101-108.

de Vries, E., de Vries, R.P., Wienholts, M.J., Floris, C.E., Jacobs, M.S., van den Heuvel, A., Rottier, P.J., and de Haan, C.A. (2012). Influenza A virus entry into cells lacking sialylated N-glycans. Proceedings of the National Academy of Sciences of the United States of America *109*, 7457-7462.

de Vries, E., Tscherne, D.M., Wienholts, M.J., Cobos-Jimenez, V., Scholte, F., Garcia-Sastre, A., Rottier, P.J., and de Haan, C.A. (2011). Dissection of the influenza A virus endocytic routes reveals macropinocytosis as an alternative entry pathway. PLoS pathogens *7*, e1001329.

Dennis, E.A., Deems, R.A., Harkewicz, R., Quehenberger, O., Brown, H.A., Milne, S.B., Myers, D.S., Glass, C.K., Hardiman, G., Reichart, D.*, et al.* (2010). A mouse macrophage lipidome. The Journal of biological chemistry *285*, 39976-39985.

Di Paolo, G., and De Camilli, P. (2006). Phosphoinositides in cell regulation and membrane dynamics. Nature *443*, 651-657.

Diaconita, G., Athanasiu, P., Petrescu, A., and Halalau, F. (1985). Morphological, histochemical and histoenzymatic investigations on the lungs of mice chronically infected with influenza virus type A. Virologie *36*, 11-14.

Dixit, E., Boulant, S., Zhang, Y., Lee, A.S., Odendall, C., Shum, B., Hacohen, N., Chen, Z.J., Whelan, S.P., Fransen, M.*, et al.* (2010). Peroxisomes are signaling platforms for antiviral innate immunity. Cell *141*, 668-681.

Dove, B.K., Surtees, R., Bean, T.J., Munday, D., Wise, H.M., Digard, P., Carroll, M.W., Ajuh, P., Barr, J.N., and Hiscox, J.A. (2012). A quantitative proteomic analysis of lung epithelial (A549) cells infected with 2009 pandemic influenza A virus using stable isotope labelling with amino acids in cell culture. Proteomics *12*, 1431-1436.

Dugan, V.G., Chen, R., Spiro, D.J., Sengamalay, N., Zaborsky, J., Ghedin, E., Nolting, J., Swayne, D.E., Runstadler, J.A., Happ, G.M.*, et al.* (2008). The evolutionary genetics and emergence of avian influenza viruses in wild birds. PLoS pathogens *4*, e1000076.

Ehrhardt, C., and Ludwig, S. (2009). A new player in a deadly game: influenza viruses and the PI3K/Akt signalling pathway. Cellular microbiology *11*, 863-871.

Eierhoff, T., Hrincius, E.R., Rescher, U., Ludwig, S., and Ehrhardt, C. (2010). The epidermal growth factor receptor (EGFR) promotes uptake of influenza A viruses (IAV) into host cells. PLoS pathogens *6*, e1001099.

Eigenbrodt, E., Reinacher, M., Scheefers-Borchel, U., Scheefers, H., and Friis, R. (1992). Double role for pyruvate kinase type M2 in the expansion of phosphometabolite pools found in tumor cells. Critical reviews in oncogenesis *3*, 91-115.

Eisfeld, A.J., Kawakami, E., Watanabe, T., Neumann, G., and Kawaoka, Y. (2011). RAB11A is essential for transport of the influenza virus genome to the plasma membrane. Journal of virology *85*, 6117-6126.

Fahy, J.V., and Dickey, B.F. (2010). Airway mucus function and dysfunction. The New England journal of medicine *363*, 2233-2247.

Fedson, D.S. (2008). Confronting an influenza pandemic with inexpensive generic agents: can it be done? The Lancet infectious diseases *8*, 571-576.

Finnegan, C.M., and Blumenthal, R. (2006). Fenretinide inhibits HIV infection by promoting viral endocytosis. Antiviral research *69*, 116-123.

Finnegan, C.M., Rawat, S.S., Cho, E.H., Guiffre, D.L., Lockett, S., Merrill, A.H., Jr., and Blumenthal, R. (2007). Sphingomyelinase restricts the lateral diffusion of CD4 and inhibits human immunodeficiency virus fusion. Journal of virology *81*, 5294-5304.

Fitch, W.M., Bush, R.M., Bender, C.A., and Cox, N.J. (1997). Long term trends in the evolution of H(3) HA1 human influenza type A. Proceedings of the National Academy of Sciences of the United States of America *94*, 7712-7718.

Forbes, N.E., Ping, J., Dankar, S.K., Jia, J.J., Selman, M., Keleta, L., Zhou, Y., and Brown, E.G. (2012). Multifunctional adaptive NS1 mutations are selected upon human influenza virus evolution in the mouse. PloS one *7*, e31839.

Freitag, J., Ast, J., and Bolker, M. (2012). Cryptic peroxisomal targeting via alternative splicing and stop codon read-through in fungi. Nature *485*, 522-525.

Frischholz, K.W., and Scholtissek, C. (1984). Influence of infection with an influenza A virus (fowl plague) on Ca++-uptake and lipid metabolism of chick embryo cells in culture. Archives of virology *80*, 163-170.

Fuhrmans, M., and Marrink, S.J. (2012). Molecular view of the role of fusion peptides in promoting positive membrane curvature. Journal of the American Chemical Society *134*, 1543-1552.

Fukazawa, N., Ayukawa, K., Nishikawa, K., Ohashi, H., Ichihara, N., Hikawa, Y., Abe, T., Kudo, Y., Kiyama, H., Wada, K.*, et al.* (2006). Identification and functional characterization of mouse TPO1 as a myelin membrane protein. Brain research *1070*, 1-14.

Furukawa, K., Hamamura, K., Ohkawa, Y., and Ohmi, Y. (2012). Disialyl gangliosides enhance tumor phenotypes with differential modalities. Glycoconjugate journal.

Fyrst, H., and Saba, J.D. (2010). An update on sphingosine-1-phosphate and other sphingolipid mediators. Nature chemical biology *6*, 489-497.

Gambaryan, A.S., Tuzikov, A.B., Pazynina, G.V., Webster, R.G., Matrosovich, M.N., and Bovin, N.V. (2004). H5N1 chicken influenza viruses display a high binding affinity for Neu5Acalpha2-3Galbeta1-4(6-HSO3)GlcNAc-containing receptors. Virology *326*, 310-316.

Gannage, M., Dormann, D., Albrecht, R., Dengjel, J., Torossi, T., Ramer, P.C., Lee, M., Strowig, T., Arrey, F., Conenello, G.*, et al.* (2009). Matrix protein 2 of influenza A virus blocks autophagosome fusion with lysosomes. Cell host & microbe *6*, 367-380.

Garten, R.J., Davis, C.T., Russell, C.A., Shu, B., Lindstrom, S., Balish, A., Sessions, W.M., Xu, X., Skepner, E., Deyde, V.*, et al.* (2009). Antigenic and genetic characteristics of swine-origin 2009 A(H1N1) influenza viruses circulating in humans. Science *325*, 197-201.

Gastaminza, P., Cheng, G., Wieland, S., Zhong, J., Liao, W., and Chisari, F.V. (2008). Cellular determinants of hepatitis C virus assembly, maturation, degradation, and secretion. Journal of virology *82*, 2120-2129.

Gastaminza, P., Kapadia, S.B., and Chisari, F.V. (2006). Differential biophysical properties of infectious intracellular and secreted hepatitis C virus particles. Journal of virology *80*, 11074-11081.

Ge, M., and Freed, J.H. (2011). Two conserved residues are important for inducing highly ordered membrane domains by the transmembrane domain of influenza hemagglutinin. Biophysical journal *100*, 90-97.

Geiss, G.K., Salvatore, M., Tumpey, T.M., Carter, V.S., Wang, X., Basler, C.F., Taubenberger, J.K., Bumgarner, R.E., Palese, P., Katze, M.G.*, et al.* (2002). Cellular transcriptional profiling in influenza A virus-infected lung epithelial cells: the role of the nonstructural NS1 protein in the evasion of the host innate defense and its potential contribution to pandemic influenza. Proceedings of the National Academy of Sciences of the United States of America *99*, 10736-10741.

Gerl, M.J., Sampaio, J.L., Urban, S., Kalvodova, L., Verbavatz, J.M., Binnington, B., Lindemann, D., Lingwood, C.A., Shevchenko, A., Schroeder, C.*, et al.* (2012). Quantitative analysis of the lipidomes of the influenza virus envelope and MDCK cell apical membrane. The Journal of cell biology *196*, 213-221.

Ghosh, M.K., and Hajra, A.K. (1986). Subcellular distribution and properties of acyl/alkyl dihydroxyacetone phosphate reductase in rodent livers. Archives of biochemistry and biophysics *245*, 523-530.

Glaser, P.E., and Gross, R.W. (1994). Plasmenylethanolamine facilitates rapid membrane fusion: a stopped-flow kinetic investigation correlating the propensity of a major plasma membrane constituent to adopt an HII phase with its ability to promote membrane fusion. Biochemistry *33*, 5805-5812.

Glaser, P.E., Han, X., and Gross, R.W. (2002). Tubulin is the endogenous inhibitor of the glyceraldehyde 3-phosphate dehydrogenase isoform that catalyzes membrane fusion: Implications for the coordinated regulation of glycolysis and membrane fusion. Proceedings of the National Academy of Sciences of the United States of America *99*, 14104-14109.

Golachowska, M.R., Hoekstra, D., and van, I.S.C. (2010). Recycling endosomes in apical plasma membrane domain formation and epithelial cell polarity. Trends in cell biology *20*, 618-626.

Goni, F.M., and Alonso, A. (2009). Effects of ceramide and other simple sphingolipids on membrane lateral structure. Biochimica et biophysica acta *1788*, 169-177.

Gravel, K.A., McGinnes, L.W., Reitter, J., and Morrison, T.G. (2011). The transmembrane domain sequence affects the structure and function of the Newcastle disease virus fusion protein. Journal of virology *85*, 3486-3497.

Grosch, S., Schiffmann, S., and Geisslinger, G. (2012). Chain length-specific properties of ceramides. Progress in lipid research *51*, 50-62.

Guan, X.L., Souza, C.M., Pichler, H., Dewhurst, G., Schaad, O., Kajiwara, K., Wakabayashi, H., Ivanova, T., Castillon, G.A., Piccolis, M*., et al.* (2009). Functional interactions between sphingolipids and sterols in biological membranes regulating cell physiology. Molecular biology of the cell *20*, 2083-2095.

Guo, L., Zhou, D., Pryse, K.M., Okunade, A.L., and Su, X. (2010). Fatty acid 2-hydroxylase mediates diffusional mobility of Raft-associated lipids, GLUT4 level, and lipogenesis in 3T3-L1 adipocytes. The Journal of biological chemistry *285*, 25438-25447.

Hagen-Euteneuer, N., Lutjohann, D., Park, H., Merrill, A.H., Jr., and van Echten-Deckert, G. (2012). Sphingosine 1-phosphate (S1P) lyase deficiency increases sphingolipid formation via recycling at the expense of de novo biosynthesis in neurons. The Journal of biological chemistry *287*, 9128-9136.

Hajra, A.K., Larkins, L.K., Das, A.K., Hemati, N., Erickson, R.L., and MacDougald, O.A. (2000). Induction of the peroxisomal glycerolipid-synthesizing enzymes during differentiation of 3T3-L1 adipocytes. Role in triacylglycerol synthesis. The Journal of biological chemistry *275*, 9441-9446.

Hakomori, S. (2000). Traveling for the glycosphingolipid path. Glycoconjugate journal *17*, 627-647.

Hakomori, S. (2003). Structure, organization, and function of glycosphingolipids in membrane. Current opinion in hematology *10*, 16-24.

Hale, B.G., Randall, R.E., Ortin, J., and Jackson, D. (2008). The multifunctional NS1 protein of influenza A viruses. The Journal of general virology *89*, 2359-2376.

Hamilton, B.S., Whittaker, G.R., and Daniel, S. (2012). Influenza virus-mediated membrane fusion: determinants of hemagglutinin fusogenic activity and experimental approaches for assessing virus fusion. Viruses *4*, 1144-1168.

Han, X., Ramanadham, S., Turk, J., and Gross, R.W. (1998). Reconstitution of membrane fusion between pancreatic islet secretory granules and plasma membranes: catalysis by a protein constituent recognized by monoclonal antibodies directed against glyceraldehyde-3-phosphate dehydrogenase. Biochimica et biophysica acta *1414*, 95-107.

Hanzal-Bayer, M.F., and Hancock, J.F. (2007). Lipid rafts and membrane traffic. FEBS letters *581*, 2098-2104.

Hao, L., Sakurai, A., Watanabe, T., Sorensen, E., Nidom, C.A., Newton, M.A., Ahlquist, P., and Kawaoka, Y. (2008). Drosophila RNAi screen identifies host genes important for influenza virus replication. Nature *454*, 890-893.

Harder, T., Scheiffele, P., Verkade, P., and Simons, K. (1998). Lipid domain structure of the plasma membrane revealed by patching of membrane components. The Journal of cell biology *141*, 929-942.

Henson, P.M., Bratton, D.L., and Fadok, V.A. (2001). The phosphatidylserine receptor: a crucial molecular switch? Nature reviews Molecular cell biology *2*, 627-633.

Herfst, S., Schrauwen, E.J., Linster, M., Chutinimitkul, S., de Wit, E., Munster, V.J., Sorrell, E.M., Bestebroer, T.M., Burke, D.F., Smith, D.J.*, et al.* (2012). Airborne transmission of influenza A/H5N1 virus between ferrets. Science *336*, 1534-1541.

Hess, S.T., Gould, T.J., Gudheti, M.V., Maas, S.A., Mills, K.D., and Zimmerberg, J. (2007). Dynamic clustered distribution of hemagglutinin resolved at 40 nm in living cell membranes discriminates between raft theories. Proceedings of the National Academy of Sciences of the United States of America *104*, 17370-17375.

Heynisch, B., Frensing, T., Heinze, K., Seitz, C., Genzel, Y., and Reichl, U. (2010). Differential activation of host cell signalling pathways through infection with two variants of influenza A/Puerto Rico/8/34 (H1N1) in MDCK cells. Vaccine *28*, 8210-8218.

Hidari, K.I., Shimada, S., Suzuki, Y., and Suzuki, T. (2007). Binding kinetics of influenza viruses to sialic acid-containing carbohydrates. Glycoconjugate journal *24*, 583-590.

Hidari, K.I., Suzuki, Y., and Suzuki, T. (2006). Suppression of the biosynthesis of cellular sphingolipids results in the inhibition of the maturation of influenza virus particles in MDCK cells. Biological & pharmaceutical bulletin *29*, 1575-1579.

Hitosugi, T., Kang, S., Vander Heiden, M.G., Chung, T.W., Elf, S., Lythgoe, K., Dong, S., Lonial, S., Wang, X., Chen, G.Z.*, et al.* (2009). Tyrosine phosphorylation inhibits PKM2 to promote the Warburg effect and tumor growth. Science signaling *2*, ra73.

Holmes, E.C., Ghedin, E., Miller, N., Taylor, J., Bao, Y., St George, K., Grenfell, B.T., Salzberg, S.L., Fraser, C.M., Lipman, D.J.*, et al.* (2005). Whole-genome analysis of human influenza A virus reveals multiple persistent lineages and reassortment among recent H3N2 viruses. PLoS biology *3*, e300.

Honsho, M., Yagita, Y., Kinoshita, N., and Fujiki, Y. (2008). Isolation and characterization of mutant animal cell line defective in alkyl-dihydroxyacetonephosphate synthase: localization and transport of plasmalogens to post-Golgi compartments. Biochimica et biophysica acta *1783*, 1857-1865.

Huang, R.T., Lichtenberg, B., and Rick, O. (1996). Involvement of annexin V in the entry of influenza viruses and role of phospholipids in infection. FEBS letters *392*, 59-62.

Huitema, K., van den Dikkenberg, J., Brouwers, J.F., and Holthuis, J.C. (2004). Identification of a family of animal sphingomyelin synthases. The EMBO journal *23*, 33-44.

Imai, M., Watanabe, T., Hatta, M., Das, S.C., Ozawa, M., Shinya, K., Zhong, G., Hanson, A., Katsura, H., Watanabe, S.*, et al.* (2012). Experimental adaptation of an influenza H5 HA confers respiratory droplet transmission to a reassortant H5 HA/H1N1 virus in ferrets. Nature *486*, 420-428.

Ina, Y., and Gojobori, T. (1994). Statistical analysis of nucleotide sequences of the hemagglutinin gene of human influenza A viruses. Proceedings of the National Academy of Sciences of the United States of America *91*, 8388-8392.

Inuzuka, M., Hayakawa, M., and Ingi, T. (2005). Serinc, an activity-regulated protein family, incorporates serine into membrane lipid synthesis. The Journal of biological chemistry *280*, 35776-35783.

Itano, M.S., Neumann, A.K., Liu, P., Zhang, F., Gratton, E., Parak, W.J., Thompson, N.L., and Jacobson, K. (2011). DC-SIGN and influenza hemagglutinin dynamics in plasma membrane microdomains are markedly different. Biophysical journal *100*, 2662-2670.

Ivanova, P.T., Milne, S.B., and Brown, H.A. (2010). Identification of atypical ether-linked glycerophospholipid species in macrophages by mass spectrometry. Journal of lipid research *51*, 1581-1590.

Jain, M., Nilsson, R., Sharma, S., Madhusudhan, N., Kitami, T., Souza, A.L., Kafri, R., Kirschner, M.W., Clish, C.B., and Mootha, V.K. (2012). Metabolite profiling identifies a key role for glycine in rapid cancer cell proliferation. Science *336*, 1040-1044.

Janke, R., Genzel, Y., Wetzel, M., and Reichl, U. (2011). Effect of influenza virus infection on key metabolic enzyme activities in MDCK cells. BMC proceedings *5 Suppl 8*, P129.

Jenkins, G.H., Fisette, P.L., and Anderson, R.A. (1994). Type I phosphatidylinositol 4-phosphate 5-kinase isoforms are specifically stimulated by phosphatidic acid. The Journal of biological chemistry *269*, 11547-11554.

Johnson, N.P., and Mueller, J. (2002). Updating the accounts: global mortality of the 1918-1920 "Spanish" influenza pandemic. Bulletin of the history of medicine *76*, 105-115.

Jorgenson, R.L., Vogt, V.M., and Johnson, M.C. (2009). Foreign glycoproteins can be actively recruited to virus assembly sites during pseudotyping. Journal of virology *83*, 4060-4067.

Josset, L., Belser, J.A., Pantin-Jackwood, M.J., Chang, J.H., Chang, S.T., Belisle, S.E., Tumpey, T.M., and Katze, M.G. (2012). Implication of inflammatory macrophages, nuclear receptors, and interferon regulatory factors in increased virulence of pandemic 2009 H1N1 influenza A virus after host adaptation. Journal of virology *86*, 7192-7206.

Kalvodova, L., Sampaio, J.L., Cordo, S., Ejsing, C.S., Shevchenko, A., and Simons, K. (2009). The lipidomes of vesicular stomatitis virus, semliki forest virus, and the host plasma membrane analyzed by quantitative shotgun mass spectrometry. Journal of virology *83*, 7996-8003.

Karlas, A., Machuy, N., Shin, Y., Pleissner, K.P., Artarini, A., Heuer, D., Becker, D., Khalil, H., Ogilvie, L.A., Hess, S.*, et al.* (2010). Genome-wide RNAi screen identifies human host factors crucial for influenza virus replication. Nature *463*, 818-822.

Kesel, A.J. (2011). Broad-spectrum antiviral activity including human immunodeficiency and hepatitis C viruses mediated by a novel retinoid thiosemicarbazone derivative. European journal of medicinal chemistry *46*, 1656-1664.

Khurana, S., Krementsov, D.N., de Parseval, A., Elder, J.H., Foti, M., and Thali, M. (2007). Human immunodeficiency virus type 1 and influenza virus exit via different membrane microdomains. Journal of virology *81*, 12630-12640.

Kilbourne, E.D., and Murphy, J.S. (1960). Genetic studies of influenza viruses. I. Viral morphology and growth capacity as exchangeable genetic traits. Rapid in ovo adaptation of early passage Asian strain isolates by combination with PR8. The Journal of experimental medicine *111*, 387-406.

Kitatani, K., Idkowiak-Baldys, J., and Hannun, Y.A. (2008). The sphingolipid salvage pathway in ceramide metabolism and signaling. Cellular signalling *20*, 1010-1018.

Klemm, R.W., Ejsing, C.S., Surma, M.A., Kaiser, H.J., Gerl, M.J., Sampaio, J.L., de Robillard, Q., Ferguson, C., Proszynski, T.J., Shevchenko, A.*, et al.* (2009). Segregation of sphingolipids and sterols during formation of secretory vesicles at the trans-Golgi network. The Journal of cell biology *185*, 601-612.

Klemperer, H. (1961). Glucose breakdown in chick embryo cells infected with influenza virus. Virology *13*, 68-77.

Kogure, T., Suzuki, T., Takahashi, T., Miyamoto, D., Hidari, K.I., Guo, C.T., Ito, T., Kawaoka, Y., and Suzuki, Y. (2006). Human trachea primary epithelial cells express both sialyl(alpha2-3)Gal receptor for human parainfluenza virus type 1 and avian influenza viruses, and sialyl(alpha2-6)Gal receptor for human influenza viruses. Glycoconjugate journal *23*, 101-106.

Koivusalo, M., Jansen, M., Somerharju, P., and Ikonen, E. (2007). Endocytic trafficking of sphingomyelin depends on its acyl chain length. Molecular biology of the cell *18*, 5113-5123.

Kolter, T., and Sandhoff, K. (2010). Lysosomal degradation of membrane lipids. FEBS letters *584*, 1700-1712.

Konig, R., Stertz, S., Zhou, Y., Inoue, A., Hoffmann, H.H., Bhattacharyya, S., Alamares, J.G., Tscherne, D.M., Ortigoza, M.B., Liang, Y.*, et al.* (2010). Human host factors required for influenza virus replication. Nature *463*, 813-817.

Kroeker, A.L., Ezzati, P., Halayko, A.J., and Coombs, K. (2012). The response of primary human airway epithelial cells to Influenza infection - A quantitative proteomic study. Journal of proteome research.

Krueger, W.H., Gonye, G.E., Madison, D.L., Murray, K.E., Kumar, M., Spoerel, N., and Pfeiffer, S.E. (1997). TPO1, a member of a novel protein family, is developmentally regulated in cultured oligodendrocytes. Journal of neurochemistry *69*, 1343-1355.

Kuerschner, L., Richter, D., Hannibal-Bach, H.K., Gaebler, A., Shevchenko, A., Ejsing, C.S., and Thiele, C. (2012). Exogenous ether lipids predominantly target mitochondria. PloS one *7*, e31342.

Kuiken, T., Holmes, E.C., McCauley, J., Rimmelzwaan, G.F., Williams, C.S., and Grenfell, B.T. (2006). Host species barriers to influenza virus infections. Science *312*, 394-397.

Kunze, M., Neuberger, G., Maurer-Stroh, S., Ma, J., Eck, T., Braverman, N., Schmid, J.A., Eisenhaber, F., and Berger, J. (2011). Structural requirements for interaction of peroxisomal targeting signal 2 and its receptor PEX7. The Journal of biological chemistry *286*, 45048-45062.

Lakadamyali, M., Rust, M.J., and Zhuang, X. (2004). Endocytosis of influenza viruses. Microbes and infection / Institut Pasteur *6*, 929-936.

Lazarow, P.B. (2011). Viruses exploiting peroxisomes. Current opinion in microbiology *14*, 458-469.

Le, Q.M., Kiso, M., Someya, K., Sakai, Y.T., Nguyen, T.H., Nguyen, K.H., Pham, N.D., Ngyen, H.H., Yamada, S., Muramoto, Y.*, et al.* (2005). Avian flu: isolation of drug-resistant H5N1 virus. Nature *437*, 1108.

LeBouder, F., Morello, E., Rimmelzwaan, G.F., Bosse, F., Pechoux, C., Delmas, B., and Riteau, B. (2008). Annexin II incorporated into influenza virus particles supports virus replication by converting plasminogen into plasmin. Journal of virology *82*, 6820-6828.

Lee, S.H., Meng, X.W., Flatten, K.S., Loegering, D.A., and Kaufmann, S.H. (2012). Phosphatidylserine exposure during apoptosis reflects bidirectional trafficking between plasma membrane and cytoplasm. Cell death and differentiation.

Lee, S.S., Pineau, T., Drago, J., Lee, E.J., Owens, J.W., Kroetz, D.L., Fernandez-Salguero, P.M., Westphal, H., and Gonzalez, F.J. (1995). Targeted disruption of the alpha isoform of the peroxisome proliferator-activated receptor gene in mice results in abolishment of the pleiotropic effects of peroxisome proliferators. Molecular and cellular biology *15*, 3012-3022.

Lemmon, M.A. (2008). Membrane recognition by phospholipid-binding domains. Nature reviews Molecular cell biology *9*, 99-111.

Leser, G.P., and Lamb, R.A. (2005). Influenza virus assembly and budding in raft-derived microdomains: a quantitative analysis of the surface distribution of HA, NA and M2 proteins. Virology *342*, 215-227.

Leung, K., Kim, J.O., Ganesh, L., Kabat, J., Schwartz, O., and Nabel, G.J. (2008). HIV-1 assembly: viral glycoproteins segregate quantally to lipid rafts that associate individually with HIV-1 capsids and virions. Cell host & microbe *3*, 285-292.

Levy, M., and Futerman, A.H. (2010). Mammalian ceramide synthases. IUBMB life *62*, 347-356.

Li, Z., Hailemariam, T.K., Zhou, H., Li, Y., Duckworth, D.C., Peake, D.A., Zhang, Y., Kuo, M.S., Cao, G., and Jiang, X.C. (2007). Inhibition of sphingomyelin synthase (SMS) affects intracellular sphingomyelin accumulation and plasma membrane lipid organization. Biochimica et biophysica acta *1771*, 1186-1194.

Lietzen, N., Ohman, T., Rintahaka, J., Julkunen, I., Aittokallio, T., Matikainen, S., and Nyman, T.A. (2011). Quantitative subcellular proteome and secretome profiling of influenza A virus-infected human primary macrophages. PLoS pathogens *7*, e1001340.

Lin, S., Liu, N., Yang, Z., Song, W., Wang, P., Chen, H., Lucio, M., Schmitt-Kopplin, P., Chen, G., and Cai, Z. (2010). GC/MS-based metabolomics reveals fatty acid biosynthesis and cholesterol metabolism in cell lines infected with influenza A virus. Talanta *83*, 262-268.

Litvak, V., Dahan, N., Ramachandran, S., Sabanay, H., and Lev, S. (2005). Maintenance of the diacylglycerol level in the Golgi apparatus by the Nir2 protein is critical for Golgi secretory function. Nature cell biology *7*, 225-234.

Liu, S.T., Sharon-Friling, R., Ivanova, P., Milne, S.B., Myers, D.S., Rabinowitz, J.D., Brown, H.A., and Shenk, T. (2011). Synaptic vesicle-like lipidome of human cytomegalovirus virions reveals a role for SNARE machinery in virion egress. Proceedings of the National Academy of Sciences of the United States of America *108*, 12869-12874.

Locasale, J.W., Grassian, A.R., Melman, T., Lyssiotis, C.A., Mattaini, K.R., Bass, A.J., Heffron, G., Metallo, C.M., Muranen, T., Sharfi, H.*, et al.* (2011). Phosphoglycerate dehydrogenase diverts glycolytic flux and contributes to oncogenesis. Nature genetics *43*, 869-874.

Lohner, K. (1996). Is the high propensity of ethanolamine plasmalogens to form non-lamellar lipid structures manifested in the properties of biomembranes? Chemistry and physics of lipids *81*, 167-184.

Lorizate, M., and Krausslich, H.G. (2011). Role of lipids in virus replication. Cold Spring Harbor perspectives in biology *3*, a004820.

Lowen, A.C., Mubareka, S., Steel, J., and Palese, P. (2007). Influenza virus transmission is dependent on relative humidity and temperature. PLoS pathogens *3*, 1470-1476.

Luan, P., and Glaser, M. (1994). Formation of membrane domains by the envelope proteins of vesicular stomatitis virus. Biochemistry *33*, 4483-4489.

Luberto, C., and Hannun, Y.A. (1998). Sphingomyelin synthase, a potential regulator of intracellular levels of ceramide and diacylglycerol during SV40 transformation. Does sphingomyelin synthase account for the putative phosphatidylcholine-specific phospholipase C? The Journal of biological chemistry *273*, 14550-14559.

Luberto, C., Yoo, D.S., Suidan, H.S., Bartoli, G.M., and Hannun, Y.A. (2000). Differential effects of sphingomyelin hydrolysis and resynthesis on the activation of NF-kappa B in normal and SV40-transformed human fibroblasts. The Journal of biological chemistry *275*, 14760-14766.

Luo, M. (2012). Influenza virus entry. Advances in experimental medicine and biology *726*, 201-221.

Ma, C., Agrawal, G., and Subramani, S. (2011a). Peroxisome assembly: matrix and membrane protein biogenesis. The Journal of cell biology *193*, 7-16.

Ma, W., Belisle, S.E., Mosier, D., Li, X., Stigger-Rosser, E., Liu, Q., Qiao, C., Elder, J., Webby, R., Katze, M.G.*, et al.* (2011b). 2009 pandemic H1N1 influenza virus causes disease and upregulation of genes related to inflammatory and immune responses, cell death, and lipid metabolism in pigs. Journal of virology *85*, 11626-11637.

Magnusson, C.D., and Haraldsson, G.G. (2011). Ether lipids. Chemistry and physics of lipids *164*, 315-340.

Maines, T.R., Chen, L.M., Matsuoka, Y., Chen, H., Rowe, T., Ortin, J., Falcon, A., Nguyen, T.H., Mai le, Q., Sedyaningsih, E.R.*, et al.* (2006). Lack of transmission of H5N1 avian-human reassortant influenza viruses in a ferret model. Proceedings of the National Academy of Sciences of the United States of America *103*, 12121-12126.

Mandel, H., Sharf, R., Berant, M., Wanders, R.J., Vreken, P., and Aviram, M. (1998). Plasmalogen phospholipids are involved in HDL-mediated cholesterol efflux: insights from investigations with plasmalogen-deficient cells. Biochemical and biophysical research communications *250*, 369-373.

Mankidy, R., Ahiahonu, P.W., Ma, H., Jayasinghe, D., Ritchie, S.A., Khan, M.A., Su-Myat, K.K., Wood, P.L., and Goodenowe, D.B. (2010). Membrane plasmalogen composition and cellular cholesterol regulation: a structure activity study. Lipids in health and disease *9*, 62.

Markham, J.E., Molino, D., Gissot, L., Bellec, Y., Hematy, K., Marion, J., Belcram, K., Palauqui, J.C., Satiat-Jeunemaitre, B., and Faure, J.D. (2011). Sphingolipids containing very-long-chain fatty acids define a secretory pathway for specific polar plasma membrane protein targeting in Arabidopsis. The Plant cell *23*, 2362-2378.

Martin, S.J., Reutelingsperger, C.P., McGahon, A.J., Rader, J.A., van Schie, R.C., LaFace, D.M., and Green, D.R. (1995). Early redistribution of plasma membrane phosphatidylserine is a general feature of apoptosis regardless of the initiating stimulus: inhibition by overexpression of Bcl-2 and Abl. The Journal of experimental medicine *182*, 1545-1556.

Matrosovich, M., Matrosovich, T., Garten, W., and Klenk, H.D. (2006a). New low-viscosity overlay medium for viral plaque assays. Virology journal *3*, 63.

Matrosovich, M., Suzuki, T., Hirabayashi, Y., Garten, W., Webster, R.G., and Klenk, H.D. (2006b). Gangliosides are not essential for influenza virus infection. Glycoconjugate journal *23*, 107-113.

Matrosovich, M.N., Matrosovich, T.Y., Gray, T., Roberts, N.A., and Klenk, H.D. (2004). Neuraminidase is important for the initiation of influenza virus infection in human airway epithelium. Journal of virology *78*, 12665-12667.

Medina, R.A., and Garcia-Sastre, A. (2011). Influenza A viruses: new research developments. Nature reviews Microbiology *9*, 590-603.

Megha, and London, E. (2004). Ceramide selectively displaces cholesterol from ordered lipid domains (rafts): implications for lipid raft structure and function. The Journal of biological chemistry *279*, 9997-10004.

Mercer, J., and Helenius, A. (2008). Vaccinia virus uses macropinocytosis and apoptotic mimicry to enter host cells. Science *320*, 531-535.

Mercer, J., Schelhaas, M., and Helenius, A. (2010). Virus entry by endocytosis. Annual review of biochemistry *79*, 803-833.

Merrill, A.H., Jr. (2011). Sphingolipid and glycosphingolipid metabolic pathways in the era of sphingolipidomics. Chemical reviews *111*, 6387-6422.

Merz, A., Long, G., Hiet, M.S., Brugger, B., Chlanda, P., Andre, P., Wieland, F., Krijnse-Locker, J., and Bartenschlager, R. (2011). Biochemical and morphological properties of hepatitis C virus particles and determination of their lipidome. The Journal of biological chemistry *286*, 3018-3032.

Miyanari, Y., Atsuzawa, K., Usuda, N., Watashi, K., Hishiki, T., Zayas, M., Bartenschlager, R., Wakita, T., Hijikata, M., and Shimotohno, K. (2007). The lipid droplet is an important organelle for hepatitis C virus production. Nature cell biology *9*, 1089-1097.

Miyauchi, K., Kim, Y., Latinovic, O., Morozov, V., and Melikyan, G.B. (2009). HIV enters cells via endocytosis and dynamin-dependent fusion with endosomes. Cell *137*, 433-444.

Molina, S., Castet, V., Fournier-Wirth, C., Pichard-Garcia, L., Avner, R., Harats, D., Roitelman, J., Barbaras, R., Graber, P., Ghersa, P.*, et al.* (2007). The low-density lipoprotein receptor plays a role in the infection of primary human hepatocytes by hepatitis C virus. Journal of hepatology *46*, 411-419.

Momose, F., Sekimoto, T., Ohkura, T., Jo, S., Kawaguchi, A., Nagata, K., and Morikawa, Y. (2011). Apical transport of influenza A virus ribonucleoprotein requires Rab11-positive recycling endosome. PloS one *6*, e21123.

Morens, D.M., Taubenberger, J.K., and Fauci, A.S. (2009). The persistent legacy of the 1918 influenza virus. The New England journal of medicine *361*, 225-229.

Moseley, C.E., Webster, R.G., and Aldridge, J.R. (2010). Peroxisome proliferator-activated receptor and AMP-activated protein kinase agonists protect against lethal influenza virus challenge in mice. Influenza and other respiratory viruses *4*, 307-311.

Mozzi, R., Andreoli, V., Buratta, S., and Iorio, A. (1997). Different mechanisms regulate phosphatidylserine synthesis in rat cerebral cortex. Molecular and cellular biochemistry *168*, 41-49.

Mullen, T.D., Hannun, Y.A., and Obeid, L.M. (2012). Ceramide synthases at the centre of sphingolipid metabolism and biology. The Biochemical journal *441*, 789-802.

Munger, J., Bennett, B.D., Parikh, A., Feng, X.J., McArdle, J., Rabitz, H.A., Shenk, T., and Rabinowitz, J.D. (2008). Systems-level metabolic flux profiling identifies fatty acid synthesis as a target for antiviral therapy. Nature biotechnology *26*, 1179-1186.

Munn, N.J., Arnio, E., Liu, D., Zoeller, R.A., and Liscum, L. (2003). Deficiency in ethanolamine plasmalogen leads to altered cholesterol transport. Journal of lipid research *44*, 182-192.

Murphy, M.G., Crocker, J.F., and Her, H. (1996). Abnormalities in hepatic fatty-acid metabolism in a surfactant/influenza B virus mouse model for acute encephalopathy. Biochimica et biophysica acta *1315*, 208-216.

Nabhan, J.F., Hu, R., Oh, R.S., Cohen, S.N., and Lu, Q. (2012). Formation and release of arrestin domain-containing protein 1-mediated microvesicles (ARMMs) at plasma membrane by recruitment of TSG101 protein. Proceedings of the National Academy of Sciences of the United States of America *109*, 4146-4151.

Nagan, N., Hajra, A.K., Larkins, L.K., Lazarow, P., Purdue, P.E., Rizzo, W.B., and Zoeller, R.A. (1998). Isolation of a Chinese hamster fibroblast variant defective in dihydroxyacetonephosphate acyltransferase activity and plasmalogen biosynthesis: use of a novel two-step selection protocol. The Biochemical journal *332 (Pt 1)*, 273-279.

Nagata, K., Kawaguchi, A., and Naito, T. (2008). Host factors for replication and transcription of the influenza virus genome. Reviews in medical virology *18*, 247-260.

Narasaraju, T., Sim, M.K., Ng, H.H., Phoon, M.C., Shanker, N., Lal, S.K., and Chow, V.T. (2009). Adaptation of human influenza H3N2 virus in a mouse pneumonitis model: insights into viral virulence, tissue tropism and host pathogenesis. Microbes and infection / Institut Pasteur *11*, 2-11.

Nayak, D.P., Balogun, R.A., Yamada, H., Zhou, Z.H., and Barman, S. (2009). Influenza virus morphogenesis and budding. Virus research *143*, 147-161.

Nayak, D.P., Hui, E.K., and Barman, S. (2004). Assembly and budding of influenza virus. Virus research *106*, 147-165.

Nelson, M.I., and Holmes, E.C. (2007). The evolution of epidemic influenza. Nature reviews Genetics *8*, 196-205.

Neuberger, G., Kunze, M., Eisenhaber, F., Berger, J., Hartig, A., and Brocard, C. (2004). Hidden localization motifs: naturally occurring peroxisomal targeting signals in non-peroxisomal proteins. Genome biology *5*, R97.

Neumann, A.K., Itano, M.S., and Jacobson, K. (2010). Understanding lipid rafts and other related membrane domains. F1000 biology reports *2*, 31.

Neumann, G., Noda, T., and Kawaoka, Y. (2009). Emergence and pandemic potential of swine-origin H1N1 influenza virus. Nature *459*, 931-939.

Nguyen, D.H., and Taub, D. (2002). CXCR4 function requires membrane cholesterol: implications for HIV infection. J Immunol *168*, 4121-4126.

Nikolaus, J., Scolari, S., Bayraktarov, E., Jungnick, N., Engel, S., Pia Plazzo, A., Stockl, M., Volkmer, R., Veit, M., and Herrmann, A. (2010). Hemagglutinin of influenza virus partitions into the nonraft domain of model membranes. Biophysical journal *99*, 489-498.

Nussbaum, O., Rott, R., and Loyter, A. (1992). Fusion of influenza virus particles with liposomes: requirement for cholesterol and virus receptors to allow fusion with and lysis of neutral but not of negatively charged liposomes. The Journal of general virology *73 (Pt 11)*, 2831-2837.

Olofsson, S., Kumlin, U., Dimock, K., and Arnberg, N. (2005). Avian influenza and sialic acid receptors: more than meets the eye? The Lancet infectious diseases *5*, 184-188.

Ono, A., and Freed, E.O. (2001). Plasma membrane rafts play a critical role in HIV-1 assembly and release. Proceedings of the National Academy of Sciences of the United States of America *98*, 13925-13930.

Oskouian, B., and Saba, J.D. (2010). Cancer treatment strategies targeting sphingolipid metabolism. Advances in experimental medicine and biology *688*, 185-205.

Perera, R., Riley, C., Isaac, G., Hopf-Jannasch, A.S., Moore, R.J., Weitz, K.W., Pasa-Tolic, L., Metz, T.O., Adamec, J., and Kuhn, R.J. (2012). Dengue virus infection perturbs lipid homeostasis in infected mosquito cells. PLoS pathogens *8*, e1002584.

Perichon, R., and Bourre, J.M. (1995). Peroxisomal beta-oxidation activity and catalase activity during development and aging in mouse liver. Biochimie *77*, 288-293.

Perry, R.J., and Ridgway, N.D. (2004). The role of de novo ceramide synthesis in the mechanism of action of the tricyclic xanthate D609. Journal of lipid research *45*, 164-173.

Peters, J.M., Shah, Y.M., and Gonzalez, F.J. (2012). The role of peroxisome proliferator-activated receptors in carcinogenesis and chemoprevention. Nature reviews Cancer *12*, 181-195.

Pettus, B.J., Baes, M., Busman, M., Hannun, Y.A., and Van Veldhoven, P.P. (2004). Mass spectrometric analysis of ceramide perturbations in brain and fibroblasts of mice and human patients with peroxisomal disorders. Rapid communications in mass spectrometry : RCM *18*, 1569-1574.

Pickl, W.F., Pimentel-Muinos, F.X., and Seed, B. (2001). Lipid rafts and pseudotyping. Journal of virology *75*, 7175-7183.

Pike, L.J., Han, X., Chung, K.N., and Gross, R.W. (2002). Lipid rafts are enriched in arachidonic acid and plasmenylethanolamine and their composition is independent of caveolin-1 expression: a quantitative electrospray ionization/mass spectrometric analysis. Biochemistry *41*, 2075-2088.

Polozov, I.V., Bezrukov, L., Gawrisch, K., and Zimmerberg, J. (2008). Progressive ordering with decreasing temperature of the phospholipids of influenza virus. Nature chemical biology *4*, 248-255.

Popa, A., Carter, J.R., Smith, S.E., Hellman, L., Fried, M.G., and Dutch, R.E. (2012). Residues in the hendra virus fusion protein transmembrane domain are critical for endocytic recycling. Journal of virology *86*, 3014-3026.

Popik, W., Alce, T.M., and Au, W.C. (2002). Human immunodeficiency virus type 1 uses lipid raft-colocalized CD4 and chemokine receptors for productive entry into CD4(+) T cells. Journal of virology *76*, 4709-4722.

Raa, H., Grimmer, S., Schwudke, D., Bergan, J., Walchli, S., Skotland, T., Shevchenko, A., and Sandvig, K. (2009). Glycosphingolipid requirements for endosome-to-Golgi transport of Shiga toxin. Traffic *10*, 868-882.

Razinkov, V.I., and Cohen, F.S. (2000). Sterols and sphingolipids strongly affect the growth of fusion pores induced by the hemagglutinin of influenza virus. Biochemistry *39*, 13462-13468.

Ribet, C., Montastier, E., Valle, C., Bezaire, V., Mazzucotelli, A., Mairal, A., Viguerie, N., and Langin, D. (2010). Peroxisome proliferator-activated receptor-alpha control of lipid and glucose metabolism in human white adipocytes. Endocrinology *151*, 123-133.

Ritter, J.B., Wahl, A.S., Freund, S., Genzel, Y., and Reichl, U. (2010). Metabolic effects of influenza virus infection in cultured animal cells: Intra- and extracellular metabolite profiling. BMC systems biology *4*, 61.

Roberts, P.C., Lamb, R.A., and Compans, R.W. (1998). The M1 and M2 proteins of influenza A virus are important determinants in filamentous particle formation. Virology *240*, 127-137.

Rodriguez-Boulan, E., Kreitzer, G., and Musch, A. (2005). Organization of vesicular trafficking in epithelia. Nature reviews Molecular cell biology *6*, 233-247.

Roe, B., Kensicki, E., Mohney, R., and Hall, W.W. (2011). Metabolomic profile of hepatitis C virus-infected hepatocytes. PloS one *6*, e23641.

Rohrbough, J., Rushton, E., Palanker, L., Woodruff, E., Matthies, H.J., Acharya, U., Acharya, J.K., and Broadie, K. (2004). Ceramidase regulates synaptic vesicle exocytosis and trafficking. The Journal of neuroscience : the official journal of the Society for Neuroscience *24*, 7789-7803.

Ronchi, P., Colombo, S., Francolini, M., and Borgese, N. (2008). Transmembrane domain-dependent partitioning of membrane proteins within the endoplasmic reticulum. The Journal of cell biology *181*, 105-118.

Rossman, J.S., Jing, X., Leser, G.P., and Lamb, R.A. (2010). Influenza virus M2 protein mediates ESCRT-independent membrane scission. Cell *142*, 902-913.

Rossman, J.S., and Lamb, R.A. (2011). Influenza virus assembly and budding. Virology *411*, 229-236.

Rothman, J.E., Tsai, D.K., Dawidowicz, E.A., and Lenard, J. (1976). Transbilayer phospholipid asymmetry and its maintenance in the membrane of influenza virus. Biochemistry *15*, 2361-2370.

Rousso, I., Mixon, M.B., Chen, B.K., and Kim, P.S. (2000). Palmitoylation of the HIV-1 envelope glycoprotein is critical for viral infectivity. Proceedings of the National Academy of Sciences of the United States of America *97*, 13523-13525.

Russell, R.J., Stevens, D.J., Haire, L.F., Gamblin, S.J., and Skehel, J.J. (2006). Avian and human receptor binding by hemagglutinins of influenza A viruses. Glycoconjugate journal *23*, 85-92.

Rust, M.J., Lakadamyali, M., Zhang, F., and Zhuang, X. (2004). Assembly of endocytic machinery around individual influenza viruses during viral entry. Nature structural & molecular biology *11*, 567-573.

Saldanha, A.J. (2004). Java Treeview--extensible visualization of microarray data. Bioinformatics *20*, 3246-3248.

Sampaio, J.L., Gerl, M.J., Klose, C., Ejsing, C.S., Beug, H., Simons, K., and Shevchenko, A. (2011). Membrane lipidome of an epithelial cell line. Proceedings of the National Academy of Sciences of the United States of America *108*, 1903-1907.

Sargent, J.R., Coupland, K., and Wilson, R. (1994). Nervonic acid and demyelinating disease. Medical hypotheses *42*, 237-242.

Sarri, E., Sicart, A., Lazaro-Dieguez, F., and Egea, G. (2011). Phospholipid synthesis participates in the regulation of diacylglycerol required for membrane trafficking at the Golgi complex. The Journal of biological chemistry *286*, 28632-28643.

Sato, K., Hanagata, G., Kiso, M., Hasegawa, A., and Suzuki, Y. (1998). Specificity of the N1 and N2 sialidase subtypes of human influenza A virus for natural and synthetic gangliosides. Glycobiology *8*, 527-532.

Scheiffele, P., Rietveld, A., Wilk, T., and Simons, K. (1999). Influenza viruses select ordered lipid domains during budding from the plasma membrane. The Journal of biological chemistry *274*, 2038-2044.

Scheiffele, P., Roth, M.G., and Simons, K. (1997). Interaction of influenza virus haemagglutinin with sphingolipid-cholesterol membrane domains via its transmembrane domain. The EMBO journal *16*, 5501-5508.

Scholtissek, C., Rohde, W., Von Hoyningen, V., and Rott, R. (1978). On the origin of the human influenza virus subtypes H2N2 and H3N2. Virology *87*, 13-20.

Schramm, M., Herz, J., Haas, A., Kronke, M., and Utermohlen, O. (2008). Acid sphingomyelinase is required for efficient phago-lysosomal fusion. Cellular microbiology *10*, 1839-1853.

Schupp, M., and Lazar, M.A. (2010). Endogenous ligands for nuclear receptors: digging deeper. The Journal of biological chemistry *285*, 40409-40415.

Seitz, C., Frensing, T., Hoper, D., Kochs, G., and Reichl, U. (2010). High yields of influenza A virus in Madin-Darby canine kidney cells are promoted by an insufficient interferon-induced antiviral state. The Journal of general virology *91*, 1754-1763.

Seo, Y.J., Blake, C., Alexander, S., and Hahm, B. (2010). Sphingosine 1-phosphate-metabolizing enzymes control influenza virus propagation and viral cytopathogenicity. Journal of virology *84*, 8124-8131.

Shackelford, D.B., and Shaw, R.J. (2009). The LKB1-AMPK pathway: metabolism and growth control in tumour suppression. Nature reviews Cancer *9*, 563-575.

Shapira, S.D., Gat-Viks, I., Shum, B.O., Dricot, A., de Grace, M.M., Wu, L., Gupta, P.B., Hao, T., Silver, S.J., Root, D.E*., et al.* (2009). A physical and regulatory map of host-influenza interactions reveals pathways in H1N1 infection. Cell *139*, 1255-1267.

Shaw, M.L., Stone, K.L., Colangelo, C.M., Gulcicek, E.E., and Palese, P. (2008). Cellular proteins in influenza virus particles. PLoS pathogens *4*, e1000085.

Shinya, K., Ebina, M., Yamada, S., Ono, M., Kasai, N., and Kawaoka, Y. (2006). Avian flu: influenza virus receptors in the human airway. Nature *440*, 435-436.

Shiratsuchi, A., Kaido, M., Takizawa, T., and Nakanishi, Y. (2000). Phosphatidylserine-mediated phagocytosis of influenza A virus-infected cells by mouse peritoneal macrophages. Journal of virology *74*, 9240-9244.

Shui, G., Cheong, W.F., Jappar, I.A., Hoi, A., Xue, Y., Fernandis, A.Z., Tan, B.K., and Wenk, M.R. (2011a). Derivatization-independent cholesterol analysis in crude lipid extracts by liquid chromatography/mass spectrometry: applications to a rabbit model for atherosclerosis. Journal of chromatography A *1218*, 4357-4365.

Shui, G., Guan, X.L., Low, C.P., Chua, G.H., Goh, J.S., Yang, H., and Wenk, M.R. (2010). Toward one step analysis of cellular lipidomes using liquid chromatography coupled with mass spectrometry: application to Saccharomyces cerevisiae and Schizosaccharomyces pombe lipidomics. Molecular bioSystems *6*, 1008-1017.

Shui, G., Stebbins, J.W., Lam, B.D., Cheong, W.F., Lam, S.M., Gregoire, F., Kusonoki, J., and Wenk, M.R. (2011b). Comparative plasma lipidome between human and cynomolgus monkey: are plasma polar lipids good biomarkers for diabetic monkeys? PloS one *6*, e19731.

Shvartsman, D.E., Gutman, O., Tietz, A., and Henis, Y.I. (2006). Cyclodextrins but not compactin inhibit the lateral diffusion of membrane proteins independent of cholesterol. Traffic *7*, 917-926.

Siddiqui, R.A., and Exton, J.H. (1992). Phospholipid base exchange activity in rat liver plasma membranes. Evidence for regulation by G-protein and P2y-purinergic receptor. The Journal of biological chemistry *267*, 5755-5761.

Sieczkarski, S.B., and Whittaker, G.R. (2002). Influenza virus can enter and infect cells in the absence of clathrin-mediated endocytosis. Journal of virology *76*, 10455-10464.

Sievers, F., Wilm, A., Dineen, D., Gibson, T.J., Karplus, K., Li, W., Lopez, R., McWilliam, H., Remmert, M., Soding, J.*, et al.* (2011). Fast, scalable generation of high-quality protein multiple sequence alignments using Clustal Omega. Molecular systems biology *7*, 539.

Silva, L.C., Ben David, O., Pewzner-Jung, Y., Laviad, E.L., Stiban, J., Bandyopadhyay, S., Merrill, A.H., Jr., Prieto, M., and Futerman, A.H. (2012). Ablation of ceramide synthase 2 strongly affects biophysical properties of membranes. Journal of lipid research *53*, 430-436.

Silva, L.C., Futerman, A.H., and Prieto, M. (2009). Lipid raft composition modulates sphingomyelinase activity and ceramide-induced membrane physical alterations. Biophysical journal *96*, 3210-3222.

Simons, K., and Vaz, W.L. (2004). Model systems, lipid rafts, and cell membranes. Annual review of biophysics and biomolecular structure *33*, 269-295.

Skehel, J.J., and Wiley, D.C. (2000). Receptor binding and membrane fusion in virus entry: the influenza hemagglutinin. Annual review of biochemistry *69*, 531-569.

St Vincent, M.R., Colpitts, C.C., Ustinov, A.V., Muqadas, M., Joyce, M.A., Barsby, N.L., Epand, R.F., Epand, R.M., Khramyshev, S.A., Valueva, O.A.*, et al.* (2010). Rigid amphipathic fusion inhibitors, small molecule antiviral compounds against

enveloped viruses. Proceedings of the National Academy of Sciences of the United States of America *107*, 17339-17344.

Su, X., Han, X., Yang, J., Mancuso, D.J., Chen, J., Bickel, P.E., and Gross, R.W. (2004). Sequential ordered fatty acid alpha oxidation and Delta9 desaturation are major determinants of lipid storage and utilization in differentiating adipocytes. Biochemistry *43*, 5033-5044.

Subathra, M., Qureshi, A., and Luberto, C. (2011). Sphingomyelin synthases regulate protein trafficking and secretion. PloS one *6*, e23644.

Sui, B., Bamba, D., Weng, K., Ung, H., Chang, S., Van Dyke, J., Goldblatt, M., Duan, R., Kinch, M.S., and Li, W.B. (2009). The use of Random Homozygous Gene Perturbation to identify novel host-oriented targets for influenza. Virology *387*, 473-481.

Tai, A.W., Benita, Y., Peng, L.F., Kim, S.S., Sakamoto, N., Xavier, R.J., and Chung, R.T. (2009). A functional genomic screen identifies cellular cofactors of hepatitis C virus replication. Cell host & microbe *5*, 298-307.

Takahashi, T., Murakami, K., Nagakura, M., Kishita, H., Watanabe, S., Honke, K., Ogura, K., Tai, T., Kawasaki, K., Miyamoto, D*., et al.* (2008). Sulfatide is required for efficient replication of influenza A virus. Journal of virology *82*, 5940-5950.

Takamori, S., Holt, M., Stenius, K., Lemke, E.A., Gronborg, M., Riedel, D., Urlaub, H., Schenck, S., Brugger, B., Ringler, P*., et al.* (2006). Molecular anatomy of a trafficking organelle. Cell *127*, 831-846.

Takeda, M., Leser, G.P., Russell, C.J., and Lamb, R.A. (2003). Influenza virus hemagglutinin concentrates in lipid raft microdomains for efficient viral fusion. Proceedings of the National Academy of Sciences of the United States of America *100*, 14610-14617.

Tan, K.S., Olfat, F., Phoon, M.C., Hsu, J.P., Howe, J.L., Seet, J.E., Chin, K.C., and Chow, V.T. (2012a). In vivo and in vitro studies on the antiviral activities of viperin against influenza H1N1 virus infection. The Journal of general virology *93*, 1269-1277.

Tan, S.H., Shui, G., Zhou, J., Li, J.J., Bay, B.H., Wenk, M.R., and Shen, H.M. (2012b). Induction of autophagy by palmitic acid via protein kinase C-mediated signaling pathway independent of mTOR (mammalian target of rapamycin). The Journal of biological chemistry *287*, 14364-14376.

Taubenberger, J.K., and Kash, J.C. (2010). Influenza virus evolution, host adaptation, and pandemic formation. Cell host & microbe *7*, 440-451.

Taubenberger, J.K., and Morens, D.M. (2010). Influenza: the once and future pandemic. Public Health Rep *125 Suppl 3*, 16-26.

Taubenberger, J.K., Reid, A.H., Lourens, R.M., Wang, R., Jin, G., and Fanning, T.G. (2005). Characterization of the 1918 influenza virus polymerase genes. Nature *437*, 889-893.

Testerink, N., van der Sanden, M.H., Houweling, M., Helms, J.B., and Vaandrager, A.B. (2009). Depletion of phosphatidylcholine affects endoplasmic reticulum morphology and protein traffic at the Golgi complex. Journal of lipid research *50*, 2182-2192.

Thai, T.P., Rodemer, C., Jauch, A., Hunziker, A., Moser, A., Gorgas, K., and Just, W.W. (2001). Impaired membrane traffic in defective ether lipid biosynthesis. Human molecular genetics *10*, 127-136.

Trajkovic, K., Hsu, C., Chiantia, S., Rajendran, L., Wenzel, D., Wieland, F., Schwille, P., Brugger, B., and Simons, M. (2008). Ceramide triggers budding of exosome vesicles into multivesicular endosomes. Science *319*, 1244-1247.

Trauner, D.A., Horvath, E., and Davis, L.E. (1988). Inhibition of fatty acid beta oxidation by influenza B virus and salicylic acid in mice: implications for Reye's syndrome. Neurology *38*, 239-241.

Trotard, M., Lepere-Douard, C., Regeard, M., Piquet-Pellorce, C., Lavillette, D., Cosset, F.L., Gripon, P., and Le Seyec, J. (2009). Kinases required in hepatitis C virus entry and replication highlighted by small interference RNA screening. FASEB journal : official publication of the Federation of American Societies for Experimental Biology *23*, 3780-3789.

Tumpey, T.M., Basler, C.F., Aguilar, P.V., Zeng, H., Solorzano, A., Swayne, D.E., Cox, N.J., Katz, J.M., Taubenberger, J.K., Palese, P.*, et al.* (2005). Characterization of the reconstructed 1918 Spanish influenza pandemic virus. Science *310*, 77-80.

Utermohlen, O., Herz, J., Schramm, M., and Kronke, M. (2008). Fusogenicity of membranes: the impact of acid sphingomyelinase on innate immune responses. Immunobiology *213*, 307-314.

Utermohlen, O., Karow, U., Lohler, J., and Kronke, M. (2003). Severe impairment in early host defense against Listeria monocytogenes in mice deficient in acid sphingomyelinase. J Immunol *170*, 2621-2628.

Valaperta, R., Chigorno, V., Basso, L., Prinetti, A., Bresciani, R., Preti, A., Miyagi, T., and Sonnino, S. (2006). Plasma membrane production of ceramide from ganglioside GM3 in human fibroblasts. FASEB journal : official publication of the Federation of American Societies for Experimental Biology *20*, 1227-1229.

van Meer, G., and Simons, K. (1982). Viruses budding from either the apical or the basolateral plasma membrane domain of MDCK cells have unique phospholipid compositions. The EMBO journal *1*, 847-852.

van Meer, G., Voelker, D.R., and Feigenson, G.W. (2008). Membrane lipids: where they are and how they behave. Nature reviews Molecular cell biology *9*, 112-124.

van Riel, D., Munster, V.J., de Wit, E., Rimmelzwaan, G.F., Fouchier, R.A., Osterhaus, A.D., and Kuiken, T. (2006). H5N1 Virus Attachment to Lower Respiratory Tract. Science *312*, 399.

Vance, J.E. (2008). Phosphatidylserine and phosphatidylethanolamine in mammalian cells: two metabolically related aminophospholipids. Journal of lipid research *49*, 1377-1387.

Vander Heiden, M.G., Cantley, L.C., and Thompson, C.B. (2009). Understanding the Warburg effect: the metabolic requirements of cell proliferation. Science *324*, 1029-1033.

Vander Heiden, M.G., Locasale, J.W., Swanson, K.D., Sharfi, H., Heffron, G.J., Amador-Noguez, D., Christofk, H.R., Wagner, G., Rabinowitz, J.D., Asara, J.M.*, et al.* (2010). Evidence for an alternative glycolytic pathway in rapidly proliferating cells. Science *329*, 1492-1499.

Vandermeer, M.L., Thomas, A.R., Kamimoto, L., Reingold, A., Gershman, K., Meek, J., Farley, M.M., Ryan, P., Lynfield, R., Baumbach, J.*, et al.* (2012). Association between use of statins and mortality among patients hospitalized with laboratory-confirmed influenza virus infections: a multistate study. The Journal of infectious diseases *205*, 13-19.

Vastag, L., Koyuncu, E., Grady, S.L., Shenk, T.E., and Rabinowitz, J.D. (2011). Divergent effects of human cytomegalovirus and herpes simplex virus-1 on cellular metabolism. PLoS pathogens *7*, e1002124.

Vluggens, A., Andreoletti, P., Viswakarma, N., Jia, Y., Matsumoto, K., Kulik, W., Khan, M., Huang, J., Guo, D., Yu, S.*, et al.* (2010). Reversal of mouse Acyl-CoA oxidase 1 (ACOX1) null phenotype by human ACOX1b isoform [corrected]. Laboratory investigation; a journal of technical methods and pathology *90*, 696-708.

Walker, A.K., Jacobs, R.L., Watts, J.L., Rottiers, V., Jiang, K., Finnegan, D.M., Shioda, T., Hansen, M., Yang, F., Niebergall, L.J.*, et al.* (2011). A conserved SREBP-1/phosphatidylcholine feedback circuit regulates lipogenesis in metazoans. Cell *147*, 840-852.

Wallner, S., and Schmitz, G. (2011). Plasmalogens the neglected regulatory and scavenging lipid species. Chemistry and physics of lipids *164*, 573-589.

Wanders, R.J., van Grunsven, E.G., and Jansen, G.A. (2000). Lipid metabolism in peroxisomes: enzymology, functions and dysfunctions of the fatty acid alpha- and beta-oxidation systems in humans. Biochemical Society transactions *28*, 141-149.

Wang, X., Hinson, E.R., and Cresswell, P. (2007). The interferon-inducible protein viperin inhibits influenza virus release by perturbing lipid rafts. Cell host & microbe *2*, 96-105.

Watanabe, T., Watanabe, S., and Kawaoka, Y. (2010). Cellular networks involved in the influenza virus life cycle. Cell host & microbe *7*, 427-439.

Wenk, M.R. (2005). The emerging field of lipidomics. Nature reviews Drug discovery *4*, 594-610.

Wenk, M.R. (2006). Lipidomics of host-pathogen interactions. FEBS letters *580*, 5541-5551.

Wenk, M.R. (2010). Lipidomics: new tools and applications. Cell *143*, 888-895.

Wiese, S., Gronemeyer, T., Ofman, R., Kunze, M., Grou, C.P., Almeida, J.A., Eisenacher, M., Stephan, C., Hayen, H., Schollenberger, L.*, et al.* (2007). Proteomics characterization of mouse kidney peroxisomes by tandem mass spectrometry and protein correlation profiling. Molecular & cellular proteomics : MCP *6*, 2045-2057.

Wolf, M.C., Freiberg, A.N., Zhang, T., Akyol-Ataman, Z., Grock, A., Hong, P.W., Li, J., Watson, N.F., Fang, A.Q., Aguilar, H.C.*, et al.* (2010). A broad-spectrum antiviral targeting entry of enveloped viruses. Proceedings of the National Academy of Sciences of the United States of America *107*, 3157-3162.

Wolff, T., O'Neill, R.E., and Palese, P. (1996). Interaction cloning of NS1-I, a human protein that binds to the nonstructural NS1 proteins of influenza A and B viruses. Journal of virology *70*, 5363-5372.

Wurdinger, T., Gatson, N.N., Balaj, L., Kaur, B., Breakefield, X.O., and Pegtel, D.M. (2012). Extracellular Vesicles and Their Convergence with Viral Pathways. Advances in virology *2012*, 767694.

Yao, D., Kuwajima, M., Chen, Y., Shiota, M., Okumura, Y., Yamada, H., and Kido, H. (2007). Impaired long-chain fatty acid metabolism in mitochondria causes brain vascular invasion by a non-neurotropic epidemic influenza A virus in the newborn/suckling period: implications for influenza-associated encephalopathy. Molecular and cellular biochemistry *299*, 85-92.

Ye, J., Mancuso, A., Tong, X., Ward, P.S., Fan, J., Rabinowitz, J.D., and Thompson, C.B. (2012). Pyruvate kinase M2 promotes de novo serine synthesis to sustain

mTORC1 activity and cell proliferation. Proceedings of the National Academy of Sciences of the United States of America *109*, 6904-6909.

Yu, A., McMaster, C.R., Byers, D.M., Ridgway, N.D., and Cook, H.W. (2004). Resistance to UV-induced apoptosis in Chinese-hamster ovary cells overexpressing phosphatidylserine synthases. The Biochemical journal *381*, 609-618.

Yu, C., Alterman, M., and Dobrowsky, R.T. (2005). Ceramide displaces cholesterol from lipid rafts and decreases the association of the cholesterol binding protein caveolin-1. Journal of lipid research *46*, 1678-1691.

Yuan, J., Bennett, B.D., and Rabinowitz, J.D. (2008). Kinetic flux profiling for quantitation of cellular metabolic fluxes. Nature protocols *3*, 1328-1340.

Yuyama, K., Sun, H., Mitsutake, S., and Igarashi, Y. (2012). Sphingolipid-modulated Exosome Secretion Promotes Clearance of Amyloid-beta by Microglia. The Journal of biological chemistry *287*, 10977-10989.

Zasloff, M., Adams, A.P., Beckerman, B., Campbell, A., Han, Z., Luijten, E., Meza, I., Julander, J., Mishra, A., Qu, W.*, et al.* (2011). Squalamine as a broad-spectrum systemic antiviral agent with therapeutic potential. Proceedings of the National Academy of Sciences of the United States of America *108*, 15978-15983.

Zhang, J., Leser, G.P., Pekosz, A., and Lamb, R.A. (2000). The cytoplasmic tails of the influenza virus spike glycoproteins are required for normal genome packaging. Virology *269*, 325-334.

Zhao, S., Xu, W., Jiang, W., Yu, W., Lin, Y., Zhang, T., Yao, J., Zhou, L., Zeng, Y., Li, H.*, et al.* (2010). Regulation of cellular metabolism by protein lysine acetylation. Science *327*, 1000-1004.

Zhirnov, O.P., and Klenk, H.D. (2007). Control of apoptosis in influenza virus-infected cells by up-regulation of Akt and p53 signaling. Apoptosis : an international journal on programmed cell death *12*, 1419-1432.

Zhong, S., Hsu, F., Stefan, C.J., Wu, X., Patel, A., Cosgrove, M.S., and Mao, Y. (2012). Allosteric activation of the phosphoinositide phosphatase Sac1 by anionic phospholipids. Biochemistry *51*, 3170-3177.

7 Appendices

7.1 Supplementary figures

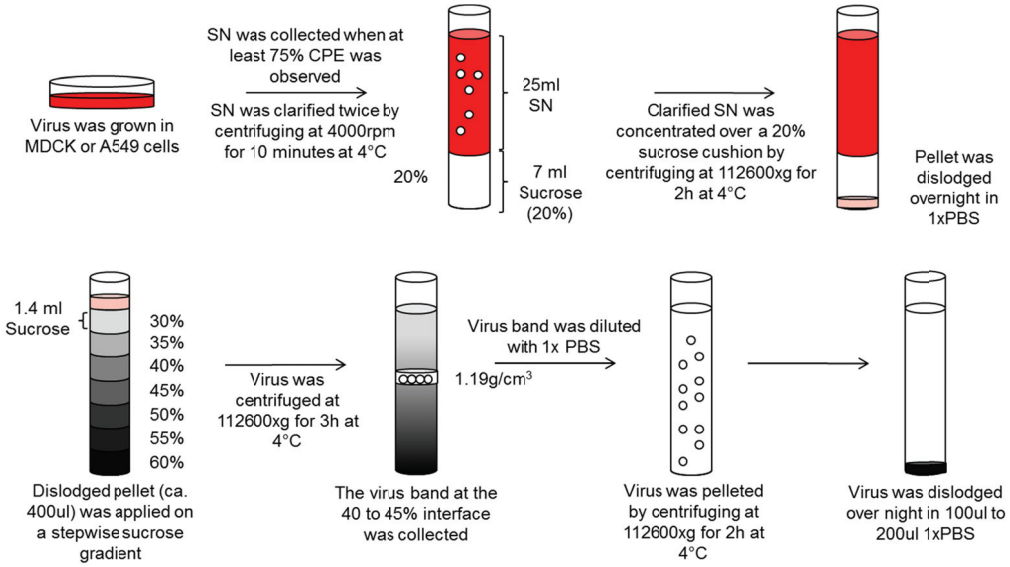

Supplementary Figure 7-1: Experimental setup of influenza virus purification according to Shaw et al, 2008.

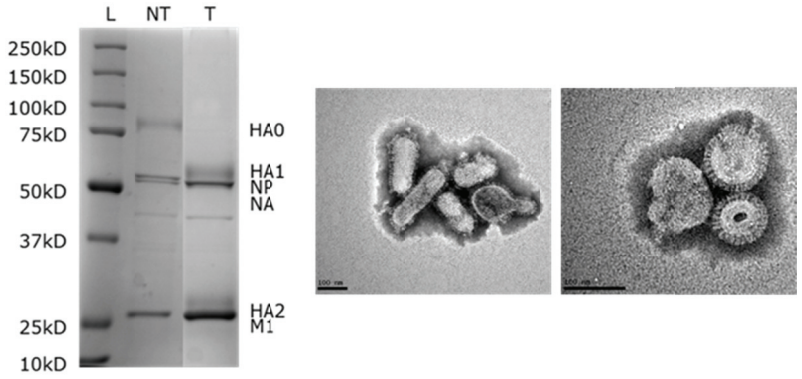

Supplementary Figure 7-2: SDS gel picture and SEM pictures from purified MDCK grown H3N2 P10 virus particles. Protein ladder (L), virus grown without trypsin (NT), virus grown in trypsin (T); Virus proteins hemagglutinin (HA0, HA1, HA2), nucleoprotein (NP), neuraminidase (NA) and matrix protein 1 (M1) were identified.

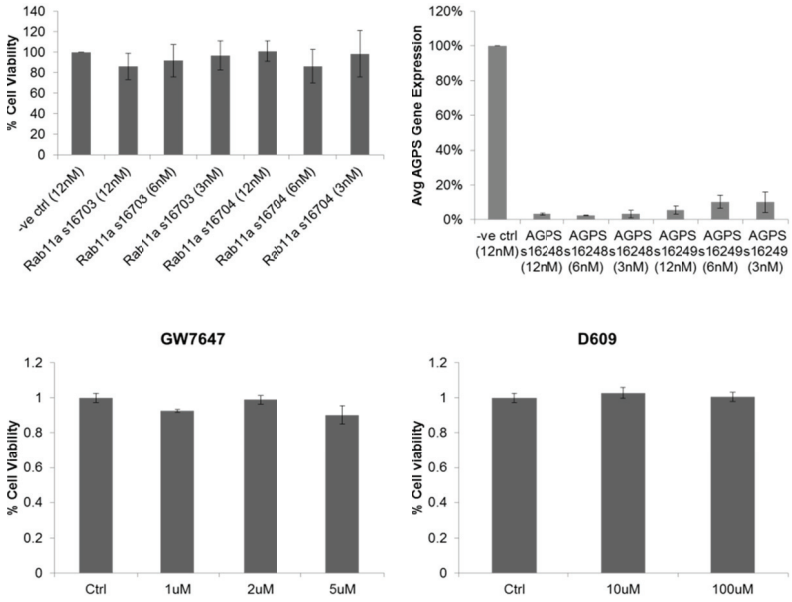

Supplementary Figure 7-3: Gene expression and cell viability (MTT) assays. AGPS & Rab11 knockdown (3 independent experiments; adapted from Charmaine Chng); cell viability assays after treatment with GW7647 and D609 inhibitors (1 experiment each with three replicates). Error bars represent standard deviations.

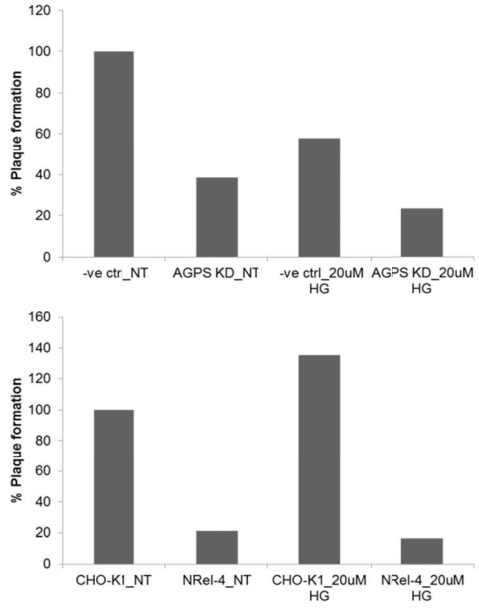

Supplementary Figure 7-4: Influenza virus production after rescue of ether lipid deficiency by HG. Influenza virus-infected AGPS depleted and NRel-4 cells were treated with 20µM 1-*O*-hexadecyl-sn-glycerol (HG) (sc-202394, Santa Cruz biotechnology). The infected cells with and without HG treatment were incubated in serum-free F12 GlutaMax media for 18 hours and subsequently, virus titres were assessed by plaque assay (Adapted from Charmaine Chng).

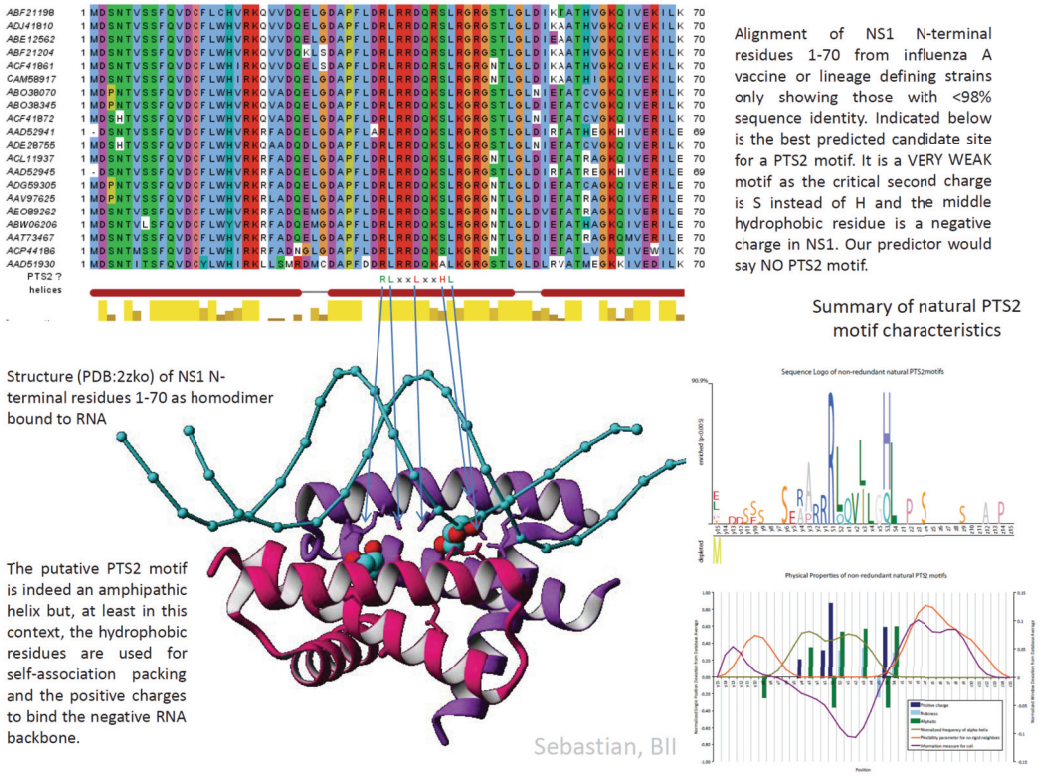

Supplementary Figure 7-5: Bioinformatics analysis of a putative PTS2 sequence in influenza virus NS1. Analysis performed by Sebastian Maurer-Stroh and Frank Eisenhaber, Bioinformatics Institute, Singapore.

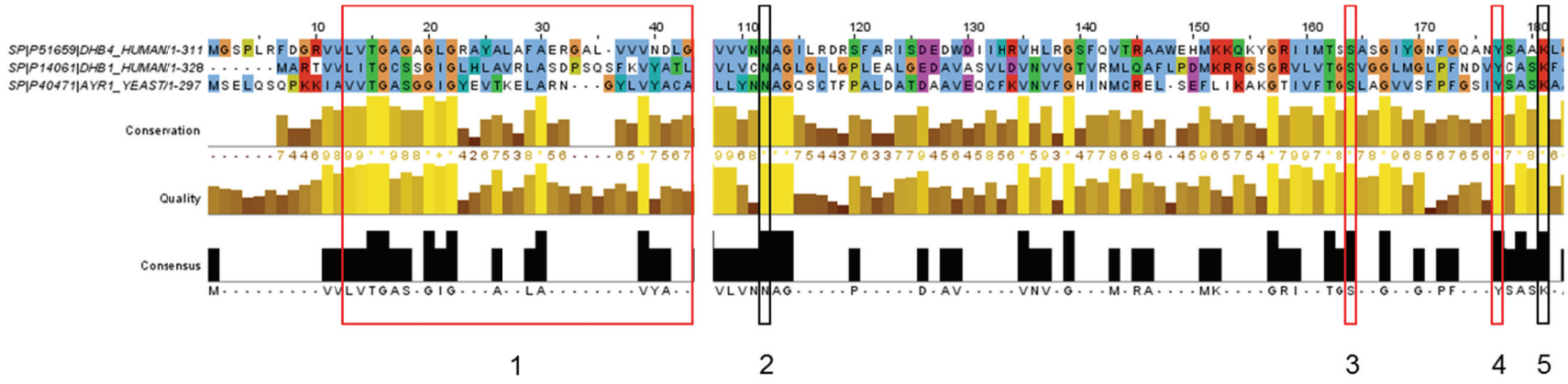

HSD17B1 (DHB1); HSD17B4 (DHB4)

1) Nucleotide Binding; NAD/NADP (HSD17B1, HSD17B4 & AYR1)
2) NAD Binding Site; via carbonyl oxygen (HSD17B4)
3) Substrate (HSD17B1, HSD17B4 & AYR1)
4) Active Site (HSD17B1, HSD17B4 & AYR1)
5) NADP Binding Site (HSD17B1)

Supplementary Figure 7-6: Alignment of the N-Terminal domain of human HSD17B4 with human HSD17B1 and yeast Ayr1p. Alignment was performed using Clustal Omega (Sievers et al., 2011) run on www.uniprot.org.

SDR	Gene names	AA	kDa (1AA~110Da)
classical	Hsd17b4, Edh17b4	735	80.85
classical	Pecr	303	33.33
classical	Pecr	260	28.6
extended	Far1, Mlstd2	515	56.65
intermediate	Kiaa0564	1905	209.55
intermediate	Pcx	1179	129.69
intermediate	Acad11	779	85.69
intermediate	Acox3	700	77
intermediate	Abcd3, Pmp70, Pxmp1	659	72.49
intermediate	Slc27a2, Acsvl1, Fatp2, Vlcs	620	68.2
intermediate	Hspa8	565	62.15
intermediate	Ces3 ,Ces1	565	62.15
intermediate	Scp2, Scp-2	547	60.17
intermediate	Krt79, Kb38	531	58.41
intermediate	Cat, Cas-1, Cas1	527	57.97
intermediate	Aldh2	519	57.09
intermediate	P4hb	509	55.99
intermediate	Nudt12	462	50.82
intermediate	Uqcrc2	453	49.83
intermediate	Got2, Got-2	430	47.3
intermediate	Amacr, Macr1	381	41.91
intermediate	Mdh2, Mor1	338	37.18
intermediate	Mdh1, Mor2	334	36.74
intermediate	Cyb5r3, Dia1	302	33.22
intermediate	Slc25a5	298	32.78
intermediate	Slc25a4	298	32.78
intermediate	Pex11a	246	27.06
intermediate	Abhd14b	210	23.1
Intermediate	Ndufa4	82	9.02

The size of peroxisomal acyl/alkyl DHAP reductase was estimated to be around 75kDa;
K_m (Acyl-DHAP) < K_m (Alkyl-DHAP) **(Datta et al, 1990).**

Supplementary Figure 7-7: Overview of SDR sequences found in peroxisomal proteins. The list of peroxisomal proteins was derived from a recent proteomics study (Wiese et al., 2007) and we identified 29 peroxisomal proteins carrying a SDR sequence (Bray et al., 2009). Proteins being similar in size than to the estimated size of mammalian acyl-DHAP reductase (Datta et al., 1990) are coloured in yellow.

7.2 Supplementary tables

Supplementary Table 7-1: Overview of samples used for quantitative MRM analysis of 159 sphingo- and phospholipid species from A549 cells infected with influenza virus A/PR/8/34 H1N1.

Time Point	Experiment 1		Experiment 2		Experiment 3	
12 hpi	Mock (n=3)	H1N1 (n=3)	Mock (n=3)	H1N1 (n=3)	Mock (n=3)	H1N1 (n=3)
18 hpi	**Mock (n=3)**	H1N1 (n=3)	Mock (n=3)	H1N1 (n=3)	Mock (n=3)	H1N1 (n=3)
24 hpi	Mock (n=3)	H1N1 (n=3)	Mock (n=3)	H1N1 (n=3)	Mock (n=3)	H1N1 (n=3)

Supplementary Table 7-2: Two by two contingency table for the calculation of lipid class enrichment in differentially regulated lipid species using a Fisher's exact test:

	Significant Lipids	MRM List
Lipid class	A	C
Other class	B	D
Total	78 (A+B)	175 (C+D)

Supplementary Table 7-3: Overview of purified influenza virus samples analysed by MRM or QTOF mass spectrometry.

	MRM			QTOF			Lipids analysed MRM	Lipids analysed QTOF
A549 grown H1N1	Exp1 (n=3)	Exp2 (n=3)					159 MRM transitions	
MDCK grown H1N1	Exp 1 (n=3)						PC species	
MDCK grown H3N2 P10	Exp1 (n=2)	Exp2 (n=2)	Exp3 (n=2)	Exp1 (n=1)	Exp2 (n=1)	Exp3 (n=1)	159 MRM transitions	PC species
MDCK grown H3N2 P0	Exp1 (n=2)	Exp2 (n=2)	Exp3 (n=2)	Exp1 (n=1)	Exp2 (n=1)	Exp3 (n=1)	159 MRM transitions	PC species

Supplementary Table 7-4: Overview of log(fold-ratios) used for hierarchical clustering.

Host response (log(H1N1/mock))						Viral lipids (log(H1N1/A549))						Virulence (log(P10/P0))		
18hpi			24hpi			A549 Exp1		A549 Exp2		A549 Exp3				
Exp1	Exp2	Exp3	Exp1	Exp2	Exp3	H1N1 Exp1	H1N1 Exp2	H1N1 Exp1	HN1 Exp2	H1N1 Exp1	H1N1 Exp2	Exp1	Exp2	Exp3

Supplementary Table 7-5: Overview of purified MDCK grown H1N1 samples used for the analysis of oxidized lipid species.

Treatment condition	Experiment 1	Experiment 2
LJ025	n=2	n=2
LJ001	n=2	n=2
JL103	n=2	n=2

Supplementary Table 7-6: Overview of MRM transitions used for phospho- and sphingolipid measurements.

Lipid Name	MRM	Flu Time Course	Flu	PI4KA
LysoPS 16:0	496.5/409.4			x
LysoPS 18:0	524.5/437.4			x
LysoPS 16:1	494.5/407.4			x
LysoPS 18:1	522.5/435.4			x
PS 32:0	734.6/647.6	x	x	x
PS 34:0	762.6/675.6	x	x	x
PS 36:0	790.6/703.6	x	x	x
PS 32:1	732.6/645.6	x	x	x
PS 34:1	760.6/673.6	x	x	x
PS 36:1	788.6/701.6	x	x	x
PS 38:1	816.6/729.6	x	x	x
PS 34:2	758.6/671.6	x	x	x
PS 36:2	786.6/699.6	x	x	x
PS 38:2	814.6/727.6	x	x	x
PS 38:3	812.6/725.6	x	x	x
PS 40:4	838.6/751.6	x	x	x
PS 40:5	836.6/749.6	x	x	x
PS 40:6	834.6/747.6	x	x	x
LysoPI 16:0	571.6/241.0		x	x
LysoPI 18:0	599.6/241.0		x	x
PI 34:0	837.6/241.1	x	x	x
PI 34:1	835.5/241.1	x	x	x
PI 36:1	863.6/241.1	x	x	x
PI 36:2	861.6/241.1	x	x	x
PI 36:3	859.6/241.1	x	x	x
PI 38:3	887.6/241.1	x	x	x
PI 38:4	885.6/241.1	x	x	x
PI 40:4	913.6/241.1	x	x	x
PI 38:5	883.6/241.1	x	x	x
PI 40:5	911.6/241.1	x	x	x
PI 38:6	881.6/241.1	x	x	x
GM3 d18:0/16:0	1153.6/290.1	x	x	x
GM3 d18:0/18:0	1181.6/290.1	x	x	x
GM3 d18:0/20:0	1209.6/290.1	x	x	x
GM3 d18:0/22:0	1237.6/290.1	x	x	x
GM3 d18:0/24:0	1265.6/290.1	x	x	x
GM3 d18:1/16:0	1151.6/290.1	x	x	x
GM3 d18:1/18:0	1179.6/290.1	x	x	x
GM3 d18:1/20:0	1207.6/290.1	x	x	x
GM3 d18:1/22:0	1235.6/290.1	x	x	x
GM3 d18:1/24:0	1263.6/290.1	x	x	x
GM3 d18:1/26:0	1291.6/290.1	x	x	x
GM3 d18:1/16:1	1149.6/290.1	x	x	x
GM3 d18:1/18:1	1177.6/290.1	x	x	x
GM3 d18:1/20:1	1205.6/290.1	x	x	x
GM3 d18:1/22:1	1233.6/290.1	x	x	x
GM3 d18:1/24:1	1261.6/290.1	x	x	x
GM3 d18:1/26:1	1289.6/290.1	x	x	x
LysoPE 16:0	452.5/196.1			x
LysoPE 18:0	480.5/196.1			x
LysoPE 16:1	450.5/196.1			x
LysoPE 18:1	478.5/196.1			x
LysoPE 18:2	476.5/196.1			x
LysoPE 18:0e	464.5/196.1			x
LysoPE 20:0e	492.5/196.1			x
PE 32:0a	690.6/196.1	x	x	x
PE 34:0a	718.6/196.1	x	x	x
PE 32:1a	688.6/196.1	x	x	x
PE 34:1a	716.6/196.1	x	x	x
PE 36:1a	744.6/196.1	x	x	x
PE 34:2a	714.6/196.1	x	x	x
PE 36:2a	742.6/196.1	x	x	x
PE 36:3a	740.6/196.1	x	x	x
PE 38:3a	768.6/196.1	x	x	x
PE 38:4a	766.6/196.1	x	x	x
PE 40:4a	794.6/196.1	x	x	x
PE 38:5a	764.6/196.1	x	x	x
PE 40:5a	792.6/196.1	x	x	x
PE 34:0e	702.6/196.1	x	x	x
PE 34:1e	700.6/196.1	x	x	x
PE 36:1e	728.6/196.1	x	x	x
PE 36:2e	726.6/196.1	x	x	x
PE 38:2e	754.6/196.1	x	x	x
PE 36:3e	724.6/196.1	x	x	x
PE 38:3e	752.6/196.1	x	x	x
PE 38:4e	750.6/196.1	x	x	x
PE 40:4e	778.6/196.1	x	x	x
PE 38:5e	748.6/196.1	x	x	x
PE 40:5e	776.6/196.1	x	x	x
PE 38:6e	746.6/196.1	x	x	x

PE 40:6e	774.6/196.1	x	x	x
PA 32:0	647.5/153.0			x
PA 34:0	675.5/153.0			x
PA 36:0	703.5/153.0			x
PA 32:1	645.5/153.0			x
PA 34:1	673.5/153.0			x
PA 36:1	701.5/153.0			x
PA 34:2	671.5/153.0			x
PA 36:2	699.5/153.0			x
PC 32:0a	734.6/184.1	x	x	x
PC 34:0a	762.6/184.1	x	x	x
PC 36:0a	790.6/184.1	x	x	x
PC 38:0a	818.7/184.1	x	x	x
PC 40:0a	846.7/184.1	x	x	x
PC 32:1a	732.6/184.1	x	x	x
PC 34:1a	760.6/184.1	x	x	x
PC 36:1a	788.6/184.1	x	x	x
PC 38:1a	816.6/184.1	x	x	x
PC 40:1a	844.7/184.1	x	x	x
PC 32:2a	730.5/184.1	x	x	x
PC 34:2a	758.6/184.1	x	x	x
PC 36:2a	786.6/184.1	x	x	x
PC 38:2a	814.6/184.1	x	x	x
PC 40:2a	842.7/184.1	x	x	x
PC 34:3a	756.6/184.1	x	x	x
PC 36:3a	784.6/184.1	x	x	x
PC 38:3a	812.6/184.1	x	x	x
PC 40:3a	840.6/184.1	x	x	x
PC 36:4a	782.6/184.1	x	x	x
PC 38:4a	810.6/184.1	x	x	x
PC 40:4a	838.6/184.1	x	x	x
PC 38:5a	808.6/184.1	x	x	x
PC 40:5a	836.6/184.1	x	x	x
PC 38:6a	806.6/184.1	x	x	x
PC 40:6a	834.6/184.1	x	x	x
PC 32:0e	720.6/184.1	x	x	x
PC 34:0e	748.6/184.1	x	x	x
PC 36:0e	776.7/184.1	x	x	x
PC 38:0e	804.7/184.1	x	x	x
PC 32:1e	718.6/184.1	x	x	x
PC 34:1e	746.6/184.1	x	x	x
PC 36:1e	774.6/184.1	x	x	x
PC 38:1e	802.7/184.1	x	x	x
PC 34:2e	744.6/184.1	x	x	x
PC 36:2e	772.6/184.1	x	x	x
PC 38:2e	800.7/184.1	x	x	x
PC 34:3e	742.6/184.1	x	x	x
PC 38:3e	798.6/184.1	x	x	x
PC 40:4e	824.7/184.1	x	x	x
PC 40:5e	822.6/184.1	x	x	x
PC 40:6e	820.6/184.1	x	x	x
PC 31:0a	720.6/184.1	x		
PC 33:0a	748.6/184.1	x		
PC 35:0a	776.7/184.1	x		
PC 37:0a	804.7/184.1	x		
PC 31:1a	718.6/184.1	x		
PC 33:1a	746.6/184.1	x		
PC 35:1a	774.6/184.1	x		
PC 37:1a	802.7/184.1	x		
PC 33:2a	744.6/184.1	x		
PC 35:2a	772.6/184.1	x		
PC 37:2a	800.7/184.1	x		
PC 33:3a	742.6/184.1	x		
PC 37:3a	798.6/184.1	x		
PC 39:4a	824.7/184.1	x		
PC 39:5a	822.6/184.1	x		
PC 39:6a	820.6/184.1	x		
LysoPC 16:0	496.5/184.1			x
LysoPC 18:0	524.5/184.1			x
LysoPC 16:1	494.5/184.1			x
LysoPC 18:1	522.5/184.1			x
LysoPC 18:2	520.5/184.1			x
LysoPC 20:4	544.5/184.1			x
LysoPC 22:6	568.5/184.1			x
SM d18:0/16:0	705.6/184.1	x	x	x
SM d18:0/18:0	733.6/184.1	x	x	x
SM d18:0/20:0	761.7/184.1	x	x	x
SM d18:0/22:0	789.7/184.1	x	x	x
SM d18:0/24:0	817.7/184.1	x	x	x
SM d18:0/26:0	845.7/184.1	x	x	x
SM d18:0/26:1	843.7/184.1	x	x	x
SM d18:1/16:0	703.6/184.1	x	x	x
SM d18:1/17:0	717.6/184.1	x	x	x
SM d18:1/18:0	731.6/184.1	x	x	x

SM d18:1/19:0	745.6/184.1	x	x	x
SM d18:1/20:0	759.6/184.1	x	x	x
SM d18:1/21:0	773.7/184.1	x	x	x
SM d18:1/22:0	787.7/184.1	x	x	x
SM d18:1/23:0	801.7/184.1	x	x	x
SM d18:1/24:0	815.7/184.1	x	x	x
SM d18:1/16:1	701.6/184.1	x	x	x
SM d18:1/18:1	729.6/184.1	x	x	x
SM d18:1/20:1	757.6/184.1	x	x	x
SM d18:1/24:1	813.7/184.1	x	x	x
SM d18:1/18:2	727.6/184.1	x	x	x
Sph d18:0	302.4/284.2			x
Sph d18:1	300.4/282.2			x
Cer d18:0/16:0	540.5/266.4	x	x	x
Cer d18:0/18:0	568.6/266.4	x	x	x
Cer d18:0/20:0	596.6/266.4	x	x	x
Cer d18:0/22:0	624.6/266.4	x	x	x
Cer d18:0/24:0	652.7/266.4	x	x	x
Cer d18:0/26:0	680.7/266.4	x	x	x
Cer d18:0/24:1	650.6/266.4	x	x	x
Cer d18:0/26:1	678.7/266.4	x	x	x
Cer d18:1/16:0	538.5/264.4	x	x	x
Cer d18:1/18:0	566.6/264.4	x	x	x
Cer d18:1/20:0	594.6/264.4	x	x	x
Cer d18:1/22:0	622.6/264.4	x	x	x
Cer d18:1/24:0	650.6/264.4	x	x	x
Cer d18:1/26:0	678.7/264.4	x	x	x
Cer d18:1/24:1	648.6/264.4	x	x	x
Cer d18:1/26:1	676.7/264.4	x	x	x
GlcCer d18:0/16:0	702.6/266.4	x	x	x
GlcCer d18:0/18:0	730.6/266.4	x	x	x
GlcCer d18:0/20:0	758.7/264.4	x	x	x
GlcCer d18:0/22:0	786.7/266.4	x	x	x
GlcCer d18:0/24:0	814.7/266.4	x	x	x
GlcCer d18:0/26:1	840.7/264.4	x	x	x
GlcCer d18:1/16:0	700.6/264.4	x	x	x
GlcCer d18:1/18:0	728.6/264.4	x	x	x
GlcCer d18:1/20:0	756.6/264.4	x	x	x
GlcCer d18:1/22:0	784.7/264.4	x	x	x
GlcCer d18:1/24:0	812.7/264.4	x	x	x
GlcCer d18:1/24:1	810.7/264.4	x	x	x

Supplementary Table 7-7: Overview of m/z values used for neutral lipid measurements

Lipid Name	Ion
DAG 32:0	586.5
DAG 34:0	614.6
DAG 32:1	584.5
DAG 34:1	612.6
DAG 36:1	640.6
DAG 34:2	610.6
DAG 36:2	638.6
DAG 36:3	636.6
DAG 36:4	634.6
DAG 38:4	662.6
TAG 44:0	768.8
TAG 46:0	796.8
TAG 48:0	824.8
TAG 52:0	880.9
TAG 54:0	908.9
TAG 56:0	936.9
TAG 58:0	964.9
TAG 60:0	992.9
TAG 44:1	766.8
TAG 46:1	794.8
TAG 48:1	822.8
TAG 49:1	836.8
TAG 50:1	850.8
TAG 52:1	878.9
TAG 53:1	864.9
TAG 54:1	906.9
TAG 56:1	934.9
TAG 58:1	962.9
TAG 60:1	990.9
TAG 44:2	764.8
TAG 46:2	792.8
TAG 48:2	820.8
TAG 49:2	834.8
TAG 50:2	848.8
TAG 52:2	876.9
TAG 53:2	862.9
TAG 54:2	904.9

TAG 56:2	932.9
TAG 58:2	960.9
TAG 60:2	988.9
TAG 46:3	790.8
TAG 48:3	818.8
TAG 50:3	846.8
TAG 52:3	874.9
TAG 54:3	902.9
TAG 56:3	930.9
TAG 58:3	958.9
TAG 60:3	986.9
TAG 48:4	816.8
TAG 50:4	844.8
TAG 52:4	872.9
TAG 54:4	900.9
TAG 56:4	928.9
TAG 57:4	942.9
TAG 58:4	956.9
TAG 60:4	984.9
TAG 52:5	870.9
TAG 54:5	898.9
TAG 56:5	926.9
TAG 58:5	954.9
TAG 60:5	982.9
TAG 52:6	868.9
TAG 54:6	896.9
TAG 56:6	924.9
TAG 58:6	952.9
TAG 60:6	980.9
TAG 52:7	866.9
TAG 54:7	894.9
TAG 56:7	922.9
TAG 58:7	950.9
TAG 60:7	978.9
TAG 54:8	892.9
TAG 56:8	920.9
TAG 58:8	948.9
TAG 60:8	976.9
TAG 54:9	890.9
TAG 56:9	918.9
TAG 58:9	946.9
TAG 60:9	974.9
TAG 54:10	888.9
TAG 58:10	944.9
TAG 60:10	972.9
Cholesterol	369.4
Cholesterol Ester	369.4